

**Daylight Design Exploration Using Parametric Processes  
and Artificial Neural Networks**

by

**Clara-Larissa Lorenz**



In partial fulfilment of the requirements for the degree of Doctor of Philosophy at  
Cardiff University

School of Architecture, Cardiff University, Wales, United Kingdom

November 2020

## Acknowledgements

I would like to acknowledge everyone who played a role in my academic accomplishments. The completion of this project could not have been possible without the endless support, motivation and advice provided by Dr. Clarice Bleil de Souza, to whom I will forever be grateful. I would also like to express my gratitude towards Dr. A. Benjamin Spaeth and Dr. Michael S. Packianather for their unwavering support and advice throughout the research process. To my parents, no words I have are enough to express my gratitude and thanks for their endless love and support. To my sister, I am thankful for her keen eye for writing and structure and her encouragements until the very end. To my love, Q. Z. Dhar, I am thankful for his continued belief in me, and for his love that has kept me going. Thank you also to my friends and others who in one way or another extended their love and help. Finally, I gratefully acknowledge BFWG Charitable Foundation and thank them for their support.

## Abstract

The integration of Artificial Neural Networks (ANNs) as surrogates for daylight simulation models within parametric design environments promises greater computational efficiency in the exploration and optimisation of design solutions. This thesis demonstrates how ANNs can be integrated in design exploration processes, specifically focusing on the investigation of design solutions for the central atrium of a school building. ANNs are validated as surrogates for climate-based-performance metrics including Daylight Autonomy (DA) and spatial Daylight Autonomy (sDA) for thresholds of 100 lux ( $DA_{100}$ ) and 300 lux ( $DA_{300}$ ). The presented work discusses the prediction accuracies and sensitivities of the developed ANN models, the efficacy of the method, and atrium design strategies aimed at improving daylight conditions in atrium adjacent spaces. The research also critically evaluates daylight performance metrics and their implications on the design outcome of optimisation. Contributions are made in terms of validating ANN prediction accuracies for annual climate-based-daylight metrics, presenting a workflow for the selection and optimisation of input features from parametric models, and identifying limitations of ANN predictions related to model complexity and number of design variables. The work also contributes to the field of atrium design research by analysing the impact of atrium design changes on daylight performance, and by employing and comparing multiple daylight performance metrics.

Thesis results showed that robust predictions could be achieved by optimising the network architecture of ANN ensembles, optimising input features, and employing cross-validation and early stopping. Overall, high accuracies were achieved for performance metrics predicting both % of occupied hours in a year and the % of space. For %time metrics, mean absolute errors were around 0.6% DA MAE (for DA ranging from 0 to 100%) for the 100 lux and 300 lux thresholds. For %space metrics, mean absolute errors were around 0.3% sDA MAE for both the 100 lux and 300 lux thresholds (for sDA ranging between 0 and 100%). Daylight simulation time was reduced by up to 71% by integrating ANNs within the design process.

The design results showed that optimum atrium design solutions varied between the  $sDA_{300/50\%}$  and  $sDA_{100/50\%}$  metric. Additionally, the favorable design solutions also varied depending on whether design solutions were explored via the %space results of the sDA metric or the %time visualisations of the DA metric. Hence, this work discusses both the target thresholds employed in daylight performance metrics and bias that can be introduced by careless implementation of them. In terms of design strategy,

southward orientations of the atrium well and reducing WWR towards the top floors increased daylight in atrium adjacent spaces on lower floors, but was met by a tradeoff, as this also reduced daylight on upper floors. The interdependencies of atrium design changes and the value and interpretability of the applied daylight performance metrics are further elaborated on in this thesis.

# Table of Contents

<b>CHAPTER 1</b>	<b>INTRODUCTION .....</b>	<b>8</b>
1.1	RATIONALE FOR IMPROVING DAYLIGHT CONDITIONS IN BUILDINGS.....	8
1.2	IMPROVING DESIGN OUTCOMES VIA EXPLORATION AND OPTIMISATION .....	10
1.3	CHALLENGES TO SIMULATION AND OPTIMISATION IN PRACTICE .....	12
1.4	RESEARCH AIMS AND OBJECTIVES .....	13
1.5	THESIS STRUCTURE.....	14
<b>CHAPTER 2</b>	<b>LITERATURE REVIEW.....</b>	<b>16</b>
2.1	DAYLIGHT PERFORMANCE ASSESSMENT .....	16
2.1.1	<i>The daylight factor .....</i>	<i>16</i>
2.1.2	<i>Climate-based-daylight-metrics .....</i>	<i>18</i>
2.1.3	<i>Identified Gaps and Conclusions.....</i>	<i>24</i>
2.2	ATRIUM DESIGN AS A DAYLIGHTING STRATEGY .....	25
2.2.1	<i>Atrium geometry .....</i>	<i>25</i>
2.2.2	<i>Atrium well splay angles .....</i>	<i>27</i>
2.2.3	<i>Vertical fenestration of the atrium well .....</i>	<i>28</i>
2.2.4	<i>Material Reflectance .....</i>	<i>29</i>
2.2.5	<i>Identified gaps and conclusions .....</i>	<i>30</i>
2.3	ARTIFICIAL NEURAL NETWORKS (ANNs) FOR BUILDING PERFORMANCE OPTIMIZATION.....	31
2.3.1	<i>ANNs as emulators for building performance simulations .....</i>	<i>32</i>
2.3.2	<i>Integration of ANN in genetic optimization.....</i>	<i>34</i>
2.3.3	<i>Optimization of ANN hyperparameters .....</i>	<i>36</i>
2.3.4	<i>Identified gaps and conclusions .....</i>	<i>40</i>
<b>CHAPTER 3</b>	<b>METHODOLOGY .....</b>	<b>41</b>
3.1	RESEARCH FRAMEWORK.....	41
3.1.1	<i>Research stages.....</i>	<i>41</i>

3.1.2	<i>Research objectives addressed in each chapter</i>	42
3.1.3	<i>ANNs as a predictive system in design exploration</i>	43
3.1.4	<i>Modelling environment</i>	44
3.1.5	<i>ANN model development</i>	45
3.1.6	<i>Measures of ANN prediction accuracy</i>	46
3.1.7	<i>Daylight performance metrics</i>	47
3.2	DETAILED DESCRIPTION OF METHODS	48
3.2.1	<i>Pilot study</i>	48
3.2.2	<i>Validation of ANNs in design exploration</i>	51
3.2.3	<i>Optimisation of ANN prediction accuracies</i>	57
3.2.4	<i>Analysis of daylight performance results</i>	61
<b>CHAPTER 4</b>	<b>PILOT STUDY: PREDICTING DAYLIGHT AUTONOMY (DA) WITH ANNS</b>	<b>62</b>
4.1	VALIDATION OF DA PREDICTIONS FOR INTERNALLY REFLECTED DAYLIGHT	62
4.1.1	<i>ANN training and test performance</i>	63
4.1.2	<i>Conclusions</i>	65
4.2	VALIDATION OF DA PREDICTIONS FOR INCIDENT DAYLIGHT	66
4.2.1	<i>ANN training and test performance</i>	67
4.2.2	<i>Conclusions</i>	71
<b>CHAPTER 5</b>	<b>ANNS IN DAYLIGHT DESIGN EXPLORATION</b>	<b>73</b>
5.1	ANN SENSITIVITIES	73
5.1.1	<i>Impact of simulation settings and modeling environment on prediction accuracies</i>	74
5.2	EFFICIENTLY MAPPING THE PERFORMANCE OF DESIGN SPACES	75
5.2.1	<i>Full-factorial validation of prediction accuracies</i>	79
5.2.2	<i>Data sampling</i>	83
5.2.3	<i>Simulated vs. predicted performance ranking of design solutions</i>	87
5.3	PREDICTING DAYLIGHT FOR WWR DISTRIBUTION OPTIONS AND MATERIAL REFLECTANCE	89
5.3.1	<i>Fractional validation of prediction accuracies</i>	91
5.4	CONCLUSIONS	94

<b>CHAPTER 6</b>	<b>OPTIMISATION OF ANN PREDICTION ACCURACIES .....</b>	<b>96</b>
6.1	INPUT FEATURE ENGINEERING .....	96
6.1.1	<i>Impact of input feature selection on prediction accuracies .....</i>	<i>96</i>
6.1.2	<i>Conclusions .....</i>	<i>105</i>
6.2	AUTOMATED INPUT FEATURE OPTIMISATION .....	106
6.2.1	<i>Ranking of input features according to relevance .....</i>	<i>111</i>
6.2.2	<i>Sequential forward selection.....</i>	<i>112</i>
6.2.3	<i>Conclusions.....</i>	<i>115</i>
6.3	FINETUNING OF HYPERPARAMETERS .....	117
6.3.1	<i>Sensitivity to network architecture and number of design variables.....</i>	<i>117</i>
6.3.2	<i>Conclusions.....</i>	<i>121</i>
<b>CHAPTER 7</b>	<b>DAYLIGHT PERFORMANCE RESULTS: EVALUATION OF ATRIUM DESIGN CHANGES.....</b>	<b>122</b>
7.1	OVERVIEW OF RESULTS .....	123
7.2	IMPACT OF ATRIUM DESIGN CHANGES ON DAYLIGHT .....	130
7.2.1	<i>Design solutions increasing daylight on lower floors.....</i>	<i>130</i>
7.2.2	<i>Design solutions decreasing daylight on lower floors.....</i>	<i>140</i>
7.2.3	<i>Design solutions increasing daylight on top floors .....</i>	<i>144</i>
7.2.4	<i>Design solutions decreasing daylight on lower floors .....</i>	<i>147</i>
7.3	CONCLUSIONS.....	155
<b>CHAPTER 8</b>	<b>SPATIAL AND TEMPORAL DAYLIGHT METRICS IN DECISION-MAKING .....</b>	<b>157</b>
8.1	OVERVIEW OF DIFFERENCES BETWEEN METRICS.....	158
8.2	EVALUATION OF METRICS AS A MEASURE OF DAYLIGHT PERFORMANCE .....	163
8.2.1	<i>Irreconcilability of metrics.....</i>	<i>163</i>
8.2.2	<i>Complementary information.....</i>	<i>167</i>
8.2.3	<i>Achievability of target criteria.....</i>	<i>170</i>
8.2.4	<i>Sensitivity to design changes .....</i>	<i>170</i>
8.3	SIGNIFICANCE OF SPATIAL AND TEMPORAL DAYLIGHT RESULTS .....	171

8.3.1	<i>Spatial daylight results</i> .....	171
8.3.2	<i>Temporal daylight results</i> .....	172
8.4	CONCLUSIONS .....	176
<b>CHAPTER 9</b>	<b>FINAL GUIDELINES AND CONCLUSIONS</b> .....	<b>178</b>
9.1	ANN-BASED PROCESSES .....	179
9.1.1	<i>ANN-based daylight performance predictions</i> .....	179
9.1.2	<i>ANNs in design exploration</i> .....	180
9.1.3	<i>Limitations and future work</i> .....	183
9.2	DAYLIGHT DESIGN EXPLORATION .....	184
9.2.1	<i>Impact of atrium design changes on daylight performance</i> .....	184
9.2.2	<i>Evaluation of metrics as a measure of daylight performance</i> .....	188
9.2.3	<i>Spatial and temporal daylight results</i> .....	191
9.2.4	<i>Limitations and future work</i> .....	193
9.3	CONCLUSIONS ON EFFICACY .....	196
9.4	POTENTIALS OF AN ANN-INTEGRATED APPROACH TO DESIGN EXPLORATION .....	198
<b>REFERENCES</b>	.....	<b>202</b>
<b>PUBLICATIONS</b>	.....	<b>212</b>
<b>APPENDIX A</b>	<b>DAYLIGHT ANALYSIS: PERCENTAGE-OF-SPACE RESULTS</b> .....	<b>213</b>
A.1	ANALYSIS OF $sD_{300/50\%}$ RESULTS .....	214
A.1.1	<i>Impact of Atrium Well Geometry on <math>sDA_{300/50\%}</math></i> .....	216
A.1.2	<i>Impact of WWR distribution on <math>sDA_{300/50\%}</math></i> .....	217
A.1.3	<i>Impact of Atrium Orientation on <math>sDA_{300/50\%}</math></i> .....	219
A.1.4	<i>Combined impact of all design changes across all floors on <math>sDA_{300/50\%}</math></i> .....	224
A.2	ANALYSIS OF $sD_{100/50\%}$ RESULTS .....	225
A.2.1	<i>Impact of atrium well geometry on <math>sD_{100/50\%}</math></i> .....	227

A.2.2	<i>Impact of WWR distribution on <math>sD_{100/50\%}</math>.....</i>	227
A.2.3	<i>Impact of orientation on <math>sD_{100/50\%}</math> .....</i>	229
A.3	ANALYSIS OF ASE RESULTS.....	235
A.3.1	<i>Impact of atrium well geometry on ASE.....</i>	236
A.3.2	<i>Impact of WWR distribution on ASE.....</i>	237
A.3.3	<i>Impact of orientation on ASE.....</i>	238
<b>APPENDIX B</b>	<b>DAYLIGHT ANALYSIS: PERCENTAGE-OF-TIME RESULTS.....</b>	<b>241</b>
B.1	IMPACT OF ATRIUM GEOMETRY ON DAYLIGHT PERFORMANCE .....	242
B.1.1	<i>Impact of atrium geometry on daylight performance on the 6<sup>th</sup> floor .....</i>	242
B.1.2	<i>Impact of atrium geometry on daylight performance on the 5<sup>th</sup> to ground floor.....</i>	245
B.2	IMPACT OF ATRIUM WWR DISTRIBUTION ON DAYLIGHT PERFORMANCE .....	250
B.2.1	<i>Impact of WWR distribution on daylight performance on the 6<sup>th</sup> to 4<sup>th</sup> floors .....</i>	250
B.2.2	<i>Impact of WWR distribution on on daylight performance on the 3<sup>rd</sup> to ground floors.....</i>	256
B.3	IMPACT OF ATRIUM ORIENTATION ON DAYLIGHT PERFORMANCE.....	262
B.3.1	<i>Impact of atrium orientation on daylight performance on the 6<sup>th</sup> floor .....</i>	264
B.3.2	<i>Impact of atrium orientation on daylight performance on the 5<sup>th</sup> floor .....</i>	267
B.3.3	<i>Impact of atrium orientation on daylight performance on the 4<sup>th</sup> floor .....</i>	272
B.3.4	<i>Impact of atrium orientation on daylight performance on the 3<sup>rd</sup> floor.....</i>	277
B.3.5	<i>Impact of atrium orientation on daylight performance on the 2<sup>nd</sup> floor.....</i>	282
B.3.6	<i>Impact of atrium orientation on daylight performance on the ground floor.....</i>	288

# Chapter 1

## Introduction

This research is concerned with a novel method introducing ANNs (artificial neural networks) to facilitate daylight design exploration in order to better inform designers on the performance of design choices. The work focuses on the efficiency of the proposed method in accelerating performance feedback on one hand, and on the value and interpretability of the applied daylight performance metrics on the other hand.

### 1.1 Rationale for improving daylight conditions in buildings

As part of the wider discussion on sustainable building design, daylighting has been found imperative for energy savings and occupant well-being. According to the 2012 CBECS survey, lighting and cooling are among the largest end-uses of electricity in commercial buildings, making up 17% and 15% of total electric consumption, respectively (EIA, 2017). Furthermore, 75% to 85% of the electric power in LED lightings is generated as heat (Ahn *et al.*, 2014), highlighting the advantage of daylighting in reducing both electric lighting consumption and cooling load. The savings potential in lighting and HVAC through best practice in daylighting has been estimated to reach up to as much as 30% of total energy consumption in open-plan high rise offices in the U.S. (Köster, 2018). Additionally, daylight-responsive lighting control systems have been shown to leverage the benefits of daylight, given a building is well designed for natural lighting (Doulos, Tsangrassoulis and Topalis, 2008; Yavuz, Yanikoglu and Güler, 2012; Klusmann and Murphy, 2015). The reported CO<sub>2</sub> emissions that can be saved per kWh electricity generation in the European Union were stated to be 295.8 g in 2016 (EEA, 2018). McHugh *et al.* (2004) found that buildings with skylights and

manually assisted or fully automated daylight responsive systems could reduce energy consumption by 0.09 or 0.15 kWh/m<sup>2</sup>a respectively. Yet another study showed that, for a six-storey office building, energy savings of 56 to 62% for lighting could be achieved with adjustments to lighting and daylighting specifications (Jenkins and Newborough, 2007). 2% of savings could be solely attributed to the addition of sky lighting (14% savings looking only at the top floor), resulting in a reduction of nearly 60Kg CO<sub>2</sub> emission per year. The aforementioned reasons make daylighting a valuable design factor for reducing critical CO<sub>2</sub> emissions.

Another strong argument for daylighting lays in the importance of daylight for human health and well-being. Light is one of the best characterised Zeitgebers of the circadian rhythm, which has profound impact on the biology of cells and hence, appropriately timed physiology and behaviour. Circadian rhythm disruption can contribute to the development of a range of disorders, including metabolic disorders, mental illnesses and insomnia (Jagannath *et al.*, 2017). A number of studies have further been able to demonstrate the importance of sufficient (day)light exposure for occupant performance and productivity. Figueiro *et al.* (2017), for instance found that circadian effective light improved the mood and sleep quality of office workers. Another study was able to extend these findings to student performance (Heschong, Wright and Okura, 2002). The latter research was corroborated by Maesano and Annesi-Maesano (2012), who found a positive association between student scores and the window to floor area ratio. The researchers also found a weaker, but nevertheless significant positive association with the percentage of window area facing south. Further evidence for the consequences of daylight on human health can be found in the review by Aries, Aarts and Van Hoof (2013).

Last but not least, daylighting serves as an architectural component to introduce natural light into the building, provide views, assist in building navigation, define public spaces (e.g. with atria), create atmosphere and shape spaces which influence social interactions. Daylighting via atrium design has been shown to increase retail sale in commercial buildings (Heschong, Wright and Okura, 2002). The study further showed that, even though customers were not aware of the presence of skylights, both customers and employees had a positive perception of skylit stores in general. To conclude, daylighting is a design tool with environmental, economic, physiological and psychological impact, thus making it a valuable design feature for optimisation in building design.

## 1.2 Improving design outcomes via exploration and optimisation

Building shape, orientation, material selection, building components and their dimensions; all of these are parameters a designer can choose to vary. Two types of difficulties arise in a traditional design approach. For one, changes are made as uncontrolled types of experiment, thus not allowing phenomena to be isolated (Schon, 1991). This contrast systematic, informed decision making. Additionally, when a change is introduced, the remaining design, views, plans or layout may need to be manually adjusted. Such a practice can be time-consuming and contrasts parametric design environments. The latter enable automatic and immediate update of changes in the model, therefore working as a “short cut” to the final model, while retaining flexibility to change and compare design choices (Eltaweel and Su, 2017). When combined with a simulation, parametric environments better align the design process with building performance investigations. They then become ‘digital laboratories’ for design exploration combined with performance testing (e.g. energy or daylight performance).

Design tools such as Design Explorer<sup>1</sup> provide interfaces to compare design choices according to their performance on set design objectives. Moreover, the automated assessment of design solutions according to set design objectives, also referred to as optimisation, has been effective in improving building performance of base case design scenarios.

Turrin et al. (2010) for examples, used the advantages of parametric modeling to explore and find skylighting design solutions that provided the best balance between solar gains and daylight transmittance. Similarly, El Daly (2014) parameterized a model to automate window and skylight allocation. The selection of optimum solutions based on daylight and solar radiation simulations resulted in an improvement of 26% in energy loads from a random initial selection of parameters. Yet another study combined parametric design environments with multiple simulation software to automatically generate design proposals that met design objectives for energy consumption, thermal performance, indoor air quality (IAQ) and daylight performance (Lauridsen and Petersen, 2014). As a result, energy consumption could be reduced to 24kWh/m<sup>2</sup>a and daylight autonomy improved, so that electric lighting was not be needed for approximately 96% of occupied hours. Thus, the generation of design alternatives in parametric modelling environments and their integration with performance simulation allows for efficient and automated exploration and optimisation of design solutions. The optimised design outcome is likely to outperform what is possible through intuitive design and manual design iteration alone.

---

<sup>1</sup> *Design Explorer v2*. Tomasetti, T., *CORE Studio*. Last updated by Peng, M. (2019). Available at: <https://tt-acm.github.io/DesignExplorer/> (accessed Oktober 21, 2019).

### 1.3 Challenges to simulation and optimisation in practice

In a survey on daylighting design in practice, it was found that the most commonly applied prediction tools for daylighting were ‘experience’, ‘computer simulation’ and ‘rules of thumb’, whereby computer simulations were mostly employed by researchers (Galasiu and Reinhart, 2008). Those not using computer simulations, indicated reasons such as long computation time, lack of information on required simulation model input and lack of clients willing to pay for simulations. Similar reasons were identified in expert interviews on obstacles to applying building performance simulation and optimisation in practice (Attia *et al.*, 2013). Among the most commonly mentioned technical obstacles were long computation times, uncertainty of simulation model input, difficulty in defining objectives and constraints and low interoperability and flexibility between different design, simulation and optimisation tools. Additionally, the requirement of high expertise and a lack of appreciation among the AEC industry were identified as general obstacles. Emphasising the aspect of time, Jonas and Reinhart (2019) found that participants with access to real-time performance feedback increased the number of tested design solutions, reported increased confidence in the design performance and the design task, and produced better-performing design solutions. Hence, in order to facilitate more widespread adaptation of optimisation and performance-driven design, it appears essential that time-efficient and feasible performance assessment processes need to be integrated in existing design workflows, if they should be accepted and adopted by designers and the industry.

## 1.4 Research aims and objectives

This work aims to facilitate the use of daylight performance assessment in parametric design explorations and comprises the following objectives:

- develop and validate emulators for daylight performance simulation to make daylight-performance driven design exploration more feasible and time-efficient (Chapters 4 to 6)
- establish the extent to which the developed emulators can move daylight-performance driven design exploration towards real-time performance feedback (answered within the chapter conclusions)
- establish a workflow that incorporates the emulators in parametric design, performance feedback and design exploration to assist in early-stage design-decision making (illustrated in Chapter 3)

Specific objectives include:

- identify appropriate metrics that assess building daylight performance and determine their strong and weak points as design targets (conducted as part of the literature review)
- identify design variables with potential impact on daylight performance suitable for early design stage investigations (conducted as part of the literature review)
- develop parametric environments to systematically generate design alternatives
- develop and validate emulators capable of predicting daylight (Chapters 4 to 6)
- identify techniques to improve the predictive performance of the developed emulators (Chapter 6)

- create a feed-back loop to the design process and make immediate emulator responses on daylight performance available in the design interface (the results of which are analysed in Chapters 7 and 8)
- explore and assess the impact of design changes on daylight performance (Chapter 7)
- determine the limitations of the performance metrics applied to assess and compare the design solutions (Chapter 8)

## 1.5 Thesis structure

This chapter has explained the context and motivation behind this research, as well as the research aim and objectives. In line with the research aims, major contributions and gaps in knowledge are identified in the literature review, Chapter 2. The chapter addresses major contributions in three fields: daylight performance assessment, in which existing metrics and targets are investigated in order to determine suitable design targets for optimisation problems, design variables with impact in the early design stages, and emulators in performance simulation and optimisation. Among those, specific attention is paid to research discussing ANNs as potential surrogates for building performance simulation software.

The 3<sup>rd</sup> Chapter details the research methods implemented in Chapters 4 to 9, with research focused on two main areas: the validation and integration of emulators predicting daylight performance in parametric environments (Chapter 4 to 6), and the exploration of design solutions and assessment of obtained daylight performance results (Chapter 7 and 8). Chapter 4 presents the results of a pilot study, demonstrating the performance of ANNs as potential emulators for daylight simulations. In Chapter 5, ANNs are integrated in a parametric design environment and applied to a case study in

order to explore daylighting design solutions for a school building. In Chapter 6, techniques are investigated to further improve the accuracies of ANN predictions. ANNs are also applied to number of daylight performance metrics and assessed with regards to their ability to predict different illuminance targets and thresholds. Chapter 7 and 8 report on the results obtained from of the daylight design explorations, considering respectively spatial daylight metrics (assessment of the percentage of space meeting a desired daylight threshold) followed by the distribution of daylight in spaces (assessment of the percentage of time a desired daylight threshold is met). Here, the impact of design changes on daylight performance is assessed (Chapter 7). Additionally, the different daylight performance metrics are compared in terms of their potential to inform design changes (Chapter 8).

Lastly, conclusions derived from the key findings presented in Chapters 4 to 8 are given in Chapter 9, with recommendations and guidelines for integrating ANNs in parametric design processes with daylight design explorations.

## Chapter 2

### Literature Review

#### 2.1 Daylight performance assessment

Daylight design considerations are part British, European and International buildings standards BS EN 17037:2018 and ISO 16817:2017. Daylighting criteria have also been adopted into major building assess rating systems such as BREEAM and LEED. A typical method used in specifications is the daylight factor (DF), which describes the percentage of indoor to outdoor illuminance. However, this metric is slowly being replaced by climate-based-daylight metrics. In 2001, matrices for annual, climate-based, dynamic daylight evaluations started emerging (Reinhart and Walkenhorst, 2001) . Although the adaptation of climate-based-daylight modelling (CBDM) has been slow, there have been several important advancements: the Illuminating Engineering Society of North America (IESNA) issued specifications for a uniform application of climate-based metrics (LM-83-2012), LEED v.4 (2013) included provisions for CBDM, and in 2013, the Education Funding Agency (EFA) made CBDM a mandatory requirement in the UK (EFA, 2014). Most recently, the European standards adopted CBDM within their specifications, and, as an alternative to CBDM, amended daylight factor calculations to incorporate climate components within the calculation (BS EN 17037:2018).

##### *2.1.1 The daylight factor*

The daylight factor became a go-to metric for practices around the world and was known for its simplicity and ease of interpretation (Mardaljevic and Christoffersen, 2016). However, the apparent ease with which the metric can be applied comes at a cost:

The DF is typically calculated for overcast sky conditions and therefore does not consider the effects of orientation and solar altitude, climate and weather or the effects of shading. Additionally, as the DF calculates the percentage of outdoor illuminance, it gives variable values that can take on different meanings depending on the outdoor illuminance under which it is calculated (Mardaljevic, Heschong and Lee, 2009). In order to counteract these shortcomings, amendments were made to the BS EN 17037:2018, specifying the outdoor illuminances for climate zones and locations. Nonetheless, prior to this amendment, the daylight factor provided neither a tangible, nor comparable (to DF results in other locations) description of available daylight. Due to these limitations, and especially for the its inability to consider orientation, the DF has been harshly criticised for its unsuitability as a design driver, as it cannot distinguish between a better or worse design approach (Reinhart, Mardaljevic, & Rogers, 2013). Experts further fear that its usage leads towards a “the more the better approach” (Reinhart, Mardaljevic, & Rogers, 2013, p.9) that can potentially worsen the energy performance of a building. By not being able to differentiate between designs, the DF also loses any basis for being applied in design optimization (Heschong Mahone Group, 2012).

Another problematic aspect concerns the daylight targets set by many standards and guidelines, which are often set to an average daylight factor (ADF) of 2% (BS 8206-2:2008, BREEAM). CIBSE LG10-1999 set up daylight factor bands to define the daylight in spaces using the DF: under 2% DF would mean the space was under-lit and required artificial lighting, between 2-5% meant that the space was adequately daylit, but may still require additional lighting, and only a DF above 5% meant that the space was well-daylit and that electric lighting would generally not be required. As such, a building barely achieving 2% threshold would be at the border of being categorised as ‘under-lit’.

The above-noted problems are further evidenced when translating the DF into absolute values. Assuming an overcast sky provides 10000 lux of unobstructed illuminance, the daylight on a horizontal calculation plane would be 200 lux. Looking at illuminance recommendations, a majority of standards and guidelines concordantly suggest a task level illuminance of 300-500 lux by daylight or artificial light to support visual tasks such as office work (DIN EN 12464-1:2011, IES-2011). 300 lux was also found to be the value to evaluate daylight sufficiency in buildings (Heschong Mahone Group, 2012). Given the difference in illuminance recommendations, one can see why many standards up to BS EN 17037:2018 were lacking. Nonetheless, there is another major aspect of criticism about the specifications, and that is use of the average daylight factor equation.

The average daylight factor can mask the daylight quality of spaces, as high illuminances achieved in close proximity to window areas can cancel out increased room depth and under-lit spaces. Furthermore, it has been shown that the ADF cannot distinguish between single and multi-aspect window designs (Mardaljevic and Christoffersen, 2016). As such, the shortcomings of the DF, ADF and the standard specifications unfold to anyone who aims to make a comparison between design solutions. Due to the risk of “perverse consequences” (Mardaljevic, Heschong and Lee, 2009, p. 3) following the application of the daylight factor, we take a look at alternative daylight matrices in the next section.

### *2.1.2 Climate-based-daylight-metrics*

Climate-based-daylight-modeling refers to the annual evaluation of daylight based on the prevailing climate on site. Using time-series data containing the annual outdoor illuminances or outdoor irradiance, several performance metrics have been developed

in order to quantify the daylight performance of a space. This section details common metrics including Daylight Autonomy (DA), continuous Daylight Autonomy (cDA), spatial Daylight Autonomy (sDA), Useful Daylight Indicators (UDIs), and Annual Sunlight Exposure (ASE), and examines their strengths and weaknesses in assessing the daylight performance.

The definition of Daylight Autonomy (DA) was first given by the Association Suisse des Electriciens in 1989 (Reinhart, Mardaljevic and Rogers, 2013) and further developed as a measure for the percentage of occupied hours in which a minimum illuminance threshold at a sensor point can be maintained by daylight alone (Reinhart and Walkenhorst, 2001). To illustrate, a DA of 80% indicates that additional lighting is not necessary for 80% of the year. The target used depends on the intended use of the space. For office work, 300 lux or 500 lux is typically used as the target. Especially for early design stages when the furniture layout is still unclear, the upper threshold of 500 lux can be used to account for missing furniture estimated to reduce light levels by approximately 50% (Anderson, 2014). In practical application, DA has been used to coordinate lighting and blind schedules for whole-building energy analysis (Reinhart, 2004), and to determine potential lighting energy savings from automated, daylight-linked lighting systems (Li, 2010).

A variant of DA is continuous Daylight Autonomy (cDA or DAcon), initially proposed by Rogers (2006). Instead of showing only when a targeted illuminance threshold is met, partial credit is given to lower illuminance levels that may still be desirable and useful in reducing electric lighting (Mardaljevic and Nabil, 2006). For example, when 500 lux has been set as the target, an area achieving 250 lux will get 50% credit instead of 0% in DA for not meeting the threshold. By doing so, the time variable is lost in this metric and the interpretation of results becomes more difficult. Thus, an

area achieving 250 lux 100% of the time would not be differentiated anymore from an area achieving 400 lux 62% of the time (both areas being weighted 0.5). In comparison to DA, which is a quantitative measure that does not give any information on the daylight availability of spaces that do not meet the requirement, cDA gives partial credit for daylight in those spaces, but the interpretation remains vague. Another aspect setting apart DA and cDA is that DA may result in an overestimation of electric lighting use (Hafiz, 2015), as all lux levels under the target are not quantified. However, such issue may be unproblematic, as overestimation (compared to underestimation) would hardly have any negative implications.

Spatial daylight autonomy ( $sDA_{300/50\%}$ ) is a metric backed by extensive research. It was developed based on a detailed comparison of existing metrics including the previously described, and based on occupant and expert assessments of 61 buildings (Heschong Mahone Group, 2012). The key intent with which the metric was developed was to determine a metric and daylight targets best suitable to ensure occupant comfort and satisfaction. As such, the metric was not developed as a tool to measure daylight quantity or improve energy performance (the main motivation of the metrics covered so far), but to ensure occupant comfort and satisfaction. In comparison to DA,  $sDA$  is purely a pass or fail metric and gives the percentage of space that can maintain a minimum of 300 lux for 50% of occupied hours in a year. A distinction is made between two possible ratings: to qualify as 'nominally acceptable', at least 55% of the space has to meet the criteria (300 lux over 50% occupied hours), to qualify as 'preferable' or 'favourable', at least 75% of analysed space has to meet the criteria.

IESNA approved of the methodology in 2012 and issued a defined methodology with which  $sDA_{300/50\%}$  was to be calculated so as to allow for a comparative assessment

across buildings (IES LM-83-2012). Specifications were made on the allowed spacing for the sensor points and the detail of the building model. Furthermore, a fixed period of working hours was defined and specifications were made for the inclusion of blinds operations.  $sDA_{300/50\%}$  then found its adaptation into EFA guidelines in 2013 and became mandatory for applications to the Priority School Building Programme. In comparison to the LM83-2012, the requirements were lowered and the sDA target threshold of  $sDA_{300/50\%}$  for 55% of space was reduced to 50% of space.

In terms of visualization, the sDA metric, as a pass and fail metric, cannot show the distribution of daylight within a space, but rather displays hard boundaries in which all sensor points achieving the target are treated as equal and all sensor points below the threshold are treated as equal. Compared to the %time metrics DA and cDA, the strength of the sDA metric mainly lies in its clear definition of a design target, which is the definition of %space required to fulfil specific %time results. As such, it can be used for the overall evaluation and comparison of design solutions. With its specific target, the  $sDA_{300/50\%}$  metric also quantifies daylight expected to ensure 'adequate' or 'preferable' daylight and can thus be used as a measure of daylight quality.

Useful daylight indicators (UDI) was first proposed by Mardaljevic and Nabil in 2005 (Mardaljevic and Nabil, 2005). As its name indicates, this metric aims to categorise daylight levels that can be considered useful. The metric initially differentiated between three categories and provided upper and lower illuminance thresholds. These were later on adjusted and supplementary categories were proposed. The initially proposed thresholds are as follows: one category was assigned to daylight levels below 100 lux (UDI<100) to define an under-lit space; another category for daylight levels ranging from 100 to 2000 lux, defined as useful daylight levels, and lastly; one category for lux

levels above 2000 (UDI>2000) to indicate the potential risk of glare. In another study, the authors highlight how UDI can be used for the rapid evaluation of design variants (Mardaljevic and Nabil, 2006). In comparison to DA, the authors indicated how the UDI metric showed the greatest sensitivity to effects of shading, as it had a provision for excessive light levels (in proximity of window areas, daylight levels visibly fell below the 2000 lux threshold by introducing shading). The consideration of low daylight levels on the other hand was deemed useful for the evaluation of deep-plan buildings or atrium adjoining spaces (Mardaljevic and Nabil, 2005).

The initially proposed UDI thresholds have been subject to change by several authors including Mardaljevic himself. Regarding the upper illuminance threshold, the authors' choice for the 2000 lux was based on a study by Roache (2002), that found that illuminances between 700 – 1800 lux were acceptable for computer- and paperwork, while illuminances over 2000 lux were likely to cause visual or thermal discomfort. Studies on indicators for glare however have very dispersed findings as a.) glare has many underlying variables, some of which are unpredictable, e.g. outside reflection from passing by vehicles and b.) the perception of glare can be temporal and subjective. Due to this, glare would be difficult to define using as simple a parameter as horizontal illuminances. In 2008, the UDI-threshold was raised to 2500 lux (Mardaljevic, 2008) and in 2012 to 3000 lux (Mardaljevic *et al.*, 2012), which is the current standard (EFA, 2014). Although the 3000 lux threshold comes close to the 2700 lux identified by Torres and Lo Verso (2015), the PIER study (2012) suggested there should be no upper illuminance threshold as occupants were more satisfied with higher illuminance levels. Mardaljevic (2015) in turn noted that these matrices could only ever give a limited perspective evaluation of the design as many instances of bright spaces of the PIER study were top lit or had diffuse lighting via light wells and diffuse glazing. He further

suggested that the UDI metric might be improved, if illuminances over 3000 lux that were achieved as a result of direct lighting, were distinguished from illuminance over 3000 lux, that was achieved by diffuse daylight. Overall, there is no consensus on upper illuminance thresholds and the interpretation of spaces identified as 'over-lit' or exceeding 3000 lux remains vague.

As for the lower threshold of the UDI metric, one possible drawback is that while lux levels of 100 are categorised the same as lux levels of 300 and above, the quality of daylight in such spaces becomes harder to assess. Following the Seattle Daylight Forum in 2005, it was suggested to subdivide UDI into further categories (Mardaljevic, 2006), and these categories, along with the current thresholds, read as follows: UDI 'fell-short' (UDI-f ) for illuminance below 100 lux, UDI 'supplementary' (UDI-s) for illuminances between 100-300 lux, UDI 'autonomous' (UDI-a) for illuminances from 300 - 3000 lux, and UDI 'exceeded' (UDI-e) where daylight exceeds 3000 lux (Mardaljevic *et al.*, 2012).

In general, the evaluations of multiple categories or thresholds of daylight allows for a better understanding of the daylight within a space. However, with multiple categories, the speed and simplicity of evaluating performance is lost. The strength of using UDI-e is the inclusion of an upper threshold as consideration for occurrences of glare. It is also possible to compare shading design strategies using this metric. On the downside however, UDI-e may bias design solutions with lower daylight levels altogether. Additionally, the metric does not differentiate between direct and indirect or diffuse lighting, and it was already noted that high illuminances resulting from indirect lighting may be desirable.

### 2.1.3 Identified Gaps and Conclusions

Taken together, the above detailed daylight performance metrics can be divided in those describing illuminances (lux levels), those describing the %time for a specified illuminances threshold, and those describing a % of space for a specified time and illuminance threshold. From the above metrics,  $sDA_{300\%/50\%}$  stands out as a metric developed to ensure occupant satisfaction and comfort. The metric does however not ensure that a minimum threshold is met and has no provision for glare. Instead, the UDI metric can ensure this, as it has established categories to measure useful illuminances that fall below 100 lux, and also an upper threshold for illuminances exceeding 3000 lux. However, the 3000 lux threshold has been contended, with research pointing out that high lux may even be desirable (Heschong *et al.*, 2012). Additionally, design solutions with more spaces exceeding the 3000 lux threshold are also likely to have more spaces passing  $sDA_{300\%/50\%}$ , therefore showing preferable daylighting conditions. Especially when high illumination is a result of reflected or diffuse lighting, the risk of glare may be reduced. A comparatively greater limitation of the UDI metric lies in its inability to distinguish between direct and indirect lighting. The metric that partially does this is the ASE metric, as it is a measure for high illuminances resulting from direct sunlight alone. However, similar to the UDI-e 3000 lux threshold, the ASE 1000 lux threshold is not backed by extensive research. There are two additional weaknesses of this metric. One concerns the inconsistency and variability of simulation results, as shown in the work of Brembilla and Mardaljevic (2019). The other relates to the above discussed research findings, which showed that it was not possible to reconcile the  $ASE_{1000,250h}$  criteria for less than 10% of spaces with the  $sDA_{300/50\%}$  criteria for more than 50% of space. Hence, the discussed metrics each provide information on certain

aspects of daylight performance, most prominently either indicating daylight sufficiency for deskwork (sDA<sub>300%50%</sub>), underlit spaces (UDI-f) or a risk of glare (UDI-e and ASE).

## 2.2 Atrium design as a daylighting strategy

Atria are a high frequency design feature that have found increased application in large-scale buildings (Hung, 2003). There are architectural, environmental and economic merits to atrium designs. From an architectural point of view, atria can provide visual connections by opening up the internal environment. They can serve as a building highlight, public gathering spaces or cultural centre, and stimulate human interaction. The additional daylight provided by an atrium can further improve the spatial and visual quality. In dense urban areas, it can even be a necessary design feature, as daylight within buildings would otherwise be too low. From an environmental point of view, the additional daylight can help reduce lighting energy consumption (Jenkins and Newborough, 2007). Lastly, from an economic point of view, atrium design has been shown to increase retail sales performance in commercial buildings, as many customers have a positive perception of skylit spaces in general (Heschong, Wright and Okura, 2002). Several design strategies have been studied in order to fully utilize the potential of atria to improve daylighting conditions, some of which are discussed in the following sections.

### 2.2.1 *Atrium geometry*

The form factor or compactness of the atrium well determines the distribution of daylight within the atrium. Square or circular forms have high atrium volume to surface area ratios, resulting in fewer reflections within the atrium and less light being absorbed by the surfaces. The internally reflected component (IRC) and daylight levels within the

atrium are therefore higher than in an atrium with equilateral triangular, rectangular or linear shapes - in that order (Sharples and Lash, 2007). For angular atria, the distribution of daylight on the atrium walls is such, that daylight levels are highest in the centre and diminish towards the edges of the atrium geometry, with higher illumination levels on the longer atrium wall (Samant and Yang, 2007; Du and Sharples, 2009). The daylight distribution in atrium adjoining spaces is therefore more even in buildings with circular and square forms than triangular or rectangular forms. That being said, rectangular shapes with lower surface to volume ratios and therefore higher light admittance areas have a higher potential of increasing daylight levels in atrium adjoining spaces, though the efficiency decreases as the depth of the atrium increases (Calcagni and Paroncini, 2004).

The advent in digital technologies in design, modeling and fabrication has expanded the possibilities for realising architecture with geometrically complex forms, such as twisted atria (Bhooshan, 2017). One example of a twisted mega-building with doubly curved facades is the Evolution Tower in Moscow, which was built on a parametric process to rationalise the model so as to construct the fully glazed facade (Hudson, 2010). The Cayan Tower in Dubai is another example, the winding shape of which was designed to provide shading in the interior spaces (Wronski, 2013). Suyoto et al. (2015) made use of this concept and optimised the angle of rotation of a spiral building to minimize heat gains. A double curvature building also showed a better energy performance in a study by Gerber and Lin (Gerber and Lin, 2013), who made a statement for unconventional, yet architecturally interesting forms. Research discussing the daylight performance for atrium wells with such a twisted geometry is limited. The shape does however seem promising in that it can withdraw surfaces to reduce exposure to direct sunlight and associated glare.

### *2.2.2 Atrium well splay angles*

The impact of the atrium well splay angles on daylight levels in atrium adjacent spaces has been investigated for 'V-shaped' or 'A-shaped' atria (Erlendsson, 2014). While maintaining the same volume, the 'V-shaped' atrium achieved higher Daylight Autonomy levels in atrium adjacent spaces than the 'A-shaped atrium'. This stands to reason, as the visible sky area is larger with such a form. In another study, it was additionally found that daylight in atrium adjacent spaces could be improved by stepping/terracing the atrium well (Alraddadi, 2004). Interestingly, overall daylight levels did not decrease despite an increase in floor area and room depth and the spaces achieved higher light uniformity. Although the increase of daylight levels in this case was largely a result of reflected light from the stepped terraces, both the studies of Erlendsson and Alraddadi showed that obtuse splay angles over 90° resulted in favourable daylighting solutions to improve daylight.

The opposite strategy is that of using splay angles of less than 90° so as to direct/reflect light deeper into the building instead of reflecting daylight back outside the building, as shown specifically for the angle of roof structures (Sharples and Shea, 1999). Laouadi (2004) found that splaying the vertical wall of a light well significantly increased daylight at its base for splay angles between 90 and 60°. This finding is backed by further studies showing that skylights with 'A-shaped' splay angles provide a better and wider daylight distribution (Parent and Murdock, 1989; Heschong Mahone Group, 2003). However, these findings pertain to skylights and daylight on the floor below the skylight, but have not yet been investigated for atrium adjacent spaces and daylight levels across multiple floors. Held against the findings of 'V-shaped' atria showing higher illumination levels in atrium adjacent spaces, and considering the associated increase in

visible sky, one may assume that splay angles over 90° more effective in providing additional daylight in adjacent spaces than splay angle less than 90°. A combination of both above-noted strategies was applied in the research of reflective systems for atrium type buildings, showing how reflective building geometry of various angles can be used to direct daylight into atrium adjacent spaces (Cunningham, Zaferiou and Lagios, 2014).

### *2.2.3 Vertical fenestration of the atrium well*

A detailed investigation of daylight illuminances in atria compared the efficiency of 4-sided, 3-sided and 2-sided atria (Boubekri and Anninos, 1996c, 1996a, 1996b). The 4-sided atrium referred to a central, top lit atrium sided by four walls, the 3-sided one to a semi-enclosed, top lit atrium side lit by one glazed wall, and the 2-sided one to a top lit atrium side lit by two glazed facades. The fully enclosed 4-sided atrium showed a higher daylight efficiency than the 3-sided atrium, which in turn performed better than the 2-sided atrium. Hence, daylight within the atrium well itself was highest for a central, fully enclosed atrium.

As for the fenestration of the atrium well, research has shown that changing the glazing distribution across storeys can increase the reflected light and therefore the daylight levels in spaces adjacent to the atria, especially on lower floors. In an attempt to find the optimal distribution of window area across floors, Aschehoug (1992) suggested that ratios of 50-, 60-, 70-, 100% from top to bottom floor worked best for a 4-storey building. For a 5-storey building with a square atrium, Cole (1990) found a distribution of 20-, 40-, 60-, 80- and 100% to be most effective. For a 5-storey building with a square-shaped atrium, Samant (2017) concluded that ratios of 50-60% WWR on the top floors gave overall better daylight levels across all floors than a ratio distribution

starting with 20-, 30- or 40% WWR on the top floors. The best daylight distribution was achieved with 60% -5<sup>th</sup>, 79%-4<sup>th</sup>, 92%-3<sup>rd</sup>, 98%-2<sup>nd</sup> and 100% ground floor.

#### *2.2.4 Material Reflectance*

The reflectance of materials in the atrium well affect the daylight efficiency within the atrium and in atrium adjacent spaces. Increasing material reflectance will increase reflected daylight within the atrium well and therefore increase illuminances in lower floors. This effect has been covered in many studies (Sharples and Lash, 2007). Iyer-Raniga (1994) compared the effect of wall reflectances on daylight in atrium adjacent spaces for wall reflectances of 25-, 50-, 75-, 85-, 90%, showing that increases in reflectance increased the reflected component, and therefore daylight. The increase in reflected component was also shown by Aschehoug (1986) in their study of a street with infinite length for diffuse wall reflectances of 40- and 90%. Depending on atrium shape and sky conditions, the potential of doubling daylight factor levels by quadrupling reflectances was shown by Boubekri (1995). In another study, Calcagni and Paroncini (2004) compared material reflectances up to 90% for square and rectangular atrium shapes and derived a simplified formula to predict the daylight factor on the atrium floor and in atrium adjoining spaces. Despite these promising findings, the effect of reflectances may be limited in tall atria, when contrasting material properties vary greatly in close distance to each another and when darker surfaces are located immediately adjacent to the atrium (Samant and Yang, 2007). The effect of specular surfaces with 23-,47-, 90% reflectance was investigated by Lau and Duan, who found that adding specular surfaces at top levels could increase daylight levels on the lower floors by 25%. In this case, resulting glare would need to be considered as well. The above studies measured the daylight factor under CIE overcast sky conditions. Daylight

levels may further increase when considering sunny sky conditions or when using climate-based daylight analysis.

### *2.2.5 Identified gaps and conclusions*

To conclude, research has provided several design strategies to improve daylight conditions in atrium buildings. These include splaying atrium well walls to a 'V-shaped' atrium well, decreasing the WWRs from bottom to top floors, and increasing material reflectance of atrium well walls. However, some design strategies come with a trade-off. For example, square shaped atria have a smaller volume to surface-area ratio, thereby allowing for more reflected daylight and deeper daylight penetration into the atrium well. By contrast, rectangular atria with larger volume to surface-area ratio have a greater light-admitting area, and could therefore increase daylight in atrium adjacent space. Another example relates to decreasing WWR on top floors in order to increase daylight on lower floors. What needs to be kept in mind here is that the loss of daylight levels on the top floors resulting from a smaller WWR is typically much larger than the achieved increase in daylight on lower floors.

Although research has investigated several atrium design strategies, according to the authors' knowledge there is little research on atria with doubly curved facades, i.e. a twisted atrium, and how such forms impact daylight in atrium adjacent spaces. Also, research is missing on the impact of tilting the atrium well towards a southward or northward orientation, i.e. by splaying atrium walls in the same direction. There is also a lack of literature investigating the combinations of the above-identified atrium design strategies and their impact on daylight, either within the atrium well or in atrium adjacent spaces.

Most research conducted on atrium design used vertical and horizontal illuminances, or the daylight factor as a measure of daylight. According to the authors' best knowledge, fewer works implemented the DA, sDA<sub>300/50%</sub> and ASE metric (i.e. Erlendsson, 2014; Mohsenin and Hu, 2015; Samant, 2017), and only one study was found using UDI for an atrium design case study (Mardaljevic, 2006). There is also a lack of research comparing optimum performing atrium design solutions according to multiple performance metrics of the same intention (i.e. optima for DA<sub>300</sub> and DA<sub>100</sub>, optimised with the intention of improving daylight quality; or optima for UDI-e and ASE<sub>1000</sub>, optimised with the intention of reducing the risk of glare). Expanding research in this field would allow for the comparison of design outcome for different daylight performance metrics and a critical evaluation of the thresholds used in the metrics. Additionally, implementing multiple metrics could highlight the impact of design changes on several aspects of daylight, including daylight sufficiency, and the occurrence of underlit or overlit areas, thus contributing to current atrium design research.

### 2.3 Artificial neural networks (ANNs) for building performance optimization

Numerous studies have proven the benefits and improvements to a design that can be achieved through design optimization. Yet, the adoption of optimization processes in architectural practices is still relatively low, partially due to long computation time (Attia et al., 2013). For a wider adoption of optimization and performance-driven design, it is therefore essential to make processes more time-efficient. A review of typical optimization methods such as particle swarm optimization, pattern searches and numerical optimization, which constitutes a central aspect of machine learning, can be

found in (Evins, 2013; Machairas, Tsangrassoulis and Axarli, 2014; Nguyen, Reiter and Rigo, 2014).

In order to reduce computational load during optimization, a number of studies turned to ANNS as potential surrogates for simulation tools. This is because, once trained on selected input and output patterns, ANNs enable instantaneous predictions of expected outputs for new unseen input in the recall mode. The following sections detail research, that have implemented ANNs as emulators of simulation tools or integrated ANNs to make design optimisation more efficient. Research findings on the optimization of ANNs are also explored.

### *2.3.1 ANNs as emulators for building performance simulations*

Several researchers have studied the application of neural networks for predicting building energy performance, including heating and cooling loads and the overall energy consumption of buildings, with positive results (Wong, Wan and Lam, 2010; Zhao and Magoulès, 2012). Studies show that the accuracy of these predictions does not fall behind that of other thermal simulation tools (Neto and Fiorelli, 2008), making neural networks a possible alternative approach to time-consuming and computationally expensive simulations. This is feasible only if the required data are within a set design scope and previous measurements are available for training the neural network. The successful application of neural networks in thermal building performance and their ability to address non-linear problems suggest that they may be applicable for daylight analysis.

Compared to the implementation of neural networks for thermal predictions, research is rather sparse on the implementation of neural networks for daylighting and illuminance predictions. However, the few results that are available are promising: In a

study by (Lopez and Gueymard, 2007), a neural network was used to predict the luminous efficacy under cloudless conditions, suggesting a possibility to predict the illuminances on surfaces based on measurements of solar irradiance. In another study, Janjai and Plaon were able to predict sky luminance for a year, giving more accurate results than the CIE model for clear and overcast skies, but not for cloudy skies (Janjai and Plaon, 2011). Comparisons have also been made between different models for predicting sky irradiance and illuminance and the neural network showed superior performance (Pattanasethanon, Lertsatitthanakorn and Atthajariyakul, 2008).

Neural network-based modeling has also been successfully applied to predicting the horizontal illuminance in an office building (Kazanasmaz, Gunaydin and Binol, 2009). The results had a low average error of 3% when compared to measured illuminances. In a classification problem, a similar study was able to determine the category of the climate based metric UDI (classification problem) for various ranges of lux levels (<100 lux, 100 – 2000 lux, >2000 lux) with a high accuracy of 96% when combining a neural network with principal component analysis (Zhou and Liu 2015). These studies suggest that neural networks can be used as a computational tool with potentially very accurate prediction capabilities, given appropriate model selection and well-defined parameters.

Achieving accurate results was a key point in the above studies. Nonetheless, it should be noted that some of the studies also faced challenges and occasional failures. This seems to be the case especially when the input parameters are complex and have a wider range of values (e.g. Janjai and Plaon 2011; Conraud-bianchi 2008), and is consistent with findings in the application of neural networks for thermal comfort predictions (Magnier and Haghghat, 2010) and those aiming to include occupant

behavioural patterns (Neto and Fiorelli, 2008). Therefore, it becomes evident that there is a necessity to accurately retrace input parameters that impact any variations in the results, and empirically search for a neural network architecture that is capable of reconstructing more complex and dynamic relationships.

### *2.3.2 Integration of ANNs in genetic optimization*

Among optimization algorithms, genetic optimization has been well established as a robust optimization method (Gen and Cheng, 2000). Genetic optimization intends to mimic the process of evolution through natural selection, whereby the selection of fitter genes can lead to a better design (Storn, & Price, 1997). Although various genetic algorithms (GAs) exist (Deb *et al.*, 2002), the methodology they apply follows similar principles. The first step consists of randomly generating an initial population covering the range of solutions. Following that, all individuals within the population are evaluated according to their performance or fitness. This is done by employing a fitness function that assigns a fitness value to each individual. Consecutively, selection takes place based on the fitness value of individuals and these individuals reproduce the population of a new generation using the three main genetic operators: replication, crossover and mutation (Tresidder, 2014). Replication takes place when neither crossover nor mutation occurs, meaning that the parent chromosome (or design) going into the next generation remains the same. During crossover, one or more genes (components of a parent chromosome or variables of the design) from one parent (or design) are swapped with one or more genes from another parent. As for mutation, this operator describes the process in which one more genes of a parent undergo change. During crossover and mutation, both the gene undergoing change and the type of change introduced are selected at random.

The aforementioned procedures entail several advantages peculiar to genetic algorithms (Ganatra *et al.*, 2011). For one, genetic algorithms effectively bypass the risk of getting stuck in local optima – a consequence of a randomly generated initial population and the introduction of variation via mutation and crossover. Another advantage innate to crossover is that it generates combinations of genes that are more fit than previous generations, thereby increasing the probability in which a fitter offspring can be selected for the population of the next generation. The genetic operation of mutation on the other hand is one to facilitate the formation of new variants that may not have arisen otherwise and may lead to improved solutions. Additionally, genetic optimisation does not require an initial guess to be made that may bias results, as would be the case for pattern search, particle swarm optimisation and any numerical optimisation (Torczon, 1995). Instead, optimisation takes place within a predetermined search range, which in theory only needs to be limited by the physical restrictions of building design.

So far, according to the authors' investigations, studies employing ANNs as within genetic optimisation seem to be limited to a few. The first studies found on the integration of ANN models within a GA were concerned with the optimisation of plant growth (Morimoto, Takeuchi and Hashimoto, 1993), particleboard manufacturing (Cook, Ragsdale and Major, 2000), optimisation of a chiller system (Chow *et al.*, 2002) and a ventilation system (Zhou & Haghghat, 2009). Another two studies applied genetic algorithms and neural networks to optimise architectural design components and reduce the energy consumption of a building (Conraud-bianchi, 2008; Magnier and Haghghat, 2010). Both studies employed back-propagation neural networks within genetic optimisation as part of its fitness function. The studies were successful in reducing the computational effort compared to stand-alone genetic optimisation while

maintaining acceptable levels of accuracy. Therefore, they illustrate the potential of ANNs in reducing simulation efforts by operating as surrogates in optimisation algorithm.

### 2.3.3 Optimization of ANN hyperparameters

With the aim of increasing the robustness of neural networks, ample research has been done on applying genetic algorithms to neural networks. Of the studies undertaken, one can distinguish between the following optimisation processes for NNs:

- a. Optimisation of neuron connections and weights to overcome the risk of getting stuck in local minima (Ritchie *et al.*, 2003)
- b. Optimisation of momentum and learning rate to achieve the lowest possible MSE (Schaffer, Whitley and Eshelman, 1992)
- c. Optimisation of the NN architecture (Koza and Rice, 1991; Tian and Noore, 2005; Benardos and Vosniakos, 2007)
- d. Optimisation of the activation function

The optimization of neural networks can be done via a brute-force approach, heuristic approach, or using genetic algorithms (GA within NN), not to be confused with feeding NN results into a GA (NN within GA). The application of genetic algorithms for the optimisation of neural network typologies typically involves the encoding of structures into gene sequences. The genetic optimisation of a neural network architecture through such an encoding of the network architecture, specifically number of hidden layers and number of neurons within the hidden layers showed the innate potential of such a process in finding more suitable architectures to improve NN prediction and classification (Hochman et al. 1996). Since then, a lot of research has

been done on improving optimisation processes for neural networks and dealing with the challenges of encoding, speeding up training and overfitting.

In their study, Tiang and Noore applied a genetic algorithm to optimise input neurons and the architecture of hidden layers of a back-propagation network trained with the Lavenberg-Marquardt algorithm with Bayesian regularisation (Tian and Noore, 2005). A function was set to force the NN to have small weights and biases to operate more smoothly and mitigate overfitting. To further reduce the risk of overfitting and improve generalisation, the Lavenberg-Marquardt algorithm with Bayesian regularisation was implemented. The genetic optimisation process was initialised with a randomised population and the fitness evaluation included a step, whereby the two chromosomes with the highest fitness were copied into the next generation without further modification through crossover or mutation. The process was halted only after all individuals reached convergence, after which the chromosomes were decoded to obtain the optimal solution.

Benardos and Vosniakos (2007), applied genetic optimisation in a similar manner. The number of hidden layers and number of neurons in the hidden layer were identified as optimisation parameters. Similar to the study by Tiang and Noore (2005), all evaluated networks were trained using the Levenberg-Marquardt algorithm. The fittest individuals were kept alive through the genetic operators fitness and selection. The weights were initialised using the Nguyen-Widrow method and early stopping was applied. A specialty of this study is that it determined the fitness through multiple criteria, namely training MSE, validation/ generalization MSE and complexity. These were aggregated in an objective function and the fittest individuals were selected to go on into the next generation.

The complexity of Neural Network optimisation increases when including the optimisation of the NN synapsis weights. Neuro Evolution has been proposed as a method to better train neural networks and substitute back-propagation. NN learning algorithms and the NN weights alongside the architecture can be evolved either through genetic algorithms or genetic programming (GP). Genetic programming is a method in which programs are used to evolve programs. The method was proposed by Koza (Koza, 1992). A main difference between GA and GP is that GPs are not limited to specific predetermined structures or lengths, which essentially means that the system or string that a GA can learn is one that has been identified beforehand. GP on the other hand seeks to find a solution based on the problem-solving process alone. This is why GPs are known to return methods and rules to solve a problem, and GAs return specific values to achieve their objectives.

The optimisation of synapsis weights using a GA builds on the encoding of different architectures into gene strings. A major issue with this is that the structure of genes may be identical, but due to a swapped order (e.g. of nodes in the hidden layer), the encoding to the genes will be different, although both result in the same solution. This is referred to as the competing conventions problem (Kearney, 2016). As a result, the genetic operation of crossover will highly likely generate damaged offspring. The repeated evaluation of such dysfunctional individuals in turn increases the computational effort of the evolutionary process. To mitigate this problem, Kearney proposed the NEAT algorithm, which uses node-based encoding and introduces historical markers to differentiate genotypes with the same functionality. Despite that, the competing conventions problem still remains during evolution. The main benefit of the taken approach is that no unnecessary evaluations are run, thereby reducing the computational effort of the process (Kearney, 2016).

As NEAT also has the ability to develop a structure, the process seems to resemble that of genetic programming, as both develop structures without limiting the possible size. A study introducing Genetic Expression Programming (GEP) was proposed for neuro-evolution by Ferreira (Ferreira, 2001). There are however noticeable differences between the two methods. Although both employ strategies to maintain syntactic correctness while developing a structure, GEP has a fixed length, meaning that it cannot continuously complexify into unknown directions (Stanley, 2015). Additionally, GEP employs neither historical markers nor speciation.

In summary, NEAT offers a good solution through the introduction of historical markers and speciation, a major strong point of which is the optimisation of input parameters. Also, the development starting from minimal structures may be considered a benefit. The counterpart however is that, as more complex structures are required, the evolutionary optimisation processes becomes more time consuming. Ganatra et al. (Ganatra *et al.*, 2011) proposed the combination of back-prop training and GA optimisation, whereby the back-prop is used to train the initial generation, from which onward GA replaces back-prop and the NN typology is optimised alongside its weights. This was proposed as a method to save time. Another critical aspect to NEAT is that there are now new parameters that may need to be optimised so that optimal or near-optimal architectures can be evolved (Kearney, 2016). So as to run NEAT, the four parameters that must be determined by the programmer are: probability of adding a connection, probability of adding a node, weight mutation power (strength in which the weight is changed) and probability of weight mutation. Choosing inappropriate values for these parameters may either result in big jumps in the error fitness landscape (NN with the lowest MSE will be overlooked), or too small changes while fitting the data

(optimisation will converge on local instead of global minima). Unsuitable parameters may also mean that the network will stop evolving the structure due to low mutation rates. Another aspect of the parameter choice is that it directly effects the number of epochs, meaning that the runtime may be substantially increased. If in addition to that a threshold has been set for the maximum number of epochs, the success of optimization becomes more restricted. Thus, the evolutionary optimisation of NN hyperparameters remains a challenging field, particularly when it comes to the optimisation of network architecture and synapsis weights between connected layers.

#### *2.3.4 Identified gaps and conclusions*

Various research has explored a range of application possibilities for ANNs to measure building performance within buildings. However, studies applying ANNs as emulators for daylight performance are few in number. In terms of climate-based predictions, ANNs have previously been trained to predict the UDI metric, but only as a category (UDI-s, UDI-a or UDI-e, not the %of hours that the illuminance thresholds are exceeded). Additionally, predictions were made for hourly, but not annual data. Thus, to the best of the authors' knowledge, there are no studies that used ANNs to predict annual cumulative climate-based metrics (neither DA, sDA, UDI nor ASE), especially in parametric design environments and for design exploration or optimisation. The lack of studies in this field therefore points to a need for validation of ANNs as emulators surrogates for daylight simulations and a thorough investigation of the advantages and limitations of ANN integration into design exploration and optimisation. The current work intends to do exactly this. In the following chapters, ANNs are validated and integrated into daylight design explorations. The specific research methods concerned with filling the identified gaps in literature are detailed in the next chapter.

# Chapter 3

## Methodology

This chapter details the framework with which the research is carried out. There are three central focal points investigated in this research: the validity and efficacy of ANNs in daylight design exploration, the comparison of daylight performance in the assessment of design solutions, and findings gathered from the design investigations carried out on and contributing to research on atrium buildings.

### 3.1 Research framework

#### *3.1.1 Research stages*

The research undertaken in this thesis is carried out in the four stages identified below:

1. Literature review (Chapter 2)
2. Pilot study testing ANNs as potential emulators for daylight simulations (Chapter 4)
3. Development of an ANN-integrated approach to daylight design exploration, performed on a case study exploring design solutions for a central atrium. Validation and optimisation of ANN prediction accuracies (Chapters 4 to 6)
4. Visualisation of daylight performance for the explored atrium design solutions. Analysis of daylight performance results for different atrium design strategies and comparison of performance metrics (Chapters 7 and 8)
5. Conclusion of research finding across the chapters, formulated as guidelines for ANN model development, design strategies to increase daylight in atrium

adjacent spaces, and design exploration methods using multiple daylight performance metrics (Chapter 9)

### *3.1.2 Research objectives addressed in each chapter*

The objective of the literature review was to: a) investigate existing daylight performance metrics, their strength and limitations, and identify suitable daylight performance metrics for design exploration, b) identify design variables with potential impact on daylight performance suitable for early design stage investigations and gaps in research for those design, and c) review existing research on ANNs in the field of design exploration and optimisation, and review methods to improve ANN models and their performance

The objective of the pilot study was to investigate the performance of ANNs as potential emulators for daylight simulations. To this end, a shoebox model was parameterised, and simple changes were implemented. ANNs were assessed on their ability to a) replace the daylight performance prediction of individual sensor points within a model, b) replace entire daylight simulations, i.e. predict daylight performance for all sensor points within a simulation.

After confirming the suitability of ANNs to emulate daylight simulation, chapters 5 and 6 explored the use of ANNs as predictive systems in design exploration. For that purpose, the objective of these chapters was to a) validate ANN predictions for a number of climate-base daylight metrics, b) identify the training input features required by the ANN models to predict daylight, c) optimise ANNs so as to produce consistently reliable results, d) establish the extent to which ANNs can accurately predict daylight (e.g. by identifying a minimum number of required training samples or a limit to the number of design variables), and e) establish the efficacy of the proposed

method in moving design exploration towards real-time performance feedback.

Following the validation and optimisation of ANN-based daylight predictions, the developed ANN models were employed to map the daylight performance of design variants for the central atrium. generated design landscape. A feedback loop of the ANN predictions to the design process allowed for the visualisation of daylight performance results in the building plan. The parametric model allowed for performance feedback in the modeling environment. The objective of chapters 7 and 8 was to a) determine the impact of atrium design changes on daylight performance and b) critically evaluate the daylight performances metrics used the design exploration process.

Finally, the objective of the last chapter was to summarise the conclusions across all chapters and extract guidelines useful to designers.

### *3.1.3 ANNs as a predictive system in design exploration*

At the core of this thesis is the integration of ANNs in a parametric modeling environment as predictive systems for daylight design explorations. Figure 3-1 illustrates the process of how this was implemented within this work. Grasshopper in Rhino was used as the parametric modeling environment. For a given case study, the design variables and their maximum and minimum bounds were specified within the model. This generated a design solution space with design variants of the base case design. From the design solution space, design variants representative of the design space were randomly selected and passed to a daylight simulation engine. Daylight simulations were conducted in Diva<sup>2</sup> for Grasshopper, a Radiance-based and validated

---

<sup>2</sup> Diva. Solemma LLC. Available at: <http://solemma.net/Diva.html> (accessed Oktober 21, 2019).

simulation tool (McNeil and Lee, 2012). From the Grasshopper model, data describing the design changes, referred to as ANN input features, were extracted alongside the corresponding daylight performance results. Subsequently, ANN models were developed by providing the extracted data to a particular network topology to undergo supervised training. Once trained, these ANN models were validated. If the model showed sufficient accuracy during validation, the ANN were used to predict the daylight performance of all design variants in the design space. The predictions were then fed back into the Grasshopper model for performance feedback within the modelling environment.

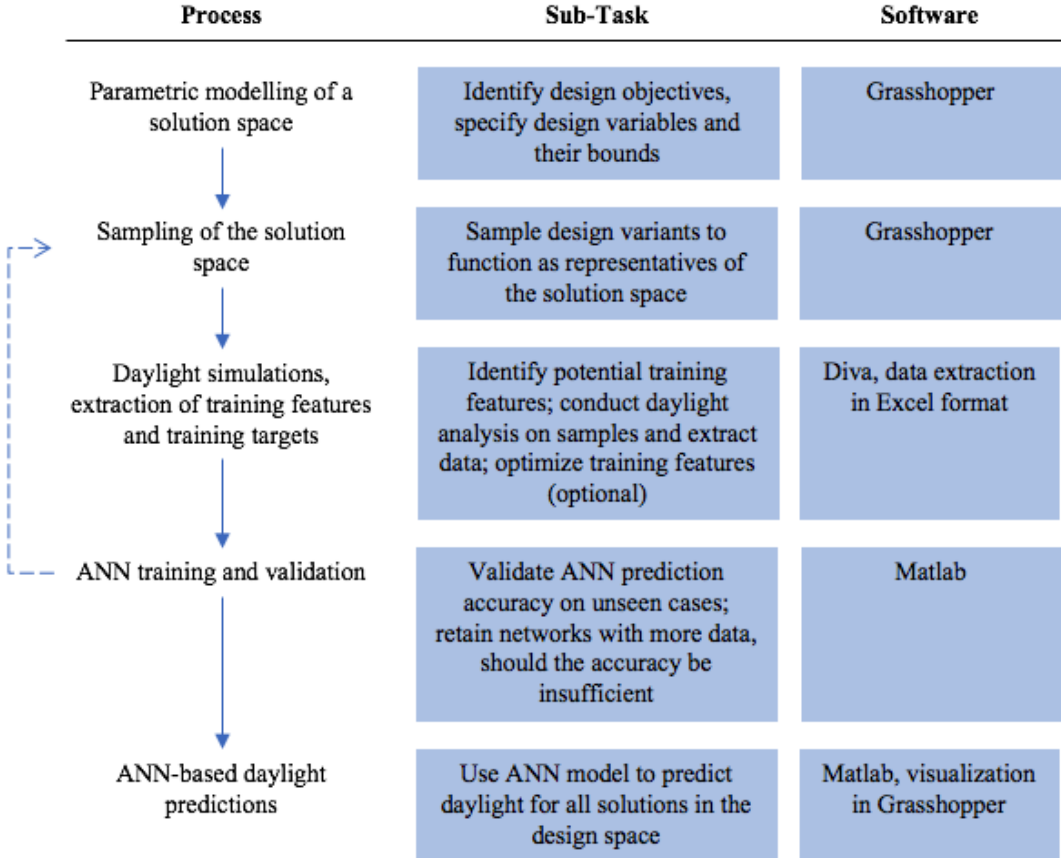


Figure 3-1 Processes underlying the integration of ANNs as a predictive system in design exploration

### 3.1.4 Modelling environment

The parametric model was set up in Grasshopper. The data required for training the ANN models were extracted in excel format from the model and imported to Matlab for

ANN training. The daylight prediction output of the ANNs was in excel format. This format was imported into Grasshopper. The performance results were then on the floor plan for visualisation of the results.

Daylight simulations were run in Diva. The work plane was set to a height of 0.8m and sensor points were distributed with 0.6m spacing from each other, unless specified differently. The input features used for ANN training were extracted for all sensor points for which daylight levels were simulated.

### *3.1.5 ANN model development*

ANNs process and pass information over a system of neurons with varying connection strengths, also called weights. *Feed-forward neural networks* are typically arranged in an input layer that receives the training data, one or more hidden layers that develop a pattern of connections to replicate functions, and an output layer that delivers the predictions (Figure 3-2). During training, the extracted input features are passed to the neurons of the input layer, and the corresponding daylight results to the neuron in the output layer. Training takes place in epochs, during which the networks adjust the connection strengths between neurons in order to minimize the mean squared error (MSE) between the simulated and predicted result. Unless where specified otherwise, the training data was divided into a subset of training, validation and test data at the ratio of 65:15:20. The training subset was used to measure training accuracy, the validation subset was used to introduce early-stopping and prevent overfitting, and the test subset was used to measure generalisation capability. Gradient descent-based backpropagation training was employed in conjunction with the Levenberg-Marquardt algorithm to adjust the connection strengths (Marquardt, 1963). A custom script was used to optimize the number of neurons in the hidden layers of the network. Each ANN

configuration was trained 10 times in parallel, with randomised initial weight settings and randomised data in each subset of training, validation and test data. Finally, the output of the 10 ANN models (also referred to as an ANN ensemble) with the lowest overall MSE was averaged to further improve the robustness of predictions.

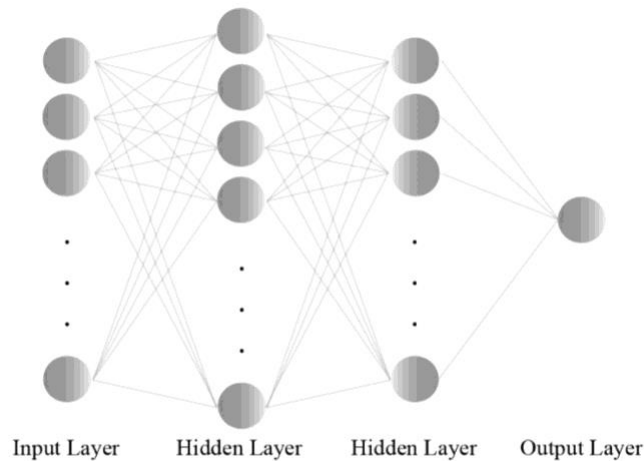


Figure 3-2 Simplified representation of an ANN architecture with an input layer, two hidden layers and an output layer. The features are passed to the input layer, and the corresponding daylight results to the output layer.

### 3.1.6 Measures of ANN prediction accuracy

The neural network output (between -1 and 1) was scaled back to daylight results (ranging 0 to 100%) before assessing the prediction accuracy. The accuracy measures used in this study are the Mean Absolute Error (MAE), the Root Mean Squared Error (RMSE) and the Mean Biased Error (MBE). MAE, RMSE and MBE are calculated by using the following equations where P is the predicted, and T the simulated daylight performance:

$$MAE = \frac{\sum_{t=1}^n |P_t - T_t|}{n}$$

$$RMSE = \sqrt{\frac{\sum_{t=1}^n (P_t - T_t)^2}{n}}$$

$$MBE = \frac{\sum_{t=1}^n (P_t - T_t)}{n}$$

In comparison on MAE and MBE, the RMSE places penalty on large errors and weighs them more heavily. Therefore, it is preferable that the MAE and RMSE are close to each other, as this would indicate that errors are consistently in the same range. If there is however a large difference in MAE and RMSE, this could be an indication of error spikes and therefore a lack of ANN robustness (Twomey and Smith, 1995). The MBE was used to assess whether ANNs typically over- or underestimated daylight predictions.

### *3.1.7 Daylight performance metrics*

From the previous literature review, several performance metrics were selected for the evaluation of design solutions. For the Daylight Autonomy (DA) metric, which describes the % of occupied hours in a year that an illuminance threshold is met, three illuminance thresholds were specified: the 100 lux threshold as an indication for underlit areas, the 300 lux threshold to indicate daylight sufficiency, and the 2000 lux threshold to indicate areas with high illuminances. These metrics are written as  $DA_{100}$ ,  $DA_{300}$  and UDI-e. Additionally, the  $ASE_{1000}$  metric was selected as an indicator for areas receiving direct sunlight and potential occurrences of glare. The named metrics describe the %time results provide for every sensor point on a work plane. For an overall assessment of the performance of an entire floor, additional metrics were selected: For the spatial Daylight Autonomy (sDA) metric, which describes the % of space that meets a DA threshold, a DA of 50% was specified for both the 300 lux and 100 lux illuminance thresholds. These metrics are written as  $sDA_{300/50\%}$  and  $sDA_{100/50\%}$ . A DA of 50% for 300 and 100 lux is also the criteria specified in the BS EN 17037:2018. The difference to the norm however is, that the % of time is supposed to be calculated for the daylight hours in a year, not the occupied hours in a year. As the standard was

published at the time of writing up, DA was simulated for the percentage of occupied hours instead. Additionally, the metric describing the % of space exceeding 1000 lux of direct sunlight for more than 250 hours in a year was selected as a daylight performance measure. This metric is written as ASE<sub>1000,250h</sub>. Both sDA<sub>300/50%</sub> and ASE<sub>1000,250h</sub> are the recommended daylight performance metrics recommended in the LM-83-2012. The targeted thresholds for the metrics were set of 50 % of space for sDA<sub>300/50%</sub> and 95% of space for sDA<sub>100/50%</sub> (as suggested in the BS EN 17037:2018). For the ASE metric, 10% of space or less was set as the target threshold. As no specific % space recommendations exist for the UDI-e metric, this metric was neglected in the spatial analysis.

## 3.2 Detailed description of methods

### 3.2.1 *Pilot study*

An initial series of experiments was undertaken in Chapter 4 to test the suitability of back propagation neural networks in predicting the climate-based DA metric. Under the hypotheses that time series weather data over the course of a year can be collapsed into an overall contribution of daylight in a year, the needed for training ANN models on all weather-, solar altitude, and sky conditions in a year was bypassed. In order to investigate ANNS as potential emulators for daylight simulation, a simple shoebox model was parameterised. A generic model of 10 x 10 m with and a centred window and a window head height of 2.7 m was chosen as the base model (Figure 3-3). DA<sub>300</sub> was simulated for sensor points at a work plane height. Changes to the model were introduced in two phases. First, only room depth was altered. This meant that the amount of daylight entering from the windows remained the same, while the daylight

distribution within the room changed (Figure 3-4). This was done to investigate ANN prediction accuracies for changes in reflected internal light. Extracted input features from the model include room the coordinates of *sensor points*, *room depth*, and *the distance to the window*.

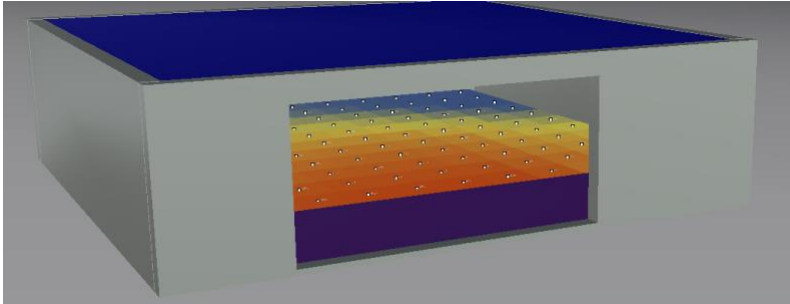


Figure 3-3 Generic shoe-box model used for daylight simulations

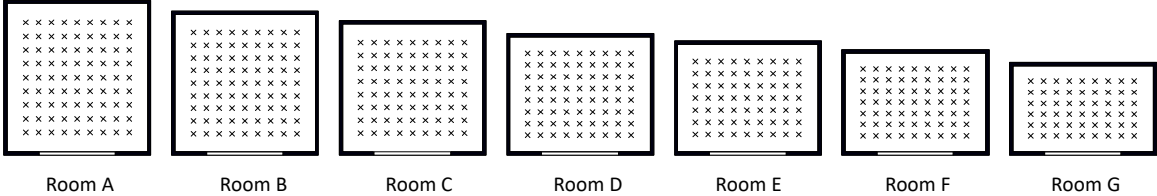
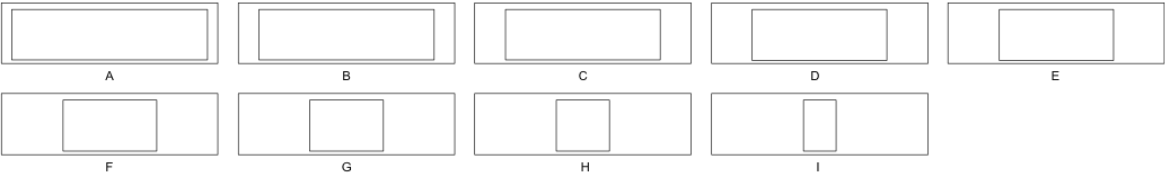


Figure 3-4 Rooms with daylight sensor points used for ANN training and testing in the first phase

Second, window dimension and window allocation on the façade were parameterised (Figure 3-5), and an external obstruction was included in the model (Figure 3-6). The obstruction was a one-storey building places 8 m across our base model. DA was simulated for 121 sensor points placed at a work plane height of 0.8 m. *Window width* and *window position on the facade* were added as input features extracted for training. Window width and its position on the south facing façade were varied by an increment of 1 m in each alteration with results designs shown in Figure 3-5. In this way, the ANNs ability to correctly predict daylight levels for a varying incident light could be tested.



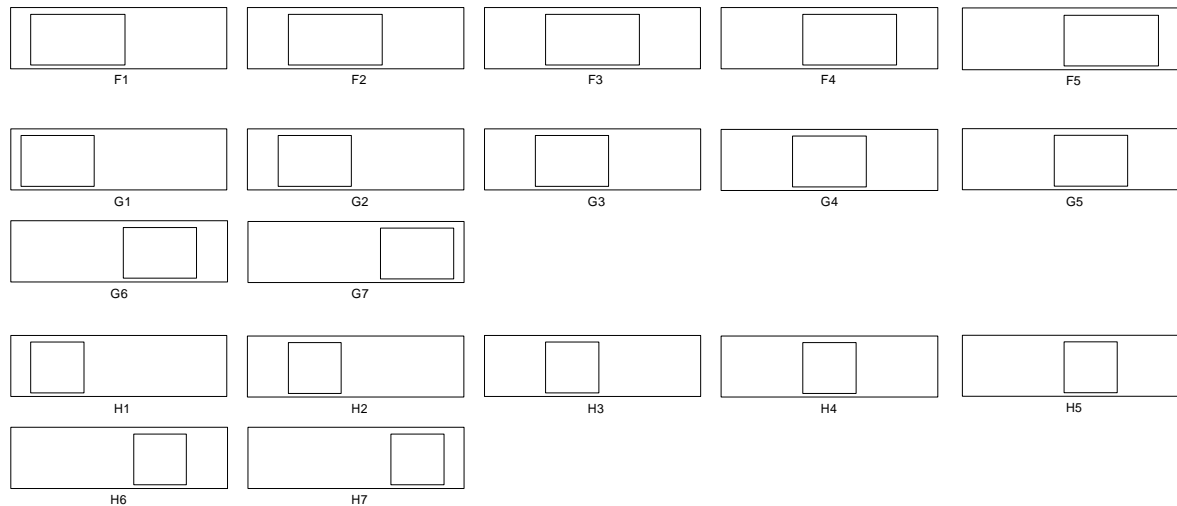


Figure 3-5 Resulting configurations for window width and allocation of the facade, used for ANN training and testing in the second phase

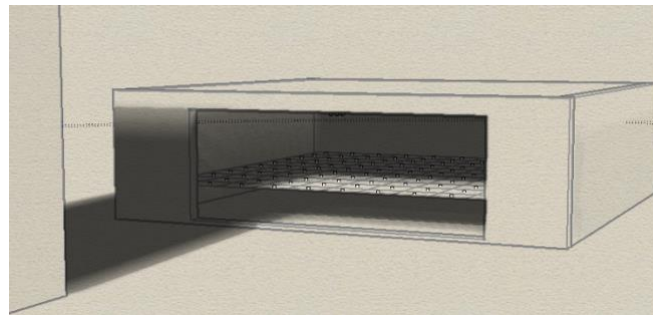


Figure 3-6 Overshadowing from an external obstruction

A simple feed-forward, back-propagation neural network was trained in the first phase of the pilot study. The extracted input features were normalised to the range of 0 to 1 and trained in Simbrain<sup>3</sup>. The relative error was used as a measure of prediction accuracy. As this was not anymore considered a suitable measure of ANN predictive performance, the MAE, MBE and RMSE were used in all other studies of this work.

In the second phase of the study, a feed-forward back-propagation neural network was trained using the Levenberg-Marquardt algorithm. Back-propagation neural networks are popular for function approximation problems (Hecht-Nielsen, 1989) and use gradient descent to adjust connection weights between neurons. As such, there is risk of getting stuck in local minima. To mitigate this risk, network settings such

<sup>3</sup> Simbrain. Available at: <https://simbrain.net> (accessed April, 2017).

as the speed or learning rate and the step size in which the network weights are adjusted as well as the initial weight setting itself become crucial factors affecting the outcome of ANN training (LeCun *et al.*, 1998). Therefore, the Levenberg-Marquardt algorithm was implemented in conjunction with back propagation for a faster convergence during training and increased robustness (Marquardt, 1963), as it switches between gradient-descent and a Newton-like update of the weights. The neural networks were modeled and trained in MATLAB and each network was trained ten times with randomised initial weight settings.

The ANN architecture, specifically the number of neurons in the hidden layer, are a paramount influencer of ANN models (Wilamowski, 2009). In this part of the study, a script was customised, testing ANN performance for different network architectures with 3 to 25 hidden neurons (HNs) in one hidden layer. All input data was normalised to the range of -1 and 1 before training, and a tan-sigmoidal activation function was employed in between the input and hidden layer and the hidden and output layer. To mitigate overfitting (Kayri, 2016), the training data set was subdivided into a validation set at the ratio 70:30 and the default MATLAB setting of 6 maximum validation failures was selected to initiate early stopping. The training epochs were set to 1000, an unnecessarily high number that was reduced in later parts of the study. Additionally, the performance of ANN ensembles was tested by averaging the prediction from multiple networks and comparing it to predictions from a single optimised network.

### *3.2.2 Validation of ANNs in design exploration*

In Chapter 5, ANN predictions of climate-based daylight metric  $DA_{300}$  and  $sDA_{300/50\%}$  were validated on a case study exploring atrium design solutions for a central atrium.

The case study building is the Katharinen School in Hamburg (Figure 3-7). The school is located and surrounded by multi-storey buildings to the east, south and west and a green area to the north. The mixed-use building consists of two blocks, with a housing and nursery and the south end of the building and school building with the atrium to the north. The deep plan of the building alongside its dense location reduce the availability of daylight inside the building. Therefore, the central atrium provides a means of bringing additional daylight into the building.

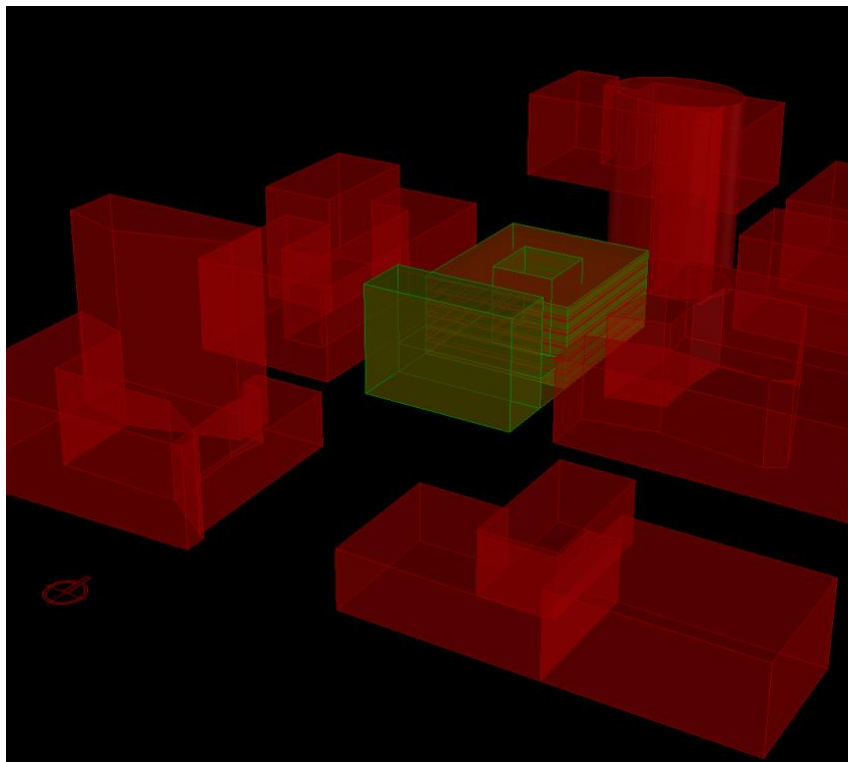


Figure 3-7 Grasshopper model of the Katharinen School (highlighted in green) with central atrium and surrounding buildings

The central atrium was taken as a base case for design explorations. Atrium geometry, atrium well orientation, window-to-wall ratios (WWR) and material reflectance were selected as design variables. The atrium well geometry was modified by scaling the atrium base area factor of 0.5 to 1, in increments of 0.1, generating 6 possible solutions with dimensions of 56.25, 81, 110.25, 144, 182.25 and 225 m<sup>2</sup> (rows in Figure 3-8). The atrium well orientation was modified by moving the atrium base and

top in opposite direction along the x-axis, in increments of 1 unit, the atrium base from -4 to 4 and the atrium top from 4 to -4. This generated 9 possible solutions for atrium well orientations (columns in Figure 3-8). The total number of combinations for both design variables thus gave a design solution space with  $6 \times 9 = 54$  possible design variants (Figure 3-8). The atrium well geometry was additionally modified by rotating the atrium base and top in opposite direction of each other by  $15^\circ$  each (Figure 3-9), resulting in  $54 \times 2 = 108$  design variants. For the atrium well facades of the first 54 design solutions, 4 WWR options were specified: a distribution of 50, 60, 70, 80, 90, 100% WWR, 20, 35, 50, 65, 80, 100% WWR, 20, 30, 40, 50, 60, 100% WWR, and 40, 40, 40, 40, 40, 100% going from top to bottom floors of the 6-storey building (Figure 3-10). The number of possible design solutions for the WWR options was therefore  $54 \times 4 = 216$ . Lastly, the diffuse reflectance of the atrium well wall in the WWR option with a distribution of 20, 30, 40, 50, 60, 100% WWR was increased from 0.8 to 0.9. The design spaces investigated in Chapter 5 therefore contained  $108 + 216 + 54 = 378$  design variants for the central atrium. All design variable categories, design variables, the maximum and minimum bounds and the number of choices for each design variable are summarised in Table 3-1.

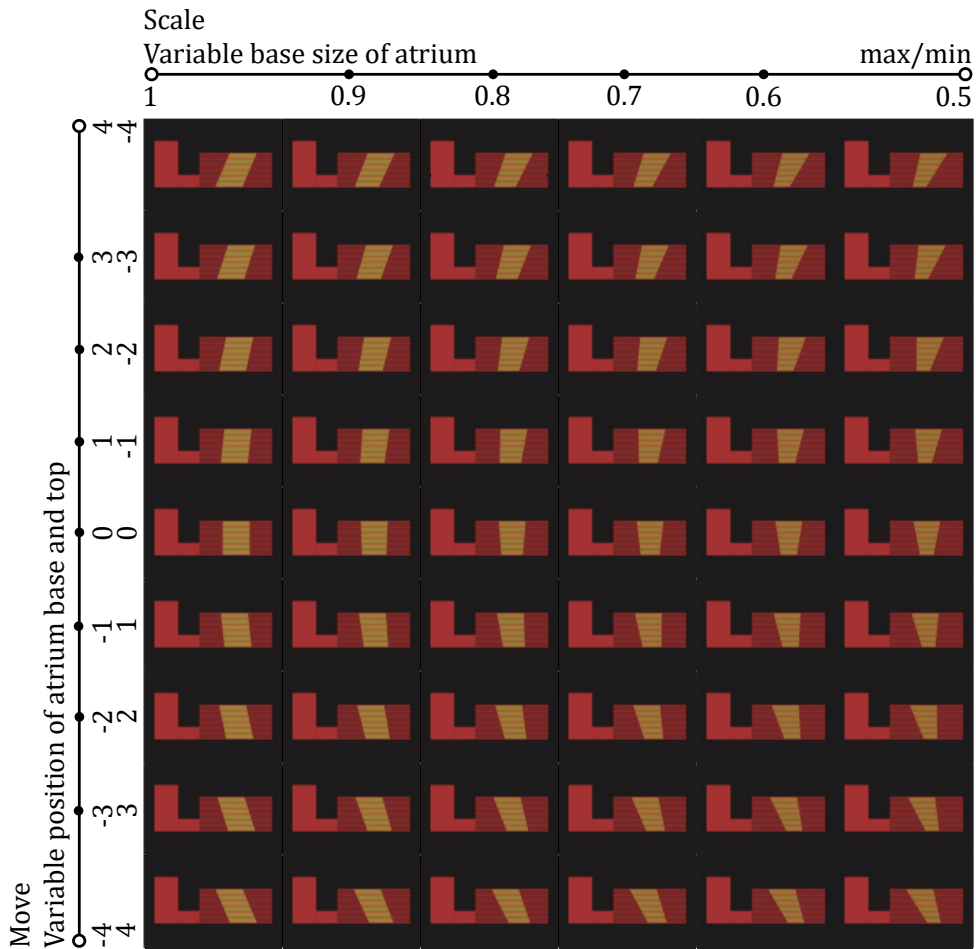


Figure 3-8 Design solution space: East elevation of the Katharinen School with 54 design variants for the central atrium. The atrium is highlighted in green. In each row of the matrix, the atrium base area becomes smaller, resulting in the 'v' shaped atrium. Down every column the orientation of the atrium changes from northward- to southward orientation

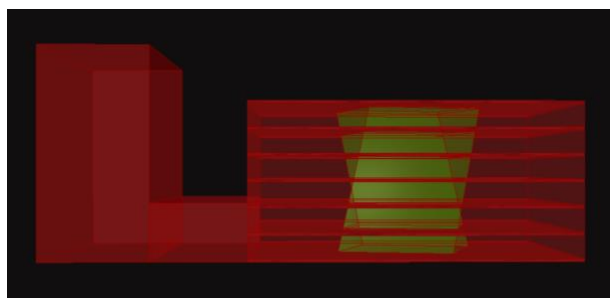


Figure 3-9 East elevation of the twisted atrium



Figure 3-10 Four possible choices for WWR distribution

Variable Category	Design Variable	Number of Choices	Maximum and Minimum Bounds
-------------------	-----------------	-------------------	----------------------------

Atrium geometry	Atrium base dimension	6	56.25 to 225 m <sup>2</sup>
Atrium orientation	Atrium top and atrium base location	9	Units along x-axis: - 4 to 4 4 to - 4
Atrium geometry	Atrium top and atrium base rotation	2	No rotation applied or +15 -15° rotation to top and base
Atrium well façade	WWR distribution	4	WWR ratios top to bottom floors: 50, 60, 70, 80, 90, 100% WWR 20, 35, 50, 65, 80, 100% WWR 20, 30, 40, 50, 60, 100% WWR 40, 40, 40, 40, 40, 100% WWR
Atrium well façade	Material reflectance	2 (only for the 20, 30, 40, 50, 60, 100% WWR series)	0.8 0.9

Table 3-1 Design variables in the proposed atrium design alterations

In Chapter 5, ANN predictions were validated surrogates of daylight simulations for the specified design changes. As part of the work carried out, the sensitivities of ANN models to the modeling environment and radiance parameter settings, as well as the number of required samples was investigated. It was also assessed, if ANNs can be trained to predict daylight performance for multiple design variables and larger design spaces, or if it was better to train multiple smaller ANNs for different design spaces. The daylight simulations of the atrium design spaces were run with the radiance parameter settings specified in Table 3-2.

Ambient bounces (ab)	6
Ambient divisions (ad)	2046

Ambient resolution (ar)	500
Ambient super-samples (as)	500
Ambient accuracy (aa)	0.1

Table 3-2 Radiance parameter settings

Regarding the training of ANN models in this part, a script was developed to automate the optimisation of the network architecture, and multiple strategies were implemented to mitigate overfitting. These strategies include cross-validation, early stopping and a weighted error approach to selecting the ANN architecture used for predictions. The weighted error approach was implemented by subdividing the training data set into training, validation and test subsets at the ratio of 65:25:15 and selecting the network architecture based on the lowest MSE for all three. Additionally, an ANN ensemble of 10 networks was trained and the division of training, validation, and test subsets was randomised for every network. The accuracies of single networks and ANN ensembles are compared in the discussion of Chapter 5. The ANN training setting are summarised in Table 3-3. The specific number training epochs used are stated within the chapters, as this varied.

Initial Mu	1
Mu decrease factor	0.8
Mu increase factor	1.5
Number of training epochs	150/ 200
Maximum number of validation failures	6

Table 3-3 ANN training parameters

The input feature extracted for ANN training and testing and bounds of the values are summarised in Table 3-4.

Training Feature	Value range	Training Feature	Value range
------------------	-------------	------------------	-------------

x, y coordinate of sensor point	.12 ... 35.5 24.9 ... 64.7 .8 ... 16.4	Distance to north, south, east, west facade	.1 ... 39.9 m .1 ... 35.5 m .1 ... 39.9 m .1 ... 35.5 m
Distance to closest atrium point	0...24.4 m	Direction of closest atrium point	0 ... 360°
Distance to atrium centre	2 ... 29.8 m	Direction of atrium centre	4 ... 360°
Glazing area at simulated floor level (4 features, one for each atrium well wall)	15.1 ... 42.3 m <sup>2</sup> 15.3 ... 46.1 m <sup>2</sup> 15.3 ... 42.3 m <sup>2</sup> 15.1 ... 46.1 m <sup>2</sup>	Glazing area across all floors	350.2 ... 1091.1 m <sup>2</sup>
Splay angles of atrium well	58.4 ... 121.9° 52.2 ... 113.2° 58.4 ... 121.9° 52.2 ... 113.2°	Dimension of the daylight calculation grid	1199 ... 1364.1 m <sup>2</sup>
Atrium dimension at the height of calculation grid	60 ... 225 m <sup>2</sup>	Dimension of the atrium base	56.3 ... 225 m <sup>2</sup>
WWR at 2 <sup>nd</sup> , 3 <sup>rd</sup> , 4 <sup>th</sup> , 5 <sup>th</sup> , 6 <sup>th</sup> floor	20 ... 90%	Location of sensor point inside or outside atrium well	0, 1
Reflectivity of atrium well walls	80, 90%	Work-plane height/ z-coordinate of sensor point	.8 ... 16.4

Table 3-4 Extracted input features and value ranges

### 3.2.3 Optimisation of ANN prediction accuracies

In Chapter 5, studies were undertaken to establish the capabilities of ANN models as a predictive system in daylight design explorations. In Chapter 6, it was attempted to further improved the obtained prediction accuracies of the developed ANN models. In

the chapter, this was done by a) optimising the selection of input features, and b) fine-tuning of ANN hyperparameters.

The input features selection was performed in two ways. First manually, then in an automated manner using sequential with sequential forward selection (SFS). Then, results and conclusions obtained from both methods were compared. The two methods are described below.

The manual selection and optimisation of features was performed on the data set of 54 generated design solutions, shown in Figure 3-8. A list of the extracted input features assessed is given in the Table 3-5.

<b>Input Feature Categories</b>
X coordinate of sensor point
Y-coordinate of sensor point
Distance to south facade
Distance to east facade
Distance to west facade
Distance to north facade
Distance to atrium closest point
Direction to atrium closest point
Distance to atrium centre
Direction to atrium centre
Atrium glazing area at the simulated floor level - west facing wall
Atrium glazing area at the simulated floor level - north facing wall
Atrium glazing area at the simulated floor level - east facing wall
Atrium glazing area at the simulated floor level - south facing wall
Atrium glazing area (all floors)

Splay angle – north facing atrium wall
Splay angle – south facing atrium wall
Area of grid plane (in m <sup>2</sup> )
Area of atrium at grid plane height (in m <sup>2</sup> )
Sensor point location (inside or outside atrium)

Table 3-5 Full set of input features extracted for 54 design solutions

In order to assess the impact of specific input features on ANN prediction accuracies, a total of 12 input features series were put together. The first evaluated series contained all features listed in Table 3-5. The other 11 input features series were selected in stages, as shown in Figure 3-11: Empirically selected input features were removed from the full set of input features, then passed an ANN ensemble for training and testing. Based on the observed results, a new selection of input features was made. The full list of the evaluated input features series is provided alongside in Chapter 6.

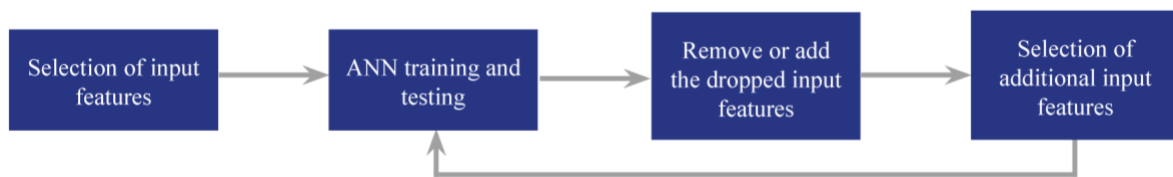


Figure 3-11 Manual selection and assessment of input features

The automated selection and optimisation of features was performed on a data set with 162 design solutions (54 x 3). The first two design variables generated 54 design solutions through changes applied to the atrium base area and atrium well orientation (as shown in Table 3-1). As a third design variable, 3 choices for the WWR distribution across floor levels was specified: a distribution of 50, 60, 70, 80, 90, 100% WWR, 20, 35, 50, 65, 80, 100% WWR, and 20, 30, 40, 50, 60, 100% WWR from the 6<sup>th</sup> to the ground floor (as shown in Figure 3-10).

To the previously extracted input features listed in Table 3-5, the window to wall ratios on the 2<sup>nd</sup> to 6<sup>th</sup> floors were added as five additional input features. The automated input features selection and optimisation process is illustrated in XX. First,

the input features were grouped into categories of similar features. Second, the input feature categories were ranked according to their impact as predictors using bagged decisions trees. Third, SFS was applied, adding the highest ranked input features first. In each iteration, the RMSE on a validation data set was observed. If the RMSE decreased, the next highest input feature was added to the data set to undergo training. If the RMSE increase, the previously added input feature was removed from the data set. In this way, all input features were selectively added or removed from the training data.

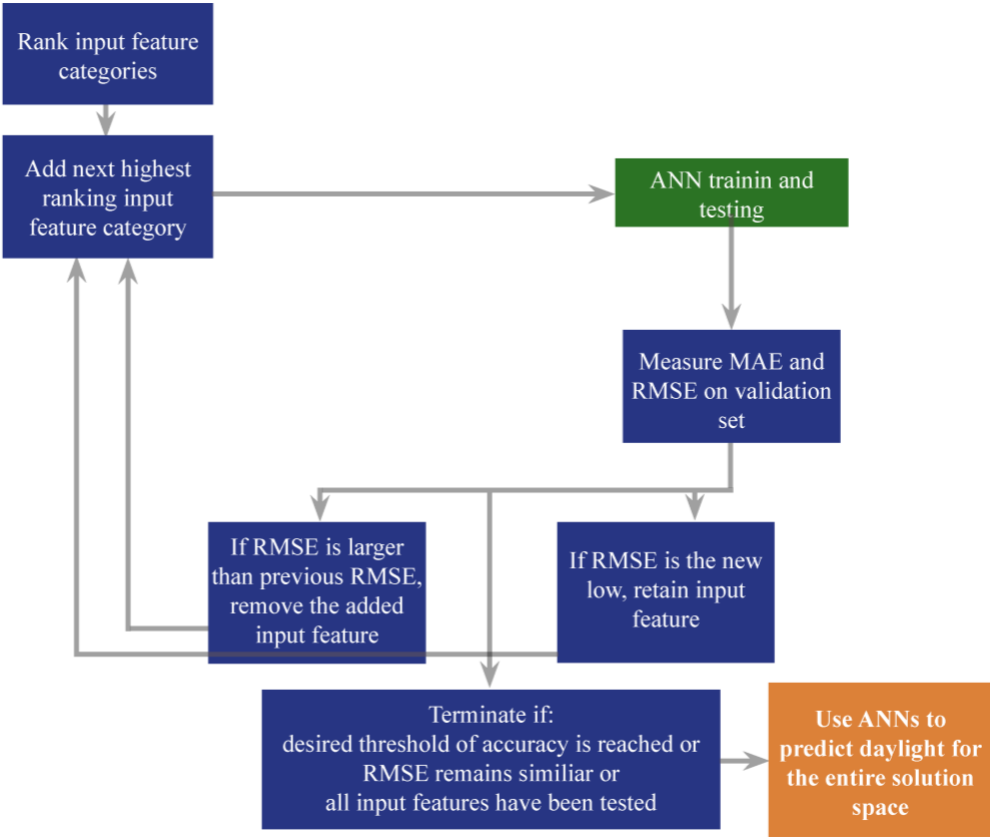


Figure 3-12 Input feature optimisation using sequential forward selection

Following the optimisation of input features, further investigations on how to improve ANN prediction accuracies were by evaluating network architectures with one and two hidden layers, by increasing the training sample size with which the model was trained, by increasing the number of design variables on which the model was trained, and by increasing the number of training epochs. Finally, the efficacy was assessed by

comparing the computational resources for optimisation and the actual improvements achieved.

### 3.2.4 Analysis of daylight performance results

The central goal of using ANNs was to efficiently map the daylight performance of all solutions in the design space. The obtained results of atrium design solutions for combinations of atrium geometry, orientation and WWR distribution are analysed and discussed in Chapters 7 and 8. Results were distinguished between % space results, discussed in Chapter 7, and % timer results, discussed in Chapter 8 (see Figure 3-13). The % space results were analysed for the  $sDA_{100/50\%}$ ,  $sDA_{300/50\%}$ , and  $ASE_{1000,250h}$  metrics. The % time results were analysed for the  $DA_{100}$ ,  $DA_{300}$ , UDI-e ( $DA_{2000}$ ), and  $ASE_{1000}$ .

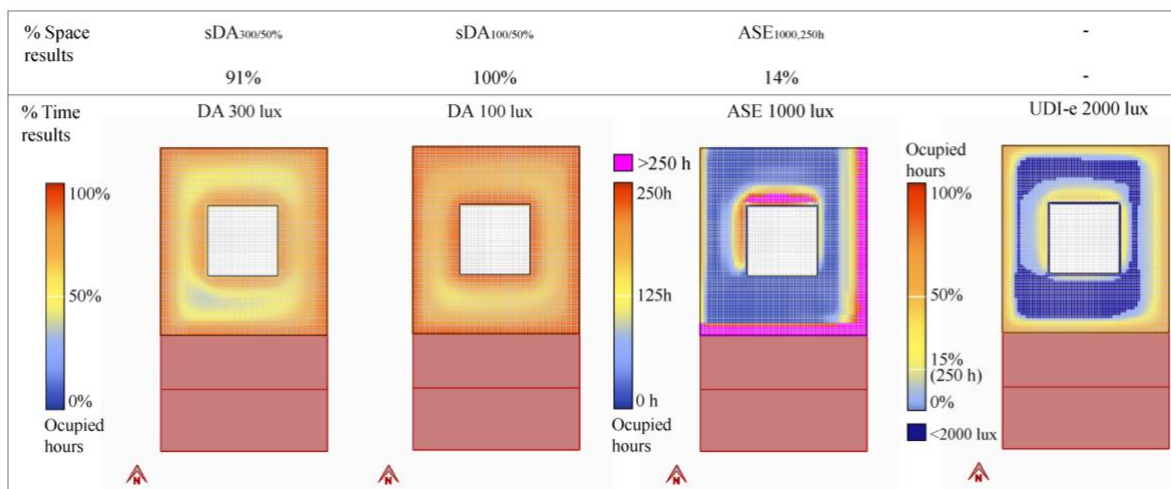


Figure 3-13 Examples of performance metrics and the two types of results

## Chapter 4

### **Pilot Study: Predicting Daylight Autonomy (DA) with ANNs**

This chapter presents an investigation on Artificial Neural Networks (ANNs) as potential emulators for daylight simulations. To this end, a shoebox model of 10m x 10m was parameterised, and simple changes were implemented. Following the methodology detailed in Chapter 3, in the first phase, only room depth was altered. This meant that the amount of daylight entering from the windows remained the same, while the daylight distribution within the room changed (results are presented in Section 4.1). In the second phase, window dimension and the position of the window on the façade were parameterised, and an external obstruction, i.e. a light obstruction surrounding building was included in the model. In this way, the ANNs accuracy for predicting daylight levels for varying amounts of daylight entering the room could be tested (results are presented in Section 4.2). Both sections deal with the question: can ANNs be used as surrogates to replace daylight simulations?

#### 4.1 Validation of DA predictions for internally reflected daylight

Daylight Autonomy for 300 lux ( $DA_{300}$ ) was predicted for a single south-facing room with varying room depth and sensor point locations. To better illustrate, the 7 generated rooms are depicted in Figure 4-1. Rooms C, G and D were used to test ANN performance, and data from the remaining rooms was used for ANN training. To train the models, the x-, and y-coordinates of the sensor points, the distance of each sensor point to the window centre point, and room depth were used as input features the model. Data from the training data set was added step by step (room by room) to the ANN model, in order to assess how much data was needed by the ANN model to make

accurate predictions. The results and conclusions are presented in the following sections.

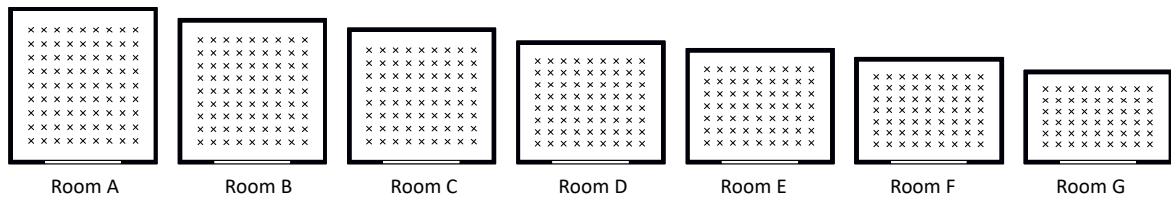


Figure 4-1 Rooms used for ANN training and testing

#### 4.1.1 ANN training and test performance

The ANN performance results during training and testing are displayed in Figure 4-2, Figure 4-3 and Figure 4-4. The results are shown for network architectures with 1 and 2 hidden layers. As shown in these figures, as the number of training data increased (by adding sensor point data from more rooms), the error margins decreased, and prediction accuracy improved. Notably, although network architectures with one hidden layer generally fit the training data better, as indicated by lower mean square errors (MSE), network architectures with two hidden layers performed better on the test data. Additionally, network architectures with two hidden layers provided lower error rates with smaller training data sets (fewer rooms used). Thus, for networks with two hidden layers, data from 3 rooms was already sufficient in providing error rates around the 3% DA MRE mark, indicating high efficacy when used as emulators for daylight simulations. Additionally, the error for the middle-sized and smallest-sized rooms were similarly low, showing that ‘extrapolating’ to the smallest room, in this instance, did not lower the predictive performance of the ANN model. The analysis however also revealed one peculiar result: neural network training for room G (Figure 4-3) led to a strong deterioration of prediction accuracy on the last point of testing. This increase in error rate from 4.46% to 28.96% MRE for a network architecture with one

hidden layer, and an increase from 1.96% to 2.07% MRE for a network architecture with two hidden layers may hint at over-fitting.

Training Data	MSE		MRE	
	One hidden Layer	Two hidden Layers	One hidden Layer	Two hidden Layers
Room A	0.0006	0.0011	41.54%	41.54%
Room A+E	0.0007	0.0014	25.18%	6.93%
Room A+E+G	0.0005*	0.0013	15.64%	6.93%
Room A+B+E+G	0.0009	0.0013	4.68%	3.10%
Room A+B+E+F+G	0.0007	0.0012	3.21%	3.32%
Room A+B+D+E+F+G	0.0008	0.0012	3.25%	3.30%

Figure 4-2 ANN training and test performance results for DA<sub>300</sub> predictions in room C

Training Data	MSE		MRE	
	One hidden Layer	Two hidden Layers	One hidden Layer	Two hidden Layers
Room A	0.0006	0.0011	78.76%	79.17%
Room A+E	0.0007	0.0014	21.11%	3.11%
Room A+C+E	0.0008	0.0012	14.52%	2.92%
Room A+B+C+E	0.0008	0.0012	13.16%	2.78%
Room A+B+C+E+F	0.0007	0.0012	4.46%	1.96%
Room A+B+C+D+E+F	0.0007	0.0012	28.96%	2.07%

Figure 4-3 ANN training and test performance results for DA<sub>300</sub> predictions in room G

Training Data	MSE		MRE	
	One hidden Layer	Two hidden Layers	One hidden Layer	Two hidden Layers
Room A+B+E+F+G	0.0006	0.0012	1.81%	2.53%

Figure 4-4 ANN training and test performance results for DA300 predictions in room D

### 4.1.2 Conclusions

The results show that ANNs are able to predict DA for variances in internally reflected daylight with high accuracy of about 3% DA MRE and could potentially replace entire simulations. Network architectures with two hidden layers typically provided more accurate DA predictions than networks with one hidden layer. Network architectures with two hidden layers were also able to learn patterns faster from the training data set, as less training data was needed to improve prediction accuracies. Interestingly, ‘extrapolating’ DA predictions to the model with the smallest design parameter setting (i.e. smallest room) did not negatively affect predictions.

Another notable finding was that training performance, as measured by the MSE, was not a good predictor of predictive performance on the test data, i.e. network architectures with two hidden layers showed higher MSE than network architectures with one hidden layer during training, but actually had a lower MRE on the test data. Therefore, the network architecture with higher MSE actually provided better prediction accuracies. This presents a problem, because the network architecture is typically selected based on network training performance. The finding therefore calls for caution when making choices based on the MSE during training. In order to mitigate the issue, in the following sections and chapters, MSE is measured on additional subsets of unseen data, which can help with the correct selection of network architecture.

Nonetheless, it may not be possible to compare architectures with different numbers of hidden layers using the MSE. Another change implemented in the following sections pertains to a change of accuracy measure (in the following sections and chapters, the MAE, MBE and RMSE will be used). The relative error used here posed a problem, in that, when DA was low (e.g. 2%), the RE, even if really close to the simulated DA (e.g. 3%), resulted in huge errors.

Lastly, the current results were produced by using a simple back-propagation network algorithm with gradient descent. In the next sections, the Levenberg-Marquardt algorithm is implemented in conjunction with back-propagation for a faster convergence during training and increased robustness, as it switches between gradient-descent and a Newton-like update of the weights in order to reduce the minimization problem arising during least squares curve fitting (Marquardt, 1963). Levenberg-Marquardt algorithm, ANN performance is further improved and the chance of overfitting or getting stuck in local optima or minima is reduced.

## 4.2 Validation of DA predictions for incident daylight

DA was again predicted for a single south-facing room. This time, prediction accuracies were assessed for different quantities of incident light. To this end, a base model of 10x10m with a centred window and a window head height of 2.7m were used. Changes were introduced to window width and the window position on the façade. Additionally, an external obstruction was included in the simulation model. The obstruction was a one-storey building placed 8 m across from the base model. Window width and window position on the south facing façade were varied by an increment of 1 m in each alteration. The resulting designs are shown in Figure 4-5 and Figure 4-6.

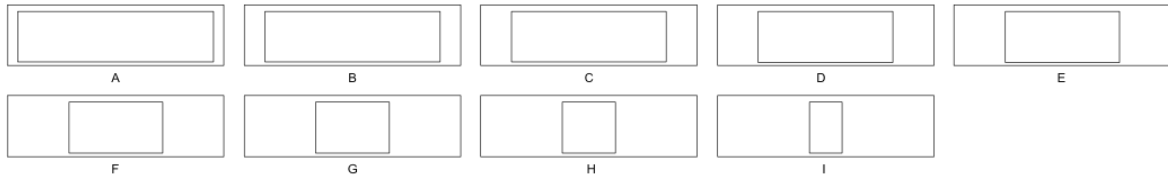


Figure 4-5 Resulting configurations for window width

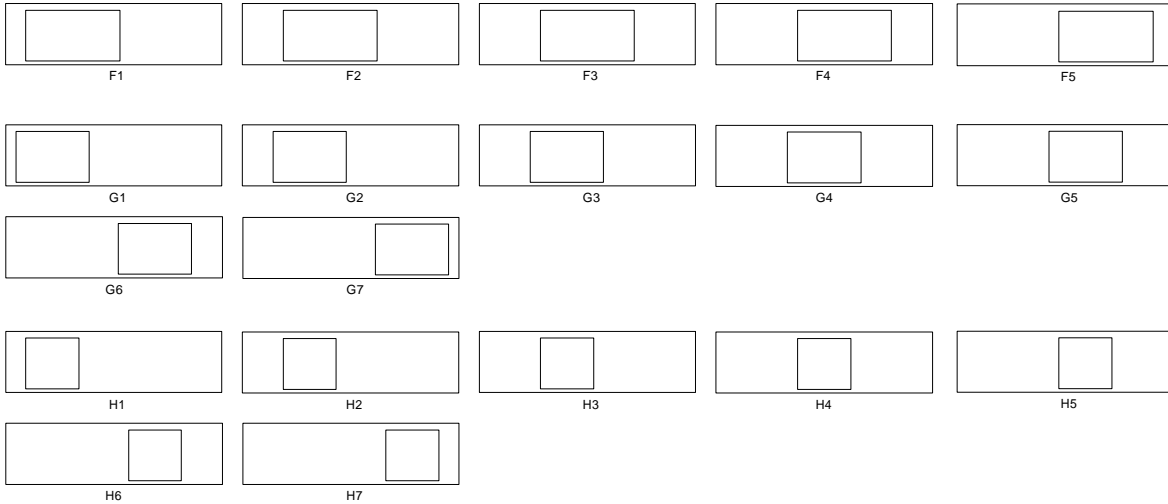


Figure 4-6 Resulting configurations for window width and window position

#### 4.2.1 ANN training and test performance

ANN performance was subsequently investigated varying window width, varying window positions and lastly for both changes combined.

First, ANN performance was investigated for varying window width. Daylight simulation results for all 121 sensor points of model A (Figure 4-5) were extracted for ANN training and testing. 90% of the data was used for training and early stopping; the remaining 10% of the data was withheld for testing. This was done once with the data from the unshaded scenario and repeated a second time with the data generated from the model that included the obstruction. The results (presented in Table 4-1) showed that ANNs could very accurately predict DA with an MAE of around 0.5% DA for sensor points within a given model. While the MAE showed that predictions typically fell 0.5 DA for the simulated result, the MBE of less than 0.1 DA showed that there was no particular tendency of over- or underestimating DA. This demonstrated that ANNs

could predict DA for sensor points within a simulation with high accuracy. The next investigation concerns whether ANNs could replace not only sensor points within a simulation but an entire simulation, without having trained on the actual model.

Predicted case		No. of hidden neurons	Errors of best trained ANN	Errors of top 5 trained ANNs	Errors of 10 trained ANNs	Elapsed training time in seconds
<b>A - Unshaded</b>	MAE	13	0.51	0.41	0.48	45.66
	MBE		-0.06	-0.10	-0.07	
	RMSE		0.63	0.49	0.55	
<b>A - Shaded</b>	MAE	13	0.55	0.51	0.54	40.31
	MBE		0.09	-0.05	-0.02	
	RMSE		0.65	0.65	0.72	

Table 4-1 ANN prediction accuracy for DA levels within a configuration

Simulation results were extracted from A to I (Figure 4-5). Data from B and H were withheld for testing and the remaining was used for training. This was done for the shaded and unshaded scenario. The prediction accuracy results on the test data from B and H are shown in Table 4-2. Predictions for B and H typically had an error below 3% DA MAE for both the shaded and unshaded scenario. However, there were two outliers among the results: The MAE of the best trained network (network with the lowest MSE during training) showed an MAE of 9.7 and 5% DA for configuration H (Table 4-2). This may indicate overfitting on the training data set or be a result of the initial weight setting of the ANN model, thus resulting in a ANN model less suitable for generalisation.

In terms of MBE, as seen previously, the errors generally remained low, showing that over-and under estimations cancelled each other out. An outlier remained for the

MBE of the ANN model with the best training performance: MBE reached -5% DA for predictions for H. In comparison, the ANN ensembles had the most reliable results, both in terms of the MAE and MBE. The results of error margins below 3% imply that ANNs could replace simulations and deliver good accuracies for design solutions with varying window dimensions.

Predicted case		No. of hidden neurons	Errors of best trained ANN	Errors of top 5 trained ANNs	Errors of 10 trained ANNs	Elapsed training time in seconds
<b>B - Unshaded</b>	MAE	23	1.01	2.55	1.67	76.71
	MBE		0.92	2.67	1.55	
	RMSE		1.22	3.30	2.09	
<b>H - Unshaded</b>	MAE	23	9.77	2.44	1.60	82.47
	MBE		0.28	-1.29	-1.13	
	RMSE		13.71	3.16	2.16	
<b>B - Shaded</b>	MAE	24	1.48	1.04	0.96	75.45
	MBE		0.56	0.13	0.36	
	RMSE		1.81	1.33	1.18	
<b>H - Shaded</b>	MAE	23	5.04	2.83	2.74	92.70
	MBE		-4.97	-2.34	-1.86	
	RMSE		7.11	4.15	3.85	

Table 4-2 Prediction accuracies for DA levels in configurations with varying window sizes

Next, ANN performance was investigated for varying window position. Simulation results were extracted from H1 to H7 (Figure 4-6). Data from H2 and H6 were withheld for testing and the remaining was used for training. The prediction accuracy results on the test data from H2 and H6 are shown in Table 4-3. Predictions for B typically had an error of 3% DA. Accuracies were not consistently better or worse

for either the unshaded and shaded scenario (i.e. with or without external daylight obstruction by surrounding buildings), indicating no significant impact of obstruction.

An outlier was again seen for the ANN with the lowest MSE, with a MAE of 7% DA.

Predicted case		No. of hidden neurons	Errors of best trained ANN	Errors of top 5 trained ANNs	Errors of 10 trained ANNs	Elapsed training time in seconds
<b>H2 - Unshaded</b>	MAE	24	2.39	1.64	2.30	77.17
	MBE		1.92	0.56	-1.94	
	RMSE		3.68	2.32	2.94	
<b>H6 - Unshaded</b>	MAE	23	7.73	2.21	1.40	68.41
	MBE		6.84	1.78	0.87	
	RMSE		9.90	3.00	1.95	
<b>H2 - Shaded</b>	MAE	23	2.06	3.58	2.15	61.28
	MBE		-1.03	3.46	1.68	
	RMSE		3.55	5.38	3.14	
<b>H6 - Shaded</b>	MAE	21	2.25	3.48	3.46	66.51
	MBE		-0.60	-0.15	-2.41	
	RMSE		3.68	4.59	4.68	

Table 4-3 Prediction accuracies for DA levels in configurations with varying window positions

Lastly, ANN performance was investigated for varying window width and window position combined. Simulation results were extracted from F1 to H7 (Figure 4-6). Data from G1, G2, G6 and G7 were withheld for testing and the remaining data was used for training. The prediction accuracy results on the test data are shown in Table 4-4. Predictions for G1, G2, G6 and G7 yielded slightly lower accuracies, with a MAE typically between 3 and 4% DA. This difference can, however, be considered marginal

in terms of interpretation of the overall daylight performance as DA ranges between 0 and 100%. Over- and underestimations were slightly more pronounced as well, especially for G2 and G7. This suggests that the magnitude of variation may be too great and additional training data may be required to improve the robustness of predictions.

Predicted case		No. of hidden neurons with lowest MSE	Errors of best trained ANN	Errors of top 5 trained ANNs	Errors of 10 trained ANNs	Elapsed training time in seconds
<b>G1 - Shaded</b>	MAE	24	3.99	2.47	2,29	135.03
	MBE		0.15	0.95	-1,33	
	RMSE		6.96	3.98	4.20	
<b>G2 -Shaded</b>	MAE		3.47	4.51	3,78	
	MBE		3.37	4.46	3.68	
	RMSE		5.07	6.39	5.48	
<b>G6 - Shaded</b>	MAE		2.71	2.90	1,39	
	MBE		-2.52	-2.59	-0.98	
	RMSE		3.44	3.76	2.02	
<b>G7 - Shaded</b>	MAE		3.46	3.32	2,38	
	MBE		-4.31	4.22	2.12	
	RMSE		6.11	5.38	3.22	

Table 4-4 Prediction accuracies for DA levels in configurations with varying window dimension and positions

**4.2.2 Conclusions**

This pilot study demonstrates that ANN models can replace simulations for variations in window design and allocation on the façade, as well as internal layout changes such as an increase in room depth. Overall results largely fell in the same range of error,

between 1 and 3 DA MAE. Using a single network, ANN models with the lowest MSE during training achieved the best as well as the worst prediction accuracies. By comparison, training multiple networks and averaging their output provided more consistently accurate predictions. This improvement in accuracies for ANN ensembles is presumed to be a result of different randomised initial weight settings for each of the ANN models within the ensemble as well as the randomised division of training samples into the training and validation subsets.

The MBE was typically close to 0, hence the ANN models did not have a particular tendency to either over- or underestimate daylight levels. Since over- and underestimations for a given model tend to cancel each other out, the overall assessment or summative value of daylight within a space (as by the sDA metric) can be expected to remain accurate. This will be examined in more detail in the following chapters.

With regard to computation time, daylight simulations on Diva<sup>4</sup> for Rhino took between 10 and 15 minutes per case on a 2.6 GHz Intel Core i7. The time required for training each ANN architecture took less than two minutes when provided with 726 data points. The training and optimisation of ANNs used for predicting DA for variations in window dimension and location (G) took slightly longer. The networks were provided with 2057 data points and took 2 minutes and 15 seconds for training. Once a neural network architecture was trained, the recall for the DA predictions took less than 1 second. Hence, ANNs are suitable surrogates for daylight simulations and are explored further as a tool for daylight performance predictions in this work.

---

<sup>4</sup> *Divia*. *Solemnia LLC*. Available at: <http://solemnia.net/Divia.html> (accessed Oktober 21, 2019).

## Chapter 5

### ANNs in Daylight Design Exploration

This chapter employs ANNs to assist in the exploration of atrium design solutions for the Katharinen School in Hamburg. The main research question here is: are ANN predictions accurate enough to emulate daylight simulation for the assessment of atrium design changes? The question is investigated for three instances. First, ANN performance and ANN sensitivities to simulation settings and the modelling environment are assessed for a single design variable modifying the central atrium of the school (Section 5.1). Second, ANN performance is assessed using full-factorial validation for a larger design solution space of 108 possible variants for the central atrium. As a part of this, the solution space is sampled to identify the number of required training samples, following which ANNs are evaluated on their ability to efficiently map the daylight performance of design solution spaces. Additionally, ANNs are assessed on their predictive performance for the summative values of a space in terms of the  $sDA_{300/50\%}$  metric (Section 5.2). Lastly, ANN performance is assessed on an additional design solution space of 270 possible variants. The trained ANN models are thusly integrated within a design process to facilitate design explorations for a central atrium (Section 5.3).

#### 5.1 ANN sensitivities

The Katharinen School in Hamburg was used as a base case to explore design solutions for a central atrium. The dimension of the atrium base (in  $m^2$ ) was selected as a design variable and scaled in order to generate 'V'-shaped atria with varying splay angles

(Figure 5-1). The atrium base was scaled by a factor of .05 to 1 in increments of .05, resulting in 20 possible design variants for the central atrium.



Figure 5-1 Left: Katharinen School in Hamburg with surrounding buildings. Right: East Elevation of the school building with the design variants for the minimum and maximum settings of the atrium base area displayed. The atrium is highlighted in green.

In order to assess prediction accuracies under different conditions, the daylight simulation settings were varied, producing different results to train the neural networks with. Changes were introduced to the grid size of the daylight calculation plane, resulting in a sensor point spacing of 0.6m and 1.2m. Ambient bounce settings were set to 2ab and 4ab, and simulations were run with the architectural model including and excluding the surrounding buildings. Data from 18 out of the 20 design variants were used for training the ANN models, the remaining 2 were used for testing ANN prediction accuracies. The ANN models were trained with 150 epochs.

### *5.1.1 Impact of simulation settings and modeling environment on prediction accuracies*

The average difference of the simulated and predicted DA for all sensor points of the two tested design variants are shown in Figure 5-2. For simulation settings with 2

ambient bounces in a simulation model without the surrounding buildings, the mean average difference between simulated and predicted DA was 2.12. As a reminder, DA values range from 0 to 100%. 1unit therefore refers to 1% of occupied hours in a year. Thus, this result is already considered as highly accurate within this work. The results became even more accurate after increasing the number of ambient bounces, in effect reducing the errors to 1.07 MAE. The result did not worsen after increasing the spacing between sensor points, even though the training data set for the larger spacing contained fewer training samples as a result of the increased spacing. Aside from a low ambient bounce setting, the inclusion of surrounding buildings also reduced prediction accuracies. Thus, errors increased to 1.8 MAE. Nonetheless, predictions generally remained close to the simulated DA results for the atrium design variants.

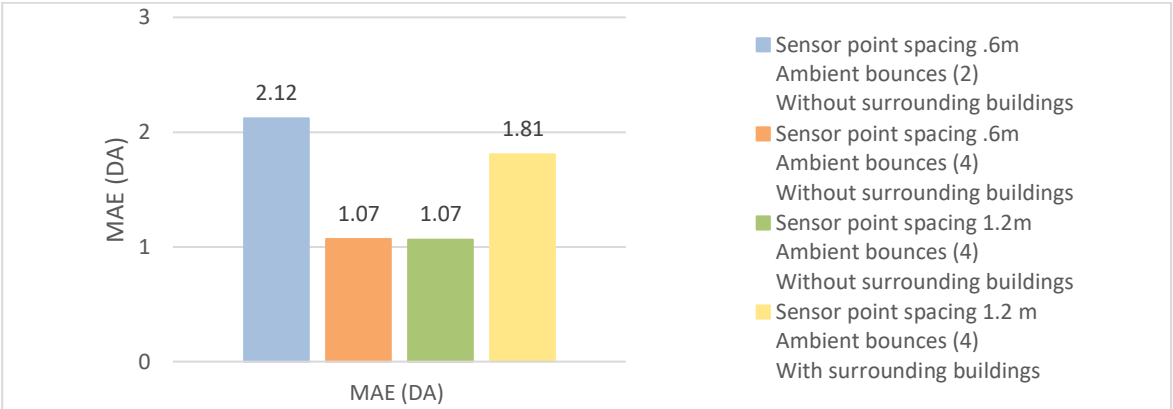


Figure 5-2 ANN sensitivities to simulation settings

## 5.2 Efficiently mapping the performance of design spaces

In this part of the study, ANNs were integrated as a prediction system in a larger solution space of 54 and 108 possible solutions. The design variables are shown in Table 5-1. The atrium base was scaled by a factor of 0.5 to 1, in increments of 0.1, generating 6 possible solutions with dimensions of 56.25, 81, 110.25, 144, 182.25 and 225 m<sup>2</sup> (Figure 5-3). Additionally, the central atrium was slanted by moving the atrium base and atrium top in opposite direction, 1 unit at a time, resulting in 9 possible

solutions for the atrium orientation (Figure 5-4). The total number of combinations for both variables thus gives a design space with  $6 \times 9 = 54$  possible design solutions (Figure 5-5). For ease of referral, the solution space is numbered 1a. As an additional variable, rotation was applied to the atrium top and base, in opposite direction each by  $15^\circ$  (Table 5-1). The solution space with the twisted variants is numbered 1b (Figure 5-6). Adding this alteration, the number of possible design solutions increased to  $54 \times 2 = 108$ . ANNs were trained to map the daylight performance for these two design spaces.

Variable Category	Design Variable	Number of Choices	Maximum and Minimum Bounds
Atrium geometry	Atrium base dimension	6	56.25 to 225 m <sup>2</sup>
Atrium orientation	Atrium top and atrium base location	9	Units along x-axis: - 4 to 4 4 to - 4
Atrium geometry	Atrium top and atrium base rotation	2	No rotation applied or $+15^\circ -15^\circ$ rotation to top and base

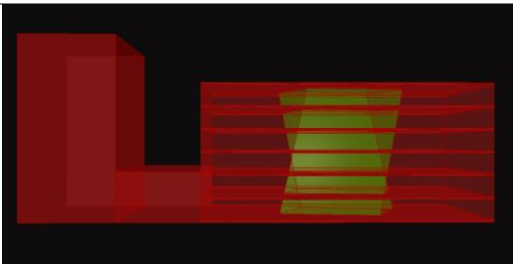
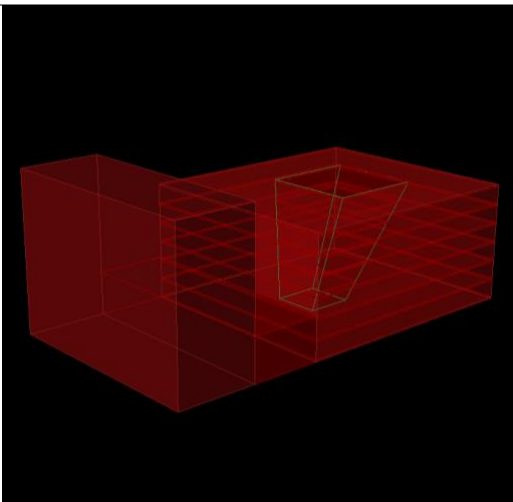


Table 5-1 Design variables used in the proposed design alterations



Figure 5-3 Six possible choices for atrium base area



Figure 5-4 Nine possible choices for atrium well orientation

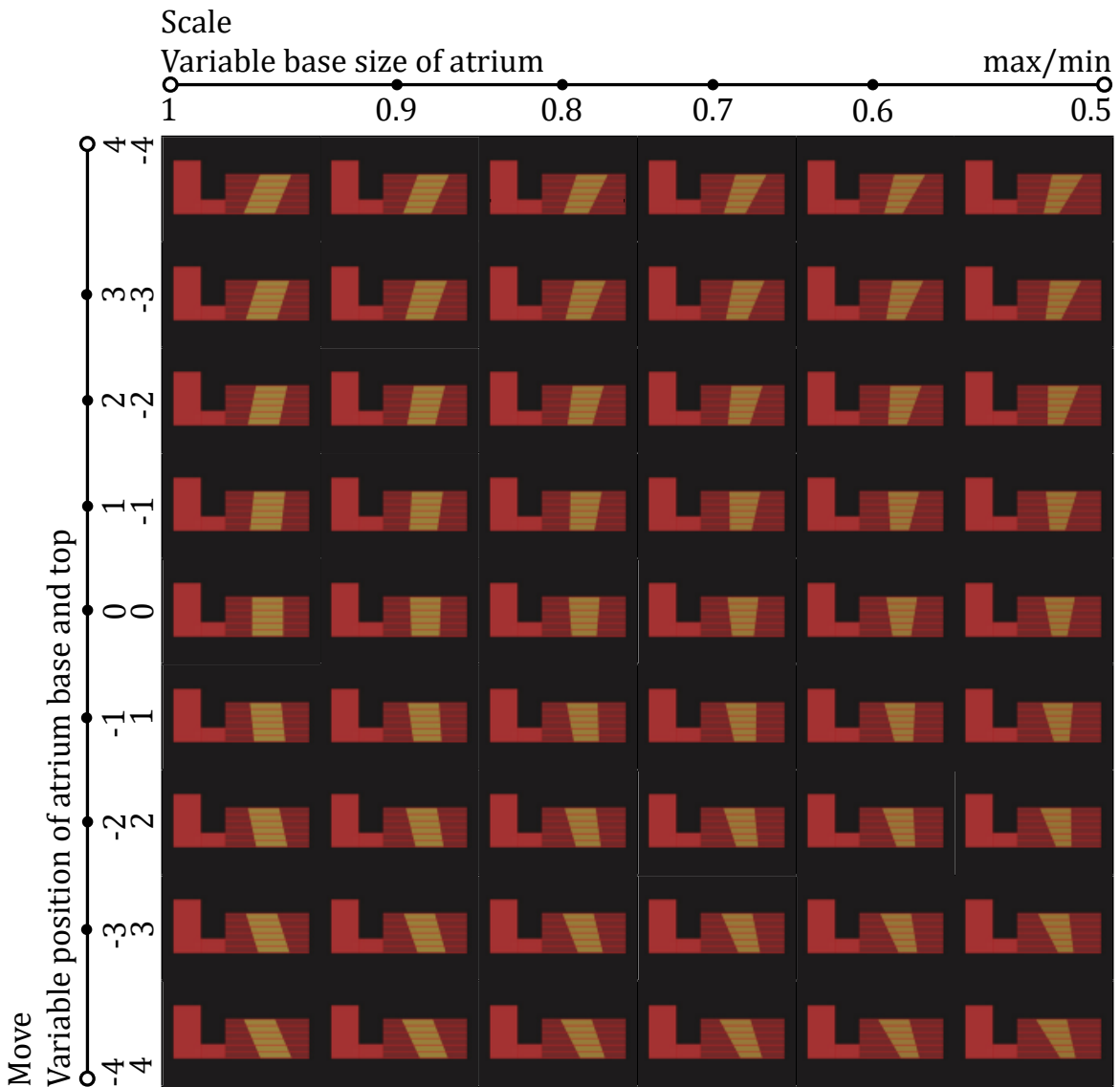


Figure 5-5 Design solution space 1a: East elevation of the Katharinen School with 54 design variants for the central atrium. The atrium is highlighted in green. In each row of the matrix, the atrium base area becomes smaller, resulting in the 'v' shaped atrium. Down every column the orientation of the atrium changes from northward- to southward orientation

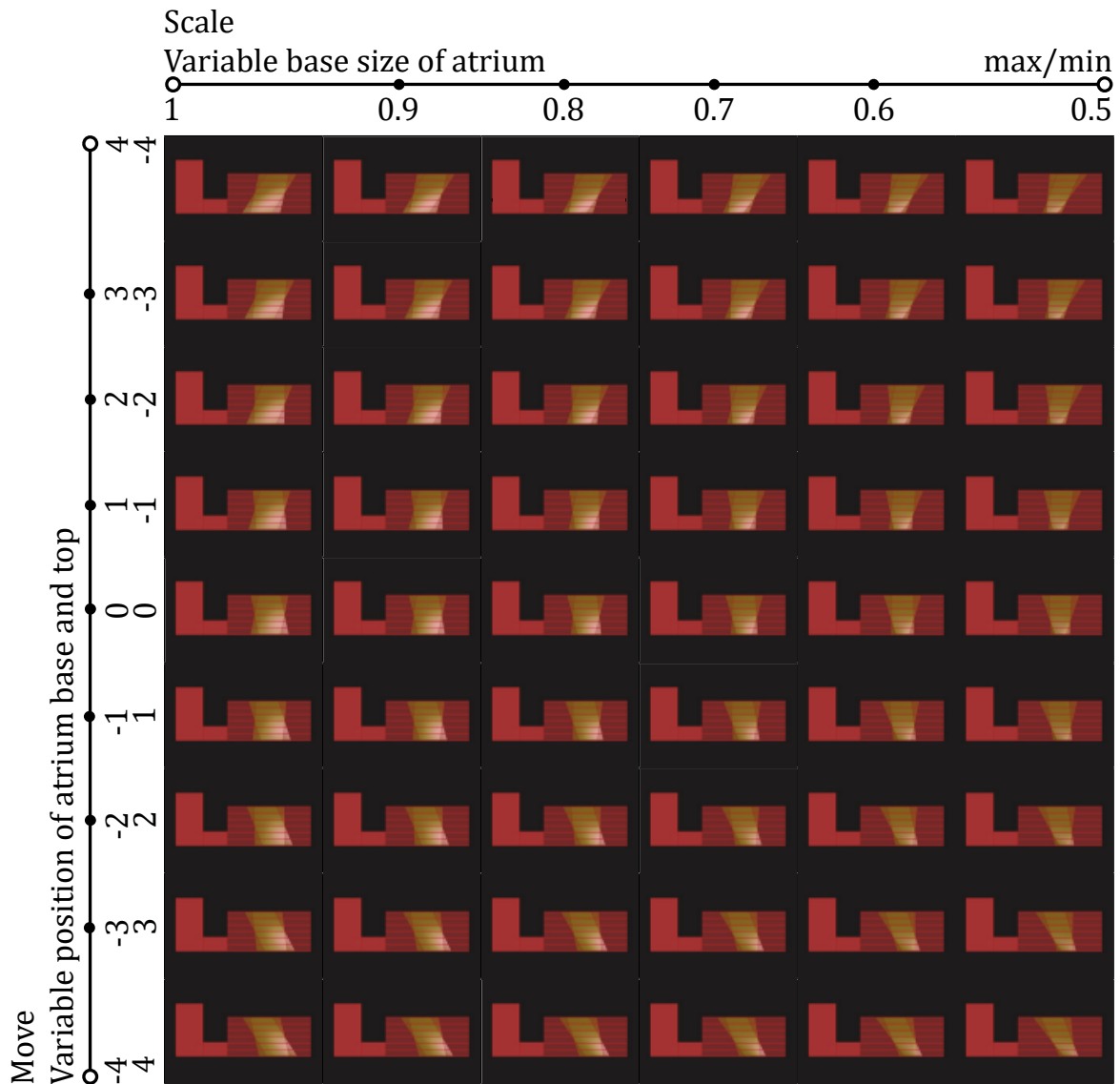


Figure 5-6 Design solution space 1b: East elevation of the Katharinen School with the 54 twisted design variants for the central atrium.

In order to generate the training data, Diva daylight simulations were run with an ambient bounce setting of 6 and sensor point spacing was set to 0.6m. The daylight model included the surrounding buildings. The previous ANN settings (max. validation failures of 6, initial mu of 1, mu decrease and increase factor of 0.8 and 1.5 respectively) were applied and the MSE during training and optimisation of the network architectures was weighted 65:15:20 for the training, validation and test subset. The number of training epochs was increased from 150 to 200. The ensemble of 10 ANNs was trained and tested for architectures with 10 to 40 hidden neurons in one hidden

layer. As a reminder (more details have previously been provided in Chapter 3), the extracted input features from the Grasshopper model include: x and y coordinates of sensor points, distance from sensor points to north, south, east, and west façade (in m), distance from sensor points to closest atrium point on the atrium well (in m), direction to the closest point on the atrium well (in °), distance to atrium centre (in m), direction to atrium centre (in °), glazing area at simulated floor level (4 features, one for each atrium well wall), total glazing area of the atrium well faced (in m<sup>2</sup>), dimension of the daylight calculation grid (in m<sup>2</sup>), splay angles of atrium well, atrium dimension at the height of calculation grid (in m<sup>2</sup>), dimension of the atrium base, location of sensor point inside or outside atrium well. The importance of these input features is further been explored in Chapter 6.

### *5.2.1 Full-factorial validation of prediction accuracies*

This section presents the results of implementing ANNs to replace simulations for the above specified design space with 108 design solutions for the central atrium. Data from 60 out of 108 simulations (30 simulations from each design space with 54 solutions) were used for training, while data from the remaining 48 simulations (24 simulations from each design space with 54 solutions) were used for testing prediction accuracies of the ANN models. Two ANN ensembles were trained individually on data from the two design spaces with 54 design solutions, and a third ANN ensemble was trained on data from the combined design space with all 108 design solutions. For design solution space 1a with 54 design solutions (Figure 5-5), the training data set consisted of 129.395 samples, the test data set of 100.412 samples. For the twisted variant, design solution space 1b with 54 design solutions (Figure 5-6), the training data set consisted of 125.604 samples, the test set of 100.505 samples. In total, this

amounted to 254.999 training samples and 200.917 test samples for the combined data set of design solution space 1a and b. The following graph shows the average MSE of the ANN ensembles during training for each of the network architectures. The lowest achieved absolute error on the unseen test data (the remaining 48 simulations) during optimisation of the ANN architecture with 10-25 and 25-40 hidden neurons is shown in Figure 5-7 alongside the respective training time.



Figure 5-7 Optimisation of ANN architecture: Training performance of ANN models with an increasing number of hidden neurons

The higher the number of hidden neurons (HNs), the better the ANN ensembles could fit to the training data, as indicated by the decreasing MSE. The MSE decreased more quickly between 10 and 25 HNs (from .005 to .001) and stagnated towards 40

HNs (at an MSE of .0005). The applied networks achieved a predictions accuracy of 0.80% DA MAE at 25 HNs, and 0.61% DA MAE at 40 HNs.

The training time increased with the number of hidden neurons. The training of an ensemble of 10 ANN models for network architectures with 10 to 25 HNs took approximately 6 hours of training on the two data sets containing data from 30 simulations (data sets from design solution space 1a and 1b). In comparison, training the ensemble for network architectures with 26 to 40 required 5 times as much time to achieve an improved accuracy of 0.19 and 0.28% DA MAE. Training the ensemble on data from all 60 simulations (combined data set 1a and b) also increased training time to around 5 times as much as training networks with 26 to 40 neurons, for an improvement of around 0.21 DA MAE in accuracy. Considering it is hardly possible to interpret the meaning of a 1% of occupied hours difference in DA performance, let alone less than 1%, this appears to be a marginal improvement in prediction accuracy for a significant increase in training time. Training an ANN ensemble on the combined datasets for all 108 design solutions marginally decreased prediction accuracies by ~0.06% DA MAE. However, in this instance, the training time on the combined dataset was approximately 10 and 12% shorter than the time required for training two datasets individually.

The prediction errors are presented in more detail in Figure 5-8. The MAE, MBE and MRSE are given for the ANN model with the lowest MSE during training, as well as ANN ensembles made up of 5 and 10 ANN models. As can be seen in the figure, there was little variation in errors for the predicted cases (blue, orange, green) or the methods of output (best-trained network vs. averaged output of ANN ensembles). The prediction errors range from 0.61 to 0.74% DA MAE. Said differently, the average difference between predicted and simulated daylight autonomy ranged between 0.61

and 0.74% DA. The difference in output between the applied models ranged from 0.02 to 0.07% DA MAE. The prediction accuracies are therefore very high, with little variation in MAE between the ANN models/ ensembles used. Nonetheless, an improved accuracy of 0.07% DA MAE was seen when predicting DA for the combined dataset, thus hinting at the superiority of ensembles.

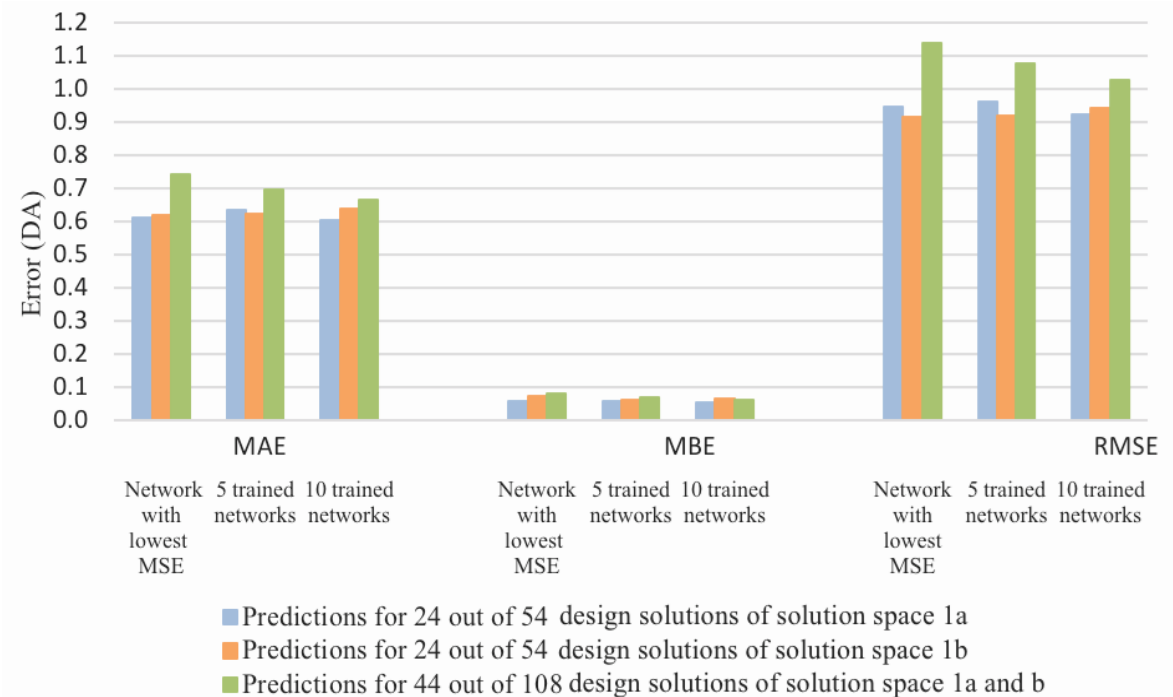


Figure 5-8 ANN prediction accuracies for design solution space 1a and b

As an illustration of the tendency of the ANN models to over- or underestimate predictions, the above figure displays the mean biased errors (MBE), for which the errors range from 0.05 to 0.08% DA. As these lie below 0,1% DA, over- and underestimations, for the most part, cancelled each other out. Although the values are very low, all are positive, which means that the ANN models showed a slight tendency to over- rather than underestimate daylight autonomy results. These overestimations are however minimal, and their relevance is discussed in a later section, when looking at prediction accuracies for the Spatial Daylight Autonomy metric.

For a display of the robustness of the networks, the RMSE has been illustrated in the above figure. As shown, the RMSE range from 0.92 to 1.14, with the largest errors

occurring when using the ANN models trained on the combined dataset (displayed in green). The RMSE also highlight a better accuracy for the ANN ensembles, especially for predictions on the combined dataset (displayed in green, Figure 5-8). Irrespective of this, the RMSEs are still very low (close to 1% DA RMSE), indicating high accuracy for all networks.

The presented accuracies were obtained when training ANN models on data from 30 out of 54 simulations. To gauge the minimum number of simulations required to obtain reliable accuracies on one hand, and to reduce computation time for simulation and ANN training on the other hand, training samples were reduced, and prediction accuracies and computational efficacies reassessed. The results are presented in the next section.

### *5.2.2 Data sampling*

In this section, ANN prediction accuracies are investigated for four training data sets comprising different sample sizes. To this end, the number of training samples from design solution space 1a was reduced by extracting training data from only 18 (data set A Figure 5-9), 12 (data set B Figure 5-9), 9 (data set C Figure 5-10) and 6 simulations (data set D Figure 5-10), as highlighted in the respective figures. The MSE during training, and MAE, MBE and RMSE during testing for these for training data sets are presented in Figure 5-11. The results were obtained for an ANN ensemble of 10 ANNs optimised with up to 40 neurons in the hidden layer.

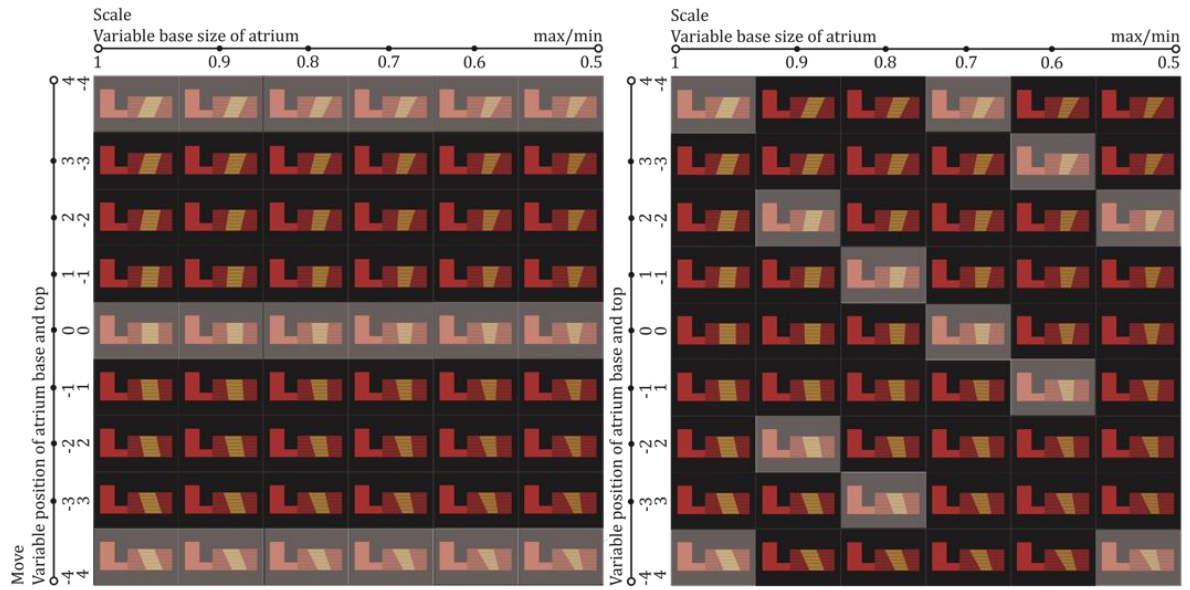


Figure 5-9 Training data set A and B (left to right). Training data set A comprises 18 simulations – 3 from every column of the matrix. Training data set B comprises 12 simulations - 2 randomly selected from every column of the matrix.

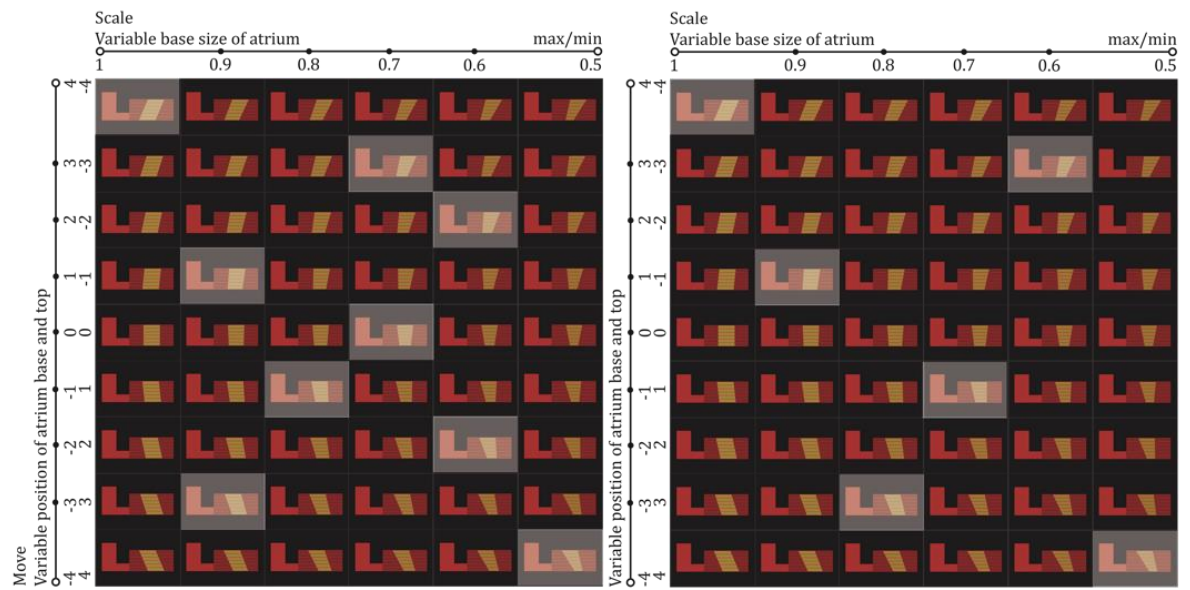


Figure 5-10 Training data set C and D (left to right). Training data set C comprises 9 simulations, 1 simulation from every row of the matrix. Training data set D comprised 6 simulations, 1 simulation from every column of the matrix.

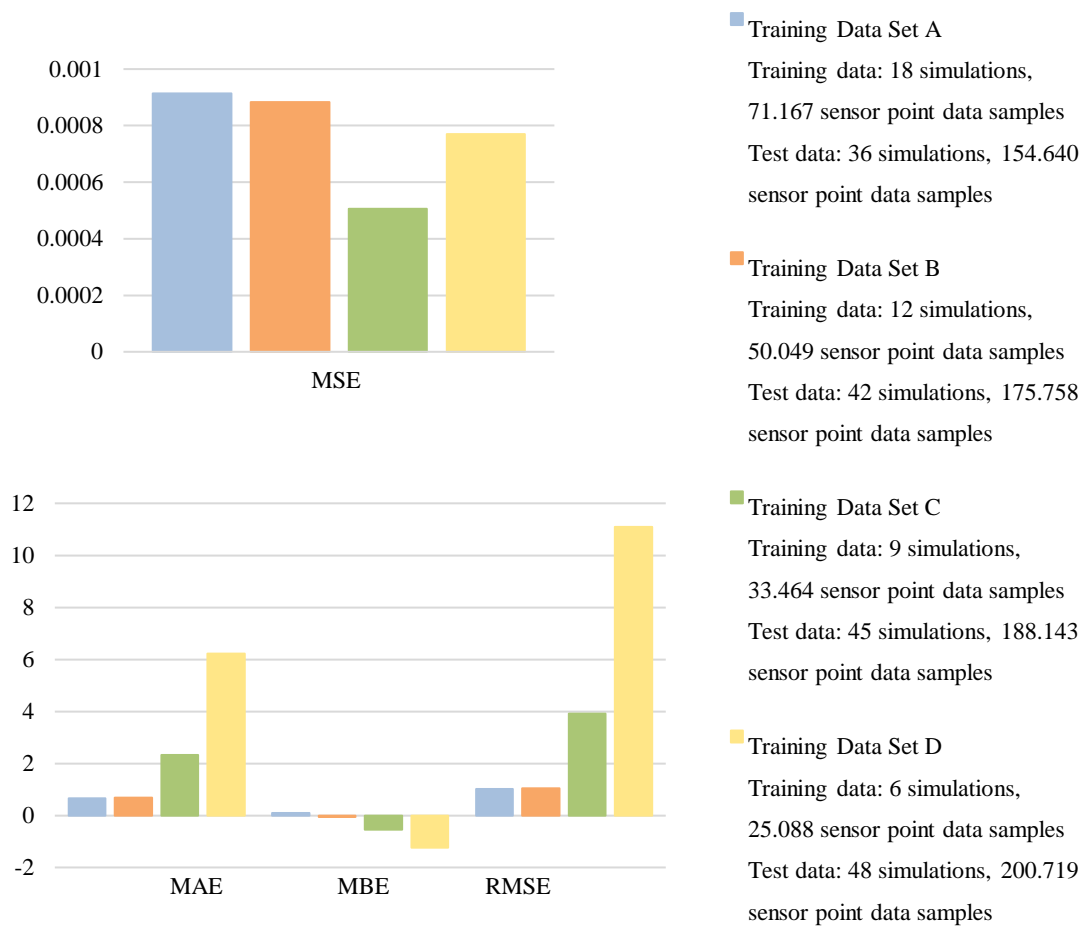


Figure 5-11 Mean Squared Errors of the trained network ensembles and resulting prediction accuracies for training data sets A to D

MSE during training ranged from 0.0005 (C displayed in green) to 0.0009 (A displayed in blue). Interestingly, while the MSE remained low for all training data sets, the MAE of the predictions increased by 314% from data set B to C (12 to 9 simulations) and by 916% from data set C to D (9 to 6 simulations). Although the MSE was low for all training data sets, it should be noted that the MSE is primarily an indicator for the ability of the ANN model to approximate a function for data it has been provided with. As such, the MSE indicates how well the network would be able to predict daylight for sensor points of design solutions which are part of the training data. As can be seen in the results, the MSE does not necessarily give insight into prediction errors on unseen

design variants: The models that were trained on data sets C (9 simulations) and D (6 simulations) were able to fit the data very well, but unable to map daylight performance of the design solution space. This becomes clear when looking at the MAE, MBE and RMSE, which were considerably higher for training sets C (9 simulations) and D (6 simulations), as compared to sets A (18 simulations) and B (12 simulations).

The MAE ranged from 0.66 and 0.68 (data sets A and B with 18 and 12 simulations displayed in blue and orange) to 2.32 (data set C with 9 simulations displayed in green) and 6.23% DA (data set D with 6 simulations displayed in yellow). Thus, even a reduced training data set comprising of data from 12 simulations was sufficient to produce ANN models capable of predicting the DA metric without losses in accuracy (0.68% DA MAE for ANNs trained with data from 12 simulations compared to 0.61% DA MAE previously obtained for ANNs trained with data from 30 simulations).

The MBE remained close to zero. Notably however, DA levels were slightly overestimated when trained on data set A (18 simulations), which coincides with previously observed overestimations when trained on data from 30 simulations. The MBE was 0.10 and 0.05% DA MBE respectively (for 18 and 30 simulations). In comparison, DA levels were underestimated when the number of training samples decreased, as seen for data sets B, C and D (12, 9 and 6 simulations respectively). Here, MBE ranged from -0.06 (12 simulations) to -1.23% DA MBE (6 simulations). It is as of yet unclear how the errors are distributed across the design variants of the design solution space, and how the error affect the overall assessment of daylight performance of each design solution. This is investigated in the next section.

### 5.2.3 *Simulated vs. predicted performance ranking of design solutions*

As a reminder, sDA metric denotes the percentage of space achieving a DA of 50% or more. By assigning a summative value to a space, the metric becomes useful for the assessment of the overall daylight performance of the space. A Grasshopper script was run to convert all DA predictions from the ANN models into sDA results. The predicted sDA results were then compared to the simulated sDA results. The prediction accuracies for the sDA metric are shown in Figure 5-12 shedding light on how closely the ANN models were able to predict the 50% DA threshold and overall daylight performance of a design solutions in terms of sDA<sub>300/50%</sub>.

Figure 5-12 gives the predicted and simulated sDA results for atrium adjacent spaces on the ground floor for training data sets A to D. The sDA results are shown according to the matrix entries in Figure 5-5 and Figure 5-6. As seen in the figure, the sDA of the 54 design solutions varied between 20 and 29%. For training data sets A and B with data from 18 and 12 simulations respectively, simulated and predicted values showed considerable and consistent overlap. The ANN models were thus shown suitable for mapping daylight performance of design solution spaces. For training sets C and D however, predictions diverged from simulated results, most noticeably so for data set D. The strong discrepancies show that training data extracted from 9 and 6 simulations were insufficient for mapping the daylight performance of the entire solution space of 54 solutions. Data from 12 simulations (data set B) on the other hand were already sufficient to accurately map the performance across the solution space.

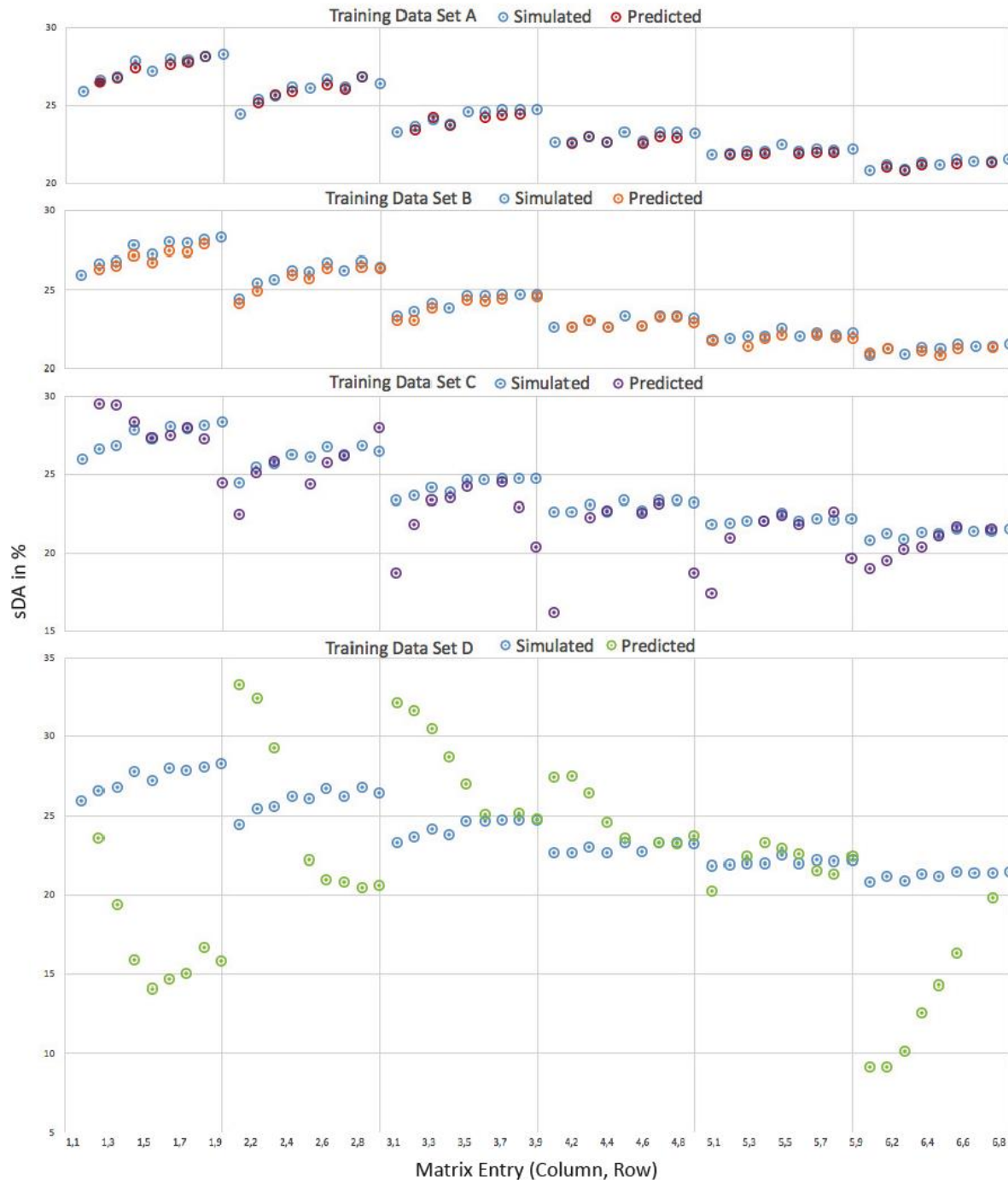


Figure 5-12 sDA performance of the 54 generated design solutions of design solution space 1a. Predicted and simulated sDA are show for training data sets A to D.

The achievable time saving from integrating ANNs in the design workflow can be calculated from the total number of replaced simulations less ANN training time. On a 2.6 GHz Intel Core i7, one daylight simulation took a little over three hours. Using ANNs to predict daylight for 42 design solutions thus reduced the time spent on

simulations by approximately 126 hours, or 125.4 hours after taking into account the time spent on training and optimizing the networks with architectures between 38-40 neurons in one hidden layer. Taking 12 simulations as the required number of training samples, ANNs replaced 78% of simulations, therefore reducing simulation time by 78%. After deducting ANN training time, overall simulation time was reduced by 77%. Nonetheless, used in a design workflow, additional simulations will be required in order to test ANN accuracies before blindly implementing them. In this section, simulations were performed on all design variants in the solution space and ANN predictions were compared to all simulated results. As this is not feasible, it is suggested to perform the validation on only a subset of solutions from the design space, as performed in work described in next section of this chapter, where ANNs are assessed on a design solution space with 270 additional atrium design variants.

### 5.3 Predicting daylight for WWR distribution options and material reflectance

In addition to the design variables affecting atrium geometry and atrium well orientation, further dimensions were added to the design solution space (Table 5-2). In order to increase daylight levels in atrium adjacent spaces on the lower floors, four options were specified for the window-to-wall ratios (WWR) on the atrium well façade. The distribution of WWR of the 6-storey building from the 6<sup>th</sup> to the ground floor were as follows: the first option had a WWR distribution of 50, 60, 70, 80, 90, 100%, the second option had a WWR distribution of 20, 30, 40, 50, 60, 100%, the third option had a WWR distribution of 20, 35, 50, 65, 80, 100%, and the fourth a WWR distribution of 40, 40, 40, 40, 40, 100% as a control case (Figure 5-13). The number of solutions in the design space was therefore  $54 \times 4 = 216$ . Finally, material reflectance was specified as a

design variable for the design space with a WWR distribution of 20, 30, 40, 50, 60, 100%. Here, the diffuse material reflectance of the opaque surfaces of the atrium façade were increase from 0.8 to 0.9. A representation of all design solution spaces in the form of 9 by 6 metrices (as in) is given in Figure 5-14.

Variable Category	Design Variable	Number of Choices	Maximum and Minimum Bounds
Atrium well façade	WWR distribution	4	WWR ratios top to bottom floors: 50, 60, 70, 80, 90, 100% WWR 20, 35, 50, 65, 80, 100% WWR 20, 30, 40, 50, 60, 100% WWR
Atrium well façade	Material reflectance	2 (only for the 20, 30, 40, 50, 60, 100% WWR series)	0.8 0.9

Table 5-2 Design variables used in the proposed design alterations

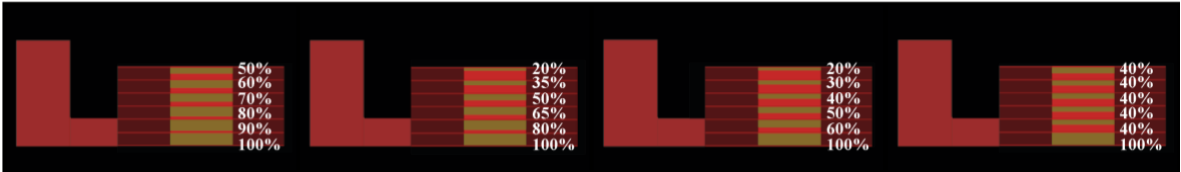


Figure 5-13 Four possible choices for WWR distribution

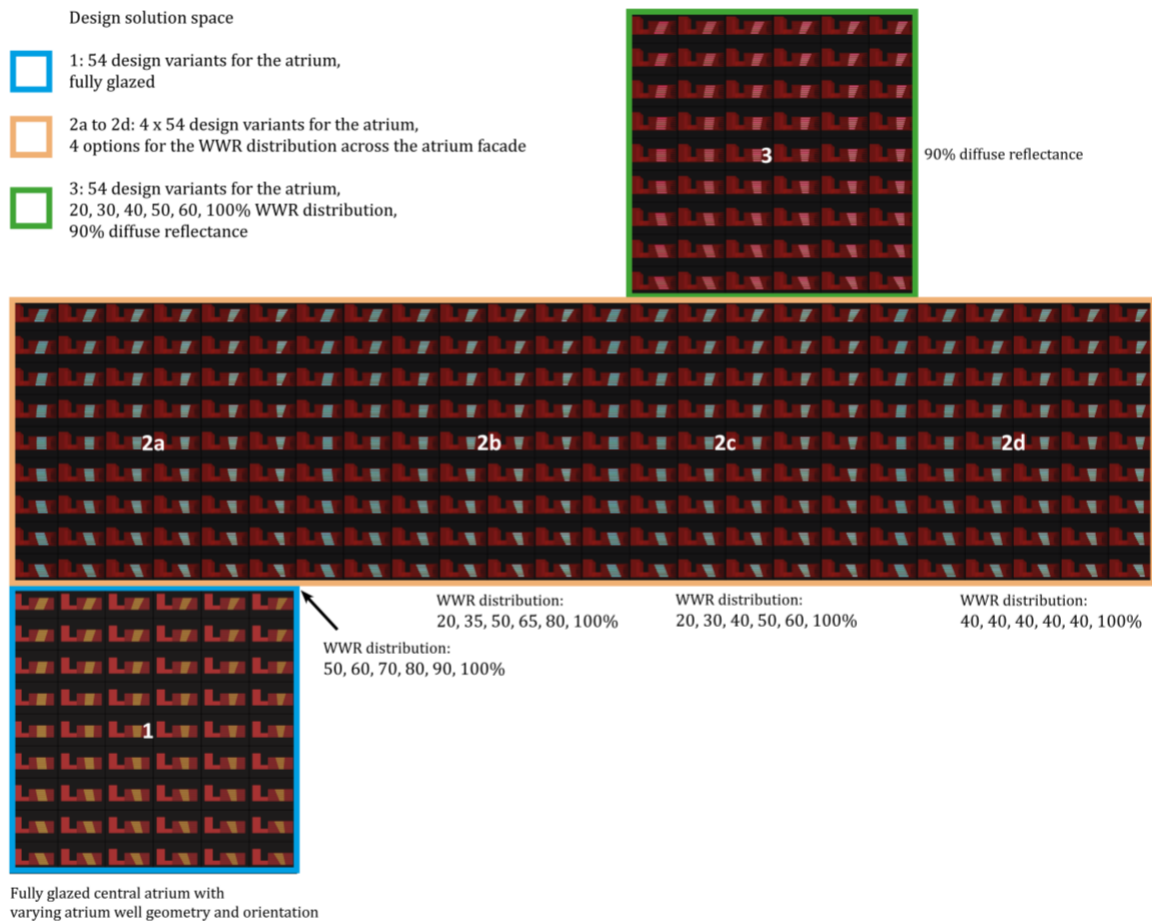


Figure 5-14 Investigated design spaces with a total of 324 design variants for the central atrium

### 5.3.1 Fractional validation of prediction accuracies

Training data was extracted from 12 simulations out of every 54 design solutions. The 12 simulations were selected randomly for every design space with the exception of two, which were specified to ensure inclusion of minimum and maximum bounds within the training data and therefore avoid extrapolation (i.e. the atrium with the largest and smallest atrium base area, northmost and southmost orientations). As for testing, 7 additional simulations were randomly selected from every 54 design solutions, amount to 13% of the total data. The 3-layerd network architecture was optimised with up to 40 HNs in the hidden layer.

The ANN prediction accuracies for all design spaces in Figure 5-14 are given in Figure 5-15. Overall, the accuracies are similar, with errors ranging between 0.68 and

0.95 DA for solution spaces 1 to 3. The lowest error were found for design space 1 with an of 0.9 DA. The highest errors occurred for the ANN model trained on all design solution spaces: 1, 2a to d, and 3. Trained on this large design space, the error of 0.95 DA came close to the error of networks trained on smaller design spaces, showing that an increase of design variables does not significantly lower prediction accuracies. However, the time for optimising the ANN models increased from 10:55 (hh:mm) in totals for three smaller networks to 15:30 for optimising and training a single larger network, on account of the larger number of input features.

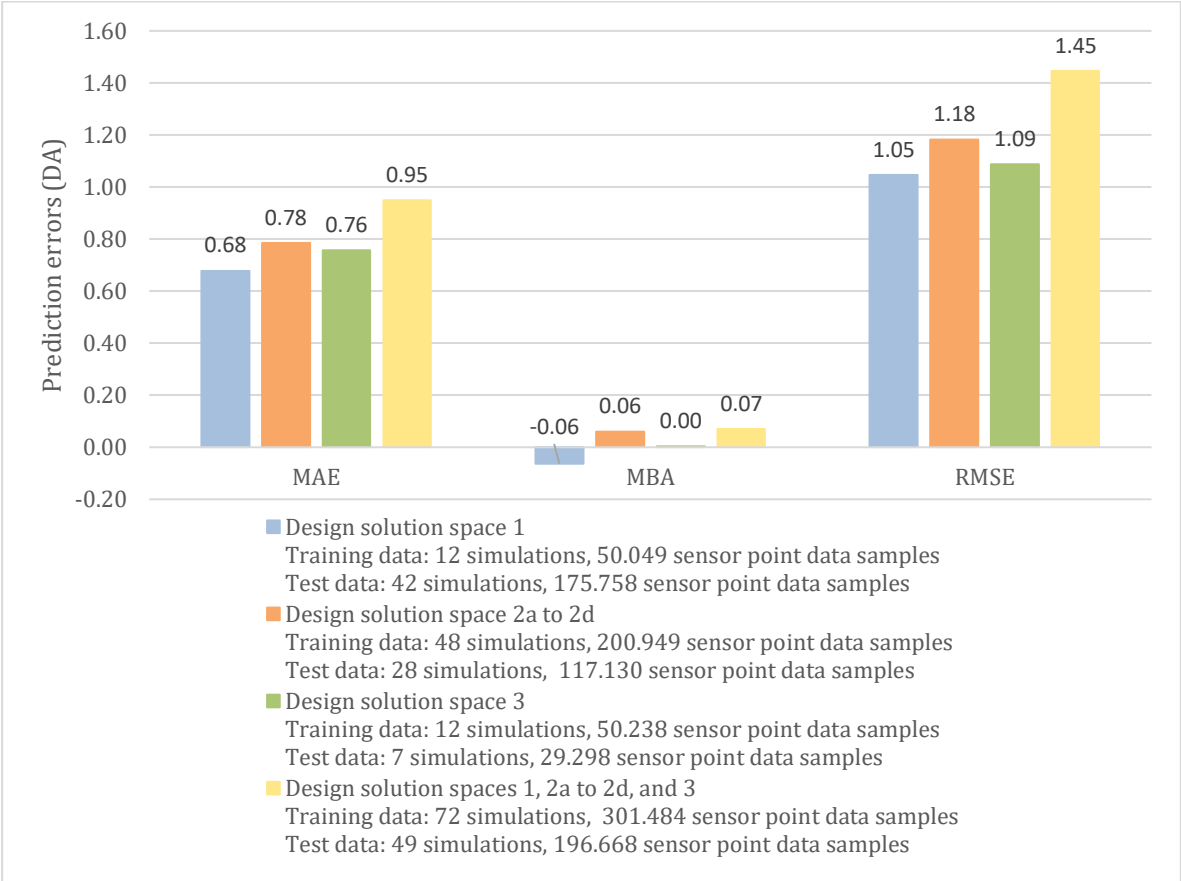


Figure 5-15 Prediction accuracies for the different design solution spaces

The ANN prediction accuracies across all floor levels for design solution space 3 in Figure 5-14 are given in Figure 5-16. Overall, where ANNs were trained individually on data from one floor, the accuracies were similar, with errors ranging between 0.76 and 0.62 DA. The lowest errors were found for predictions on the 6<sup>th</sup> floor with a MAE

of 0.62 DA. The highest errors occurred when training an ANN to predict daylight across multiple floors. Here, the errors increased to 1.24 MAE. This increase in absolute error by about 200% to errors obtained for predictions on the top floor may pose a concern. Arguably, the increase in error may be a result missing input features describing the different daylight conditions on each floor level. After all, the only input feature added to the training data set described the height of the sensor point location (z-coordinate). However, there are major differences between the floors: the ground floors for example has an adjoining building on its south, accessed via the ground and second floors. Therefore, natural light is only provided on three facades. This changes for the 3<sup>rd</sup> and top floors, which have access to daylight on all four sides of the building. Additionally, daylight conditions will also be different on the 3<sup>rd</sup> floor, which receives additional reflected light from the roof of the connecting building, and is more affected from overshadowing than the top floor. Therefore, lacking descriptors are likely to have caused the error spike. In conclusion, training multiple smaller ANNs provides a possibility to bypass extensive features engineering, if design scenarios vary greatly. Alternatively, when design variables differentiating designs are of similar nature (e.g. WWR), ANNs were shown to provide good accuracies, despite a marginal increase in errors for larger design spaces. In the next chapter, this is investigated in more detail for additional daylight performance metrics.



Figure 5-16 Prediction accuracies across floor levels for design solution space 3

## 5.4 Conclusions

A question raised in chapter was whether it is better to train multiple smaller ANN ensembles on different design variable vs. one larger ANN ensemble on multiple design variables. Prediction accuracy for the  $DA_{300}$  metric marginally dropped when training one, as opposed to two ANN ensembles on the design variables *atrium well orientation* and *atrium well geometry* (by twisting the atrium well and scaling the atrium base area). Whether this holds true for other, similar design spaces as well (i.e. for different WWR distribution series), is addressed in the next chapter. Nonetheless, where there was a larger difference between design spaces, prediction accuracies dropped. Specifically, accuracies were significantly lower when one ANN ensemble was trained to predict the daylight performance of all six floors of the atrium building, in comparison to six ANN

ensembles trained to predict daylight performance for each floor. This result is easily explained, as each floor has a different daylight availability, a consequence of differences in floor height and the relationship to adjacent/surrounding buildings. For the ANN models to retain their accuracy when trained on all floors together, missing descriptors describing the differences in context for each floor level may need to be captured as input features for ANN training (in the current work, only floor height was used as an additional input feature describing differences between floors). Alternatively, increasing training sample from the design spaces may improve accuracy. Both options however would increase overall training time of the models.

Overall, this chapter has shown that high prediction accuracies of less than 1  $DA_{300}$  and  $sDA_{300/50\%}$  are achievable for different design spaces and design variables. By training ANNs as emulators for daylight simulations, ANNs replaced 78% of simulations for the design spaces specified in this chapter. After deducting ANN training time, overall simulation time was reduced by 77%. Once trained on a design solution space, the ANN models allowed for instantaneous predictions to be made and daylight performance results could be explored in real-time within the Grasshopper interface. Nonetheless, real-time exploration while designing/building the CAD model was not possible, as a.) part of the simulations still needed to be run to generate the training data for the ANN models, and b.) the ANN models needed to be trained. With ~200.000 training samples generated from 12 simulations, the minimum training time (without optimisation of ANN hyperparameters and one hidden layer) was possible in less than 30 minutes for the design spaces and accuracies described in this chapter.

## Chapter 6

### Optimisation of ANN Prediction Accuracies

Having established the accuracies for climate-based-daylight predictions, further improvements to the ANN models were made by adjusting and optimising training input features and finetuning ANN hyperparameters. In the first section of this chapter, the impact of input features on prediction accuracies are assessed. 12 different input series containing different features are tested against each other, highlight training features required by the ANN model. In the second section of this chapter, the process of optimising the training features is automated via sequential forward selection (SFS). Lastly, ANN hyperparameters are adjusted and improvements to predictions accuracy are assessed.

#### 6.1 Input feature engineering

This section details the optimisation of input features for the first 54 generated design solutions (Figure 5-5). A data set with 71.167 samples (data from 18 out of 54 simulations) was used as training data and predictions were made for 154.640 test cases. The data extracted from the models contained 23 features, listed in Table 6-1. An ANN ensemble with one hidden layer was trained and optimised with 37 to 40 neurons in the hidden layer.

##### *6.1.1 Impact of input feature selection on prediction accuracies*

The prediction errors of the ANN model with the lowest MSE, the ANN ensembles of 5 ANNs with the lowest MSE and the ANN ensemble of 10 ANNs are shown in Figure 6-1, Figure 6-2 and Figure 6-3. For the 12 input feature series, refer to Table 6-1.

Input Feature Series 1	Input Feature Series 2	Input Feature Series 3	Input Feature Series 4	Input Feature Series 5	Input Feature Series 6	Input Feature Series 7	Input Feature Series 8	Input Feature Series 9	Input Feature Series 10	Input Feature Series 11	Input Feature Series 12
X coordinate of sensor point	X coordinate of sensor point	X coordinate of sensor point	X coordinate of sensor point	X coordinate of sensor point	X coordinate of sensor point	X coordinate of sensor point	X coordinate of sensor point	X coordinate of sensor point	X coordinate of sensor point	X coordinate of sensor point	X coordinate of sensor point
Y-coordinate of sensor point	Y-coordinate of sensor point	Y-coordinate of sensor point	Y-coordinate of sensor point	Y-coordinate of sensor point	Y-coordinate of sensor point	Y-coordinate of sensor point	Y-coordinate of sensor point	Y-coordinate of sensor point	Y-coordinate of sensor point	Y-coordinate of sensor point	Y-coordinate of sensor point
Distance to south facade	-	-	-	Distance to south facade	-	Distance to south facade	Distance to south facade	Distance to south facade	Distance to south facade	Distance to south facade	Distance to south facade
Distance to east facade	-	-	-	Distance to east facade	-	Distance to east facade	Distance to east facade	Distance to east facade	Distance to east facade	Distance to east facade	Distance to east facade
Distance to west facade	-	-	-	Distance to west facade	-	Distance to west facade	Distance to west facade	Distance to west facade	Distance to west facade	Distance to west facade	Distance to west facade
Distance to north facade	-	-	-	Distance to north facade	-	Distance to north facade	Distance to north facade	Distance to north facade	Distance to north facade	Distance to north facade	Distance to north facade
Distance to atrium closest point	Distance to atrium closest point	Distance to atrium closest point	-	Distance to atrium closest point	Distance to atrium closest point	-	Distance to atrium closest point				
Direction to atrium closest point	Direction to atrium closest point	Direction to atrium closest point	-	Direction to atrium closest point	Direction to atrium closest point	-	Direction to atrium closest point				
Distance to atrium centre	-	Distance to atrium centre	Distance to atrium centre	Distance to atrium centre	Distance to atrium centre	Distance to atrium centre	-	Distance to atrium centre			



Atrium glazing area (all floors)	Atrium glazing area (all floors)	Atrium glazing area (all floors)	Atrium glazing area (all floors)	Atrium glazing area (all floors)	Atrium glazing area (all floors)	Atrium glazing area (all floors)	Atrium glazing area (all floors)	Atrium glazing area (all floors)	Atrium glazing area (all floors)	Atrium glazing area (all floors)	Atrium glazing area (all floors)
Splay angle - north facing atrium wall	Splay angle - north facing atrium wall	Splay angle - north facing atrium wall	Splay angle - north facing atrium wall	Splay angle - north facing atrium wall	Splay angle - north facing atrium wall	Splay angle - north facing atrium wall	Splay angle - north facing atrium wall	Splay angle - north facing atrium wall	-	-	-
Splay angle - south facing atrium wall	Splay angle - south facing atrium wall	Splay angle - south facing atrium wall	Splay angle - south facing atrium wall	Splay angle - south facing atrium wall	Splay angle - south facing atrium wall	Splay angle - south facing atrium wall	Splay angle - south facing atrium wall	Splay angle - south facing atrium wall	-	-	-
Area of grid plane (in m <sup>2</sup> )	Area of grid plane (in m <sup>2</sup> )	Area of grid plane (in m <sup>2</sup> )	Area of grid plane (in m <sup>2</sup> )	Area of grid plane (in m <sup>2</sup> )	Area of grid plane (in m <sup>2</sup> )	Area of grid plane (in m <sup>2</sup> )	Area of grid plane (in m <sup>2</sup> )	Area of grid plane (in m <sup>2</sup> )	Area of grid plane (in m <sup>2</sup> )	Area of grid plane (in m <sup>2</sup> )	Area of grid plane (in m <sup>2</sup> )
Area of atrium at grid plane height (in m <sup>2</sup> )	-	-	-	-	-	-	-	-	-	-	Area of atrium at grid plane height (in m <sup>2</sup> )
Sensor point location (inside or outside atrium)	Sensor point location (inside or outside atrium)	Sensor point location (inside or outside atrium)	Sensor point location (inside or outside atrium)	Sensor point location (inside or outside atrium)	Sensor point location (inside or outside atrium)	Sensor point location (inside or outside atrium)	Sensor point location (inside or outside atrium)	Sensor point location (inside or outside atrium)	Sensor point location (inside or outside atrium)	Sensor point location (inside or outside atrium)	Sensor point location (inside or outside atrium)

Table 6-1 Input features used for training the ANN models

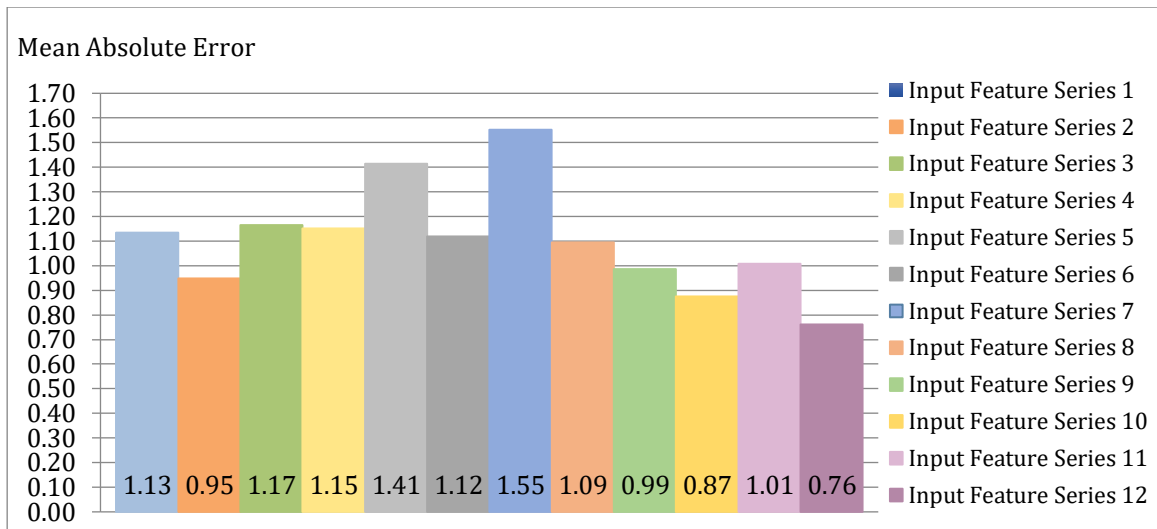


Figure 6-1 Prediction accuracies using the network with the lowest MSE

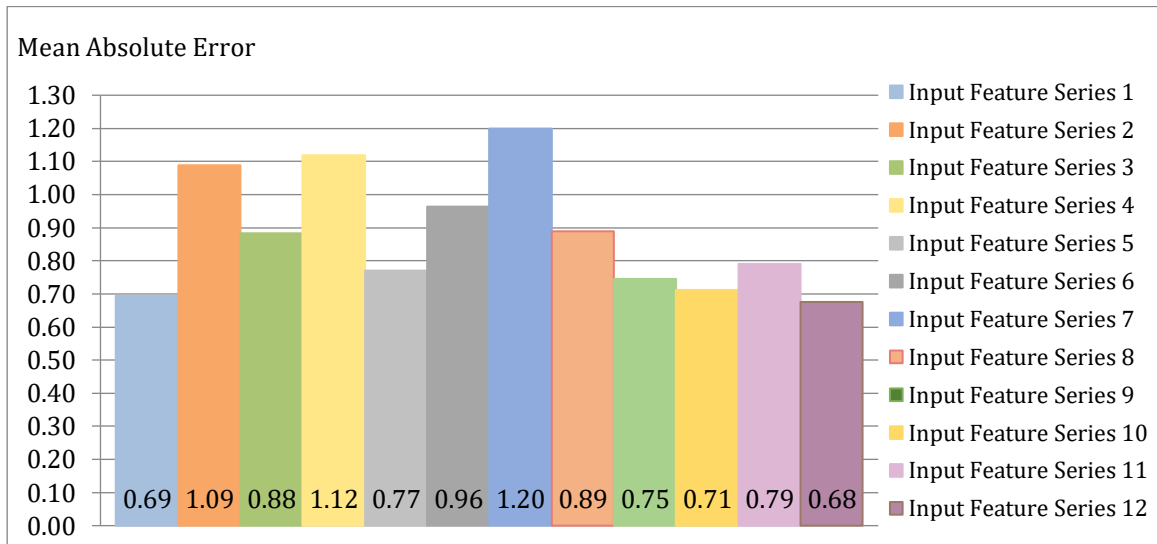


Figure 6-2 Prediction accuracies using the average of five trained networks

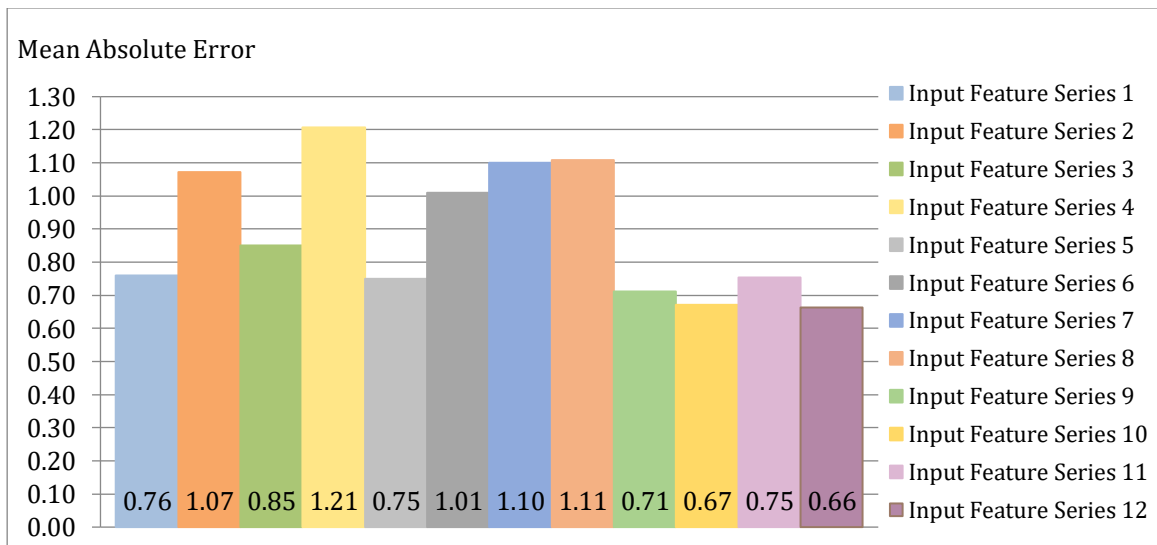


Figure 6-3 accuracies using the average of ten trained networks

In the first out of 12 data series, all 20 extracted training features were used (input feature series 1). As for the second feature series, all information on *distance of sensor points to the façades*, *distance and direction of sensor points to the atrium centre*, and also the *atrium dimension at simulated floor level* (the inverse of the calculation grid area) was removed (input feature series 2). Note that the sensor point identifiers, i.e. the coordinates of the sensor point would still have remained as features linking to the removed information, should the networks have been able to make such connections. In the third feature series, *distance and direction of sensor points to the atrium centre* were added back in (input feature series 3). Then, *distance and direction to the atrium closest point* was removed from the training data (input feature series 4), while still keeping information on the *distance of sensor points to the façade* and the *atrium dimensions* withheld from the training data.

Results showed that, compared to the data set containing all training parameters, the MAE increased by 0.39 and 0.31 for the training features in input feature series 2 for network outputs from five and ten trained networks (Figure 6-2 and Figure 6-3). Although the increase is itself small and an error of 1.09, 1.07 MAE remains low, it adds up to an increase of 36% and 29% from the original error. The error from using the output from a single network with the lowest MSE showed a different result in that the MAE improved by 0.18, that is 16% from the original error (Figure 6-1). Prediction accuracies improved from series 2 for two model outputs after returning *distance and direction of sensor points to the atrium centre* as training features, the MAE of five trained networks by 0.21, the MAE of ten trained networks by 0.22. Only the error of one trained network increased by 0.22. After removing *distance and direction of sensor points to the atrium closest point* (input feature series 4), the error again worsened by 0.42 MAE and 0.45 MAE and 0.03 from series 1 for predictions using five,

ten and one trained networks, respectively, showing a higher impact for *distance and direction to the atrium closest point* than for *distance and direction of sensor points to the atrium centre*.

Following these results, input features series 5 to 8 were set up. In input feature series 5, distance to the four façades was returned as training data and only the *area of atrium* was withheld. Input feature series 6 looks at the error after removing *distance of sensor points to the façade*; input feature series 7 to 8 look at the increase in error after removing *direction to atrium closest point* and *distance and direction to atrium centre* one at a time, while including the four input features describing the *distance of sensor points to the façade*.

Results showed that, after including *distance of sensor points to the façade in the training data*, the predictions were more accurate than input feature series 2, 3 and 4. In comparison to the original training data set that had *area of atrium* as a training parameter (input feature series 1), there were minor changes in prediction accuracy using five and ten trained networks: the MAE of five trained networks worsened by 0.08 and the MAE of ten trained networks improved by 0.01, showing that the inclusion of atrium dimension as training feature bore no significance in this combination of training parameters. The MAE using the best-trained network however increased by 0.28 and showed an MAE of 1.41.

Input feature series 6 showed slightly lower errors than series 2 and 4, in which *distance and direction of sensor points to closest point* and *atrium centre* had been additionally removed. The accuracy was 0.27 and 0.25 MAE lower than input feature series 1 for predictions using five and ten trained networks and 0.02 MAE better using the best-trained network.

Removing *distance and direction of sensor points to closest point* (input feature series 7) increased the error by 0.54 and 0.34 MAE and with 1.2 and 1.1 MAE gave worse prediction accuracies than input feature series 2, in which *distance to façade* had been additionally removed. The error of predictions using a single network increased in this instance as well, providing the worst performance for this training data set with an MAE of 1.55. Similarly, prediction accuracies worsened for input feature series 8 after removing *distance and direction of sensor points to atrium centre*. Specifically, there was an increase of 0.2 using the average output of five trained networks and an increase of 0.34 using the average output of ten trained networks. Using a single network, predictions slightly improved by 0.04 MAE.

Following these results, input features series 9 to 12 were set up. In input feature series 9, *atrium glazing area at the simulated floor* consisting of four input features was removed. The *atrium dimension* was kept out of the training data in this input feature series and for series 10 and 11. This was done, because *atrium dimension* was shown to have no significant impact on the results and was the reverse of the input feature *area of the calculation gird*. In input feature series 10, the *atrium splay angle* constituting two input features was removed from the training data and *atrium glazing area at the simulated floor* was added back. Next, both *atrium glazing area at the simulated floor* and *atrium splay angle* were removed from the training data (input feature series 11). Lastly, as input feature series 9 achieved the lowest errors (in Figure 6-1, Figure 6-2 and Figure 6-3), the same input features were used, but *atrium dimension* was returned as input for training the networks.

After removing *atrium glazing area at the simulated floor* (input feature series 9), prediction accuracies were very close to those of input feature series 1, which contained all extracted features: the MAE improved by 0.05 and 0.15 using the output

of ten and one network, and worsened by 0.05 using the output of five trained networks. Even lower errors occurred using input feature series 10, which had *atrium splay angle* removed. The MAE improved by 0.09 and 0.26 using ten and a single ANN model and worsened by 0.02 using five trained networks.

Although removing *atrium glazing area at the simulated floor* and *atrium splay angle* individually from the training data provided better accuracies, removing both features at a time (input feature series 11) led to higher errors than input feature series 9 or 10. In comparison to series 1, which contained all training parameters, the error improved by 0.01 and 0.13 MAE using the average output of ten networks and one trained network, but increased by 0.1 using the average of five network outputs.

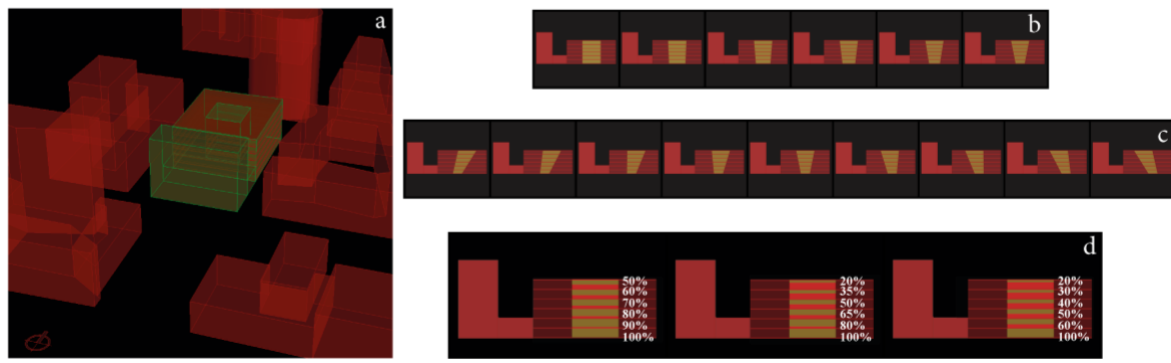
Input feature series 12 had the lowest prediction error among all tested combinations of training features, with an MAE of 0.68, 0.66 and 0.76 and an improvement of 0.01, 0.1 and 0.37 from the original data set for predictions using five, ten and one neural network. Noticeably, prediction accuracies using the best trained network fell closer to those achieved by averaging the output of networks for the data series that had removed either *atrium glazing area at the simulated floor* or *atrium splay angle*, suggesting that the networks were less able to form the correct relationships using both parameters simultaneously as input. There are several possible explanations for this: Firstly, worse accuracies using both features may be due to noise within the data, or, secondly, the small training sample size may have made it difficult for the ANN model to integrate a large number of complex training features. By increasing the sample size, the networks may have been able to make the right connections between features or learned to deal with the noise. Other aspects that may have had an impact on the obtained results are the limited number of hidden neurons tested and the selection of networks based on a random subdivision of training data.

### 6.1.2 Conclusions

This summary refers mostly to results obtained from the ANN ensembles, as they provided the most robust results. Overall, prediction errors increased after removing *distance and direction of sensor points to the atrium centre* and *distance and direction of sensor points to the atrium closest point* from the training data, while the latter feature showed a higher impact on prediction accuracies. Removing *distance to façade* increased errors to a similar extent as removing *distance and direction of sensor points to the atrium centre* and *atrium closest point* did. However, removing *distance to façade* alongside either of the other parameters did not increase errors much further. Removing either *atrium glazing area at the simulated floor* or *atrium splay angle* improved prediction accuracies, but led to higher errors when both features were discarded at a time. Removing *area of the atrium* as an input feature showed little impact on the results using five and ten networks, but was included in the training data that led to the highest accuracies. Overall, predicting daylight by averaging the output of the five networks with the lowest MSE gave a mean absolute error of 0.88, while the average output of ten networks gave an MAE of 0.89. For the most part, predictions made using both methods had errors similar to each other and both methods showed, overall, the same tendencies towards changes in input parameters. The ANN model that had the best training performance however showed a different directionality in error for many of the cases, and produced larger errors than the other two methods. The average MAE across all data series was 1.1. This is in line with findings from previous chapters, showing that the ANN model with the lowest MSE is often not able to generalise as well to new data as ANN ensembles.

## 6.2 Automated input feature optimisation

This section details the optimisation of input features for 162 generated design solutions (54 x 3). As a reminder, as a first design variable, atrium base dimension was reduced from 225m<sup>2</sup> to 56.25m<sup>2</sup>, as a second design variable, the atrium well was slanted northward or southward orientation, and as a third design variable, 3 possible WWR distributions were specified across floor levels of the 6-storey building (Figure 6-4). A data set with 150.706 samples (data from 12 out of 54 simulations) was used as training data. The network architecture was optimised with 38 to 40 neurons in one hidden layer.



Variable Category	Design Variable	Number of Choices	Maximum and Minimum Bounds
Atrium geometry	Atrium base dimension	6	56.25 to 225 m <sup>2</sup>
Atrium orientation	Atrium top and atrium base location	9	Units along x-axis: - 4 to 4 4 to - 4
Atrium well facade	WWR distribution	3	WWR ratios top to bottom floors: 50, 60, 70, 80, 90, 100% WWR 20, 35, 50, 65, 80, 100% WWR 20, 30, 40, 50, 60, 100% WWR

Figure 6-4 a: The school building and surrounding buildings. b: Six variations resulting from a change to the atrium base dimension (the atrium well is highlighted in green). c: Nine variations for atrium well orientation. d: Three variations for the WWR distribution across floor levels

The selection of ANN input features matters, because the number of input features increase training time (affects efficiency), while too few input features may result in high prediction errors (affects accuracy). In order to determine the best possible input features series, it is possible to test all possible combinations of input features. This is however typically infeasible due to the number of training runs it would require. Therefore, research has suggested sequential feature selection to more efficiently determine sustainable input features.

The two common methods of sequential selection are Sequential Forward Selection (SFS) and Sequential Backward Selection (SBS). SFS employs a bottom-up approach that starts with an empty set of features to which features are iteratively added (Whitney, 1971). Its counterpart, SBS, starts from the complete set from which features are iteratively removed (Marill and M. Green, 1963). Inevitably, both methods inhibit a nesting problem, whereby potentially important features, once removed, cannot be re-introduced. To ensure that important features remain in the training data, mixed method approaches have been introduced (Pudil, Novovi and Kittler, 1994). A comparative evaluation of methods is provided by Zongker and Jain (1996). As forward-based methods have been shown to be faster than backward-based methods, the current sections shows the implementation of a SFS approach in combination with a machine learning algorithm to determine the sequence of input features in the selection process.

The steps of the proposed process of input feature optimisation combined with ANN model development and optimisation are shown in Figure 6-5. Performance data was collected from selected design variants of the above specified design solution space (A). The data was extracted from daylight simulations performed on 21 out of 162 design variants. It recorded training input features describing the design changes and

the corresponding training targets describing the daylight results. While a portions of data was used for training, another part containing data from 21 daylight simulations (13% of the design solution space) was retained for validation of the ANN models (D). After data was extracted from the daylight simulation models, a machine learning technique called bagged decision trees were used to determine a sequence for the sequential forward selection of input features (B). The sequence of input features was established according to their relevance in predicting daylight. During SFS, the ANN models were first trained with the input features that showed the highest potential as predictors.

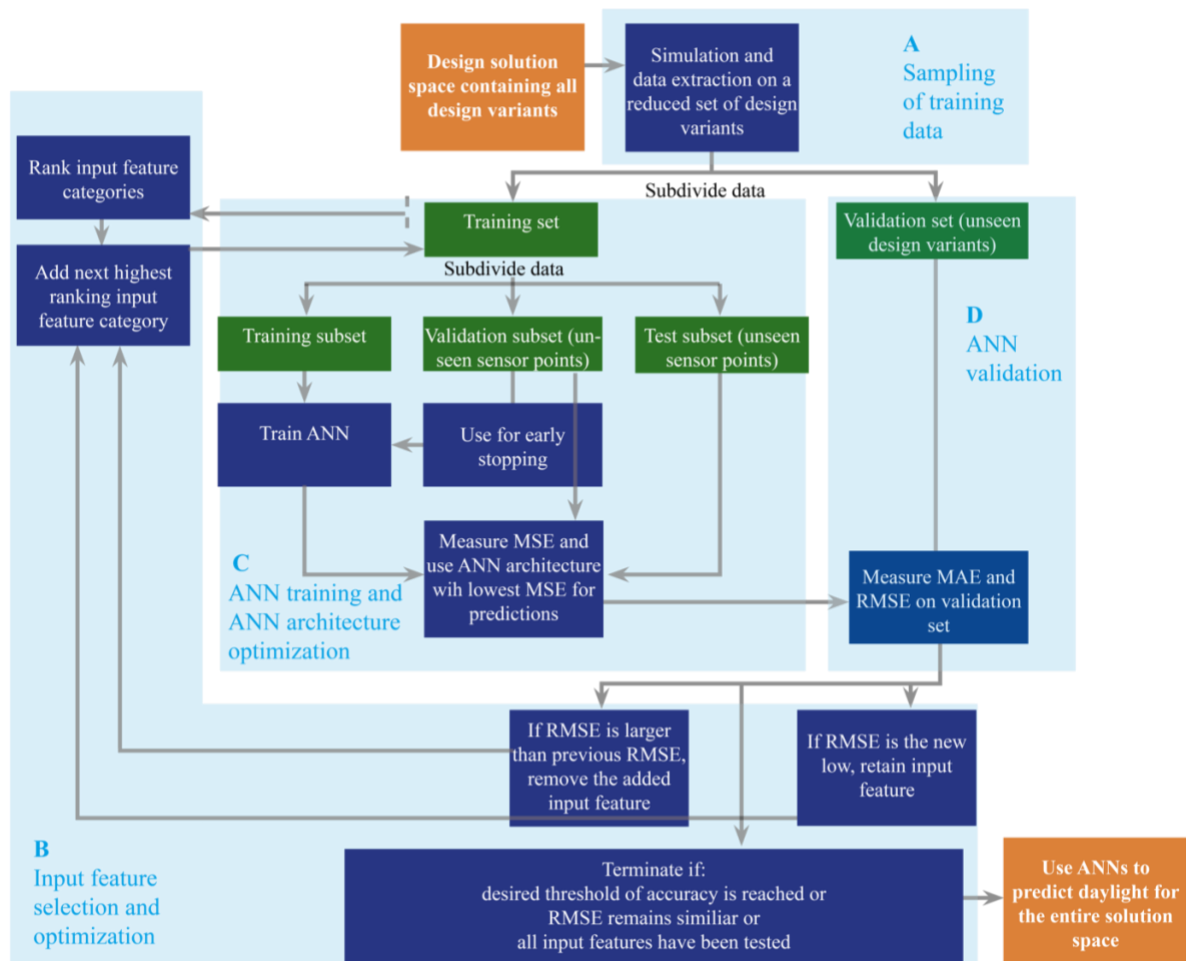


Figure 6-5 Workflow for ANN model development comprising four main steps: sampling of training data, ANN training and ANN architecture optimisation, Input features selection and optimisation and ANN validation

The ANN training data set was subdivided into a training subset, a validation subset and a test subset at the ratio of 65:25:15. The training subset was used to measure the training accuracy, the validation subset was used to avoid over-fitting, and the test subset was used to determine its generalisation capability (C). Then, an ANN ensemble with 10 networks was trained with different architectures. During training, a different randomized initial weight setting was applied for each network, and training data was randomly divided into different training, validation and test subsets. The mean squared error (MSE) was observed on all subsets and the ANN architecture with the lowest error was used for predictions (C). The prediction of ten ANNs was then averaged to improve generalization.

A complete list of extracted input features is shown in Figure 6-6. As shown in the figure, 26 input features were extracted from the simulation model in total and grouped according to categories. In a next step, these categories (as encircled in the figure) were ranked according to their impact on predictions.

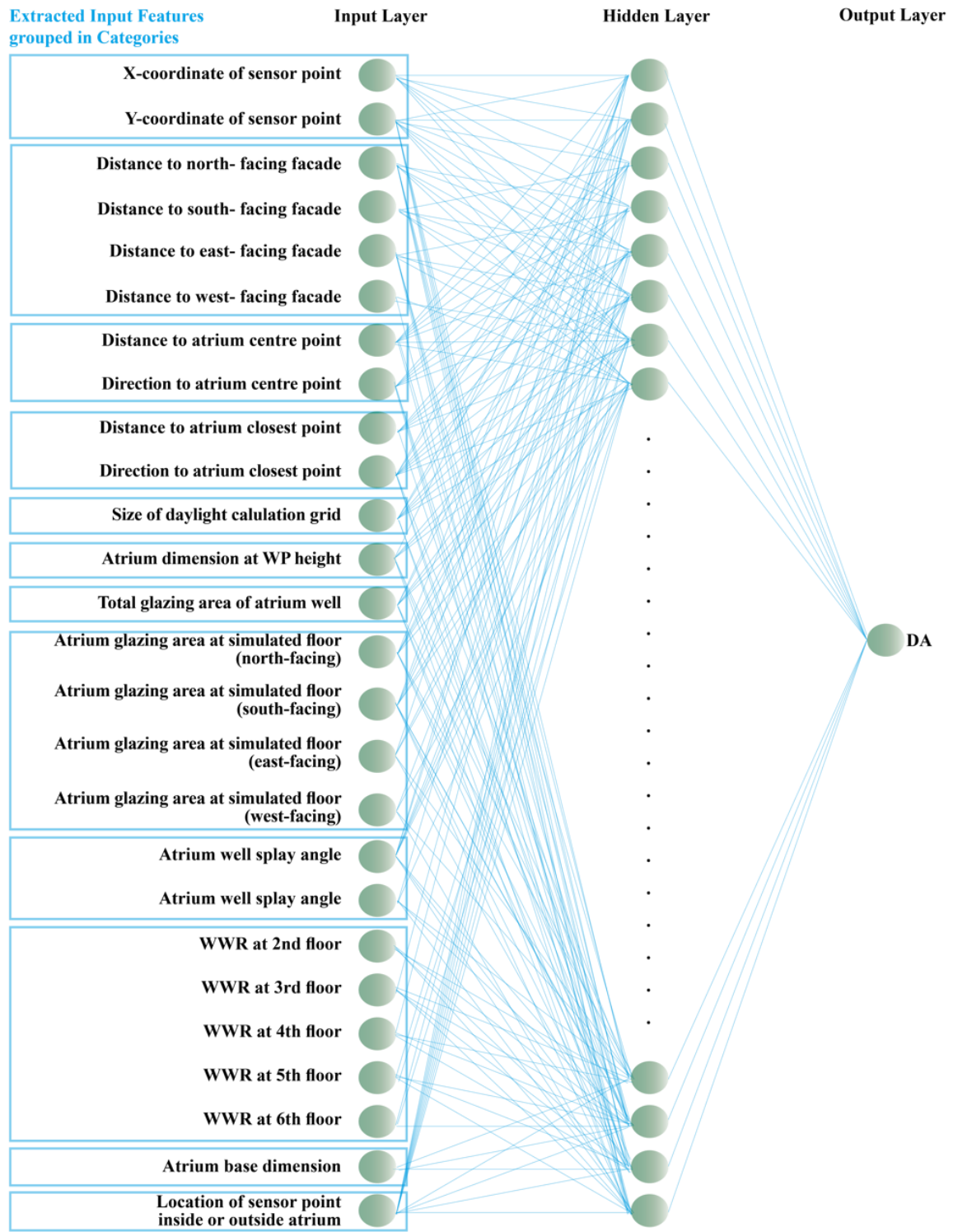


Figure 6-6 Representation of the ANN architecture as a construct of neurons with an input layer, a hidden layer and an output layer. The extracted input features were passed to the input layer of the model and the daylight performance data (in DA) to the output layer.

### 6.2.1 Ranking of input features according to relevance

In order to assess the relevance of the extracted input features as predictors for daylight performance, the training data set were passed to a number of machine learning (ML) algorithms. For this task, tested ML techniques included: linear regression models, fine, medium and coarse trees, boosted tree ensembles, liner, quadratic, cubic, fine Gaussian support vector machines and Gaussian process regression models. From these tested models, bagged decision trees showed the lowest root mean squared error (RMSE) during fitness approximation, and therefore superior performance compared to the other models. Additionally, the computation time was low, with approximation taking around four minutes. Therefore, bagged decision trees were selected as suitable models to identify the feature selection sequence. ANNs, which could have also been used to identify significant input features, were not used as they are much more computationally expensive.

The training data set with the full set of input features was then passed to the bagged decision trees. Next, every input feature category was individually removed and the corresponding variance in RMSE was measured (Table 6-2). The input features were ranked according to the variance they inflicted on the error, with features resulting in the largest variance ranked highest. The RMSE during approximation and the resulting sequence of input feature categories are shown in Table 6-2.

<b>Input Feature Category</b>	<b>Sequence Order</b>	<b>RMSE</b>	<b>Input Feature Category</b>	<b>Sequence Order</b>	<b>RMSE</b>
Distance and direction to atrium closest point (2 features)	1	1.19	X-, Y-coordinates of sensor points (2 features)	7	.87
Distance to façade (4 features)	2	.99	Glazing area at simulated floor level (5 features)	8	.85
Distance and direction to atrium centre point (2 features)	3	.96	Glazing area across all floors (1 feature)	9	.84
WWR (5 features)	4	.90	Atrium base dimension (1 feature)	10	.84

Location of sensor point inside or outside atrium (1 feature)	5	.90	Atrium dimension at work plane height (1 feature)	11	.84
Atrium well spay angles (2 features)	6	.89	Daylight calculation grid size (1 feature)	12	.84

Table 6-2 Ranking of input features according to the afflicted variance in errors

### 6.2.2 Sequential forward selection

During SFS, the ANN models were first trained with the input features that showed the highest potential as predictors. In each training iteration, one input feature category was added according to the determined sequence (as shown in Table 6-2). If the error on the validation data set increased after adding an input feature category, then that specific input feature category was deemed redundant and removed from the training data set before the next iteration.

The MSE on the training data set (36/162 simulations with 150.706 sensor point data samples) and the RMSE and MAE on the validation set (21/162 simulations with 87.850 sensor point data samples) were recorded at each iteration of the sequential search. The MAE and RMSE on the validation data set are shown in Figure 6-7 and Figure 6-8. The validation data set was used to determine the removal or addition of training features. The sequences at which an added input feature category increased the error and was therefore removed from the training data set have been highlighted in yellow. The optimum set of input features, where errors were at the minimum, has been highlighted in red. For comparison, the MSE on the training data set is shown in Figure 6-9.

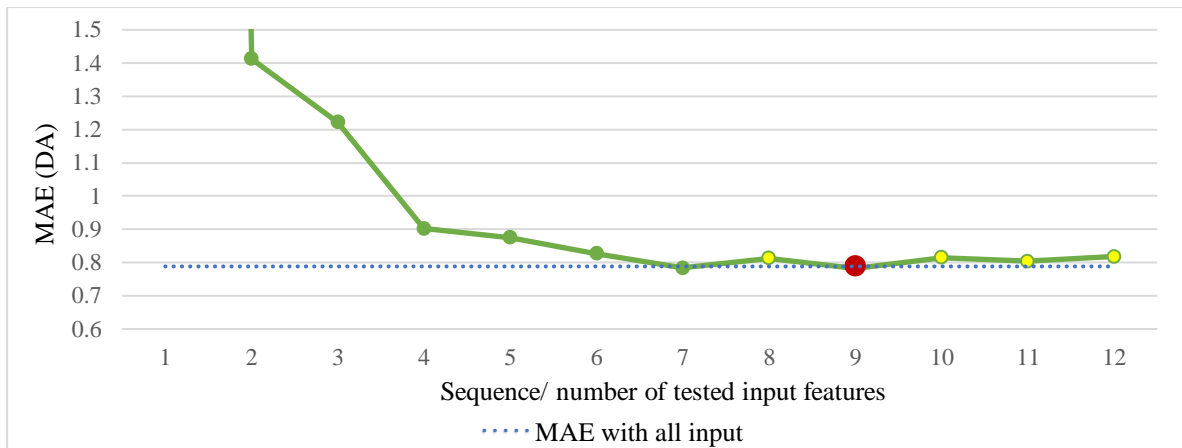


Figure 6-7 MAE on the validation data set at every iteration of the SFS

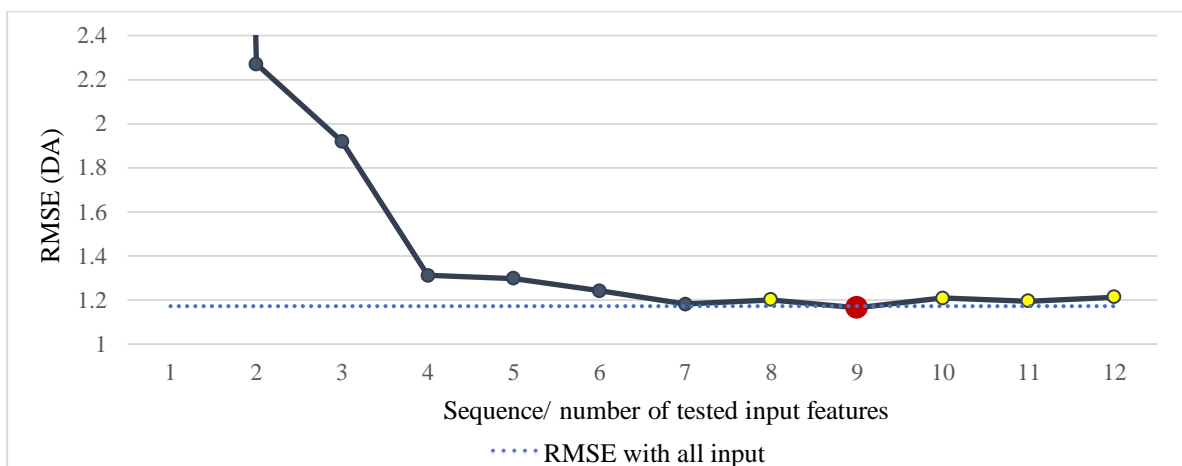


Figure 6-8 RMSE on the validation data set at every iteration of the SFS

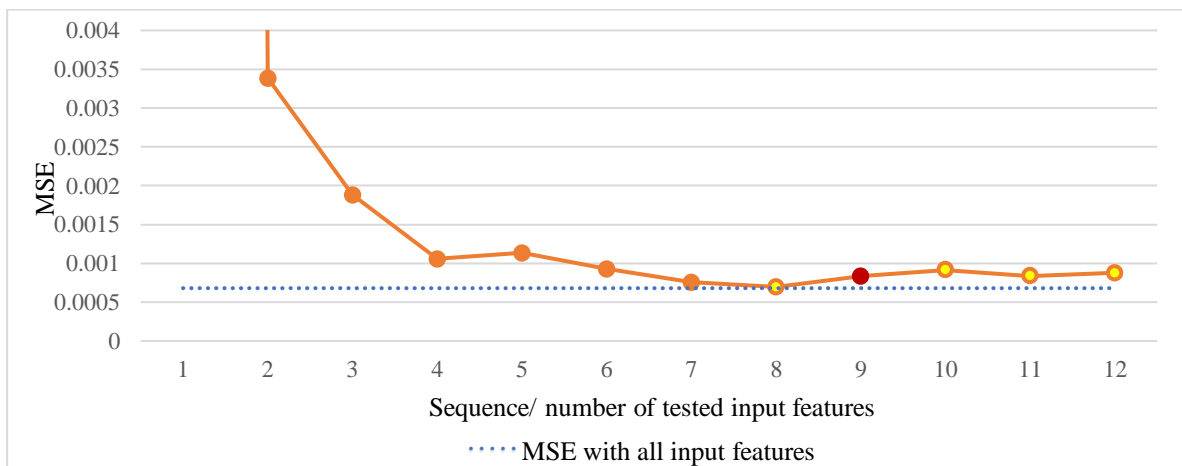


Figure 6-9 MSE on the training data set at every iteration of the SFS

Results showed that the MAE and RMSE on DA predictions remained consistently low after the 7<sup>th</sup> input feature category (*coordinates of sensor points*) was added to the training data. This indicates that the first 7 input feature categories (Table

6-2) suffice in predicting DA for the given design solution space. The MSE dropped below 0.01 after including six input feature category (*atrium well splay angels*) and remained below this threshold in the consecutive iterations.

The lowest MSE on the training data was reached after including the 8<sup>th</sup> input feature category (describing *glazing areas on the simulated floor level*). The MAE and RMSE on the validation data however increased, resulting in the feature being removed from the feature set. The minimum MAE and RMSE were reached at 0.78 MAE and 1.16 RMSE during the 9<sup>th</sup> sequence of the SFS after including 8, and removing 1 input feature categories. This was therefore considered the 'optimum' set of input features. In comparison to the complete set of 12 extracted input feature categories however, the improvement in accuracy was only marginal, as the original feature set showed errors of 0.79 MAE and 1.17 RMSE (indicated by a dashed blue reference line in Figure 6-7, Figure 6-8, Figure 6-9). Although this shows that the input feature selection did not result in a significant improvement of accuracies, not all input features were required for DA predictions, and overall training time could be reduced.

The training time of ANN models (including optimization of ANN architecture) was measured on a 2.6 GHz Intel Core i9 processor. ANN training of the model that included all 12 input features (26 individual features) had a duration of 05:55 (hh:mm). In comparison, training of the 'optimal' feature set with 8 input feature categories (19 individual features) took 03:23 hours. When further limiting the data to 7 added feature categories (16 individual features), training time was 02:32 hours. Predictions on the validation set were made in less than 1 second. Thus, using the proposed method, accuracies marginally improved compared to the empirically selected full set of input features. However, the training time for the ANN models could be reduced by 43% with the

optimum number of training features. After further input feature reduction, training time was reduced by 57% without significantly compromising the accuracies.

### 6.2.3 *Conclusions*

Several of the conclusions, that can be drawn from the work described in this section reinforce previous findings. During SFS, the MSE on the training data set did not directly correlate with the MAE and RMSE on the validation data set, as the prediction accuracies could improve (lower MAE and RMSE) even though the ability of the network to fit the data decreased (higher MSE). This was seen previously in the results of chapter 4 and 5. In chapter 4, the ANN architecture was optimized towards the MSE, which did not necessarily correlate with the MAE on the validation data set, especially when the number of hidden layers increased. In chapter 5, different numbers of training samples were tested. Again, the MSE did not necessarily correlate with the MAE, especially when the number of training samples was particularly low. The described discrepancy in MSE and MAE may also point to a weakness of the implemented SFS. Because the selection is based on the MAE of the reduced validation data set (13% of data from the entire design space), results may not be representative for the entire design solution space. This may even more so be the case when MSE and MAE differ from each other, i.e. when either one increases while the other decreases. A solution for the future work may be to remove an input feature only under the condition that both MSE and MAE decrease.

Another two limitations of the proposed SFS were identified. One pertains to the method on identifying the selection sequence. Consider the example, where the impact of design features on the daylight performance varies. Some features, such as the window to wall ratios, may result in a large variance in daylight results. Other features, such as the atrium well splay angles, may only result in small changes in daylight results. Nonetheless,

the splay angles are a crucial feature differentiating design solutions (i.e. according to orientation). The selection method may therefore bias features that show a greater impact on daylight results, while other features, despite necessary, are at risk of being discarded. Future work will have to ensure that this does not happen.

The other limitation pertains to the feasibility of the approach. The proposed method remains computationally expensive, as it requires multiple training runs with already computationally demanding ANNs. It would therefore be useful to through the SFS using smaller and more feasible network architectures (i.e. with 20, rather than 40 hidden neurons). Additionally, it may also be an option to completely rely on computationally less expensive ML models for feature selection. A comparison to alternative feature selection methods is therefore recommended.

In terms of input features required for predicting daylight in atrium buildings, *atrium distance and direction to atrium closest point* and *distance and direction to atrium centre* stood out as important input features. From the two, former showed a greater significance, as it was ranked first. The same results were confirmed in Section 6.1 of this chapter, in the manual selection and optimisation of input features, despite being performed on a different design space. Both features were required, which shows differences in illumination along the atrium well walls (e.g. center or edge). This aligns with the findings of Du and Sharples (2009), who showed different unobstructed vertical illuminances at different positions of the atrium width (i.e. at the center, 30%, 10% distance to atrium edge/corner).

The SFS also showed that having superfluous input features did not significantly lower accuracies (e.g. calculation grid size and atrium dimension at WP height). It did however increase training time. On the other hand, too few input features (i.e. before sequence 4 in Table 6-2) compromised prediction accuracies. The training time for ANNs could be reduced by 43% with the optimum number of training features, and up to 57%

without significantly compromising the accuracies. After further input feature reduction, training time was reduced by 57% without significantly compromising the accuracies. Due to potential bias from the sequence definition however, as explained above, it may be a better choice to select optimum input feature series with the lowest errors as opposed to the one with minimalized computational effort.

Overall, the empirically selected input feature series performed well in this study. In more complex design scenarios however, where the number of design variables is greater, it may become more difficult to empirically identify the appropriate training features. In such cases, the proposed selection method may prove to be valuable in sorting and identifying input features.

## 6.3 Finetuning of hyperparameters

For the design solutions space of 162 design variants, potential improvements to  $DA_{300}$  and  $sDA_{300/50\%}$  were investigated. Changes are made to the number of hidden layers in the network architecture, the training sample size, the number of design variables a model is trained on, and the number of training epochs.

### 6.3.1 *Sensitivity to network architecture and number of design variables*

Prediction accuracies were investigated following adjustments to ANN training data and network setting. ANN models were trained with data from 12 vs. 15 out of 54 simulations and one vs. two hidden layers. Additionally, one ANN ensemble was trained to predict  $DA_{300}$  and  $sDA_{300/50\%}$  for all WWR distribution series vs. three ensembles ANN ensembles trained to predict for one WWR series each.

Figure 6-10 shows the error margins in  $DA_{300}$  predictions for the investigated adjustments. As shown in the figure, prediction accuracies for  $DA_{300}$  increased either by

increasing the training data or increasing the number of hidden layers to two (as indicated by a decreasing MAE and RMSE). Three smaller ensembles trained individually performed better than one larger ensemble trained to predict for all WWR distribution series. When training the ANN ensemble with 300, instead of 200 epochs, accuracies slightly deteriorated. Over – and under estimations for DA<sub>300</sub> cancelled each other out for the most part, with a minor over-estimation of less than 0.01 DA prevalent for all ANN models.

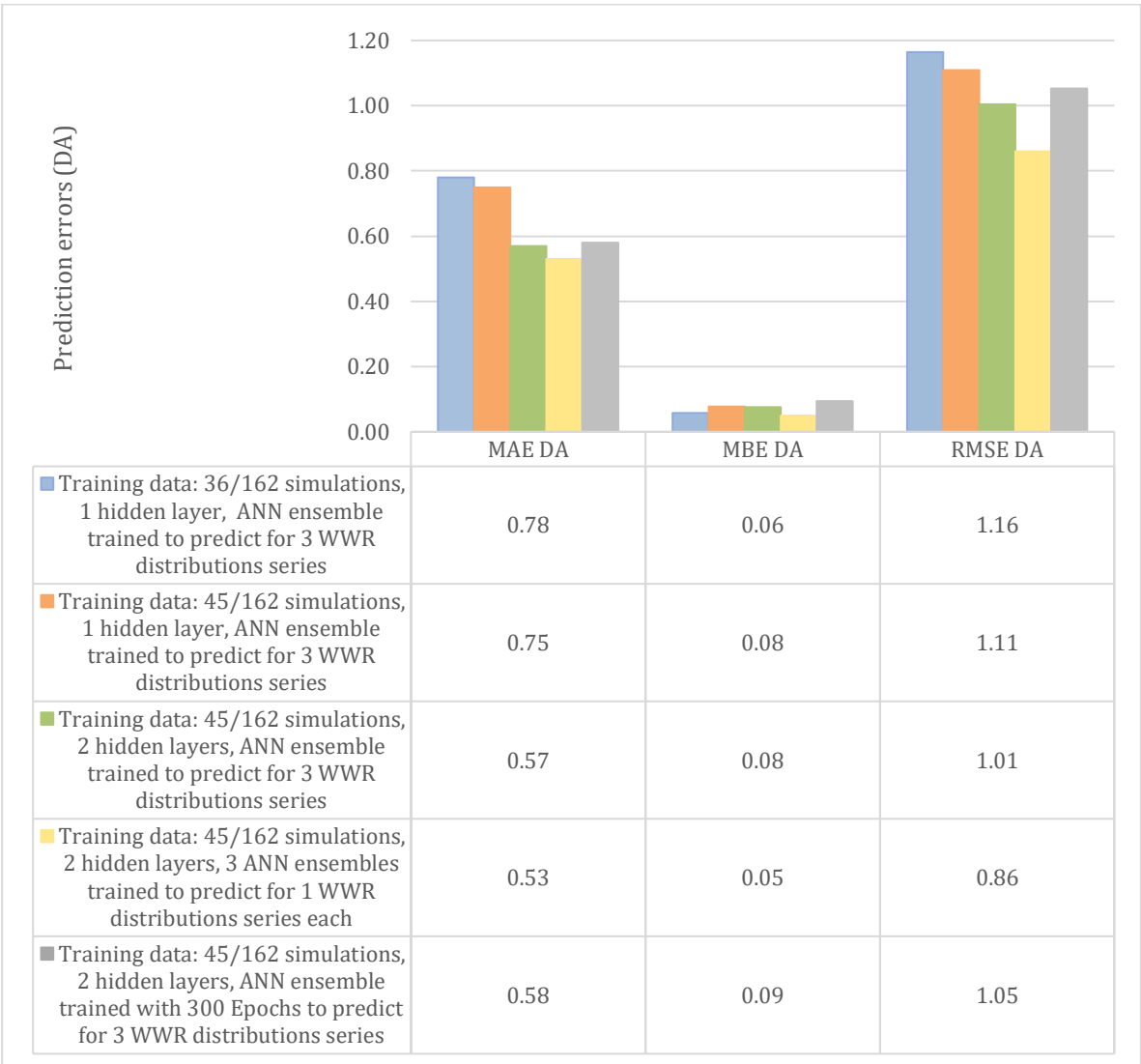


Figure 6-10 MAE, MBE and RMSE for DA<sub>300</sub> predictions

The results observed for the DA<sub>300</sub> predictions did not translate to sDA<sub>300/50%</sub> predictions. Figure 6-11 shows the error margins sDA<sub>300/50%</sub> predictions for the

investigated adjustments. Despite improvements in accuracy of around 0.3%  $DA_{300}$ , errors for  $sDA_{300/50\%}$  remained similar. Only a slight increase in errors was observed when using ANN ensembles with one, instead of two hidden layers, and also when training ANN ensembles individually on the WWR distribution series, latter of which stands in contrast to previous observations. Interestingly, another contrast to  $DA_{300}$  prediction accuracies is that  $sDA_{300/50\%}$  was consistently underestimated, as indicated by the MBE. Moreover, the MBE marginally increased with the number of training samples and hidden layer size, again contrasting results for  $DA_{300}$  predictions. In order to shed more light on this matter, the variance in errors (for  $sDA_{300/50\%}$ ) was investigated. Results are presented in Table 6-3.

The variance in absolute errors showed that most consistent prediction accuracies were achieved with ANN ensembles trained with two hidden layers, on all three WWR distribution series, and with 300 training epochs. In contrast to the results obtained for  $DA_{300}$  predictions, ANNs trained on multiple design variables of similar natures (i.e. the WWR distribution), were able to predict the DA 50 threshold more accurately (see MAE, RMSE in Figure 6-11) and with a lower variance in errors (see Table 6-3).

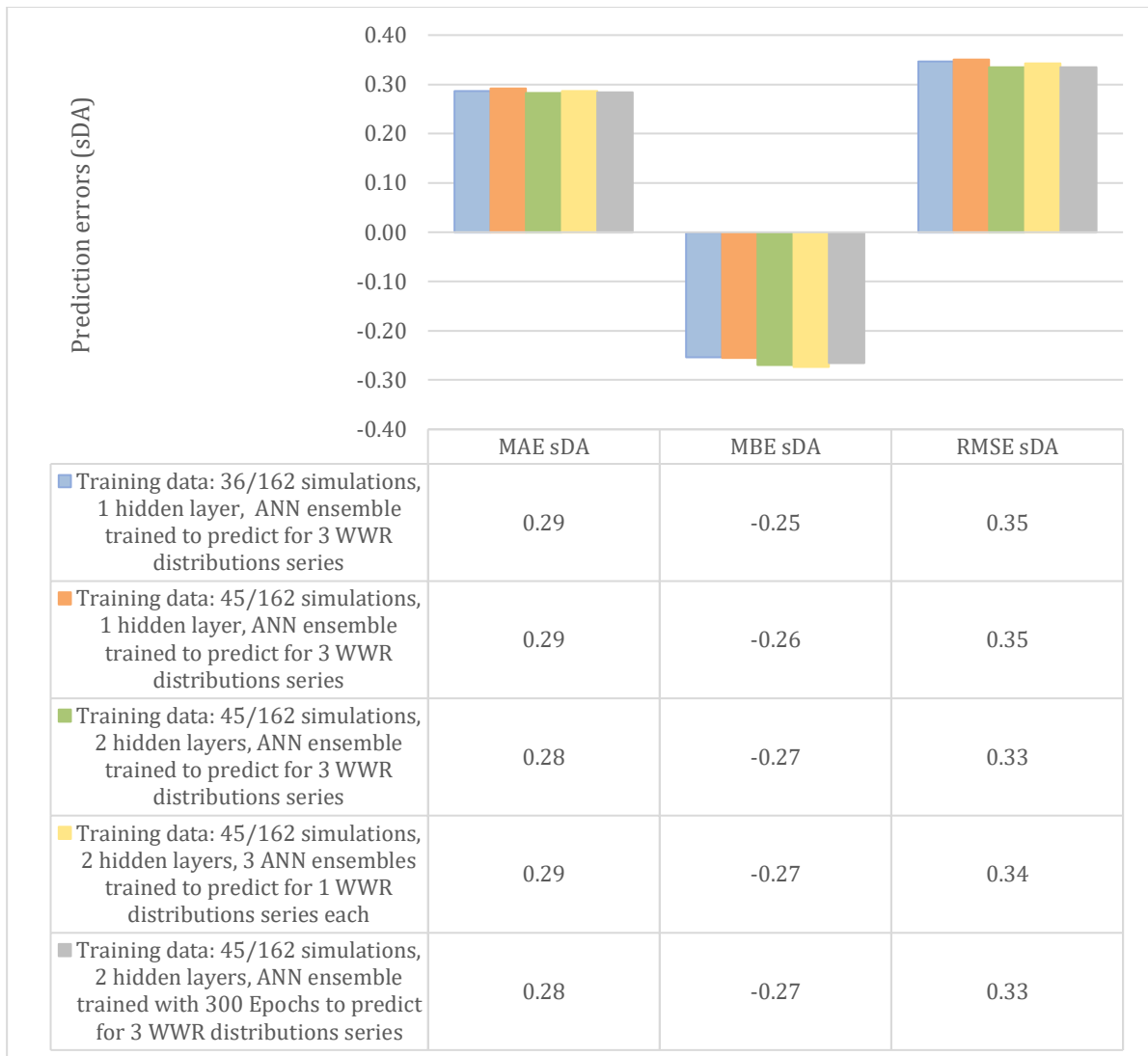


Figure 6-11 MAE, MBE, RMSE for sDA<sub>300/50%</sub> predictions

	Training data: 36/162 simulations, 1 hidden layer, ANN ensemble trained to predict for 3 WWR distributions series	Training data: 45/162 simulations, 1 hidden layer, ANN ensemble trained to predict for 3 WWR distributions series	Training data: 45/162 simulations, 2 hidden layers, ANN ensemble trained to predict for 3 WWR distributions series	Training data: 45/162 simulations, 2 hidden layers, 3 ANN ensembles trained to predict for 1 WWR distributions series each	Training data: 45/162 simulations, 2 hidden layers, ANN ensemble trained with 300 Epochs to predict for 3 WWR distributions series
Variance in absolute errors	0.038	0.038	0.033	0.036	0.032

Table 6-3 Variance in sDA<sub>300/50%</sub> prediction accuracies

### 6.3.2 Conclusions

Deeper ANN architectures outperformed shallow networks. The improvement in prediction accuracy was however more noticeable for the  $DA_{300}$  metric than the  $sDA_{300/50\%}$  metric. Mean biased errors for  $DA_{300}$  predictions were close to 0, indicating no particular tendency of over- or underestimating results. Interestingly however,  $sDA_{300/50\%}$  was consistently underestimated. This means that there is a possibility to apply a correcting factor to the 50 DA threshold so as further improve the emulated results.

In line with previous findings, prediction accuracies for  $DA_{300}$  dropped, the more design variables the ANN was trained on, or the larger the design solutions space. The findings in this chapter however also showed, that ANNs trained on a larger design solution space were able to fit the DA50 threshold better, thus providing more reliable results and better accuracies for  $sDA_{300/50\%}$ . As this may vary with the test data used, this will need to be examined more thoroughly in future work.

## Chapter 7

# Daylight Performance Results: Evaluation of Atrium Design Changes

The central goal of using ANNs was to efficiently map the daylight performance of all solutions in the design space. The obtained results of atrium design solutions for combinations of atrium geometry, orientation, and WWR distribution are presented in this and the following chapter. Results are based on the following performance metrics:  $DA_{100}$ ,  $DA_{300}$ ,  $DA_{2000}$ ,  $sDA_{100/50\%}$ ,  $sDA_{300/50\%}$ , UDI-e and  $ASE_{1000,250h}$  (see Figure 7-1).  $DA_{100}$  and  $sDA_{100/50\%}$  are the inverted results for UDI-f (UDI-‘fell short’, where daylight would be considered insufficient, as proposed by Mardaljevic *et al.*, 2012).  $DA_{2000}$  is written as UDI-e (UDI-‘exceeded’, where daylight would be considered excessive and cause glare). These daylight metric results can be distinguished between those describing the % of time for a specified illuminance threshold, and those describing a % of space (aggregated performance) for a specified time and illuminance threshold (as illustrated in Figure 7-1).

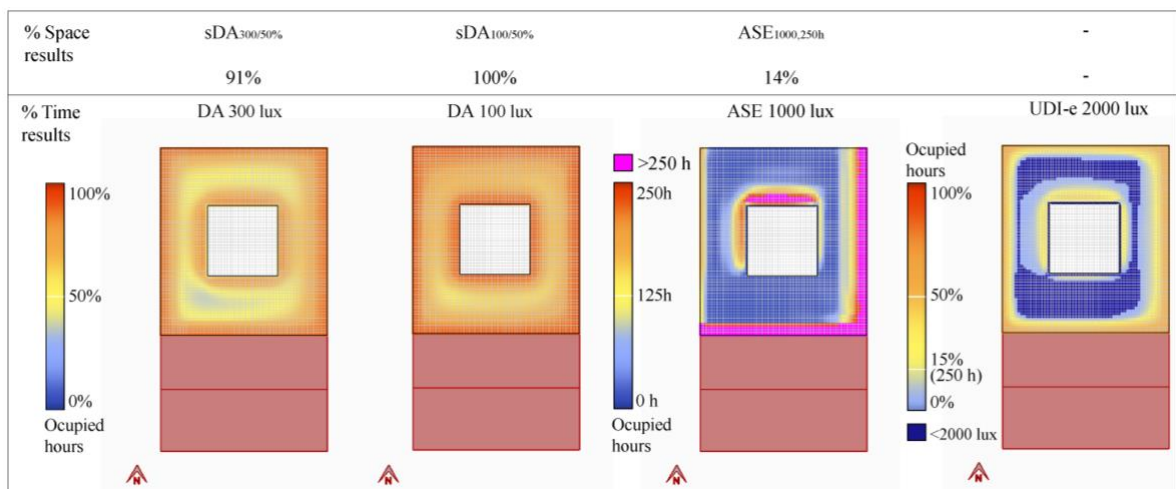


Figure 7-1 Examples of performance metrics and the two types of results

First, the %-space results are presented to give an overview of the obtained metric results for all design solutions. This chapter then focuses on key findings in terms of the efficiency of different atrium design strategies for improving daylight penetration into the atrium and atrium adjacent space. Chapter 8 focuses on key findings resulting from the comparison and evaluation of different daylight metrics and their potential to inform atrium design. All key findings are based on the in-depth analysis of results and discussion in 'Appendix A -Daylight Analysis: Percentage-of-Time Results' and 'Appendix B – Daylight Analysis: Percentage-of-Space Results'.

The findings are drawn from trends and patterns in the %-space results, in combination with %-time results. The latter were not only found to provide explanations for the observed %-space results, but also revealed new causalities for the impact of atrium design changes on daylight performance.

## 7.1 Overview of results

This section provides an overview of %-space results for all 162 design solutions. Results of all six floors for  $sDA_{300/50\%}$ ,  $sDA_{100/50\%}$ , and  $ASE_{1000,250h}$  are briefly presented. To improve legibility, the %-time results are presented in graphical format, to be read as shown in Figure 7-2: The orientation of each atrium design solution is indicated at the head, and the atrium base area (atrium geometry) at the foot of the illustration. Atrium design solutions with a central orientation are highlighted with a filled-in marker. The specific WWR distribution of the design solution is indicated by the hue of the markers; the darkest hue for the distribution series of 50, 60, 70, 80, 90, 100% WWR, and the lightest hue for a distribution series of 20, 30, 40, 50, 60, 100% WWR.

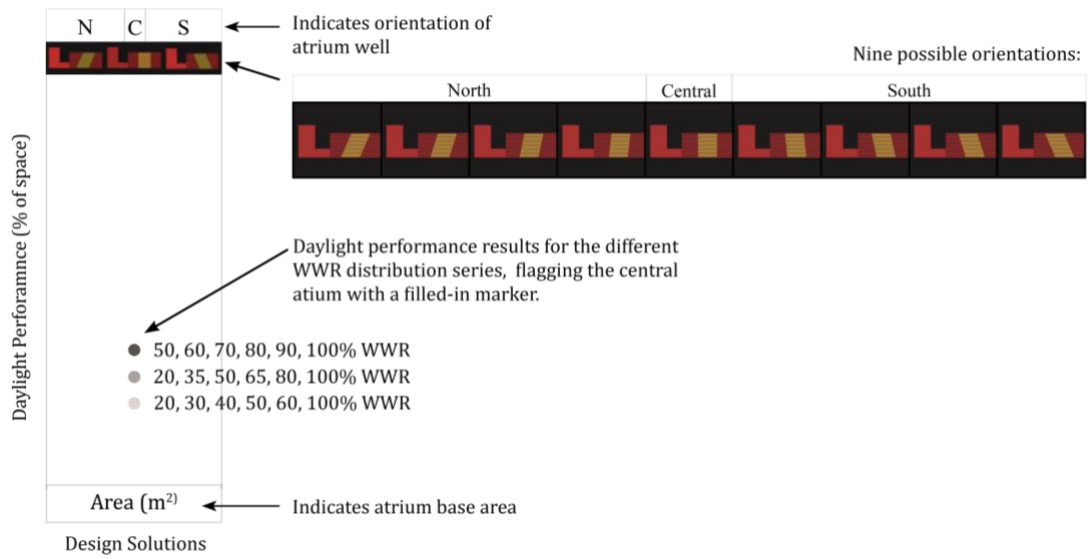


Figure 7-2 Graphic format in which results are presented

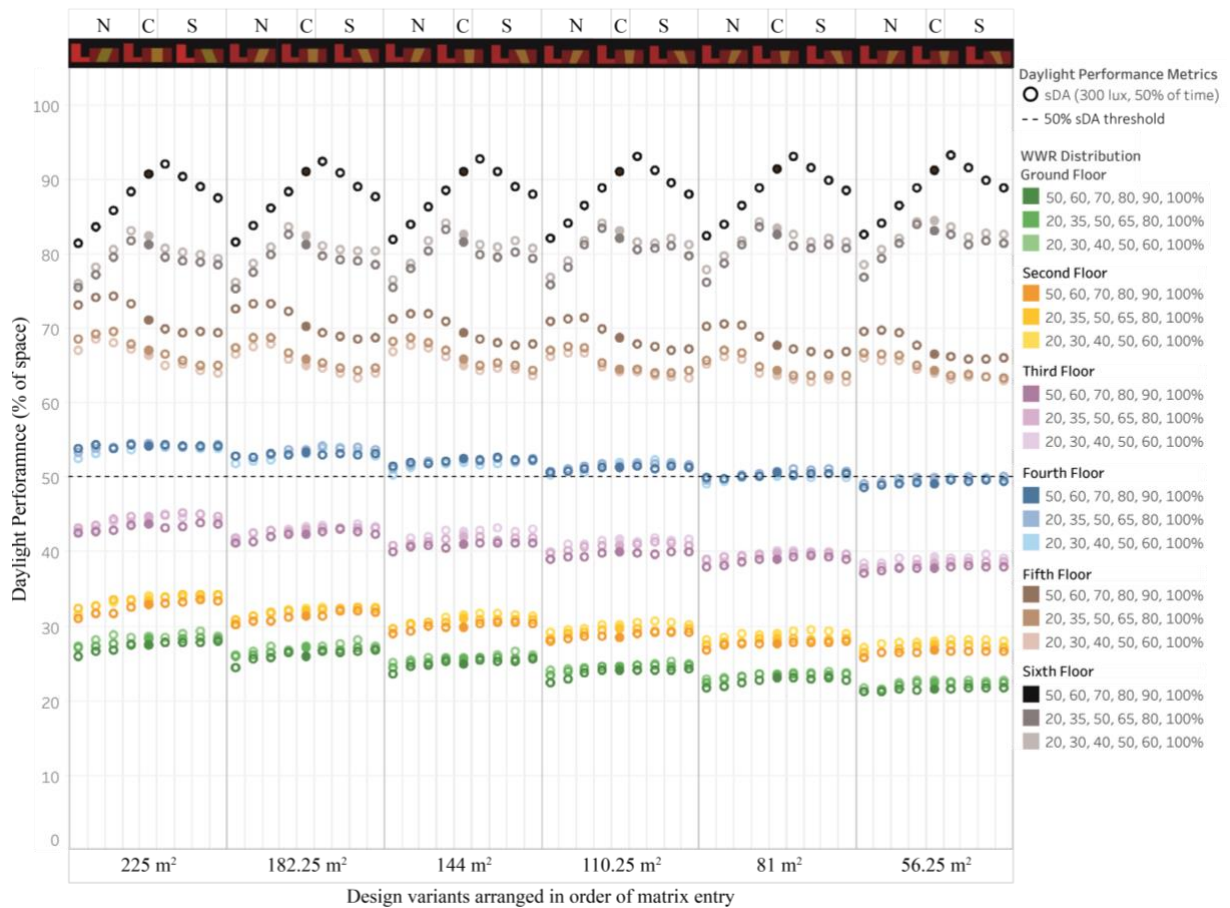


Figure 7-3 sDA<sub>300/50%</sub> performance in atrium adjacent spaces: ground to top floor

sDA<sub>300/50%</sub> results are presented in Figure 7-3. As shown in the figure, sDA<sub>300/50%</sub> levels in atrium adjacent spaces varied across floor levels, ranging from 21% on the ground floor to 93% on the sixth floor, increasing in value with each floor level. Initial

observations could be made regarding the influence of the three design variables atrium geometry, atrium well orientation, and WWR distribution on daylight levels. Patterns were most varied on the top two floors and less so on the lower floors, with the fourth floor showing the least variation in results. In terms of atrium geometry, reducing the atrium base area reduced  $sDA_{300/50\%}$  on the lower five floors. On the fifth floor, this pattern began to reverse for the smallest two atrium base areas. On the sixth floor, reducing the atrium base area marginally increased  $sDA_{300/50\%}$  throughout.

In terms of WWR distribution, the series starting with 20% WWR showed higher  $sDA_{300/50\%}$  on the lowest three floors. However, for the fourth floor, there were barely any differences in daylight levels between the WWR series. For the top two floors, an opposite trend to the lower floors was observed, such that WWR distribution series starting with 50% WWR showed the highest  $sDA_{300/50\%}$  results. Again, the magnitude of variation between results based on changing the WWR distribution was much higher on the top two floors than on the lower floors.

In terms of orientation, patterns appeared to be consistent on the lower four floors and indicated that southward orientations were the more favourable solution to increase  $sDA_{300/50\%}$ . This pattern was different on the top two floors. For these floors, northward orientations performed better for the most part, with slightly southward orientations showing higher  $sDA_{300/50\%}$  for the 50% WWR distribution series on the sixth floors. Differences could also be seen in the magnitude of variation between results related to changing the orientation. For the lower floors, the variation was marginal, whereas for the top floors, changes in orientation resulted in vastly different outcomes in daylight performance.

Taken together, patterns and trends changed depending on the combination of design variables and the floor level. The influence of atrium geometry, atrium

orientation, and WWR distribution on  $sDA_{300/50\%}$  could therefore not be expressed in a unified manner across floors: whereas reducing the atrium base area reduced  $sDA_{300/50\%}$  on the lower floors, the opposite effect was seen on the top floor. Furthermore, southward orientations improved  $sDA_{300/50\%}$  on lower floors only, while northward or more central orientations provided higher  $sDA_{300/50\%}$  results on top floors. Lastly, reducing overall glazing areas improved  $sDA_{300/50\%}$  on lower floors. The contrary was evidenced on top floors. Considering that the spaces on lower floors achieved daylight levels below the recommended threshold, it may be advisable to focus on strategies aimed at improving daylight on those floor levels, despite the choices being less effective (as indicated by a smaller variation in results on those floors). To gain further insight into the influence of the design variables on daylight, the  $sDA_{100/50\%}$  metric results are presented next.

$sDA_{100/50\%}$  results are shown in Figure 7-4. As indicated by the figure,  $sDA_{100/50\%}$  in atrium adjacent spaces ranged from 47% on the ground floor to 100% from the fourth floor onwards. In terms of the influence of design variables, reducing the atrium base area reduced daylight levels. This aligns with the observations made for the  $sDA_{300/50\%}$  metric (Figure 7-3), although the magnitude of variation between results is greater for  $sDA_{100/50\%}$ .

In terms of WWR distribution, the results echoed those seen for the  $sDA_{300/50\%}$  metric, with distribution series with the lowest overall glazing area (series starting with 20% WWR) achieving higher results on the ground to third floor. From the fourth floor onwards, results cannot be compared, as the entire floor area achieved 100%  $sDA_{100/50\%}$  (displayed in black in Figure 7-4, as data points overlap).



Figure 7-4 sDA<sub>100/50%</sub> performance in atrium adjacent space: ground to top floor

In terms of orientation, optimal orientation on the ground floor changed with every smaller atrium base area, from more northward to central orientations. For larger areas (e.g., 225m<sup>2</sup>), northward orientations achieved the highest sDA<sub>100/50%</sub> results, whereas central and even slightly southward orientations showed higher sDA<sub>100/50%</sub> for smaller areas (e.g., 56.25 m<sup>2</sup>). This pattern was reflected on the second floor as well, although the magnitude of variation was smaller, and change occurred more gradually. On the third floor, northward orientations showed higher sDA<sub>100/50%</sub> for the majority of design solutions. A change in pattern was only visible for the daylight distribution series starting with 50% WWR and the smallest atrium base area (56.25 m<sup>2</sup>).

The next section takes a closer look at ASE, a metric intended to highlight potentially overlit areas, which increases the risk of glare and visual discomfort. The

calculation method varies from the previous two metrics in that the simulation was run with 0 ambient bounces. As a result, only direct sunlight contributions were measured. The ASE results for all floors are shown in Figure 7-5.

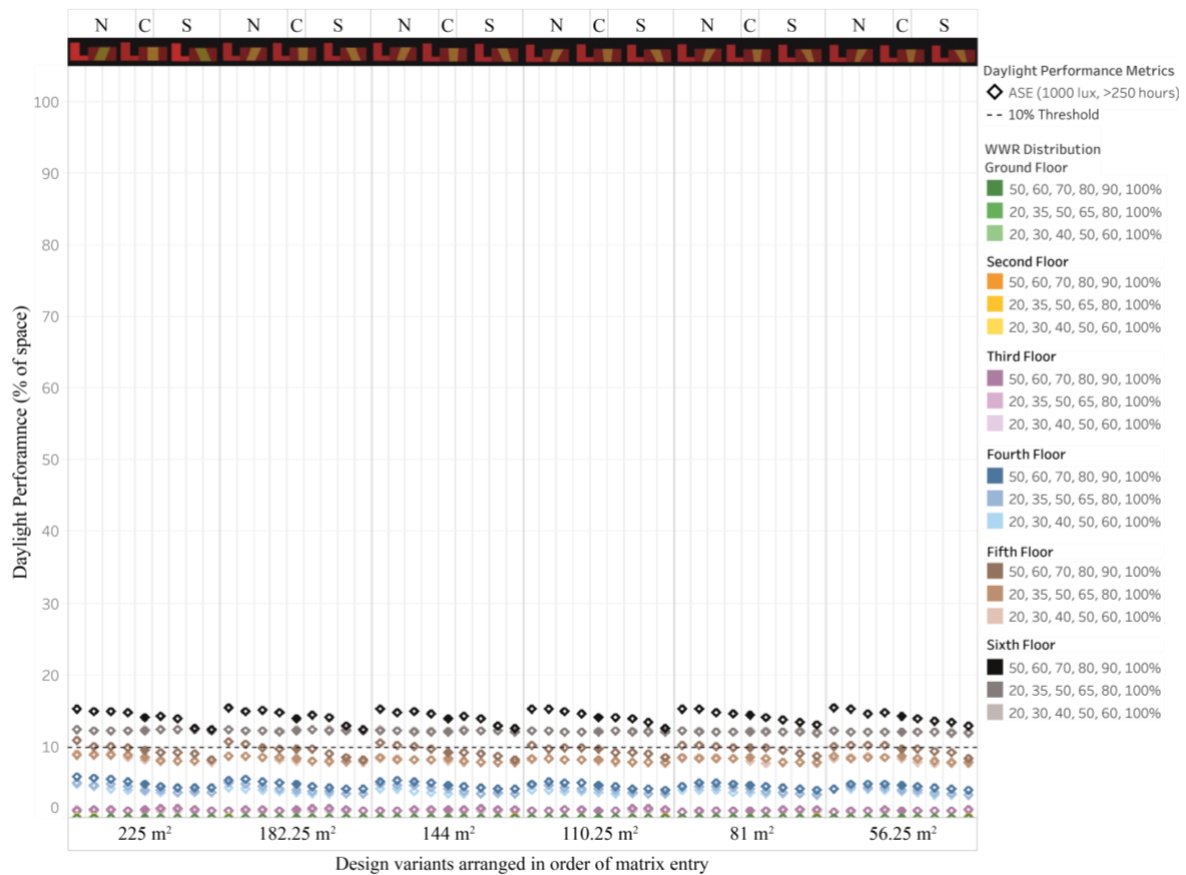


Figure 7-5 ASE performance in atrium adjacent space: ground to top floor

As seen in the figure, ASE ranged from 0 to 16% and varied across floor levels. On the first two floors, no area was hit by direct sunlight for more than 250 of occupied hours. From the third floor onwards, exposure to direct sunlight increased. Patterns and trends differentiating the various design solutions became more visible on higher floor levels, where Atrium design changes had a greater impact on ASE results.

In terms of atrium base area, ASE results were barely affected. In terms of WWR distribution, the figure shows that the greater the overall glazing area, the greater the sunlight exposure. Specifically, the WWR distribution series starting with 50% WWR showed distinctly higher ASE than the WWR series starting with 20% WWR. The

magnitude of variation in results between the two increased with the floor level, attributable to the greater daylight availability on upper floors (due to the lack of obstructions).

In terms of atrium well orientation, northmost orientations showed a higher ASE on the sixth and fifth floors. On the fourth floor, a shift in trend became visible, whereby less steeply northward orientated atria showed higher ASE, the smaller the atrium base area. Only the 20% WWR distribution series on the sixth floor was not affected by changes in orientation (due to the narrow window area). The variation in results from the third to ground floors was too small to decisively uncover trends.

Taken together, atrium design changes in terms of WWR distribution showed consistent and predictable patterns, as larger window areas showed higher ASE. In contrast, the other two metrics showed shifts in trends from top to lower floors, with smaller overall glazing areas showing higher results on the lower floors. In terms of orientation, shifts in trends were noticeable for all three metrics. Whereas northmost orientations showed the highest ASE on the 6<sup>th</sup> and 5<sup>th</sup> floors, this changed from the fourth to lower floors.  $sDA_{300/50\%}$  showed the highest results mostly for northward orientations on the 6<sup>th</sup> and 5<sup>th</sup> floors, and highest results for southward orientations from the 4<sup>th</sup> to the ground floor.  $sDA_{100/50\%}$  showed metric optima for different orientations depending on the atrium base area and floor level. For the second and ground floors, larger atria showed higher  $sDA_{100/50\%}$  for northward orientations, and smaller atria had higher  $sDA_{100/50\%}$  for more central orientations, with northward and northmost orientations showing the lowest  $sDA_{100/50\%}$ . Thus, all three metrics provide a different perspective on the consequences of design choices.

To conclude, ASE allowed tracing direct sunlight exposure, while the sDA metrics additionally indicated reflected daylight. ASE showed little variation in results

and suggested that only little direct sunlight penetrated deep into the atrium well and reached atrium adjacent spaces. All metrics are limited by an absolute threshold (e.g. 250 h for ASE, 50% DA for  $sDA_{300/50\%}$ ) and thus do not provide information on the distribution of daylight within the atrium and atrium adjacent spaces. Therefore, the %-time results (simulation plots for the design solutions) are presented alongside observations in the next sections to lend support to the findings on the impact of atrium design changes on daylight performance.

## 7.2 Impact of atrium design changes on daylight

### 7.2.1 *Design solutions increasing daylight on lower floors*

Initial observations were made regarding the influence of the three design variables atrium geometry, WWR distribution, and atrium well orientation on daylight performance on the lower floors. Reducing the atrium well geometry resulted in lower  $sDA_{300/50\%}$  and  $sDA_{100/50\%}$  performance (starting from the 5<sup>th</sup> floor downwards). Reducing the overall glazing area, in comparison, resulted in higher  $sDA_{300/50\%}$  and  $sDA_{100/50\%}$  performance (starting from the 4<sup>th</sup> floor downwards), as the WWR distribution series with 20, 30, 40, 50, 60, 100% WWR, and 20, 35, 50, 65, 80, 100% WWR from top to ground floors outperformed the WWR distribution series with 50, 60, 70, 80, 90, 100% WWR. Regarding orientation, southward orientated atria showed a higher  $sDA_{300/50\%}$  performance (starting on the 4<sup>th</sup> floor).  $sDA_{100/50\%}$  results were more mixed, showing optima for different orientations depending on the floor level and atrium base area. The impact of both WWR distribution and atrium well orientation are presented in more detail in the following.

To illustrate the impact of WWR distribution on daylight performance on lower floors, %time results are shown for four representative design solutions on the ground floor. The selected design solutions are highlighted in Figure 7-6. The four design variants have northmost and southmost orientations and a WWR distribution of 50, 60, 70, 80, 90, 100% and 20, 30, 40, 50, 60, 100%.

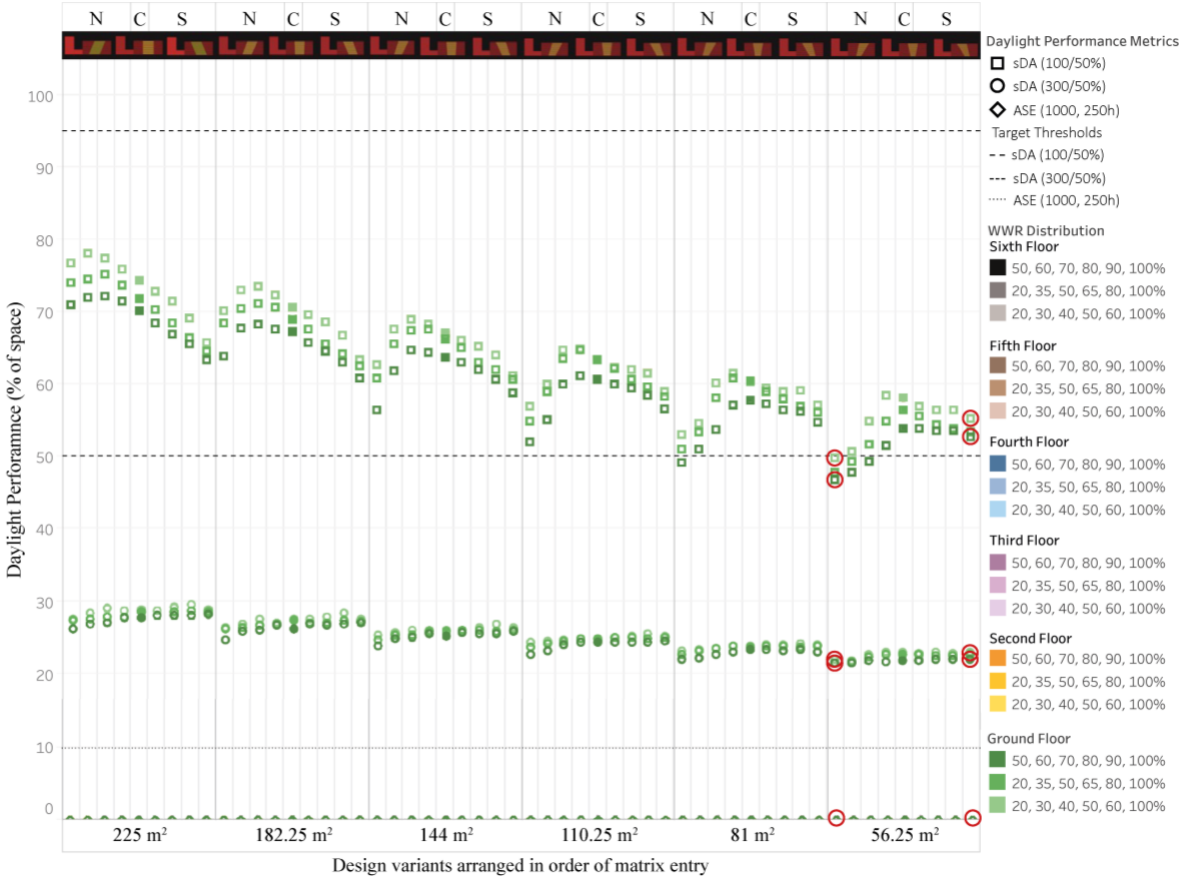
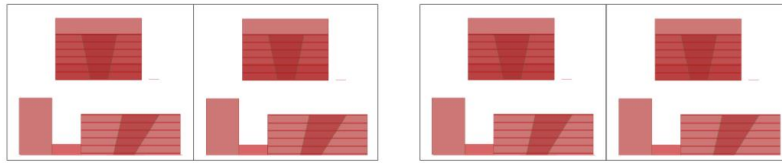


Figure 7-6 sDA<sub>300/50%</sub>, sDA<sub>100/50%</sub> and ASE results on the ground floor.

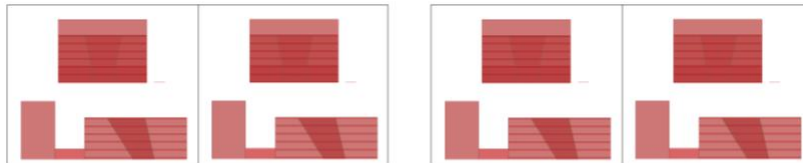
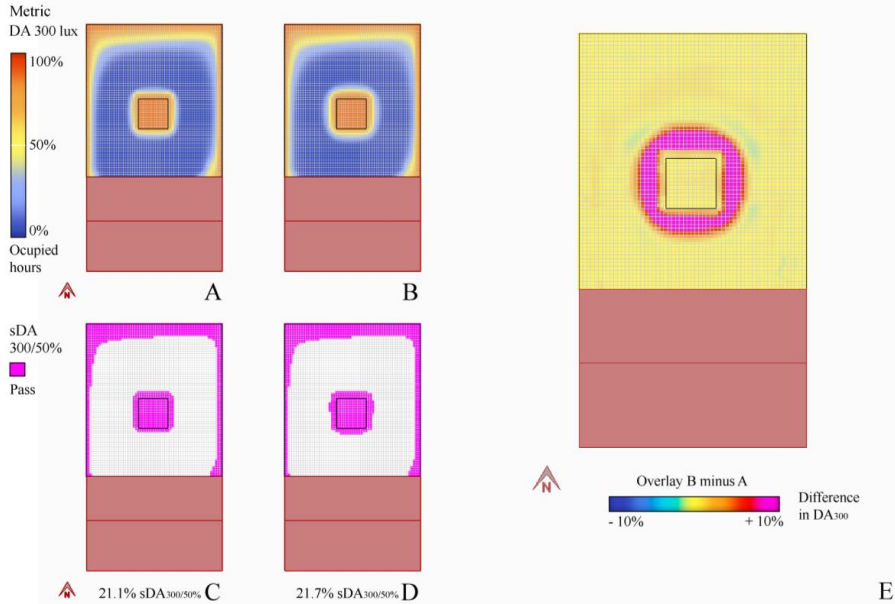
DA<sub>300</sub> and sDA<sub>300/50%</sub> plots for the specified design solutions on the ground floor are shown in Figure 7-7. DA<sub>100</sub> and sDA<sub>100/50%</sub> plots are shown in Figure 7-8. The increase in daylight resulting from lower WWR across the atrium façade is displayed by means of an overlay of DA<sub>300</sub> plots in Figure 7-7 and DA<sub>100</sub> plots in Figure 7-8. As shown in the figures, the WWR distributions series with 20, 30, 40, 50, 60, 100% showed a deeper daylight penetration into atrium adjacent spaces. Areas surrounding the atrium were able to achieve DA<sub>300</sub> and DA<sub>00</sub> for at least 10% more

occupied hours in a year (see pink hue Figure 7-7 , Figure 7-8 E, E2). These findings can be explained by the reduction of glazing area (light admitting area), and therefore an increase of reflected daylight within the atrium well, resulting in a deeper daylight penetration into the atrium well and atrium adjacent space. This effect was especially noticeable on the third floor, where the majority of design solutions with a smaller window area of 50% WWR showed higher  $sDA_{300/50\%}$  than those with a larger window area of 65% WWR. The displayed difference of 1%  $sDA_{300/50\%}$  (Figure 7-7 D2), and 3.1%  $sDA_{100/50\%}$  (Figure 7-8 D) equate to an additional floor area of 14 m<sup>2</sup> and 42 m<sup>2</sup> meeting the thresholds respectively. This improvement is particularly notable, as it occurred on lower floors where daylight levels fell below recommended thresholds, and the additional daylight reached beyond what was visible from the %space results alone (as shown by the overlays). To simulate the full impact of reflected daylight within the atrium, a higher number of ambient bounces than those used for the current analyses may be advisable.

Figure 7-9 presents the ASE and UDI-e result plots, to further illustrate the impact of WWR distribution on daylight levels on lower floors. The overlay of UDI-e results, in particular, showed an increase of illuminances exceeding 2000 lux in the atrium and in atrium adjacent spaces (Figure 7-9 J, J2). For northmost orientations,  $DA_{2000}$  mostly increased in the atrium and in spaces to the north of the atrium well. For southmost orientations, the increase in  $DA_{2000}$  was noticeably deeper into atrium adjacent spaces than seen for northmost orientations. Here,  $DA_{2000}$  increased most notably in spaces to the south, east, and west when reducing overall glazing area. Thus, reducing the overall glazing area across the atrium well façade, especially by reducing WWR on the top floors, improved daylight penetration into atrium adjacent spaces on lower floors.



Floor level Ground floor  
 Atrium base area 56.25m<sup>2</sup>  
 WWR distribution 50, 60, 70, 80, 90, 100% 20, 30, 40, 50, 60, 100%  
 Orientation Northmost (1) Northmost (1)



Floor level Ground floor  
 Atrium base area 56.25m<sup>2</sup>  
 WWR distribution 50, 60, 70, 80, 90, 100% 20, 30, 40, 50, 60, 100%  
 Orientation Southmost (9) Southmost (9)

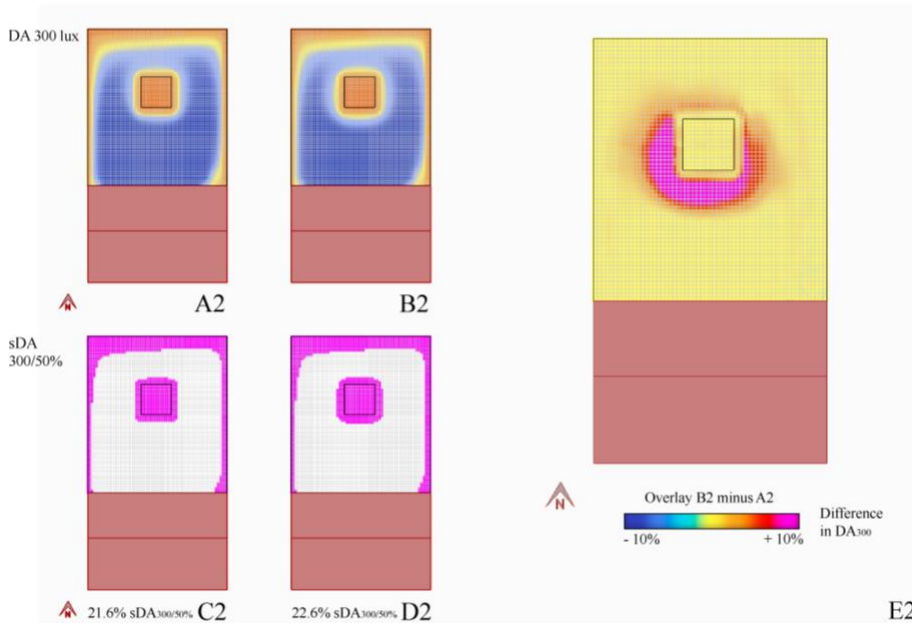


Figure 7-7 DA<sub>300</sub> and sDA<sub>300/50%</sub> result plots for the specified design solutions, highlighting the impact of WWR distribution on daylight results on the ground floor. The %space sDA results provided below the plots refer to atrium adjacent spaces only.

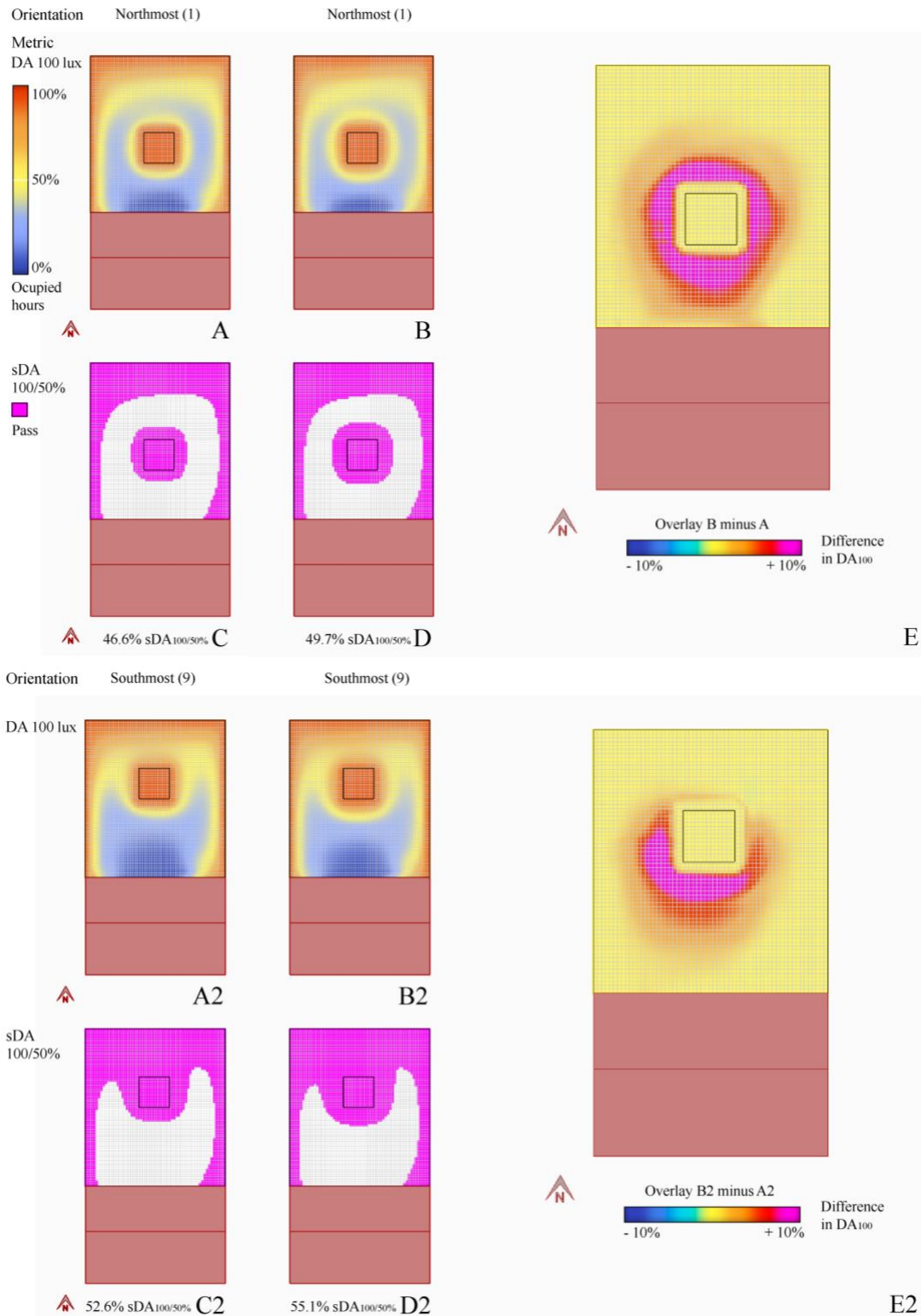


Figure 7-8 DA<sub>100</sub> and sDA<sub>100/50%</sub> result plots for the specified design solutions on the ground floor. The %space sDA results provided below the plots refer to atrium adjacent spaces only.

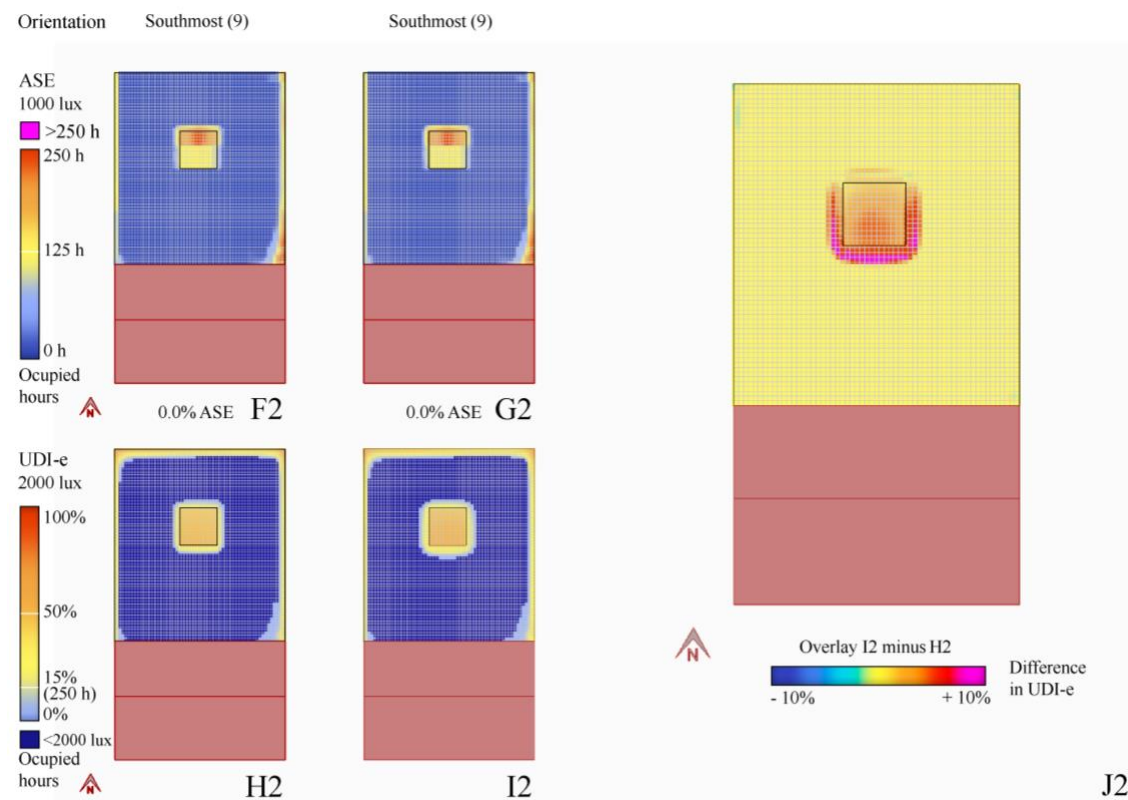
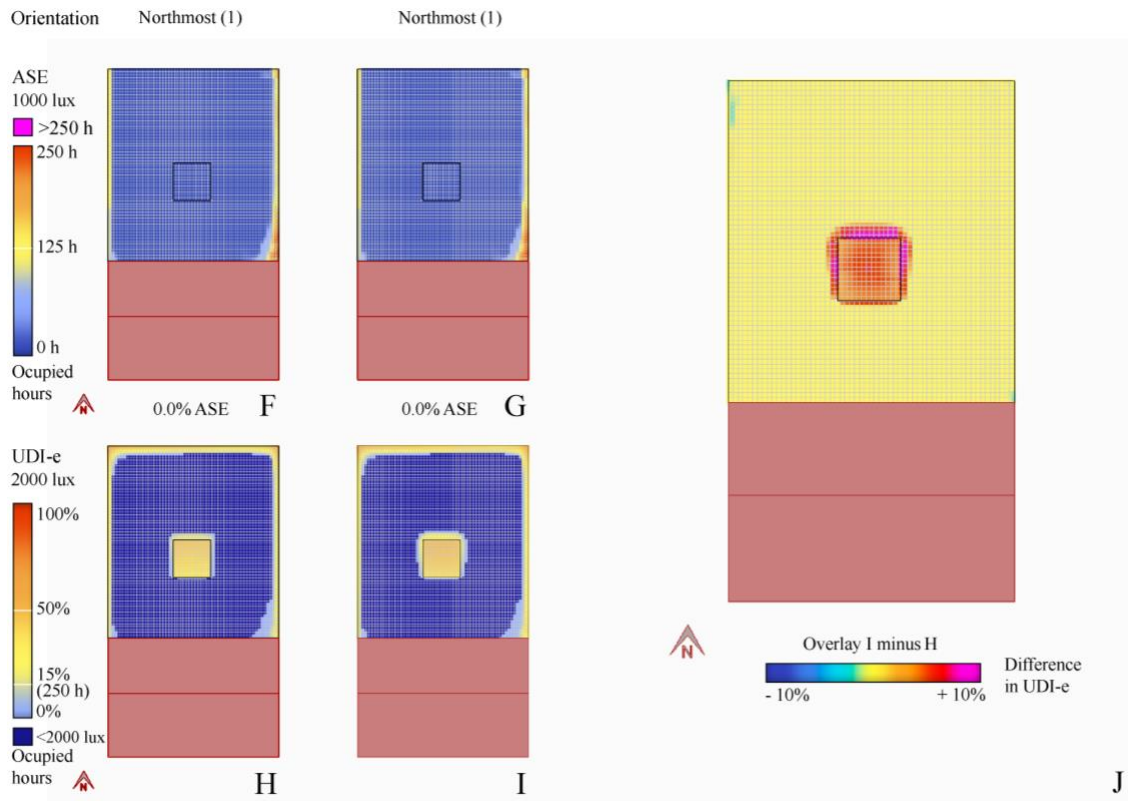


Figure 7-9 ASE and UDI-e result plots for the specified design solutions on the ground floor.

To illustrate the impact of orientation on daylight performance on lower floors, %time results are shown for four representative design solutions on the ground floor. The selected design solutions are highlighted in Figure 7-10. The selected design solutions have a northmost, northward, central, southward, and southmost orientation with an atrium base area of 56.25m<sup>2</sup>. Results are shown for design solutions from the WWR distribution series starting with 50% WWR.

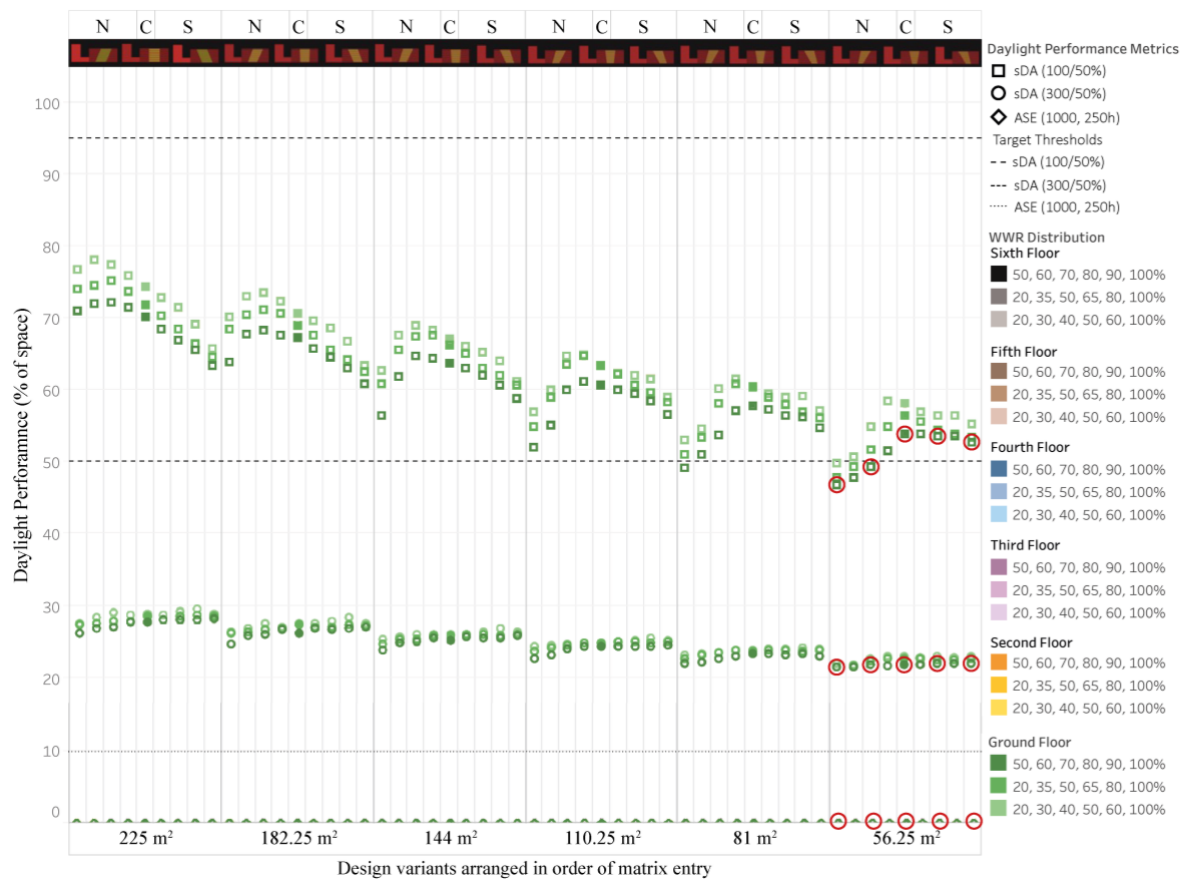


Figure 7-10 sDA<sub>300/50%</sub>, sDA<sub>100/50%</sub> and ASE results on the ground floor.

Figure 7-11 shows the DA<sub>300</sub> and sDA<sub>300/50%</sub> plots for the specified design solutions on the ground floor. Figure 7-12 shows the DA<sub>100</sub> and sDA<sub>100/50%</sub> plots. The latter results were heavily influenced by the position of the atrium well within the floor plan, and the increasing room depth and overshadowing from the attached building associated therewith. In comparison, the differences in sDA<sub>300/50%</sub>, although marginal, occurred in spaces directly surrounding the atrium well only. Thus, when looking to

generalise results, sDA300/50% results point to an increase of daylight into atrium adjacent spaces for southward orientations. An increase could be confirmed by looking at the UDI-e and ASE plots in Figure 7-13. ASE results showed that southmost orientations received the most direct sunlight at the atrium base, resulting from an alignment of the atrium well with solar altitude angles (Figure 7-13 N2, O2). UDI-e plots also showed a deeper daylight penetration into atrium adjacent spaces for southward, rather than northward orientations (light blue hue all around the atrium well instead of only to the north of the atrium, Figure 7-13 S2, T2). To further highlight the difference in DA<sub>300</sub>, DA<sub>100</sub>, and DA<sub>2000</sub> for different orientations, the DA results for the northmost orientation were subtracted from the DA results for the southmost orientation by superimposing both results at the location of the atrium well (Figure 7-14). The overlays for DA<sub>300</sub>, DA<sub>100</sub>, and DA<sub>2000</sub> all showed an overall deeper daylight penetration into atrium adjacent spaces for southward orientations. This is especially noticeable in spaces to the south, east, and west of the atrium well. The northward orientations, by comparison, showed higher DA<sub>300</sub>, DA<sub>100</sub>, and DA<sub>2000</sub> in a small area to the north of the atrium well (Figure 7-14). This result can be explained by the alignment of the atrium well with solar altitude angles for southward orientations (resulting in a deeper daylight penetration into the atrium well), as well as the splaying of atrium well façades towards the skylight (resulting in more daylight in atrium adjacent spaces to the north of the atrium well when the south-facing atrium well façade is splayed towards the skylight in northward orientations, and daylight in atrium adjacent spaces to the south of the atrium well when the north-facing atrium well façade is splayed towards the skylight in southward orientations).

In conclusion, two design changes improve daylight penetration into atrium adjacent spaces on lower floors: reducing overall glazing area of the atrium well façade

by reducing WWR on the top floors to increase reflected light, and a more southward orientation of the atrium well to align the atrium well with solar altitude angles.

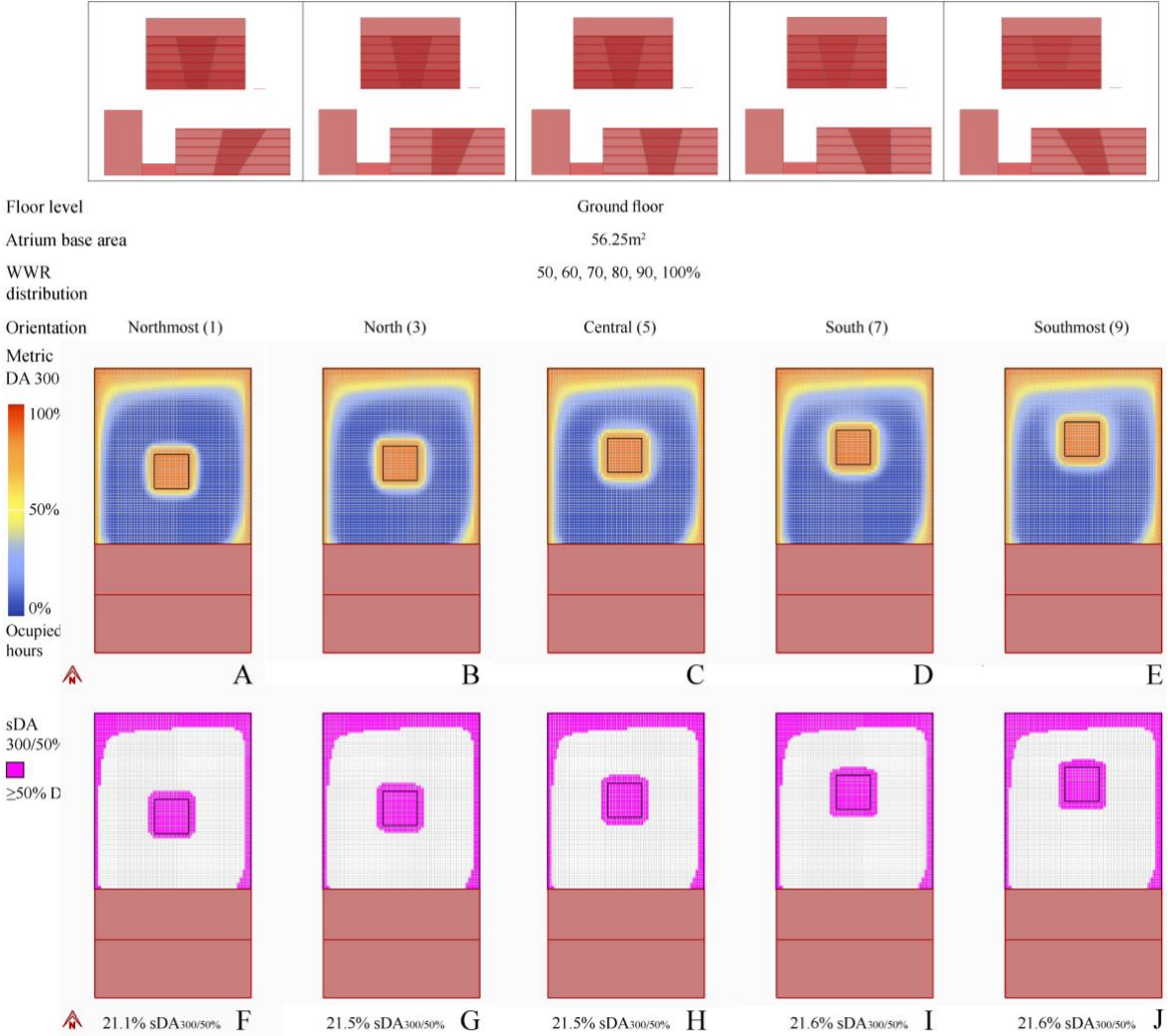


Figure 7-11 DA<sub>300</sub> and sDA<sub>300/50%</sub> result plots for the specified design solutions, highlighting the impact of atrium area orientation on daylight performance on the ground floor. The %space sDA results provided below the plots refer to atrium adjacent spaces only.

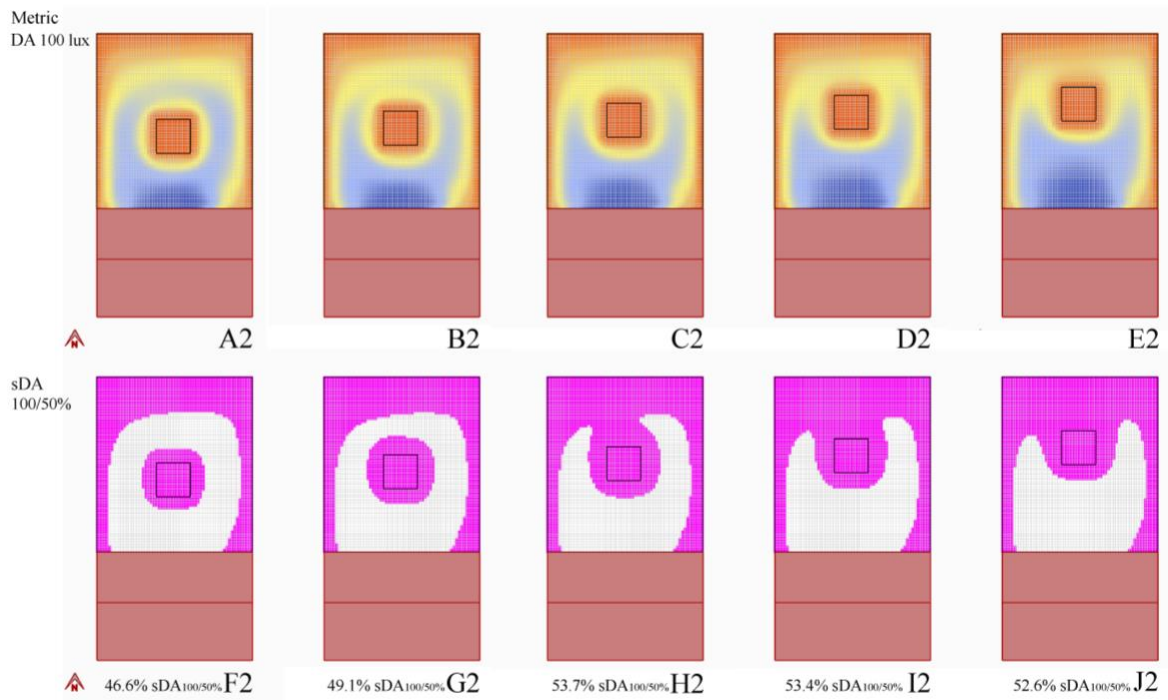


Figure 7-12 DA<sub>100</sub> and sDA<sub>100/50%</sub> results plots for the specified design solutions on the ground floor. The %space sDA results provided below the plots refer to atrium adjacent spaces only.

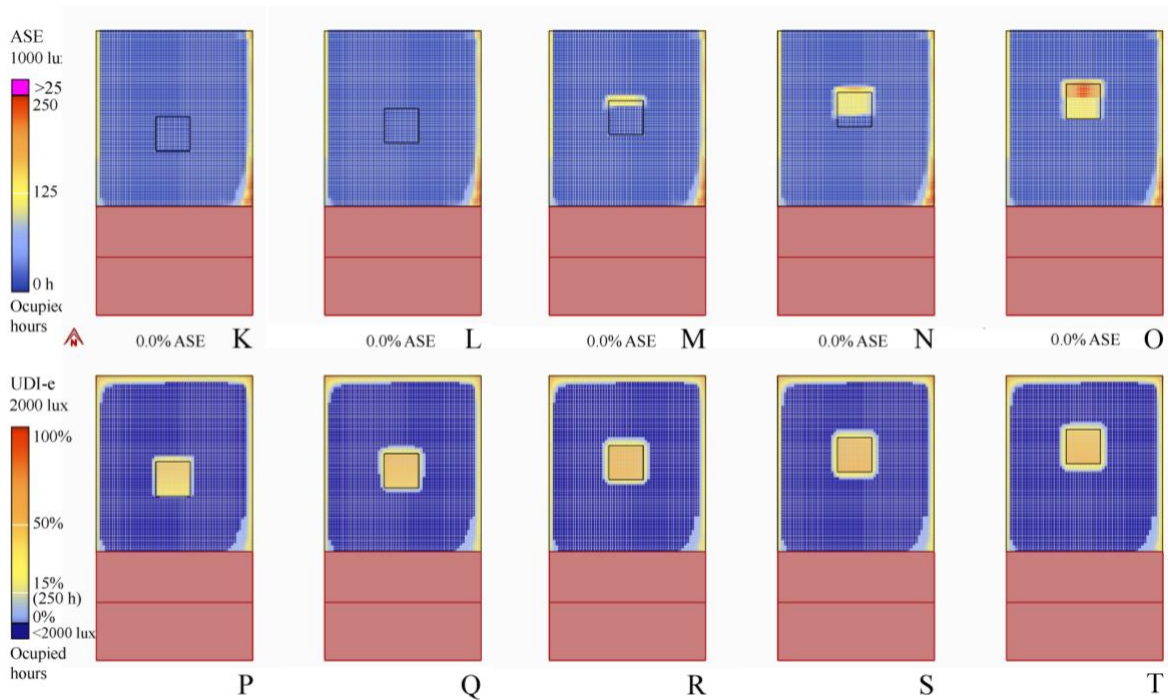


Figure 7-13 ASE and UDI-e result plots for the specified design solutions on the ground floor.

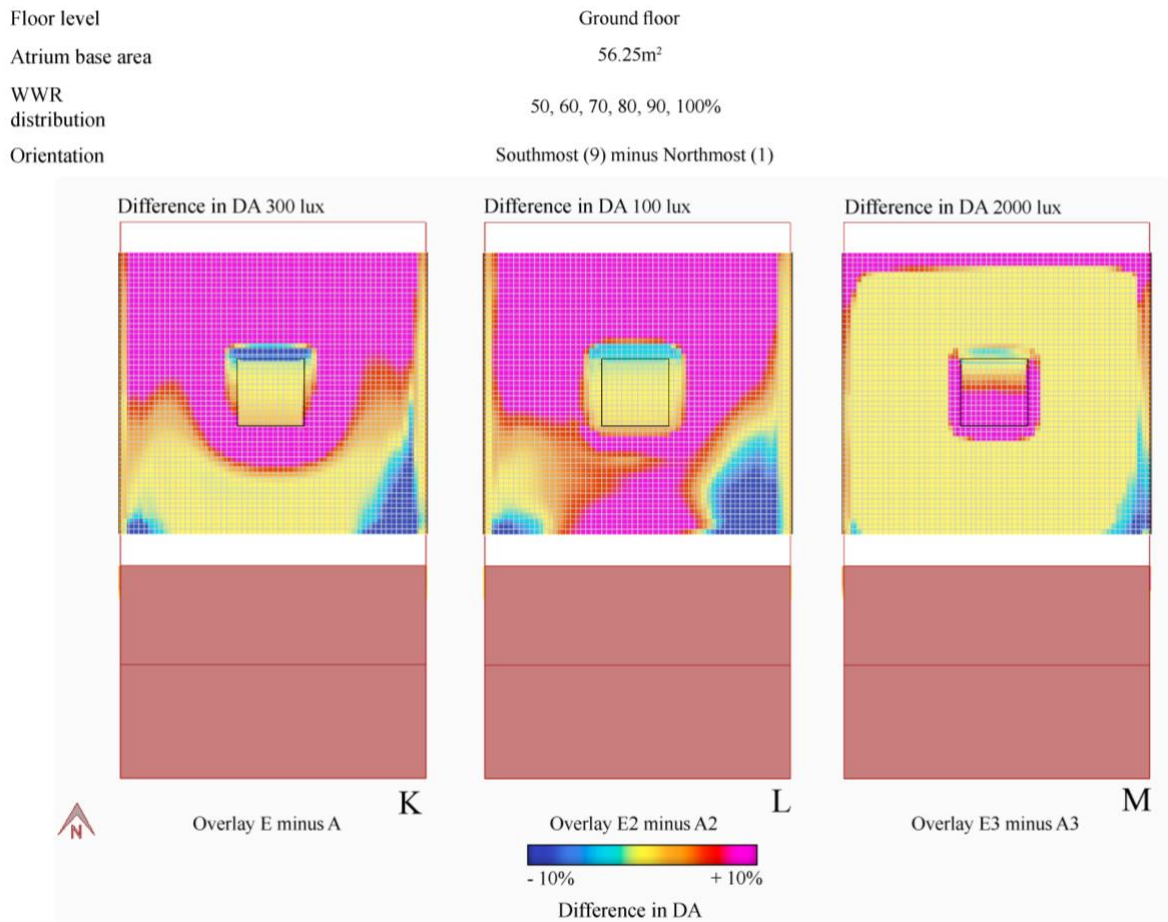


Figure 7-14 Overlay of DA<sub>300</sub>, DA<sub>100</sub>, DA<sub>2000</sub> result plots for northmost and southmost orientations on the ground floor.

### 7.2.2 Design solutions decreasing daylight on lower floors

The influence of atrium geometry on daylight performance across floors was unmistakable. Reducing the atrium well area resulted in lower sDA<sub>300/50%</sub> from the 5<sup>th</sup> to the ground floor, lower sDA<sub>100/50%</sub> from the 3<sup>rd</sup> to the ground floor, and marginally lower ASE from the 5<sup>th</sup> to the 3<sup>rd</sup> floor.

To aid in further understanding the impact of atrium geometry on daylight performance, %time results are shown for three selected design solutions on the 3<sup>rd</sup> floor. The selected design solutions are highlighted in Figure 7-15. The three design variants have a central orientation and a WWR of 50% on the 3<sup>rd</sup> floor.

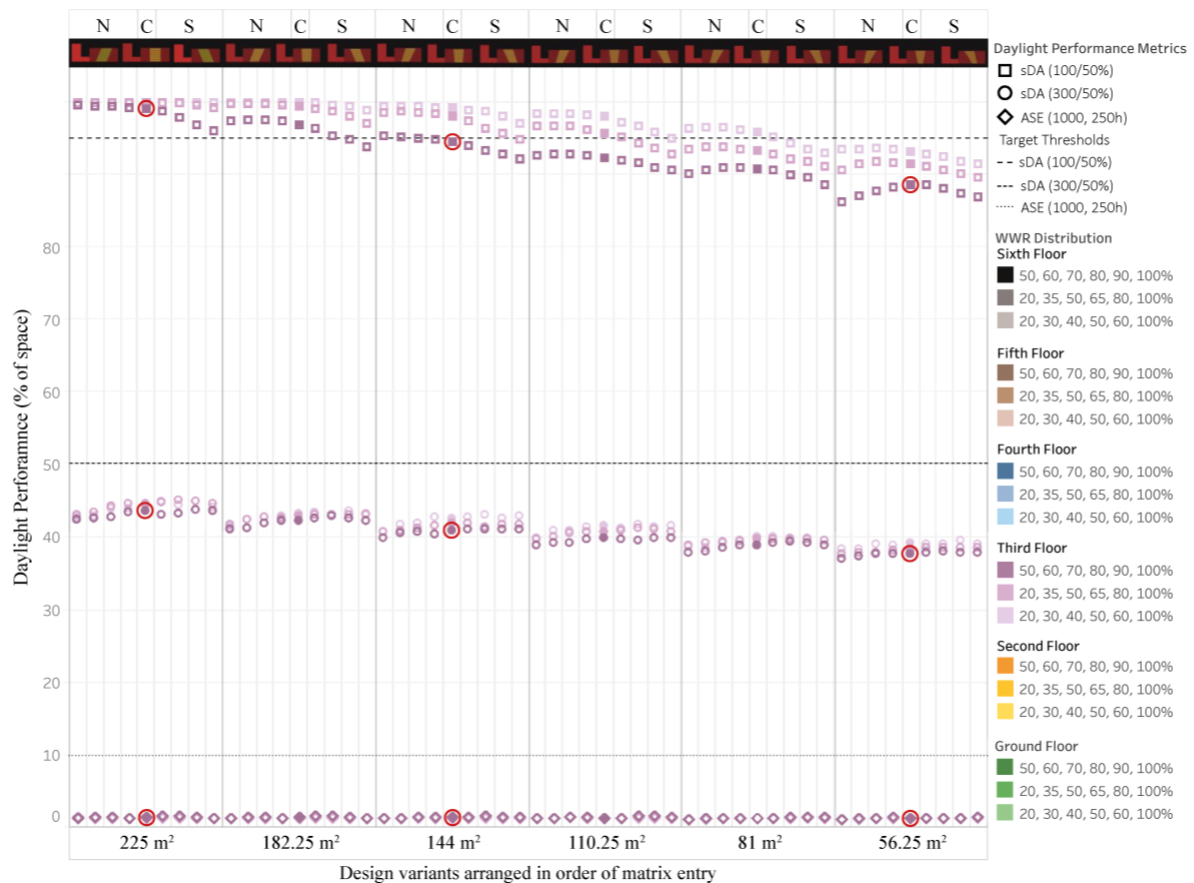


Figure 7-15 sDA<sub>300/50%</sub>, sDA<sub>100/50%</sub> and ASE results on the 3rd floor.

DA, sDA, ASE, and UDI-e plots for the specified design solutions on the 3<sup>rd</sup> floor are shown in Figure 7-16, Figure 7-17, and Figure 7-18. Decreasing the atrium base area reduced daylight performance. The plots and overlays show that the decrease in %-space performance could be attributed to the increase in room depth. For sDA<sub>300/50%</sub>, the increase in floor area for smaller atria resulted in a lower %-space threshold meeting the target criteria, despite a deeper daylight penetration into atrium adjacent spaces for the V-shaped atrium (marginally thicker ring around the atrium well in Figure 7-16 C, F, G). For sDA<sub>100/50%</sub>, the increase in room depth combined with the obstruction from the adjoining building resulted in larger areas failing to meet the target threshold in spaces to the south of the atrium well (Figure 7-17 K to M). The overlay of UDI-e again shows higher DA deeper into atrium adjacent spaces for the splayed/V-shaped atrium geometry with smaller atrium base area, although the

additionally daylit areas could not offset the increase in room depth (Figure 7-18 U). In conclusion, a V-shaped atrium geometry increases the depth of daylight penetration into atrium adjacent spaces as a result of splaying the atrium well walls to a more perpendicular position towards the skylight. However, when the V-shape is produced as a result of decreasing the atrium well area and increasing the floor area, the increase in room depth far outweighs the increase in daylight penetration, so that reducing the atrium base area overall reduces daylight performance.

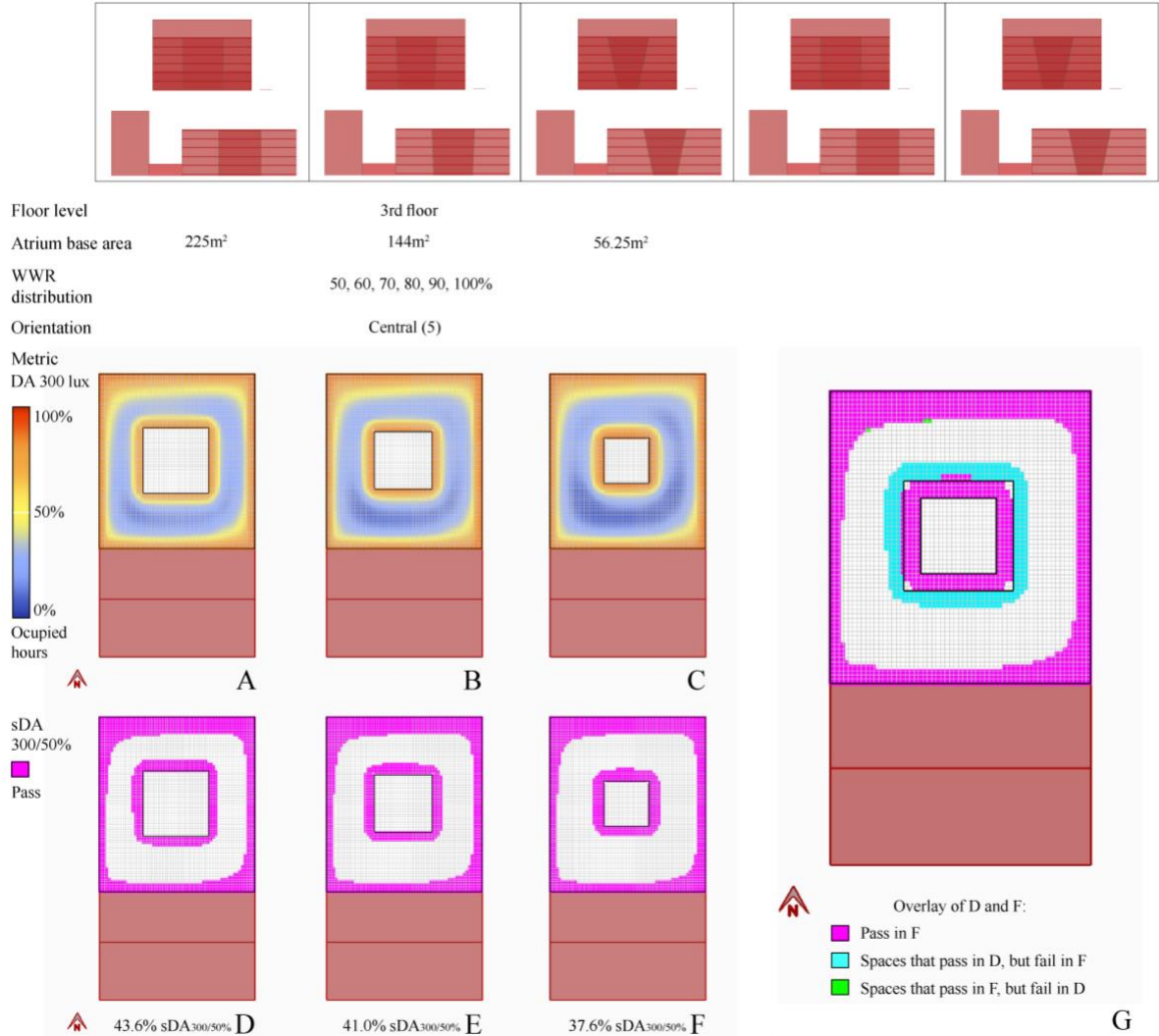


Figure 7-16 DA<sub>300</sub> and sDA<sub>300/50%</sub> results plots for the specified design solutions, highlighting the impact of atrium geometry on daylight results on the 3rd floor.

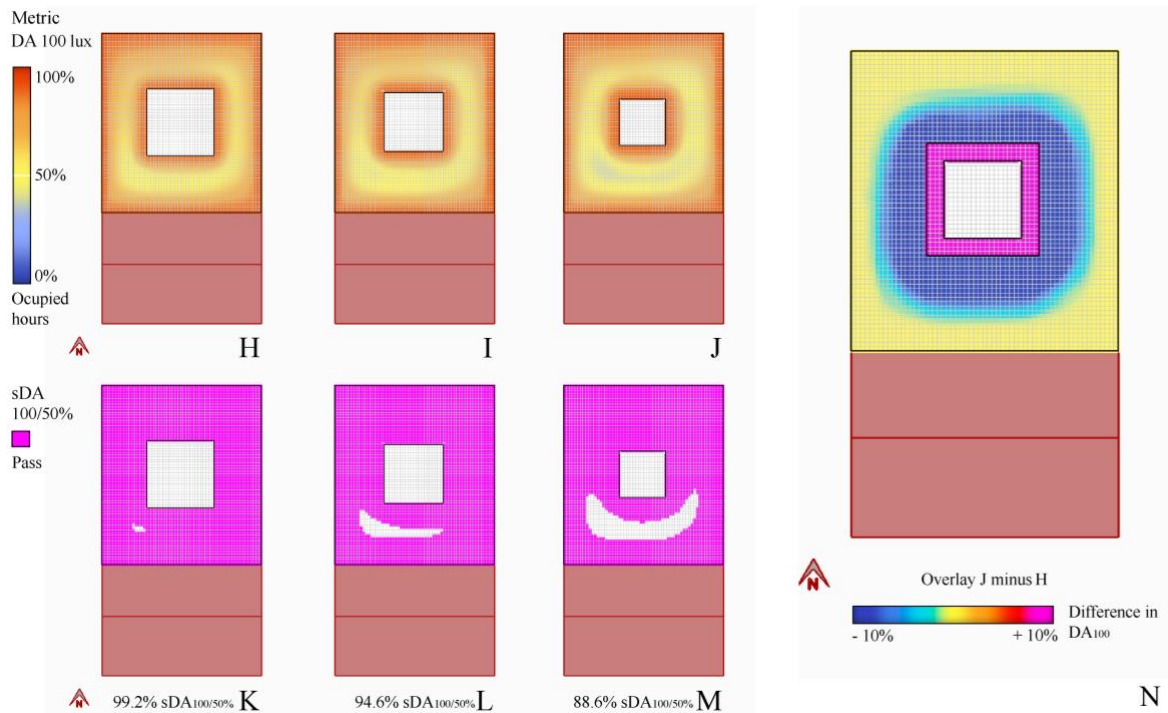


Figure 7-17 DA<sub>100</sub> and sDA<sub>100/50%</sub> results plots for the specified design solutions, highlighting the impact of atrium geometry on daylight results on the 3rd floor.

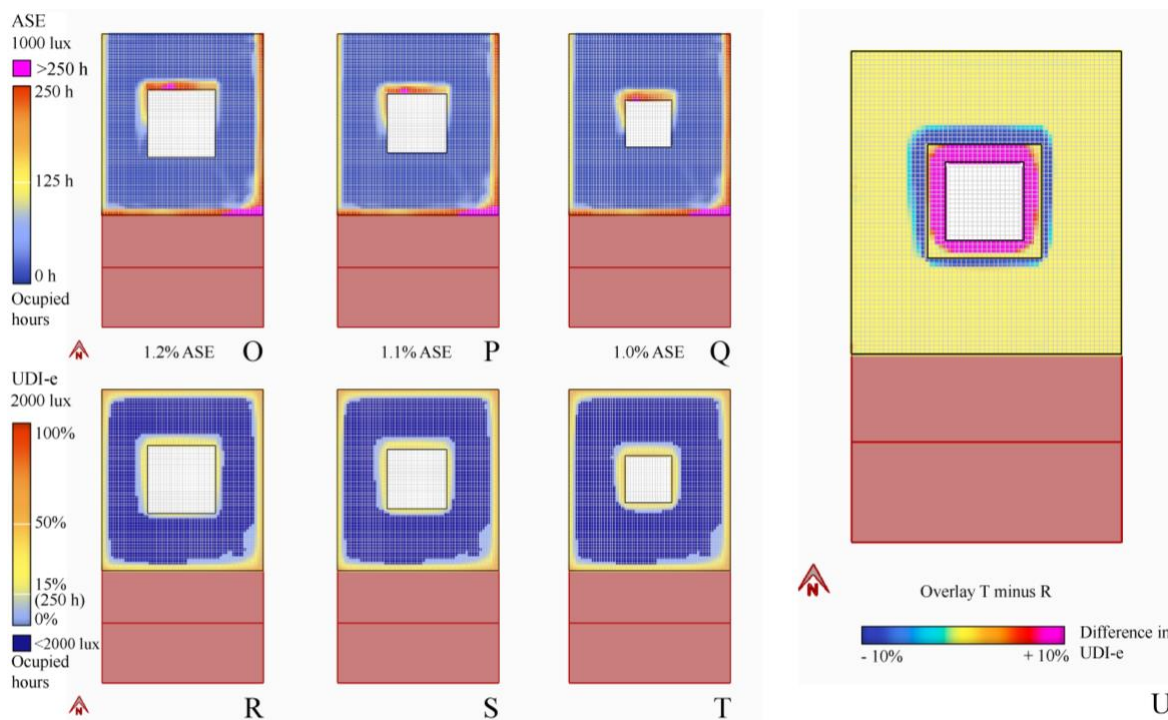


Figure 7-18 UDI-e and ASE results plots for the specified design solutions, highlighting the impact of atrium geometry on daylight results on the 3rd floor.

### 7.2.3 Design solutions increasing daylight on top floors

Initial observations were made regarding the influence of atrium well geometry, WWR distribution, and atrium well orientation on the 6<sup>th</sup> and 5<sup>th</sup> floors. Whereas lowering the WWR resulted in lower  $sDA_{300/50\%}$  performance and lower ASE, results for optimum orientations according to  $sDA_{300/50\%}$  were mixed and will be discussed in the next section. In terms of atrium geometry, reducing the atrium well base area resulted in higher  $sDA_{300/50\%}$  and ASE on the 6<sup>th</sup> floor, but lower  $sDA_{300/50\%}$  and ASE starting from the 5<sup>th</sup> floor downwards. To better understand the impact of atrium geometry, %time results are shown for three selected design solutions on the 6<sup>th</sup> floor. The selected design solutions are highlighted in Figure 7-19. The three design variants have a central orientation and a WWR of 50%.

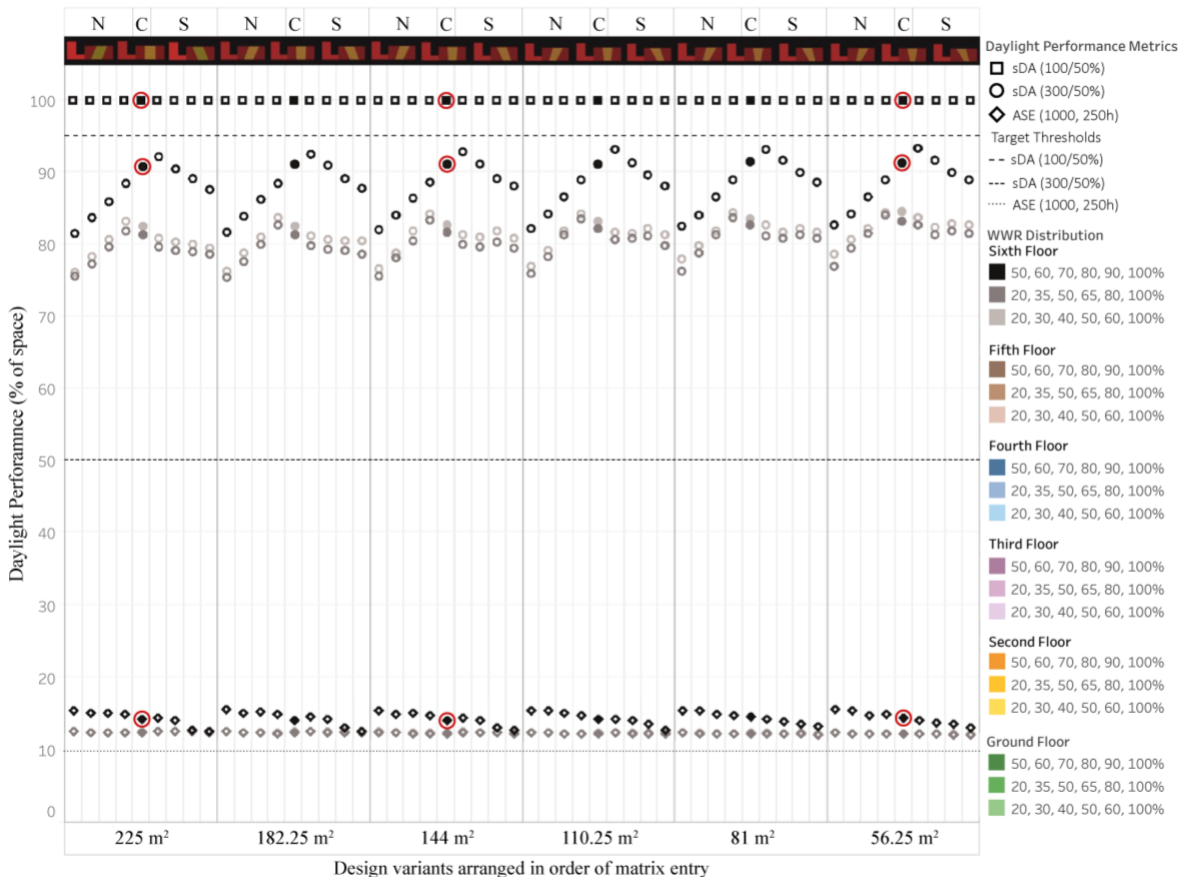


Figure 7-19  $sDA_{300/50\%}$ ,  $sDA_{100/50\%}$  and ASE results on the 6<sup>th</sup> floor. Metric results for the marked design solutions are plotted in Figure 7-20 and Figure 7-21.

DA<sub>300</sub> and sDA<sub>300/50%</sub> plots for the specified design solutions on the 6<sup>th</sup> floor are shown in Figure 7-20. Decreasing the atrium base area showed a marginal increase in sDA<sub>300/50%</sub> with every smaller atrium base area. An overlay of the plot from the largest and smallest atrium base areas is illustrated below (Figure 7-20, G). The areas highlighted in blue show additional spaces that passed the sDA<sub>300/50%</sub> threshold. For central oriented design solutions, these spaces were mostly in areas directly surrounding the atrium well, as slanting the atrium well façades exposed more floor area to the skylight. Therefore, an increase could be seen in sDA<sub>300/50%</sub> results despite the increase in room depth, which reduced %space results on other floor levels. This increase in room depth was 1 m on each side of the atrium well, or 27 m<sup>2</sup> when comparing the largest to the smallest atrium base area (Figure 7-20, G, highlighted in blue).

UDI-e and ASE results are shown in Figure 7-21. Both show a marginal increase in daylight levels exceeding 1000 lux, the smaller the atrium base areas. An overlay highlights this difference between UDI-e for the largest and smallest atrium base areas by subtracting the results (Figure 7-21, N). Especially areas to the north of the atrium receive more daylight when reducing the atrium base area, a consequence of splaying the south-facing atrium well walls to be more perpendicular to solar altitude angles.

In conclusion, the identified trend in which reducing the atrium base area reduces sDA<sub>300/50%</sub> on lower floors can largely be explained by the increase in the floor area of atrium adjacent spaces and the associated increase in overall room depth. The reverse effect for the 5<sup>th</sup> floor onwards can be explained by the splay angles of the atrium well walls increase visible sky area (top light rather than side light). This increases sDA<sub>300/50%</sub> despite the slight increase in room depth. Thus, splaying atrium

well angles into a 'V-shape' improves daylight penetration into atrium adjacent spaces. Adjusting the atrium well geometry in this way can however only improve overall daylight performance, if an increase in room depth does not offset the additional depth of daylight penetration. This work investigated "V-shaped" atrium well by reducing the atrium base area. Setting a constraint to maintain the atrium well volume across the design changes would deliver a better basis for analysis in future work, as higher sDA results may then be seen on floors besides the top floor.

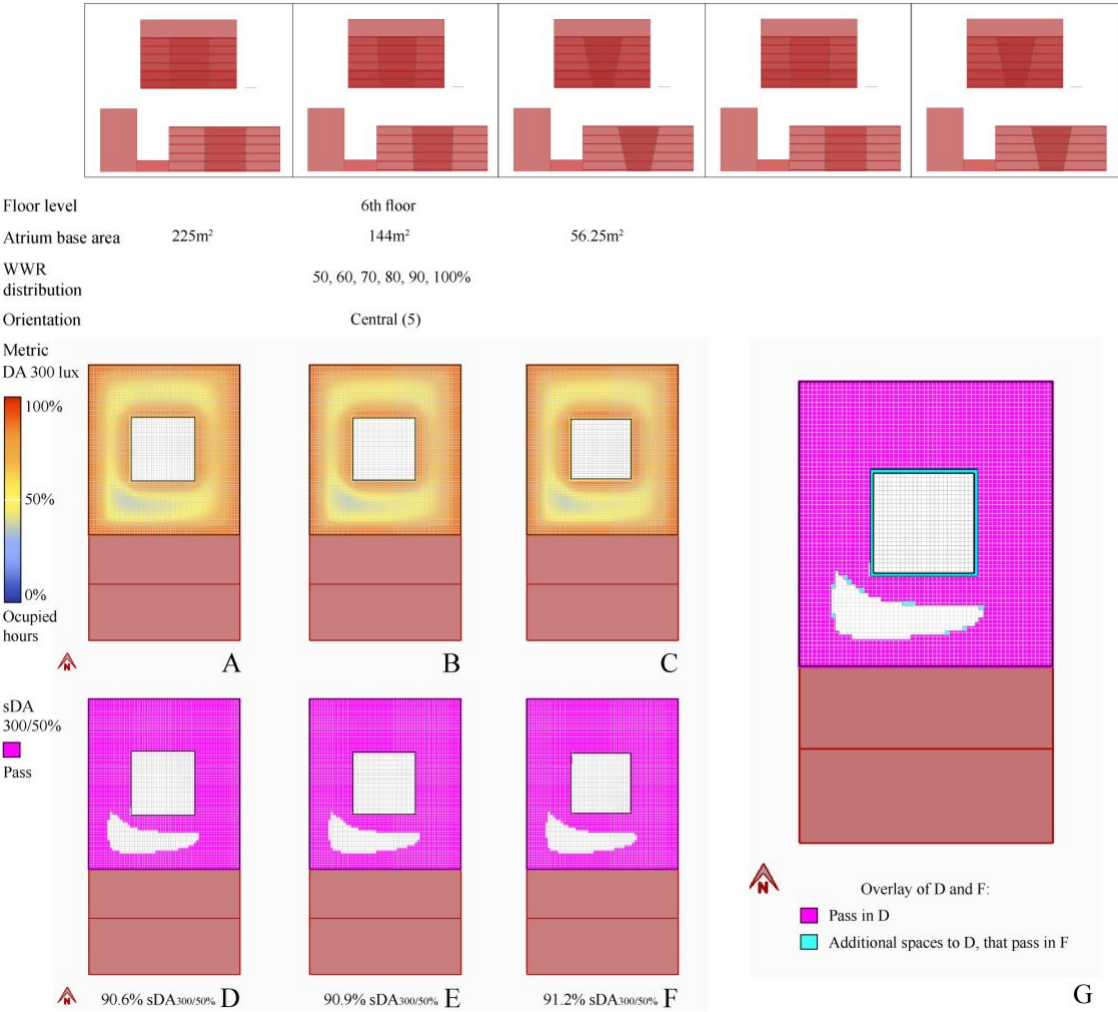


Figure 7-20 DA<sub>300</sub> and sDA<sub>300/50%</sub> results plots for the specified design solutions, highlighting the impact of atrium geometry on daylight results on the 6<sup>th</sup> floor.

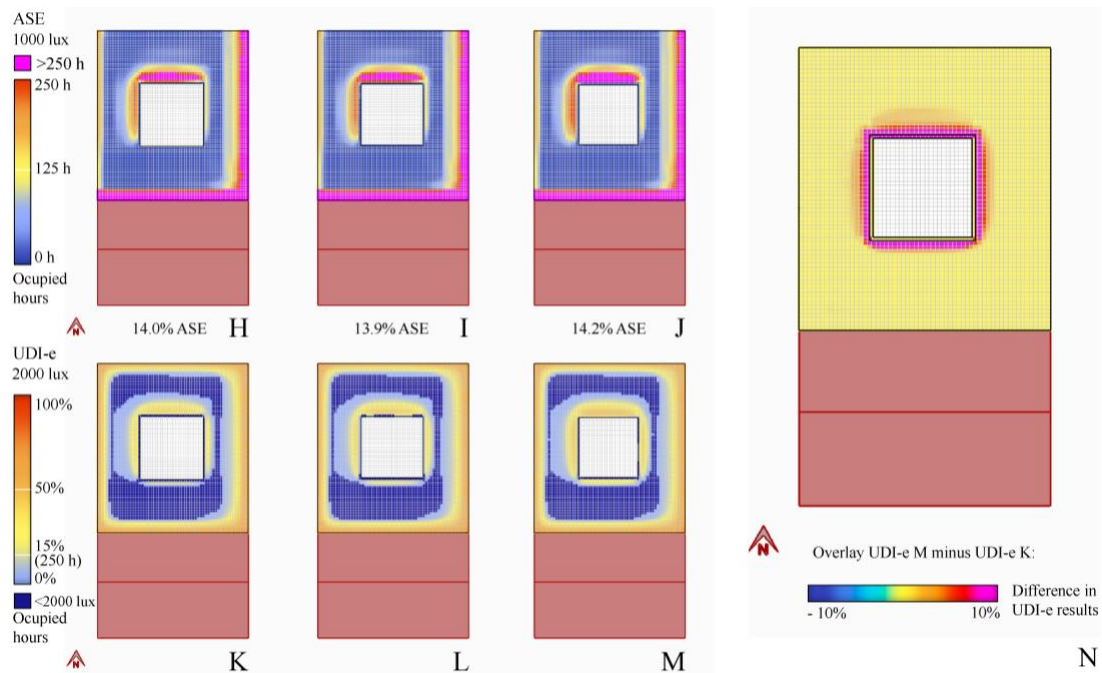


Figure 7-21 ASE and UDI-e results plots for the specified design solutions, highlighting the impact of atrium geometry on daylight results on the 6th floor.

#### 7.2.4 Design solutions decreasing daylight on lower floors

As previously mentioned, a lower WWR resulted in lower  $sDA_{300/50\%}$  performance on the 6<sup>th</sup> and 5<sup>th</sup> floors, with a turning point visible on the 4<sup>th</sup> floor. ASE results were also lower for smaller WWR on the 6<sup>th</sup> to 3<sup>rd</sup> floors. The difference in ASE results between different WWR distribution series differed more for northward, than southward orientations on the 6<sup>th</sup> to 4<sup>th</sup> floor. In terms of orientation,  $sDA_{300/50\%}$  results were mixed from the 6<sup>th</sup> to 5<sup>th</sup> floors: On the 6<sup>th</sup> floor, slightly northward/slightly southward oriented atria showed the highest  $sDA_{300/50\%}$  results, depending on the WWR distribution series. On the 5<sup>th</sup> floor, northward orientations displayed the highest  $sDA_{300/50\%}$  performance, and southward orientations the lowest, regardless of WWR distribution series. On the 4<sup>th</sup>, a shift was visible towards southward orientations showing higher  $sDA_{300/50\%}$  results, and northmost orientations showing the lowest  $sDA_{300/50\%}$ . As for ASE, result were highest for northmost orientations on the 6<sup>th</sup>, and partially on the 5<sup>th</sup> floor. On the 5<sup>th</sup> and 4<sup>th</sup> floors, a shift in trend was noticeable and

ASE for northmost orientations dropped, so that less steeply northward orientated atria showed the highest ASE on the 4<sup>th</sup> floor. These mixed results make it especially difficult to draw conclusions on the impact of atrium well orientation on daylight penetration into atrium adjacent. In this section, %-time plots are used to shed light on the %-space results for both WWR distribution and atrium well orientation.

To illustrate the impact of WWR distribution on daylight levels, %time results are shown for four selected design solutions on the 5<sup>h</sup> floor. The selected design solutions are highlighted in Figure 7-22. The four design variants have northmost and southmost orientations and a WWR of 60% and 30% on the 5<sup>th</sup> floor.

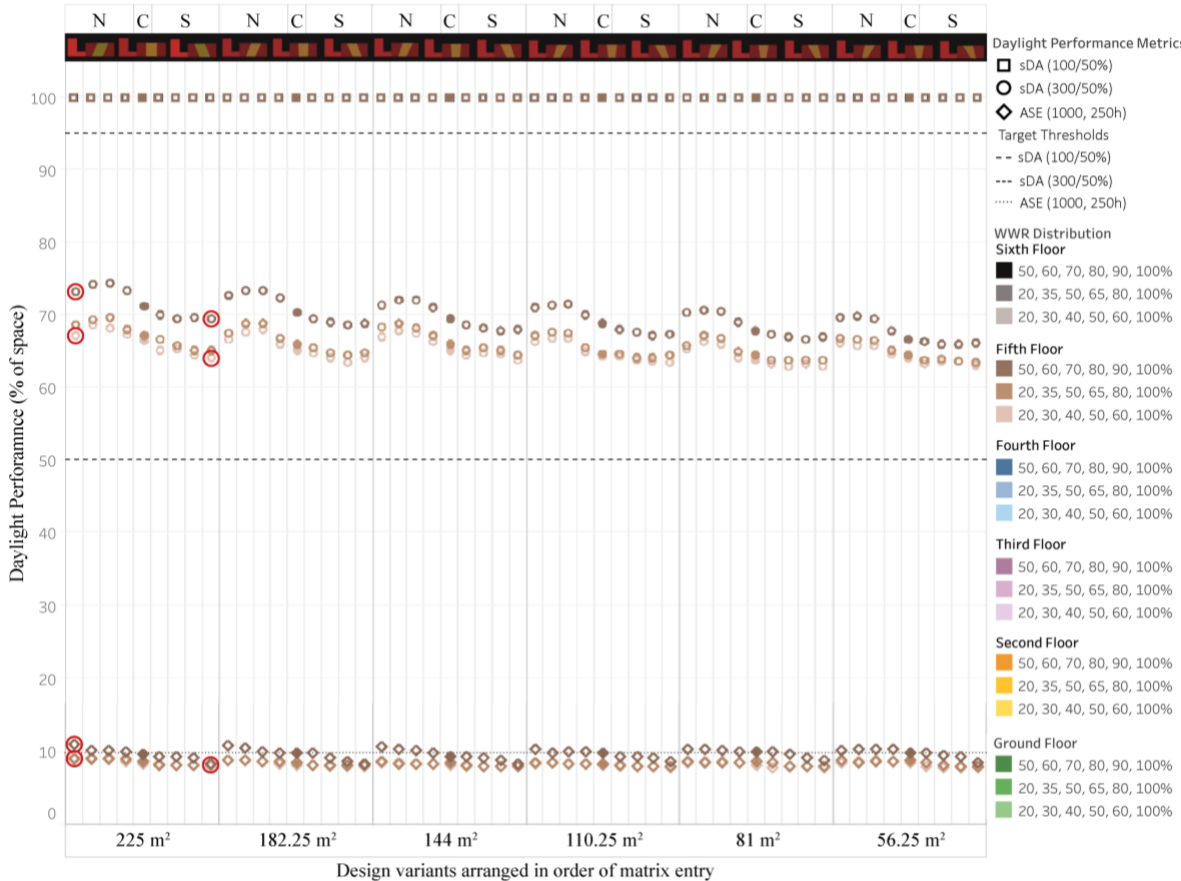


Figure 7-22 sDA<sub>300/50%</sub>, sDA<sub>100/50%</sub> and ASE results on the 5<sup>th</sup> floor.

DA<sub>300</sub> and sDA<sub>300/50%</sub> plots for the specified design solutions on the 5<sup>th</sup> floor are shown in

Figure 7-23. The WWR distribution series starting with 50% WWR (with a WWR of 60% on the 5<sup>th</sup> floor) showed a higher sDA<sub>300/50%</sub> performance than the WWR distribution series starting with 20% (with a WWR of 30% on the 5<sup>th</sup> floor). This result is self-explanatory, considering the difference in light-admitting window area. The difference in DA<sub>300</sub> with increasing WWR was especially noticeable in areas to the south of the atrium when the atrium had a northward orientation, and vice versa, in areas to the north of the atrium when the atrium had southward orientations (see depth of daylight penetration,

Figure 7-23 E and E2). These findings resulted from splaying either the north- or south-facing atrium well façades towards the skylight.

UDI-e and ASE results are shown in Figure 7-24. These ASE plots additionally show how northward orientations, where the south-facing atrium well façades are splayed towards the skylight, had increased direct sunlight exposure compared to southward orientations, where the south-facing atrium well façade was withdrawn (obtuse angle of façade to the skylight). These results explain the difference in ASE in connection with orientation. Hence, northward orientations showed a greater sensitivity to changes in WWR for the ASE metric. The findings show how orientation affects the sensitivity to changes in WWR. The question of which orientation allows for a deeper daylight penetration into atrium adjacent spaces is answered next.

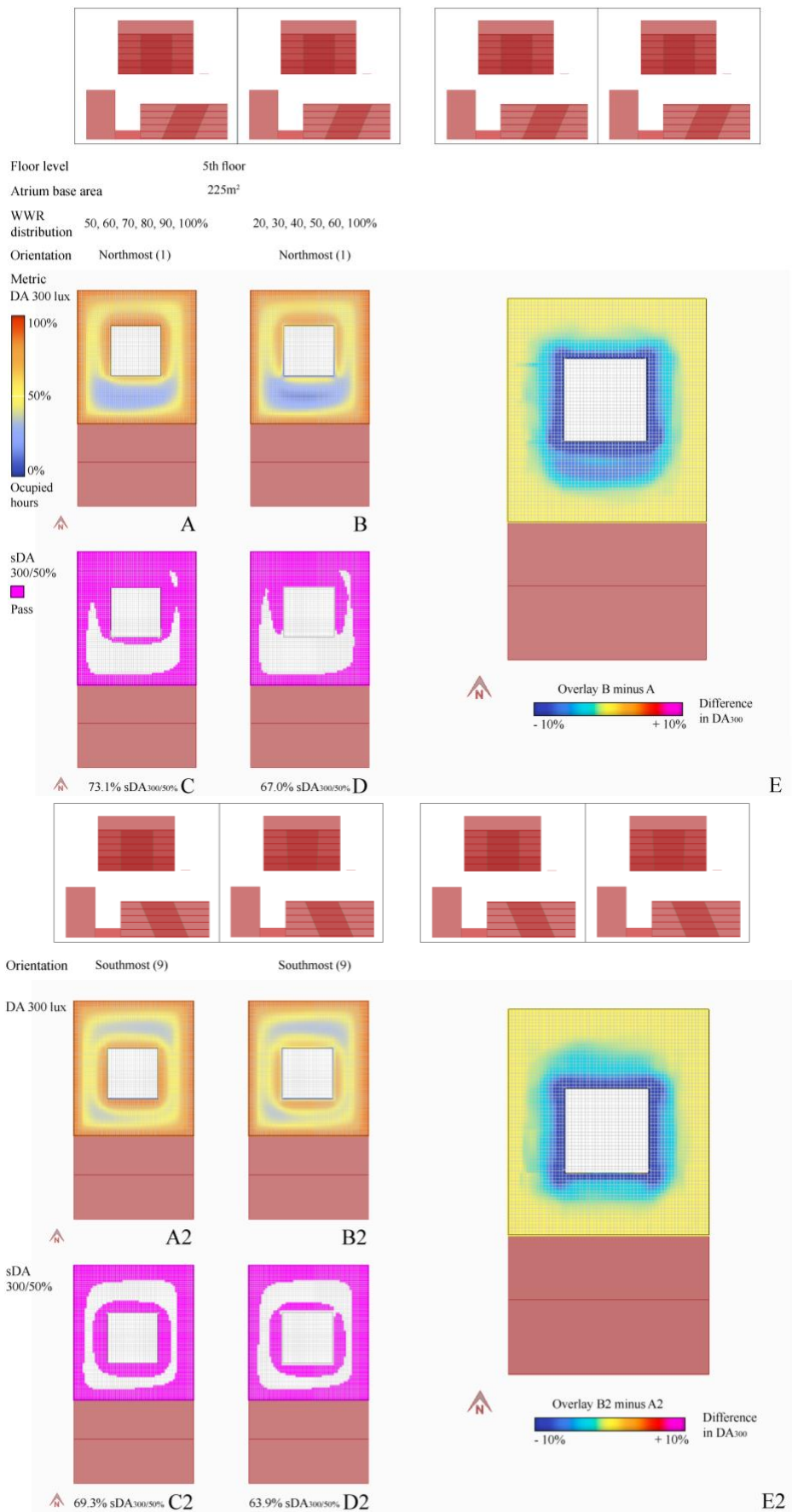


Figure 7-23 DA<sub>300</sub> and sDA<sub>300/50%</sub> result plots for the specified design solutions, highlighting the impact of WWR distribution on daylight results on the 5<sup>th</sup> floor.

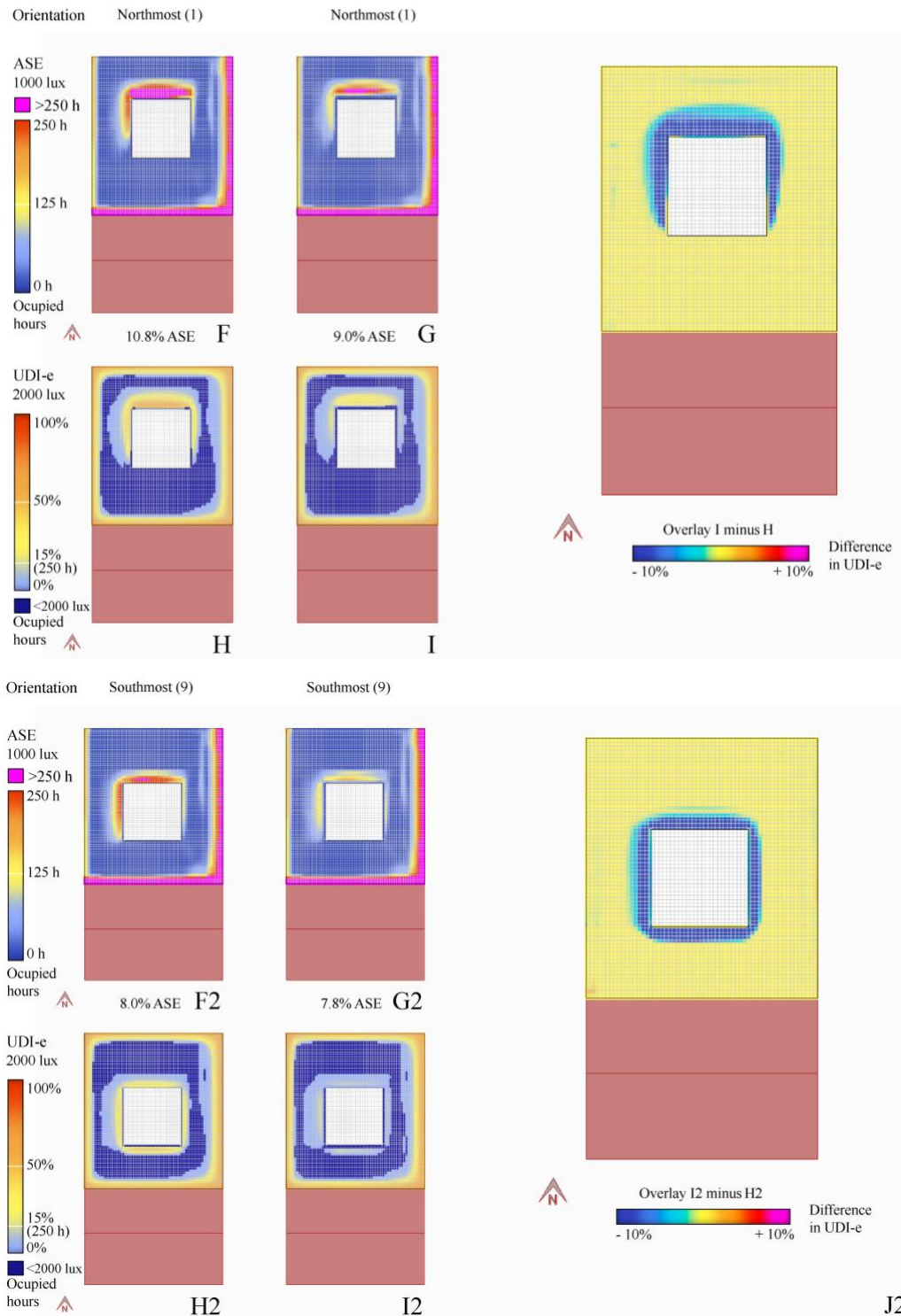


Figure 7-24 ASE and UDI-e result plots for the specified design solutions on the 5<sup>th</sup> floor.

To better understand the impact of atrium well orientation on daylight levels in atrium adjacent spaces, %time results are shown for five selected design solutions on the 5<sup>th</sup> floor (Figure 7-25.). The selected design variants have a northmost, northward, central, southward, and southmost orientation and a WWR of 60% on the 5<sup>th</sup> floor.

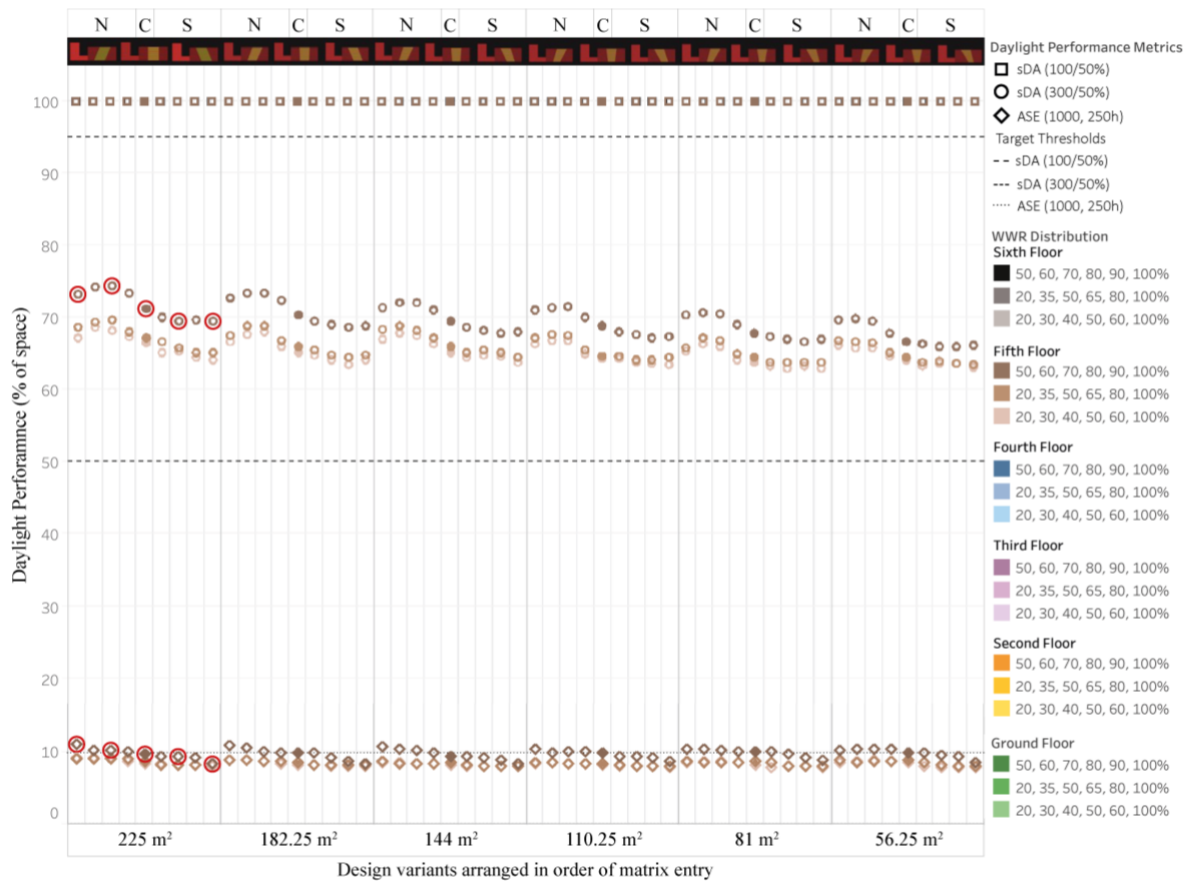


Figure 7-25 sDA<sub>300/50%</sub>, sDA<sub>100/50%</sub> and ASE results on the 5<sup>th</sup> floor.

Figure 7-26 shows DA<sub>300</sub> and sDA<sub>300/50%</sub> results for the selected design solutions on the 5<sup>th</sup> floor. UDI-e and ASE results are shown in

Figure 7-27. As visible in the plots, southward orientations showed a more even distribution of daylight to all sides of the atrium well (see orange/ yellow hue surrounding the atrium well Figure 7-26 A to E and

Figure 7-27 P to T), whereas northward orientation showed higher DA<sub>2000</sub>, deeper into spaces adjacent to the north of the atrium well (e.g. Figure 7-26 A,

Figure 7-27 P). This is further highlighted in the overlay of results for the

northmost and southmost orientations in Figure 7-28, B, where higher illuminances

were seen deeper into atrium adjacent for northward orientations (indicated by the

dark blue hue).

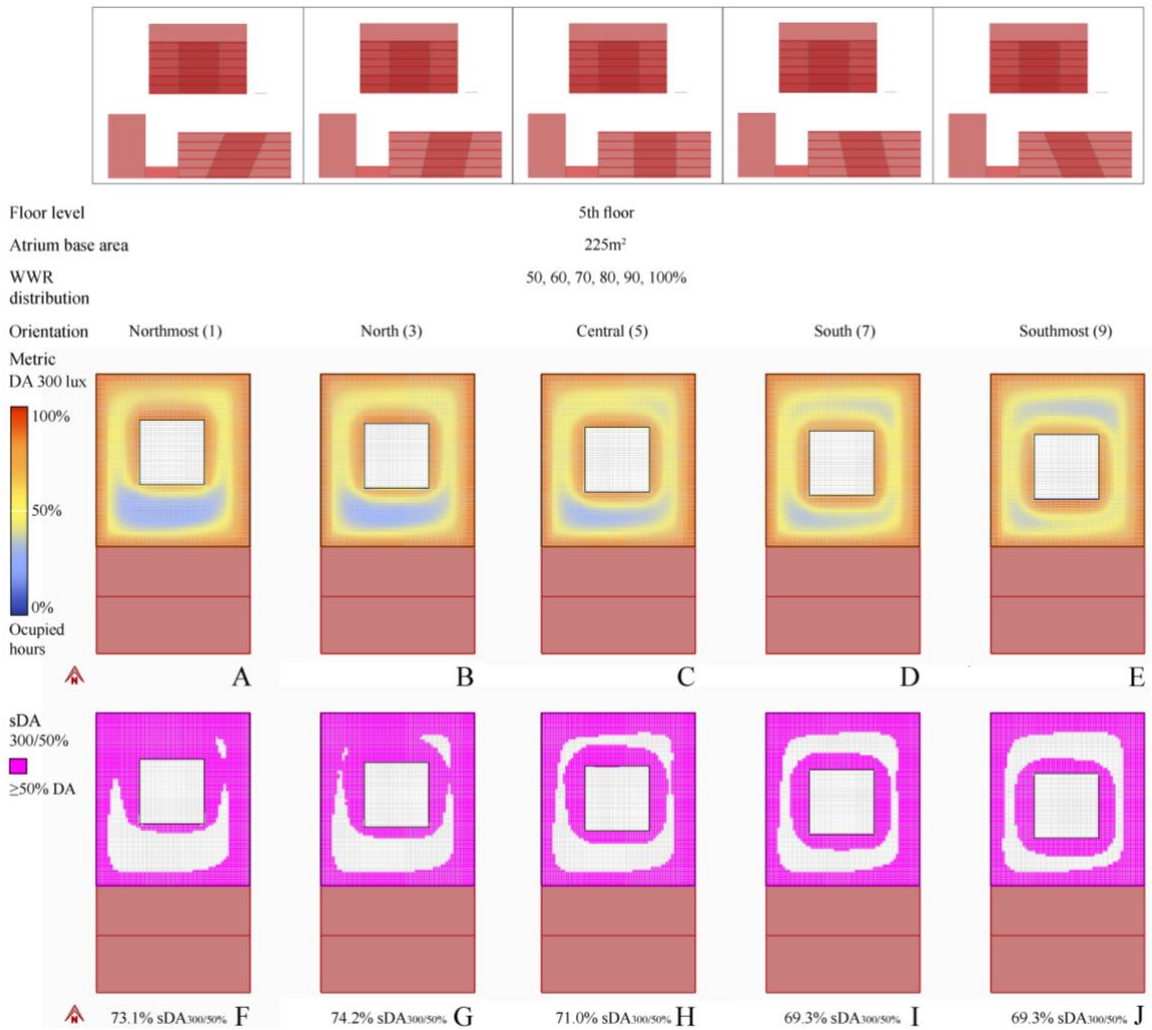


Figure 7-26 DA<sub>300</sub> and sDA<sub>300/50%</sub> result plots for the specified design solutions on the 5<sup>th</sup> floor.

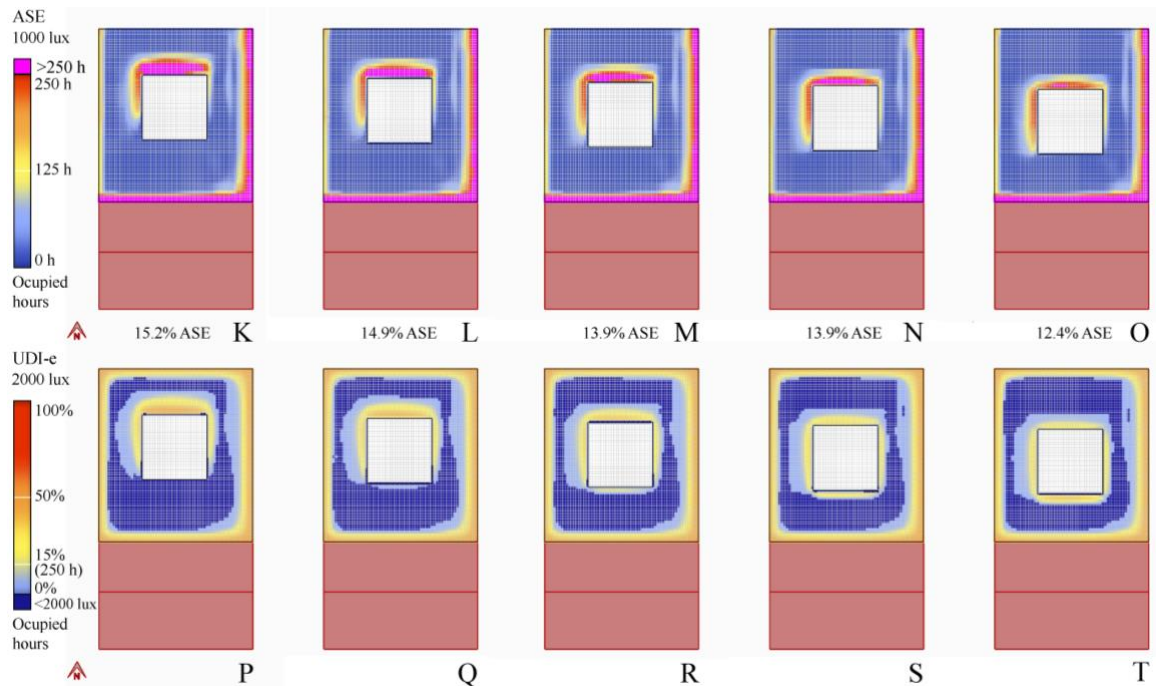


Figure 7-27 ASE and UDI-e result plots for the specified design solutions on the 5<sup>th</sup> floor.

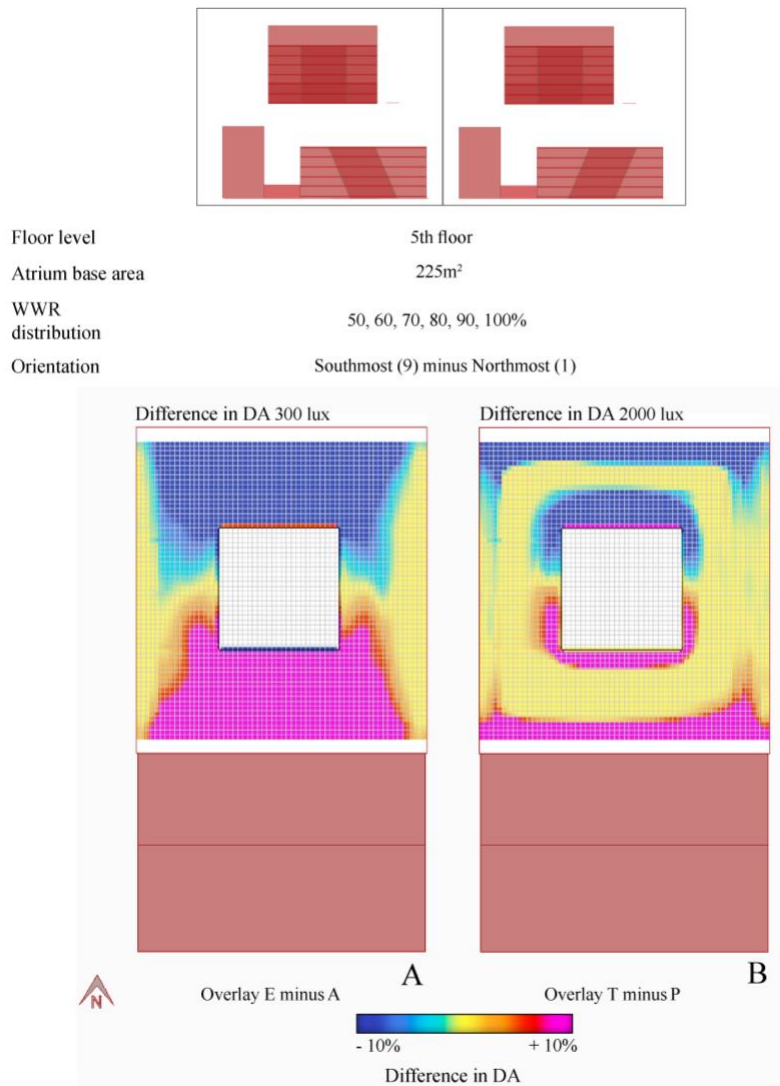


Figure 7-28 Overlay of DA<sub>300</sub>, and DA<sub>2000</sub> result plots for northmost and southmost orientations on the ground floor.

In conclusion, on floors where direct sunlight is available and reflected light matters less (i.e. on top floors), increasing the window area increases daylight in atrium adjacent spaces. However, increasing the window area also increases the risk for glare. Additionally, atrium well orientation influences which spaces surrounding the atrium well receive higher DA. Here, splaying south-facing walls (northward orientations) increases daylighting potential in spaces to the north of the atrium well while also increasing the risk for glare resulting from direct sunlight (as shown by the ASE results). On the other hand, southward orientations, which show overall lower DA in atrium adjacent spaces, reach areas on all four sides of the atrium well.

### 7.3 Conclusions

The central atrium was introduced to bring additional daylight into the building. Results however showed that improving daylight levels in atrium adjacent spaces on the lower floors proved difficult. Overall variation of daylight levels as a result of changing WWR distribution and atrium orientation remained small on the lowest four floors for the  $sDA_{300/50\%}$  (in the presented case study less than 3 percentage points), and was considerably higher for the top two floors (up to 13 percentage points). The design factor that showed the biggest impact on lower floors was the reduction of the atrium base area, which led to a decrease in  $sDA_{300/50\%}$  performance (around 9 percentage points) resulting from the increase in room depth.

Nonetheless, two design choices were found to improve daylighting in atrium adjacent spaces on lower floors. These are: 1) reducing the WWR on top floors to increase the reflected daylight in the atrium well, and 2.) a more southward orientation, which allowed for a deeper daylight penetration into the building due to an alignment with solar altitude angles. The improvements seen for the presented case study are less than 3 percentage points for the  $sDA_{300/50\%}$  metric.

Improvements to daylighting on the lower floors were met with trade-offs on the top floors. This is because reducing WWR on top floors meant reducing daylight there (up to 13 percentage points for the  $sDA_{300/50\%}$  metric). In terms of orientations, a southward orientation increased DA in spaces to the north of the atrium well, and a northward orientation increased DA in spaces to the south of the atrium well. From the two options, northward orientations appeared to result in deeper daylight penetration, but also increased the risk of glare due to an increased exposure to direct sunlight. Interestingly, reducing the atrium base area –a design choice that reduced daylight

performance on the ground floor –improved daylight performance on the top floor (2 percentage points for the  $sDA_{300/50\%}$  metric). This result indicates that a v-shaped atrium well geometry increases daylight penetration into atrium adjacent spaces.

## Chapter 8

### Spatial and Temporal Daylight Metrics in Decision-Making

This section summarises the main findings of the analysis of the %time results, or more accurately, the distribution of %time results for  $DA_{300}$ ,  $DA_{100}$ ,  $DA_{2000}$  and  $ASE_{1000}$  that led to the previously detailed results for  $sDA_{300/50\%}$ ,  $sDA_{100/50\%}$ , and  $ASE_{1000,250h}$ . With this, some of the previous results can be explained. Interestingly, different conclusions can be drawn from the %time and %space results. By comparing these conclusions, the set target thresholds of the %space results (i.e. 50% time for 50% of space for  $sDA_{300/50\%}$ ; 50% time for 95% of space for  $sDA_{100/50\%}$  and 10% for  $ASE_{1000,250h}$ ) are scrutinised. Thus, the limitations of setting such thresholds as target criteria and the severe implications this can have for optimisation processes are discussed in this chapter.

$DA_{300}$ ,  $DA_{100}$ ,  $DA_{2000}$  and  $ASE_{1000}$  results for all six floors of the 162 design solutions were obtained from the ANN models and were visualised in Grasshopper, resulting in a total of  $4 \times 6 \times 162 = 3888$  visualisations for the daylight distribution. From these 3888 visualisations, select examples were used to analyse the influence of atrium well geometry, WWR distribution, and orientation on daylight distribution. These examples also help explain previous findings for  $sDA_{300/50\%}$ ,  $sDA_{100/50\%}$ , UDI-e, and  $ASE_{1000,250h}$ .

The analysis is structured in accordance with the main findings from the previous chapter on the impact of atrium well geometry, atrium well orientation, and WWR distribution on daylight performance in Sections 8.1, 8.2, and 8.3, respectively. The sections are sub-structured to present the key results for each floor, going from the 6<sup>th</sup> to the ground floor. Thus, current %time results are always compared with the findings

from the previous chapter, highlighting how %time and %space results can explain each other or provide additional information crucial to understanding the impact of design changes.

## 8.1 Overview of differences between metrics

Similar to the 'Overview of results' section in the previous chapter (Section 7.1), this section presents the %-results for all 162 design solutions, but discusses them in a different context. Central to the discussion are notable differences between performance metrics and the thresholds at which design targets are achieved.

sDA<sub>300/50%</sub> results are presented in Figure 8-1. As shown in the figure, sDA<sub>300/50%</sub> ranged from 21% to 93% across floors. The sDA<sub>300/50%</sub> threshold was met from the fourth floor onwards. The lowest three floors therefore constituted problematic zones, requiring further design interventions to improve daylight levels.

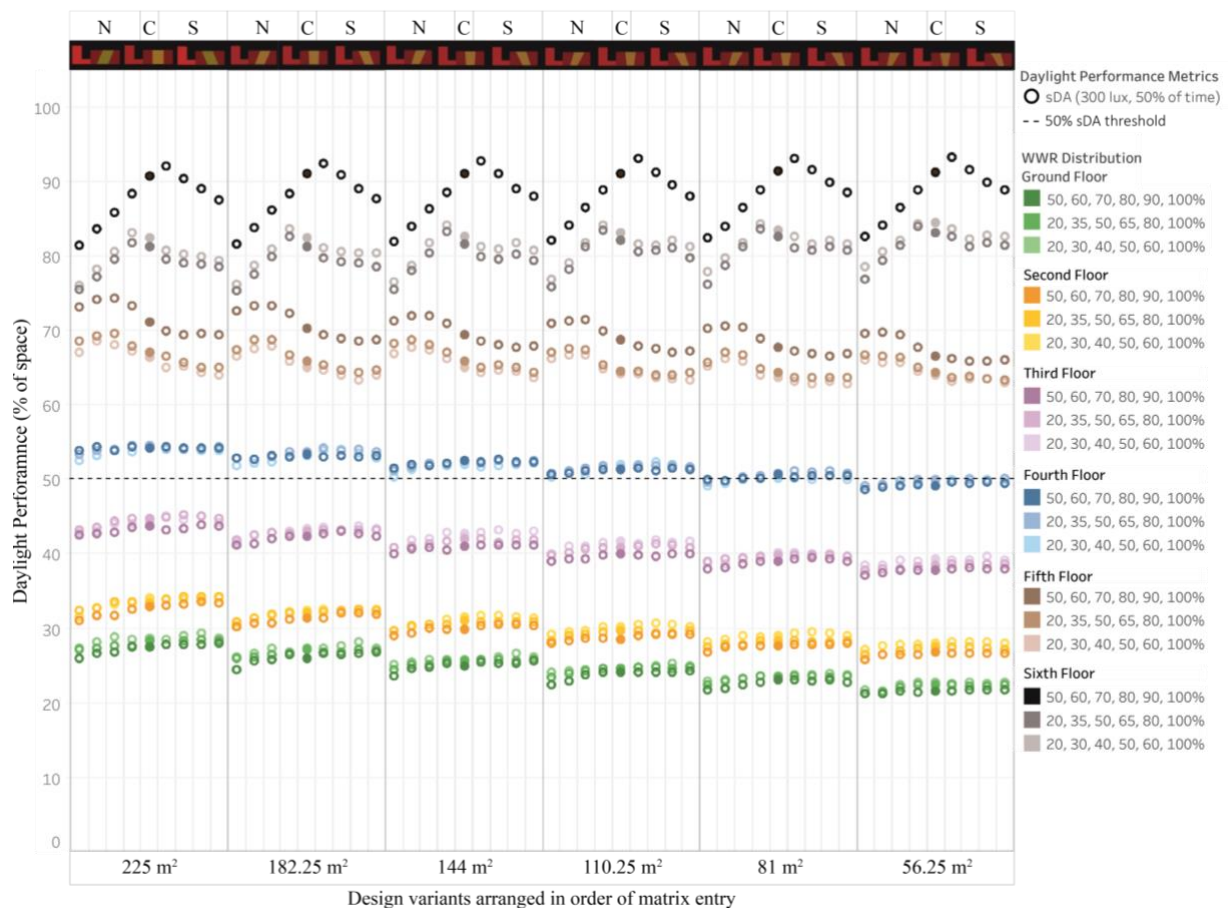


Figure 8-1 sDA<sub>300/50%</sub> performance in atrium adjacent spaces: ground to top floor

sDA<sub>100/50%</sub> results are shown in Figure 8-2. As indicated by the figure, sDA<sub>100/50%</sub> in atrium adjacent spaces ranged from 47% on the ground floor to 100% from the fourth floor onwards. The recommended target of 95% was partially achieved by design solutions on the third floor, with the lowest three floors at risk of not meeting the daylight targets. Compared to the sDA<sub>300/50%</sub> metric, where the target was only met by part of the design solutions from the fourth floor onwards, this threshold therefore appears to be more lenient. Additionally, observations on the impact of atrium design changes and optimum design solutions differ between metrics. First, southward orientations showed higher sDA<sub>300/50%</sub> performance on lower floors, while northward orientations showed higher sDA<sub>100/50%</sub> performance for most solutions on the lower floors. Second, sDA<sub>300/50%</sub> performance patterns for the optimal orientation were consistent across atrium base areas. Thus, the same or similar orientations showed

higher  $sDA_{300/50\%}$ , even as the atrium base area changed. In contrast, optimum orientations for  $sDA_{100/50\%}$  varied depending on the atrium base areas, from northward to central orientations showing higher  $sDA_{100/50\%}$ .

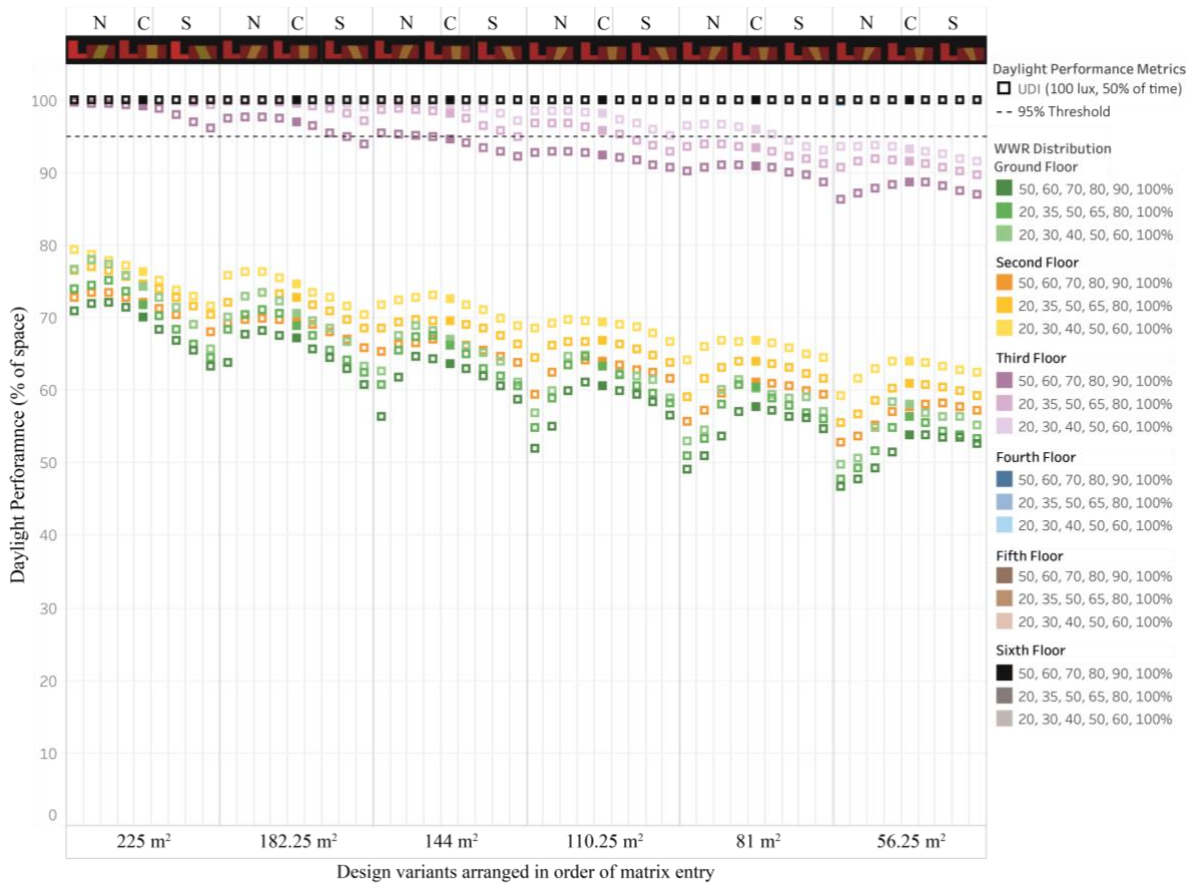


Figure 8-2  $sDA_{100/50\%}$  performance in atrium adjacent space: ground to top floor

Another notable difference between  $sDA_{300/50\%}$  and  $sDA_{100/50\%}$  stems from the difference in variance between results. The magnitude of variation for  $sDA_{100/50\%}$  results (percentage difference between results) was much higher on lower floors than seen for  $sDA_{300/50\%}$ . However,  $sDA_{100/50\%}$  results were not able to capture differences on top floors, as all design solutions achieved the target criteria for 100% of space. Thus, when overall daylight availability was low (as seen for lower floors) the  $sDA_{100/50\%}$  metric showed a greater sensitivity to design changes. Where  $sDA_{100/50\%}$  and  $sDA_{300/50\%}$  align, i.e., show similar trends, this makes it easier to read the impact of design changes (i.e. for the impact of WWR distribution and atrium well area). However, the  $sDA_{100/50\%}$

metric was not usable to compare design changes in better-daylit areas (i.e. on upper floors where 100% of space easily achieved the DA<sub>100</sub> target for 50% of occupied hours).

The next section takes a closer look at ASE, the metric intended to highlight potentially overlit areas, and calculated with 0 ambient bounces in order to capture only direct sunlight penetration. The ASE results for all floors are shown in Figure 8-3. ASE ranged from 0 to 16%. The recommended 10% threshold was exceeded from the fifth floor onwards by part of the design solutions.

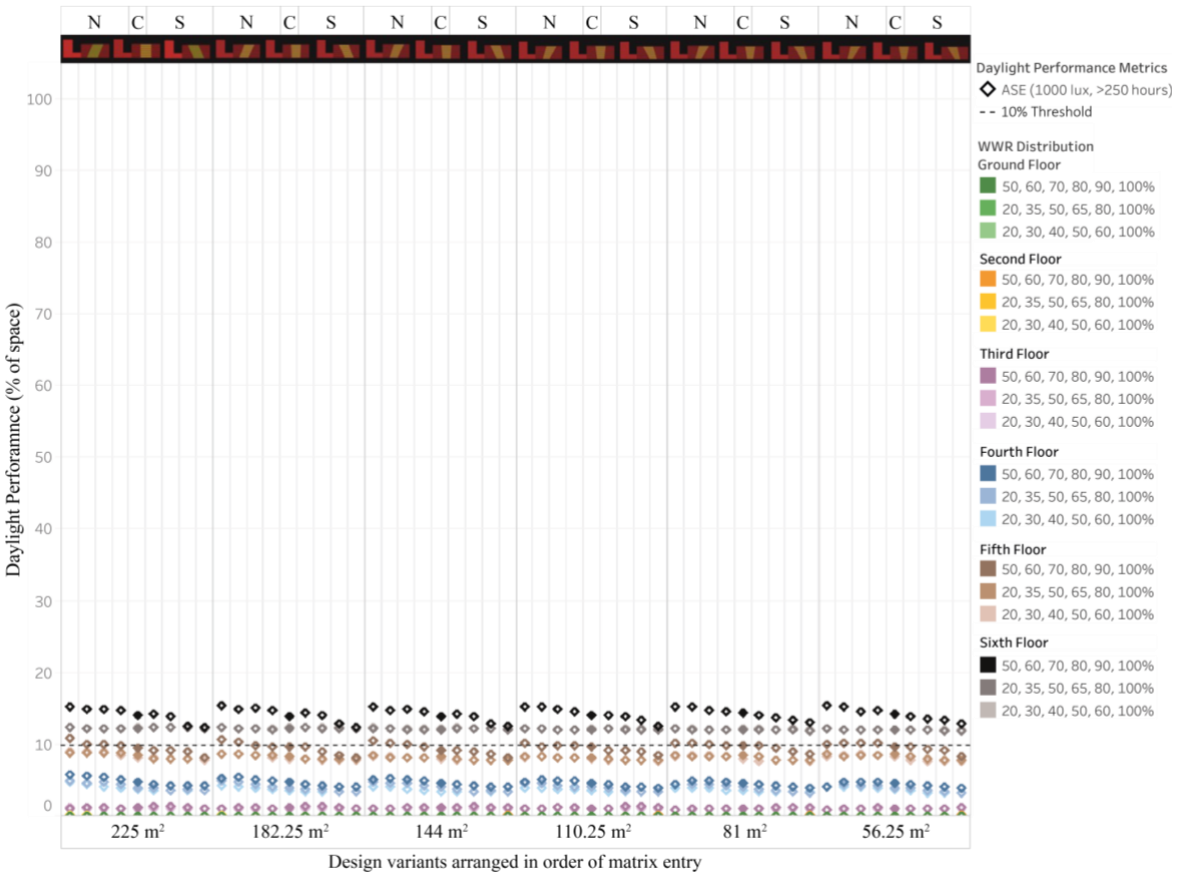


Figure 8-3 ASE performance in atrium adjacent space: ground to top floor

In terms of atrium design changes, the impact could be seen from the fourth floor onwards. A key difference between ASE, sDA<sub>300/50%</sub>, and sDA<sub>100/50%</sub> can be seen when interpreting the results on the impact of WWR distribution. ASE results showed higher ASE for larger window areas and larger overall glazing area across the atrium well

façade. In contrast,  $sDA_{300/50\%}$  and  $sDA_{100/50\%}$  metrics showed higher performance results for the WWR distribution series starting with 20% on lower floor levels, so that even though a floor had a smaller window area, the resulting  $sDA_{300/50\%}$  and  $sDA_{100/50\%}$  performance was still higher for that floor. This difference can be attributed to the simulation of inter-reflected light for  $sDA_{300/50\%}$  and  $sDA_{100/50\%}$ . It highlights that sDA results in atrium adjacent spaces stem from reflected, rather than direct sunlight alone, and attests to an increase of reflected light within the atrium well when overall glazing (light admitting area) is reduced.

In terms of design targets, the metrics could not all be reconciled in meeting the targeted thresholds. Especially the ASE target conflicts with the  $sDA_{300/50\%}$  and  $sDA_{100/50\%}$  targets. For example, on the upper floors that achieved the  $sDA_{300/50\%}$  and  $sDA_{100/50\%}$  target, the ASE target of 10% was exceeded. And vice versa, on the lower floors where ASE was within the 10% threshold,  $sDA_{300/50\%}$  and  $sDA_{100/50\%}$  targets were not always met. However, as already noted, the implications of an exceeded ASE target on overheating and the risk of glare are still ill-defined and may vary between the simulation methods used, making ASE the more questionable metric. Nonetheless, daylight design optimisation remains a trade-off between choices that can have both positive and negative implications for the building. The next sections discuss in more detail similarities and differences between metrics and the information they hold as tools for design decision making. The findings are based on the detailed analysis undertaken in Appendix A and Appendix B, as well as the results presented in the previous chapter.

## 8.2 Evaluation of metrics as a measure of daylight performance

### 8.2.1 *Irreconcilability of metrics*

The  $sDA_{100/50\%}$ ,  $sDA_{300/50\%}$ , and  $ASE_{1000,250h}$  metrics were used to assess the performance of design variants for a central atrium. Daylight performance assessments using such metrics are typically done to either achieve target thresholds set by building standards, or to improve and optimise daylight performance. For both cases, the above results showed that metrics were not always reconcilable with each other. Specifically, the ASE target could not always be simultaneously achieved with the  $sDA_{300/50\%}$  and  $sDA_{100/50\%}$  targets. All three target thresholds were only simultaneously achieved by part of the design solutions on the 5<sup>th</sup> and 4<sup>th</sup> floors, with sDA targets being met on the upper floors, and ASE on the lower floors (Figure 8-1, Figure 8-2, Figure 8-3). Although additional design changes may help move the design towards the desired target, the results point to the difficulty of integrating both, as they are conflicting.

Similarly, the above-described results demonstrated that design optima varied between metrics. To give one example, southward orientations showed the highest  $sDA_{300/50\%}$  on lower floors, but not always the highest  $sDA_{100/50\%}$  (Figure 8-4.). In fact, for part of the design solutions with larger atrium base areas, design optima for the  $sDA_{100/50\%}$  metric had northward orientations. This is problematic because both metrics are used with the objective of increasing daylight but lead to contrasting design choices in the decision-making process.

To aid in further understanding the findings described, %time results are shown for ten selected design solutions on the 2<sup>nd</sup> floor, which have a northward and southward orientation as the design optimum. The selected design solutions are highlighted in Figure 8-4. Plots are shown for northmost, northward, central,

southward, and southmost orientations for an atrium base area of 182.25m<sup>2</sup> and 56.25m<sup>2</sup>.

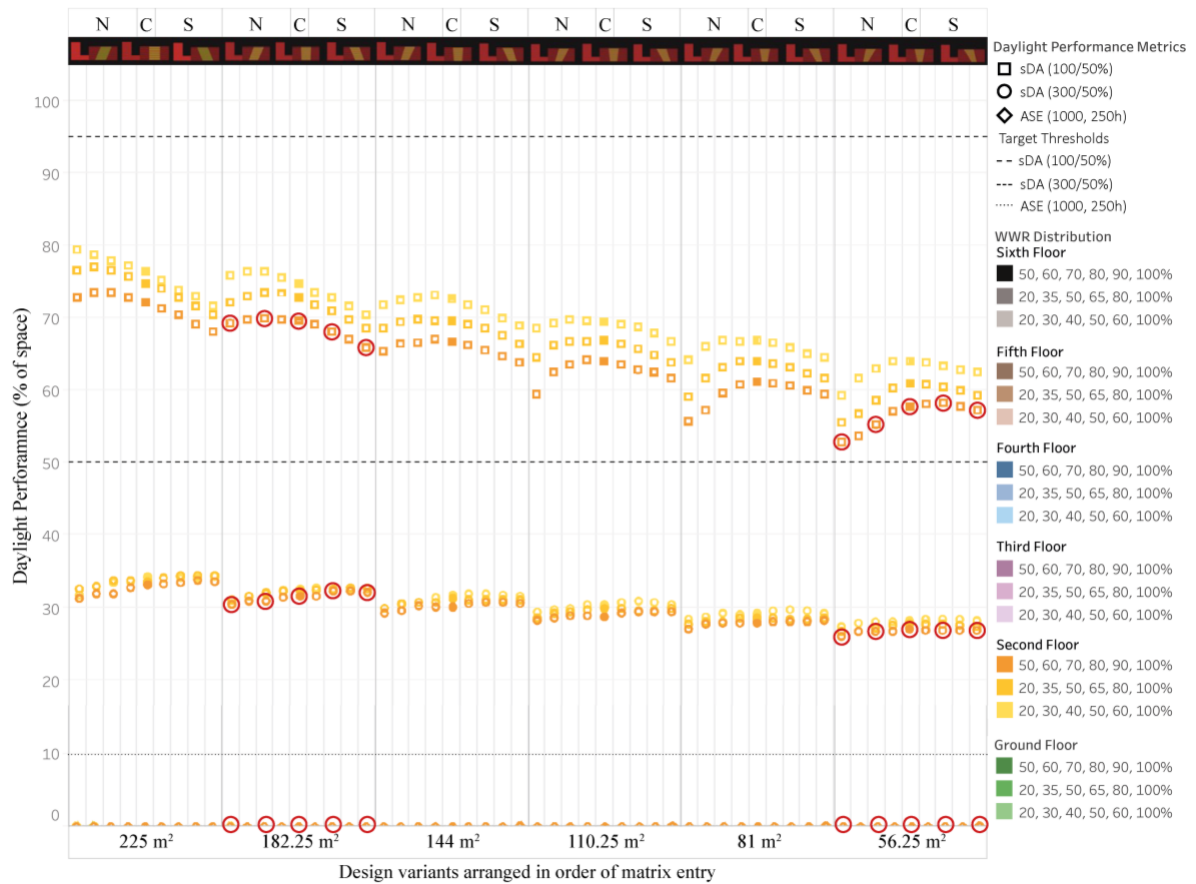


Figure 8-4 sDA<sub>300/50%</sub>, sDA<sub>100/50%</sub> and ASE results on the 2<sup>nd</sup> floor

DA<sub>300</sub> and sDA<sub>300/50%</sub> plots for the specified design solutions on the 2<sup>nd</sup> floor are shown in Figure 8-5. The patterns for DA<sub>300</sub> were straightforward. With an increase of room depth, areas with especially low DA increased for southward orientations as a result of overshadowing from the adjoining building (dark blue patches in Figure 8-5 A to E, A2 to E2). Looking at the sDA<sub>300</sub> plots, only spaces directly surrounding the atrium well met the threshold, therefore indicating that more daylight from the atrium well reached atrium adjacent spaces for central to southmost orientations.

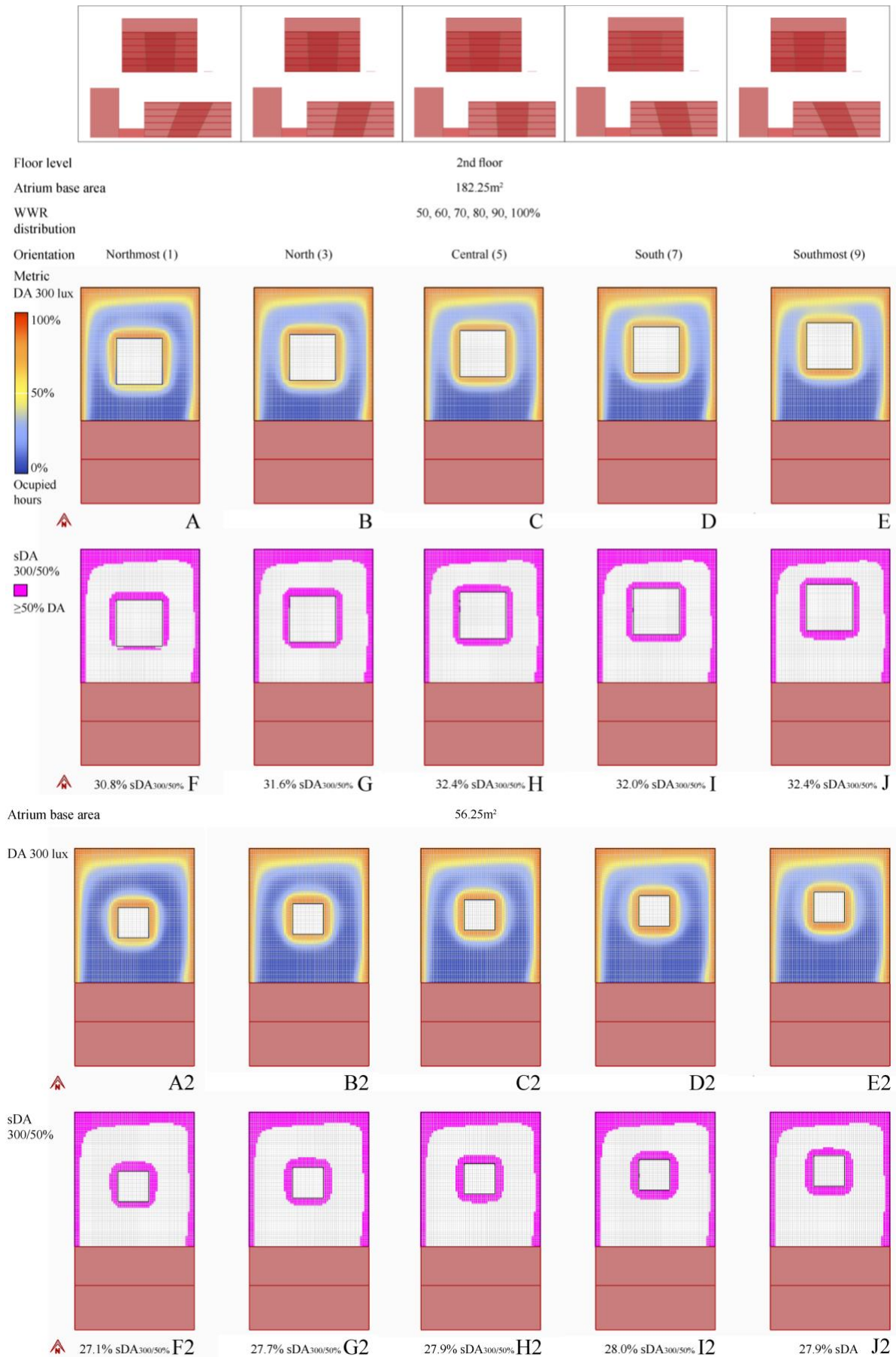


Figure 8-5 DA<sub>300</sub> and sDA<sub>300/50%</sub> result plots for the specified design solutions on the 2<sup>nd</sup> floor.



Figure 8-6 DA<sub>100</sub> and sDA<sub>100/50%</sub> result plots for the specified design solutions on the 2<sup>nd</sup> floor.

As with the DA<sub>300</sub>, the DA<sub>100</sub> and sDA<sub>100/50%</sub> plots (Figure 8-6) show that, with an increase of room depth, areas with especially low DA increased for southward

orientations as a result of overshadowing from the adjoining building (dark blue patches, Figure 8-6 A to E, A2 to E2). In contrast to  $sDA_{300/50\%}$  however, areas achieving the 100lux threshold varied depending on the location of the atrium, the size of the atrium, and the resulting room depth. For larger atria (resulting in less room depth), areas to the north of the atrium well still met the thresholds for northward orientations, while this was no longer the case for smaller atria. Therefore, the  $sDA_{100/50\%}$  results were a consequence of the design context, rather than a result of the atrium well orientation.

To conclude, spatial metric results are not always reconcilable. Keeping in mind that design optima can point towards entirely different design choices depending on the selected lux thresholds, the visualisation of temporal results (DA plots) can provide useful information to assist with better-informed decision making: in the above-detailed case, for instance, a southward oriented atrium can be placed in areas towards the south of the building, where daylight levels are especially low. As such information cannot be extracted from the spatial results alone, design optimisation methods using such metrics may be questionable, as results can be arbitrary.

### *8.2.2 Complementary information*

Although metrics were not always reconcilable in terms of the design outcome, the differences in patterns and trends between the three metrics (e.g. in terms of optima) also meant that each metric provided unique additional information. With the previous example (Figure 8-5, Figure 8-6),  $sDA_{300/50\%}$  was higher for southward orientations on the lower floors, but at the same time, underlit areas increased for the same design solutions, resulting in lower  $sDA_{100/50\%}$ . Therefore,  $sDA_{300/50\%}$  showed the influence of

splaying the atrium well walls, while  $sDA_{100/50\%}$  showed the impact of the atrium well location, which changed as a result of the parametric operation.

Similarly,  $sDA_{300/50\%}$  and ASE results also highlighted daylight performance from two different angles. To give an example, performance results will be discussed for the 5<sup>th</sup> floor (Figure 8-25). Here, although northward orientations outperformed southward orientations in terms of  $sDA_{300/50\%}$ , ASE results showed that the risk of glare resulting from direct sunlight penetration was higher for northward orientation.

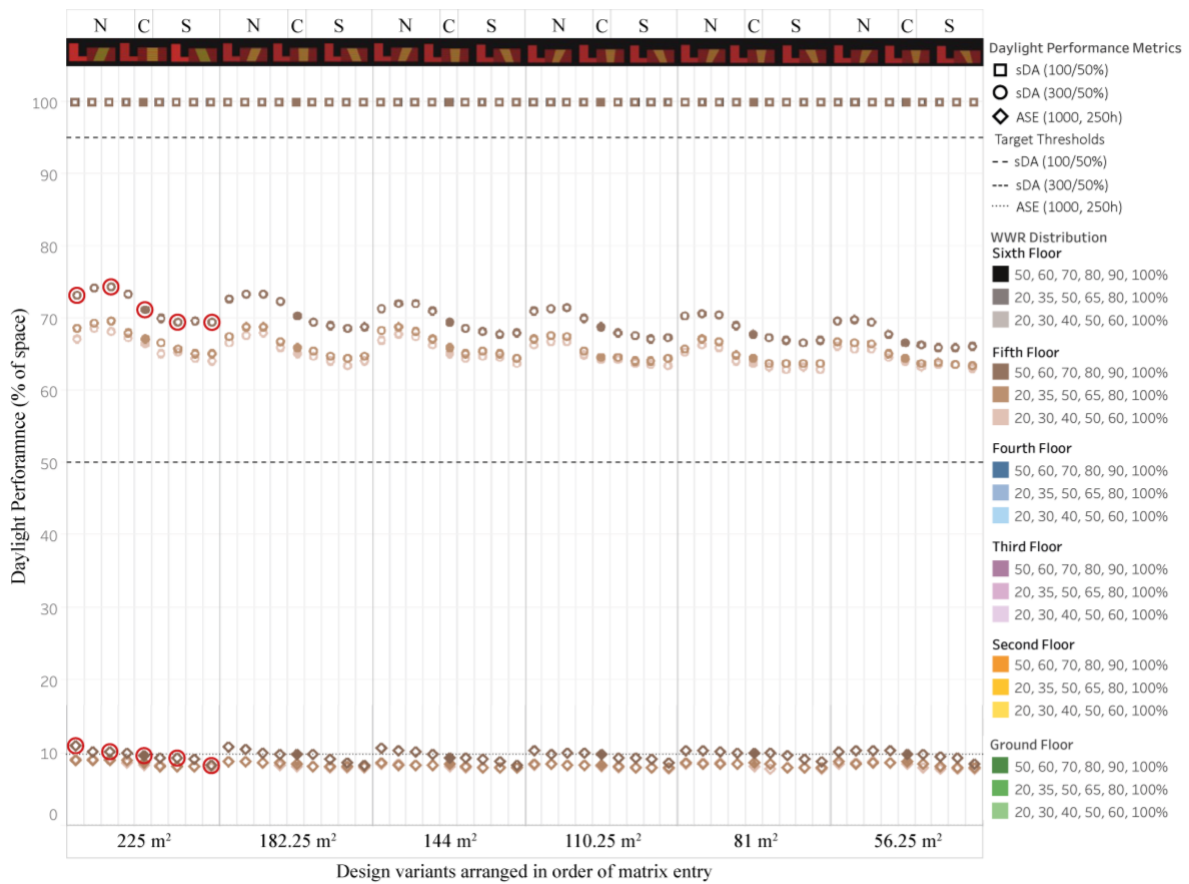


Figure 8-7  $sDA_{300/50\%}$ ,  $sDA_{100/50\%}$ , and ASE results on the 5<sup>th</sup> floor.

The higher ASE results for northward orientations suggest that splaying the south-facing atrium well walls in more perpendicular positions towards solar altitude angles may have made substantial contributions. To confirm this theory, ASE and UDE-e result plots are shown for five selected design solutions highlighted in Figure 8-7. In line with expectation, the plots (Figure 8-8) show that northmost-oriented atria

received the most direct and reflected sunlight in areas to the north of the atrium well, a result of splaying the south-facing well walls. Southmost orientations in turn received the least direct sunlight.

To conclude, using different performance metrics can provide valuable insights, as each can highlight design challenges from a different angle. The temporal plots visualised the distribution of daylight in the atrium building. Thus, alongside the spatial performance metrics, they helped determine the specific locations in a design that are prone to being overlit- or underlit.

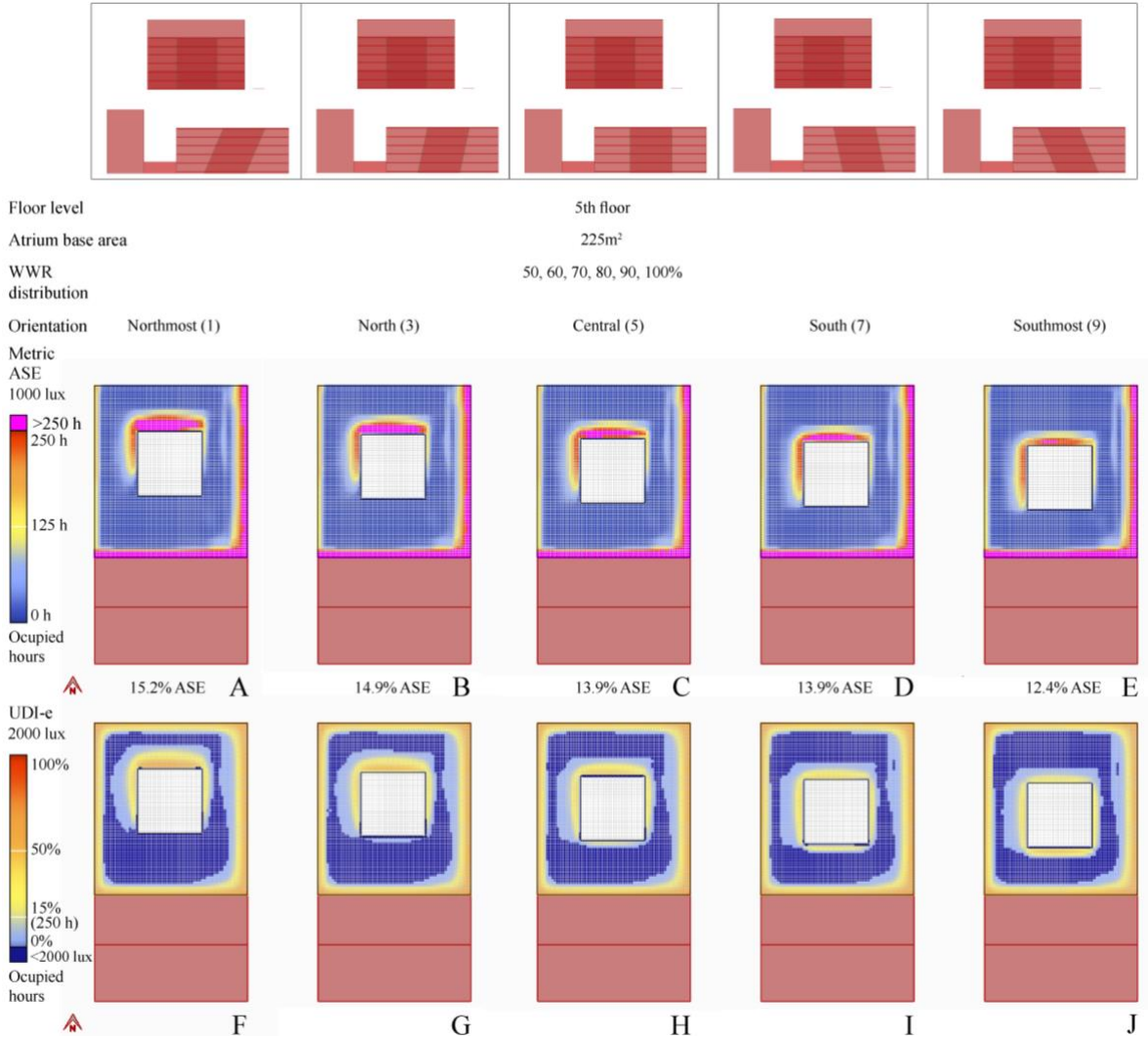


Figure 8-8 ASE and UDI-e result plots for the specified design solutions on the 5<sup>th</sup> floor.

### *8.2.3 Achievability of target criteria*

In the presented study, some metric thresholds were more easily achieved than others. Particularly the  $sDA_{100/50\%}$  target for 95% of space was a more lenient target compared to the  $sDA_{300/50\%}$  target for 50% space, seeing how  $sDA_{100/50\%}$  was still achieved by part of the design solutions on the 3<sup>rd</sup> floor, while the  $sDA_{300/50\%}$  target was only achieved from the 4<sup>th</sup> floor onwards. This may however be necessary, seeing how  $sDA_{100/50\%}$  works to ensure that a minimum threshold for daylight is met (aka a design constraint), while  $sDA_{300/50\%}$  provides targets to achieve a 'well-daylit' design. As findings on achievability of target criteria may differ between case studies, further research is recommended.

### *8.2.4 Sensitivity to design changes*

$sDA_{300/50\%}$ ,  $sDA_{100/50\%}$ , and ASE each showed a different sensitivity to design changes, such that the magnitude of variation was different for each metric. In particular,  $sDA_{100/50\%}$  showed the largest variations in results on lower floors, where daylight availability was low.  $sDA_{300/50\%}$ , in comparison, showed greater variations on upper floors, where conditions for daylighting were good. Here,  $sDA_{100/50\%}$  could not be used to compare design solutions, as the threshold was met by 100% of space. Similarly, ASE could not be used to compare design solutions on the lower floors, as hardly any direct sunlight reached there.

To conclude, when performance metrics align (i.e. design solutions with a higher  $sDA_{300/50\%}$  also have a higher  $sDA_{100/50\%}$ ), changing the lux threshold of metrics can help to better visualise the impact of design choices. However, when optimum design solutions vary between metrics, lux thresholds cannot simply be replaced by another, as each threshold highlights the design from a different angle and can provide

useful additional information. Lastly, in cases where a specific lux threshold is met by all or not met by any design solution (as was the case for  $sDA_{100/50\%}$  on the top floors and ASE on the lower floors), metrics lose their usefulness in comparing designs.

## 8.3 Significance of spatial and temporal daylight results

### 8.3.1 *Spatial daylight results*

Overall, spatial results make optimisation feasible, as they provide an aggregated value for daylighting in a building. Nonetheless, this aggregation leads to information loss. Although multiple thresholds can be used to supplement information, there is reason to scrutinise design outcomes produced by optimising %space results. This is because the target criteria give an absolute threshold (e.g. DA 50), whereas in reality daylight is continuous. Judging merely based on threshold criteria may therefore lead to a misinterpretation of results and misguided design choices. This can be shown with an example. Taking the previous results on the 5<sup>th</sup> floor (Figure 8-7), additional  $DA_{300}$  plots are provided below (Figure 8-9). As shown in the figure, northward orientations showed the highest  $sDA_{300/50\%}$  results, and southmost orientations the lowest. For northward oriented atria, the majority of areas failing to meet the threshold were located to the south of the atrium well and showed especially low DA. For southward orientations, however, areas failing to meet the target threshold were spread in areas surrounding the atrium well, but DA levels did not fall as low. Therefore, going by the temporal results, central to southmost orientations appear favourable, as the distribution of daylight is better and DA does not fall as low. This is also the case for the previously discussed  $DA_{100}$  results on the ground floor (Figure 8-6). To conclude, design optimisation with %space metrics may not always lead to the best design outcome,

because the hard DA threshold neglects DA levels in areas failing the threshold, which may nonetheless be close to the desired threshold.

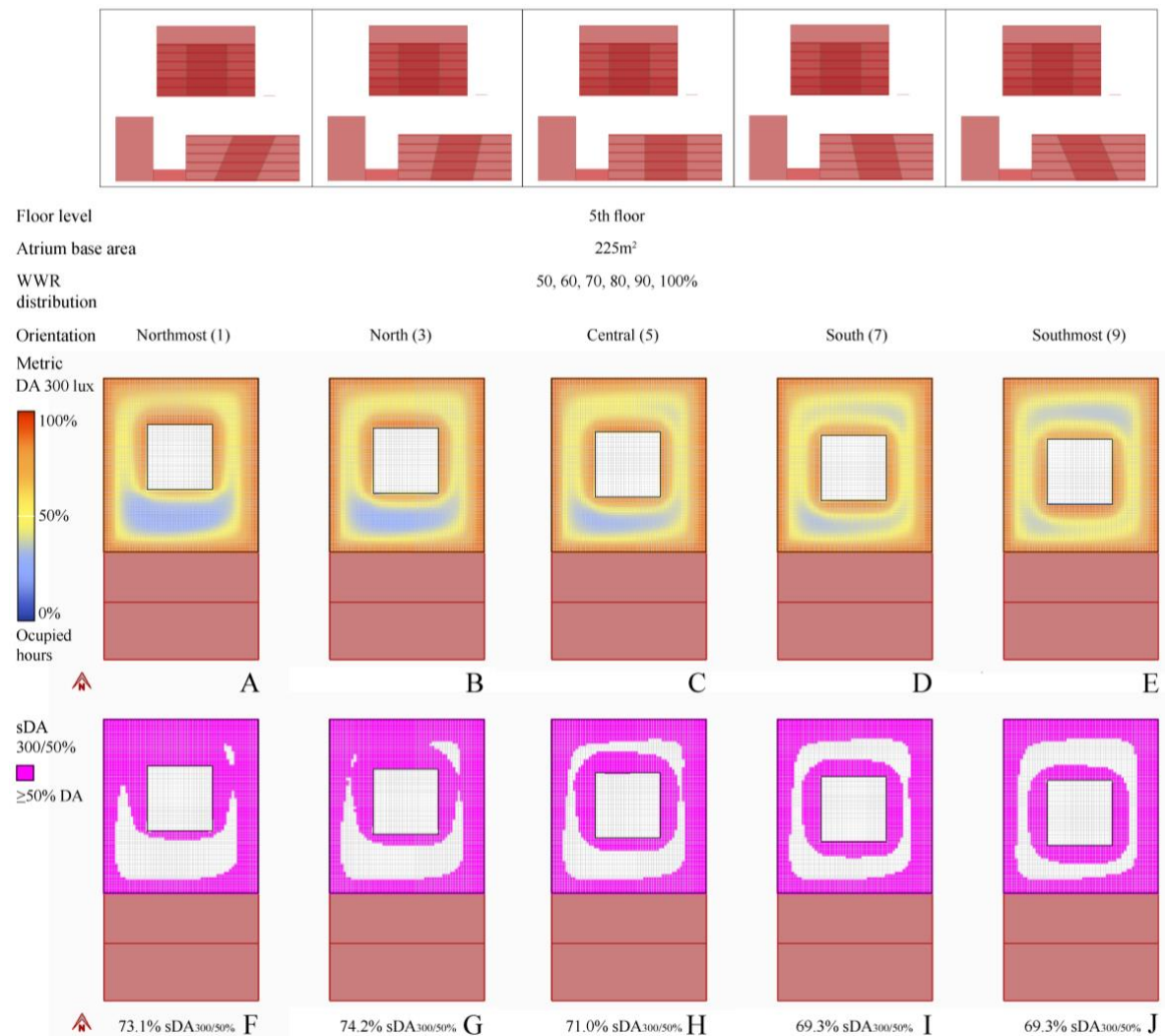


Figure 8-9 DA<sub>300</sub> and sDA<sub>300/50%</sub> result plots for the specified design solutions on the 5<sup>th</sup> floor.

### 8.3.2 Temporal daylight results

The %-time results helped to more accurately understand the impact of design changes on daylight performance. The results provided explanations for the observed patterns and trends in daylight performance analysed in the previous chapter and uncovered additional information and differences between design solutions that were not evident from the %-space results alone. Several examples of this will be given in the following.

For one, %-time plots made particularly under- or overlit locations visible (see Figure 8-8, Figure 8-9), thereby highlighting the problematic zones of a design solution. Such information can be used to inform layout designs (e.g., to place hallways where less daylight is available, and classrooms where there is more daylight available) or interventions (e.g., where the risk of glare is higher). This makes the %time results a valuable design tool for the early design stages.

Taking another example, %-time results provide explanations for the observed %-space results. In the current work, a deeper daylight penetration for southward orientations was traceable with the temporal ASE and UDI-e plots of the ground floor. This partially explained the higher  $sDA_{300/50\%}$  results on the lower floors. To illustrate, ASE and UDI-e results on the ground floor are shown in Figure 8-10. The ASE results at the atrium base highlight a deeper daylight penetration into the atrium well, a consequence of aligning the atrium well orientation with solar altitude angles. Additionally, the plots made differences in ASE visible that could not be read from the %-space results (as %-space results were 0% for all design solutions). Specifically, results showed that southward orientations increased direct sunlight penetration in spaces to the north, east, and west of the atrium well.

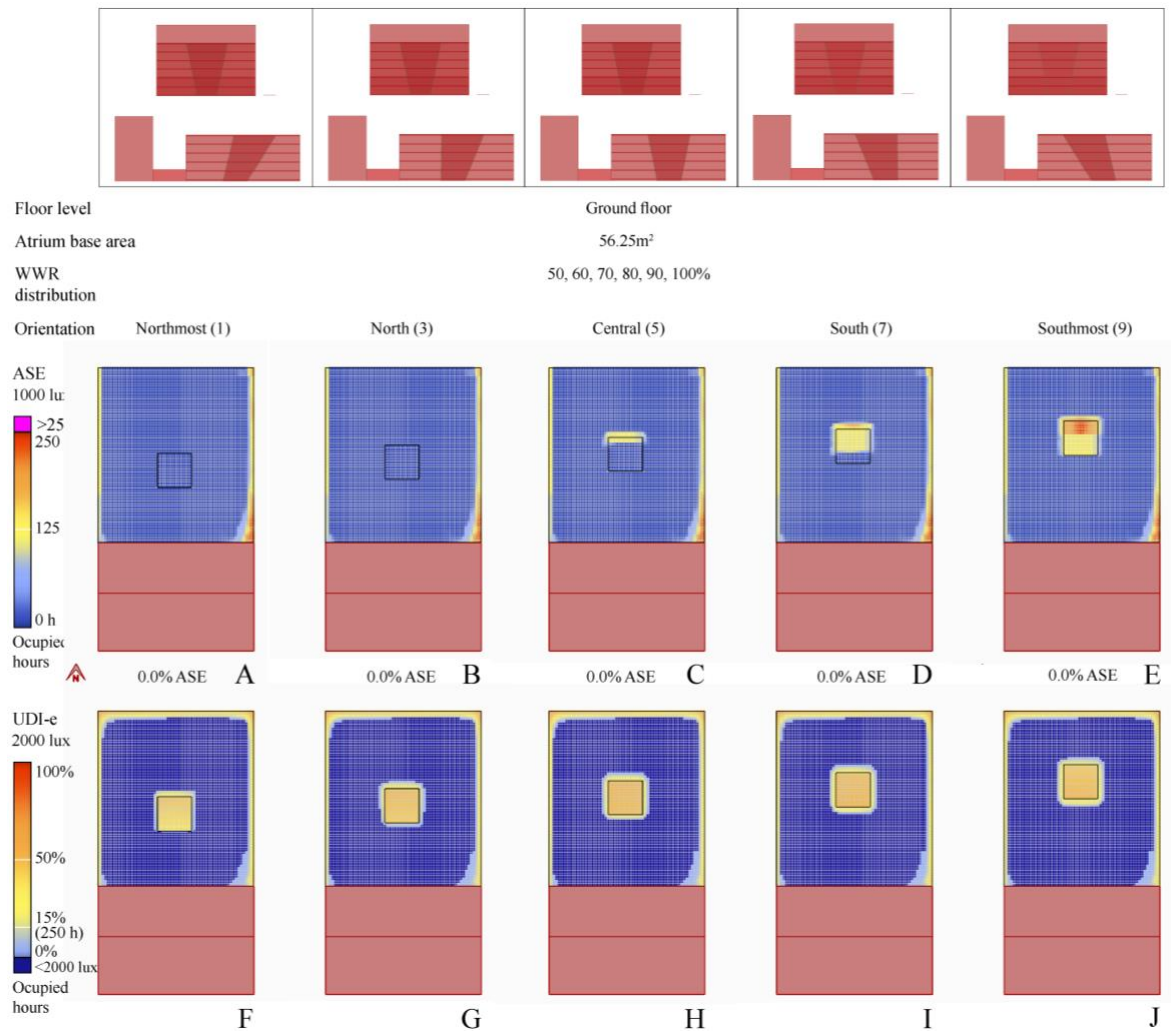
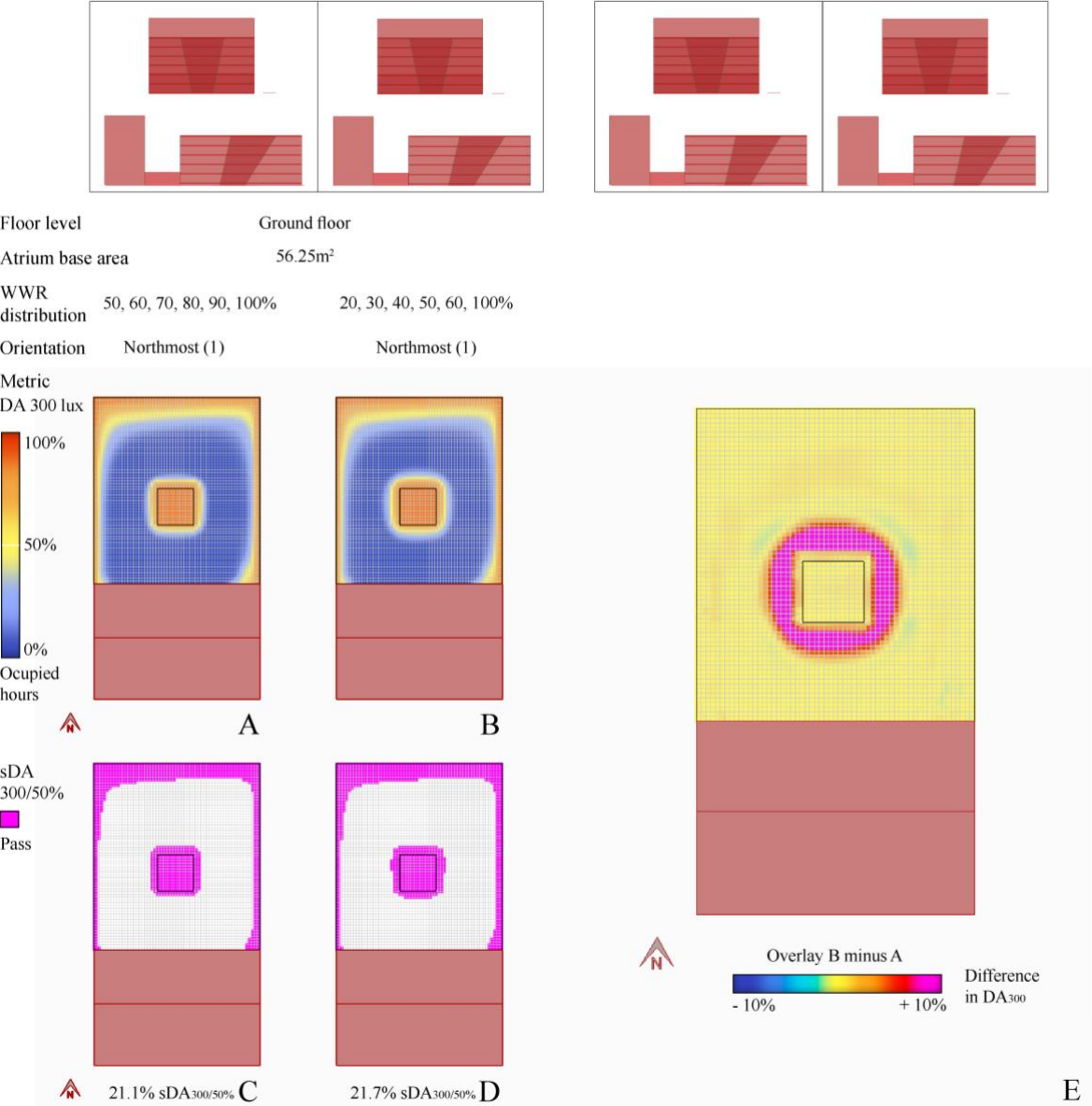


Figure 8-10 ASE and UDI-e result plots for the specified design solutions on the ground floor.

Regardless of the afore-described benefits of using temporal results to guide design decision making, there are also some limitations. The readability of %-time results is conditional on the available daylight in a building and the thresholds used. This means that %-time visualisations may require adjustments to the colour scale or require overlays to highlight the differences in daylight, especially when the impact of design changes is subtle. For example, on lower floors, the 2000 lux threshold was rarely exceeded. Hence, in this work, the UDI-e colour scale was adjusted to avoid single-colour plots for the metric (e.g. compare DA and UDI-e colour scale in this chapter).

Similarly, when assessing the impact of design changes on daylight performance, some designs were difficult to differentiate visually. For example, the impact of WWR distribution on lower floors was apparent in the %-space results but not in the %-time results (see Figure 7-8). Therefore, overlays may help highlight the differences between designs (as shown in Figure 7-8).



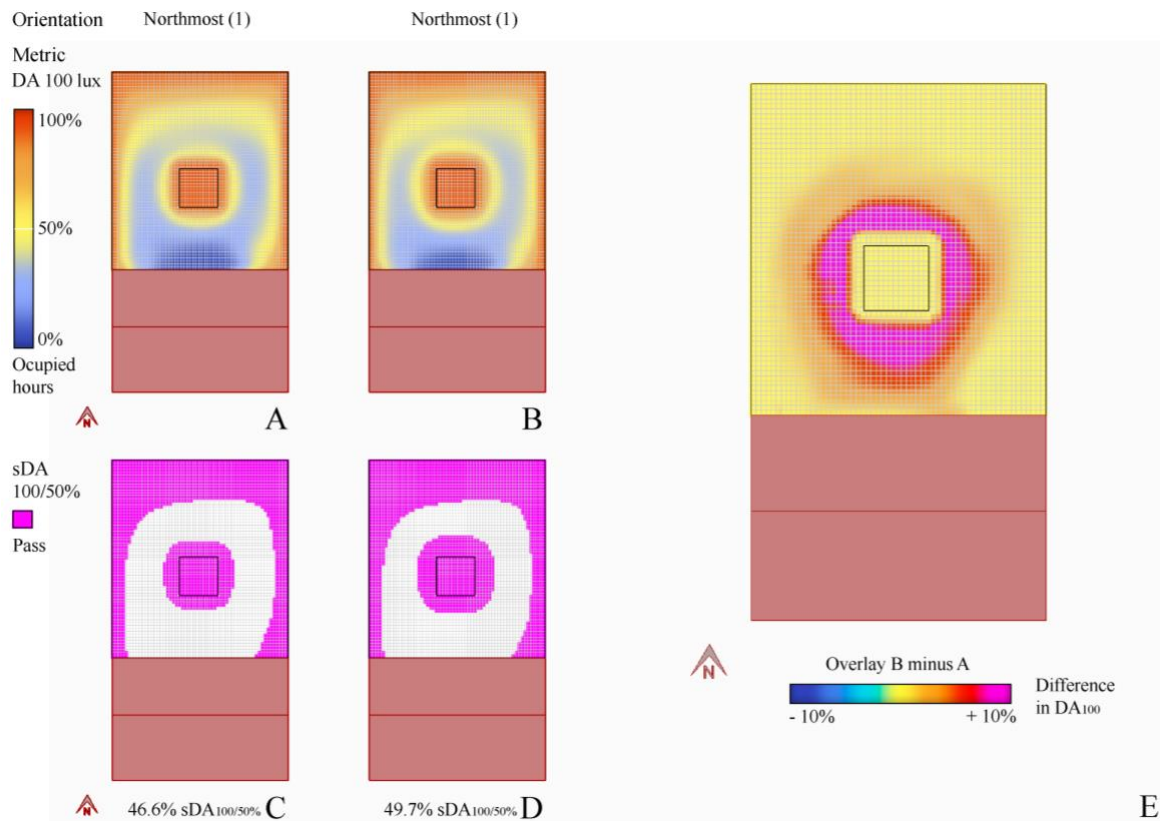


Figure 8-11 DA<sub>300</sub> and sDA<sub>300/50%</sub>, DA<sub>100</sub>, and sDA<sub>100/50%</sub> result plots for design solutions on the ground floor. The %space sDA results provided below the plots refer to atrium adjacent spaces only.

To conclude, whereas important information may be withheld in %-space performance metrics (e.g. on the distribution of daylight), %-time explorations may also be unable to capture or highlight differences between designs depending on the colour scale and lux thresholds applied. Additionally, temporal plots currently cannot be used in performance optimisation, as such processes require an aggregated value that describes the performance of a design solution. These limitations would need to be addressed in design exploration tools for designers, to provide the necessary information required for decision-making. The current work could be extended by looking further into such topics (i.e., information required by designers).

## 8.4 Conclusions

All daylight performance metrics had different sensitivity to design changes. sDA<sub>100/50%</sub>, in particular, showed large variations in performance between design

variants on lower floors, i.e. when daylight availability was low. In comparison,  $sDA_{300/50\%}$  showed greater variations on upper floors, i.e. when the conditions for daylighting were good. Where trends in  $sDA$  results for the 300 and 100 lux thresholds aligned (i.e. similar design optima), the variation in performance was much larger for the  $sDA_{100/50\%}$  than the  $sDA_{300/50\%}$  metric. In conclusion, changing the thresholds of the metrics can help to better visualise the impact of some design changes on daylight performance. However, optimum solutions can also vary between metrics. In such cases, one threshold cannot simply be used to replace another, as each threshold provides different information.

Importantly, %-space results did not always lead to the best design outcome, given the implementation of a hard threshold (i.e. DA50 for  $sDA_{300/50\%}$ ). This was because DA levels in areas failing the threshold were neglected. To counteract the negative effects of enforcing a hard threshold, one may consider combining  $sDA$  metrics with  $cDA$ , or apply uniformity measures.

Finally, this chapter pointed out the importance of %time results as design tools to gain an understanding of design consequences. In addition, temporal plots can be used to highlight well-daylit, overlit, or underlit zones to inform layout design. However, %time results also have their restrictions in that they rely on a visual comparison of results and thus cannot be used in design optimisation to compare a myriad of design variants. Further restrictions concern readability, as visualisations may require adjustments to the colour scale or overlays in order to highlight differences in performance.

## Chapter 9

### Final Guidelines and Conclusions

This section summarises the main conclusions drawn from findings discussed in chapters 4 to 8. Conclusions regarding ANN-based processes are presented first (chapters 4 to 6), followed by conclusions on daylight design exploration (chapters 7 and 8). Additionally, general conclusions are offered regarding the overarching topics of efficacy and the potentials of an ANN-integrated approach to design exploration. The conclusions and guideline are thus structured as follows:

#### 9.1 ANN-based processes

9.1.1 ANN-based daylight performance predictions (Chapter 4, 5)

9.1.2 ANNs in design exploration (Chapter 5)

9.1.3 ANN optimisation (Chapter 6)

9.1.4 Limitations and future work

#### 9.2 Daylight design exploration

9.2.1 Impact of atrium design changes on daylight performance (Chapter 7, 8)

9.2.2 Evaluation of daylight metrics as a measure of daylight performance (Chapter 7)

9.2.3 Percentage of space and percentage of time results (Chapter 7, 8)

9.2.4 Limitations and future work

#### 9.3 Conclusions on efficacy (general conclusions)

#### 9.4 Potentials of an ANN-integrated approach to design exploration (general conclusions)

## 9.1 ANN-based processes

### 9.1.1 ANN-based daylight performance predictions

Chapter 4 investigated ANN training methods for daylight predictions. The conclusions drawn laid the groundwork for the subsequent chapters and are detailed in the following. Given the breath of information discussed, subheadings are included, improving structure and readability –particularly for topics discussed later on in this chapter.

*Surrogates.* ANNs predicted DA<sub>300</sub> with high accuracy, typically within 3% DA MAE. ANNs were found to be suitable for 1.) replacing sensor points within simulations, and 2.) replacing entire simulations. In both cases, computational effort could be reduced without much impact simulation accuracy.

Above accuracies were obtained for five scenarios, which were tested individually. In the first scenario, the daylight distribution within a room changed by altering only the room depth. In the second scenario, the amount of daylight entering a space changed by altering only the window sizes in design variations. In the third scenario, the location of the window in the façade was changed, whereas in the fourth scenario, both window location and window size were altered in design variations. Finally, in the fifth scenario, an outside obstruction was added to the simulation model, therefore partially obstructing daylight entering the designed space. In this case, accuracies were slightly lower than in the other scenarios, but nonetheless remained within 4% DA MAE. To conclude, ANNs can replace simulations for variations in room depth, variations in window size and window position on the façade, also when introducing external daylight obstructions in the form of surrounding buildings.

*Correlation of MSE during training and MAE during testing.* Interestingly, MSE on the training data was not a good measure of predictive performance of an ANN model, especially when comparing ANNs with a different number of hidden layers. Although network architectures with two hidden layers typically showed higher MSE than network architectures with one hidden layer during training, the error on the test data were lower. In conclusion, the MSE during training cannot be used to evaluate the predictive performance of ANNs with a varying number of hidden layers.

*Ensembles.* In line with the above finding, the best trained ANN model (the ANN model that achieved the lowest MSE during training) did not always provide the most accurate results on unseen cases. Instead, averaging the output of an ensemble of ten trained network overall provided the most accurate results. Each of the ten networks were trained with randomised initial weights and also a randomisation division of data into validation and test subsets used during ANN training. It is therefore assumed, that this reduced the risk of implementing models that were trapped in local minima or began overfitting. In conclusion, training and test performance do not necessarily correlate, and implementing ANN ensembles improves the generalisation capability of ANN models.

### *9.1.2 ANNs in design exploration*

In Chapter 5, ANNs were applied to predict daylight for design variations of a central atrium. First, sensitivities to daylight simulation model were tested. Then, ANN models were used to map the daylight performance of entire design landscapes.

*Number of design variables an ANN should be trained on.* A question raised in Chapter 5 was whether it is better to train multiple smaller ANN ensembles on different design variable vs. one larger ANN ensemble on multiple design variable. The results of

the tests conducted are, however, inconclusive, and this appears to be a case-dependant problem. Prediction accuracy for the  $DA_{300}$  metric marginally dropped when training one, as opposed to two ANN ensembles on the design variables *atrium well orientation* and *atrium well geometry* (by twisting the atrium well and scaling the atrium base area). However, in subsequent Chapter 6, training one, as opposed to three ANN ensembles on different WWR distribution series, overall improved  $sDA_{300/50\%}$  predictions and the accurate mapping of the daylight performance of that specific design solution space.

In one case however, accuracies dropped clearly. Specifically, accuracies were significantly lower when one ANN ensemble was trained to predict the daylight performance of all six floors of the atrium building. Here, predictions were more accurate, when six ANN ensembles were trained to predict the daylight performance for each floor individually. This result is easily explained, as each floor has a different environment impacting daylight levels. For example, the lowest two floors are connected to an attached building, whereas the upper floors receive daylight from all cardinal directions. The daylight on each floor is also differently impacted by the overshadowing from the surrounding buildings. In order for the ANN models to not drop in accuracy when trained on all floors together, these missing descriptors would first need to be captured as input features for ANN training. In conclusion, the number of design variables, that an ANN model can be trained on at a time, is case-dependent. Notably, the more variables an ANN model is trained on, the higher the number of training input features, and the longer the training time required by the ANN model.

To conclude, it may be worthwhile to train multiple smaller ensembles if parameters greatly differ between simulated design scenarios. As more variables are likely to require more input features, ANN training time may increase. On the other hand, if multiple design variables are similar, it may be advantageous to train one larger

ensemble in order to improve ANN accuracies for spatial metrics. This may also lead to a reduction of required training samples, which in turn reduces ANN training time.

*ANN efficacy.* When training ANN models to predict new design solution spaces, three parameters (aside from the hyperparameters of model training) were found to greatly affect the efficacy of the ANN model and its accuracies: the number of design variables or input features, the size of ANN architecture, and the training sample size (i.e. number of samples required from the design solution space to train accurate models).

Regarding the number of input features, training time required for training a single larger, or multiple smaller ANN ensemble remained similar on the condition that the number of input features remained similar (one or two additional features, as shown in Chapter 5). However, overall training time increased as input features were added (larger ensembles require more input features describing all variables, as shown in Chapter 6). Therefore, when deciding on how to split/ train ANN ensembles on different design variables, the additional amount of input features for training a larger ANN ensemble need to be considered.

Regarding the size of ANN architecture, alongside the decision on how to split models on different design variables, choices on the ANN architecture greatly affect the efficacy of the approach. It was found that ANN training and prediction performance converged. As a result, improvements seen on the model performance were marginal when continuing to increase the ANN architecture. Conversely, training time greatly increased with the size of the ANN architecture i.e. number of hidden layers and hidden neurons). For example, results showed that training time increased five-fold for an improvement of 0.1% DA in accuracy (see Chapter 5). As prediction accuracy converges, several boundaries can be defined in order to keep ANN training time to a

minimum: a maximum number of nodes and hidden layers to be tested, training stop once a desired prediction accuracy is met, or training stop once improvements in accuracy stagnate.

### *9.1.3 Limitations and future work*

The results described in Chapter 5 and 6 demonstrated that ANNs are a good method for emulating daylight simulations and provide high prediction accuracies for a number of design variables and a number of daylight performance metrics. Despite the strengths of this research, a notable limitation concerns the unanswered question of how the ANN models will perform on other or more complex design scenarios. It is also not known if there is a limit to the number of design variables with which the models can still reliably predict daylight performance. Although one solution would be to train multiple neural networks when the number of design variables is too large, a method to automatically detect this limit still needs to be identified.

Another limitation of the current work concerns the practicality of an ANN-integrated approach. The parametrisation of the architectural model, alongside ANN feature extraction and ANN training, require time. In addition, this work promotes ANN integration in early design stages. In practice however, design strategies may change quickly and by the time a parametric model has been developed and an ANN model trained, the design may have already progressed in a new, unforeseen direction. Such spontaneous changes may in and of themselves already be difficult to implement in a parametric model. Adding to the complication, for ANN training, the model would need to be retrained on the new design variables using transfer learning. Because of the additional effort and time required for such processes, the currently proposed method may not yet appear practical to designers. Additionally, the required expertise to

develop both parametric and ANN prediction models may put off designers even further. Future work is therefore still required to develop design tools that simplifies such processes and makes them appealing to designers.

## 9.2 Daylight design exploration

We now leave the topic of ANN-based approaches and turn towards a discussion of daylight design explorations, starting with a presentation of the conclusions derived from explorations of design variants of a central atrium, presented in Chapter 7 and 8.

### 9.2.1 *Impact of atrium design changes on daylight performance*

*Overall impact of atrium design changes on  $sDA_{300/50\%}$ .* The central atrium was introduced to bring additional daylight into the building. Results however showed that improving daylight levels in atrium adjacent spaces on the lower floors proved difficult. Overall variation of daylight levels as a result of changing WWR distribution and atrium orientation remained small on the lowest four floors for the  $sDA_{300/50\%}$  metric (typically less than 3 percentage points), and was considerably higher for the top two floors (up to 13 percentage points for the  $sDA_{300/50\%}$  metric). The design factor that showed the biggest impact on lower floors was reduction of the atrium base area, which led to a decrease in  $sDA_{300/50\%}$  performance (around 9 percentage points) resulting from the increase in room depth.

*Design solutions increasing daylight on lower floors.*  $sDA_{300/50\%}$  in atrium adjacent spaces on lower floors could be increased by: 1) changing the WWR distribution to smaller WWRs on the top floors (e.g. to 20, 40, 60, 80 and 100% WWR from top to bottom floors), as the lower overall glazing area increased reflected daylight within the atrium, and 2) choosing a more southward orientation, which allowed for a deeper

daylight penetration into the building due to alignment with solar altitude angles. The two methods' success in terms of deeper daylight penetration could be seen when looking at the %-time results for ASE and UDI-e mapped onto the floor plan of the ground floor (see Chapter 8.3.6). Daylight levels on lower floors may further increase when adjusting radiance parameter settings (e.g. ambient bounces).

*Optimum orientations for the 300 lux and 100 lux thresholds.* Although southward orientations showed an increase in  $sDA_{300/50\%}$  for the lower floors, optimal solutions for  $sDA_{100/50\%}$  varied from northward to southward orientations on the lower floors. As explained by the %-time results mapped onto the floor plan, the decrease was mainly a result of the location of the atrium on the floor plan shifting with the tilt of the atrium to the north. This greatly increased the room depth in spaces to the south of the atrium well, which were the spaces failing to meet the 100 lux threshold. For the 300 lux threshold however, only spaces in direct proximity of the atrium well met the threshold on the lower floors. Here, the influence is as described in the previous paragraph. In short, rather than resulting from the atrium orientation, the performance results for  $sDA_{100/50\%}$  were a product of overshadowing in the south and the positioning of the atrium well within the floor plan. One might therefore argue, that southward orientations are advantageous, in that they allow for deeper daylight penetration into the building, and northward orientations are advantageous in that the amount of especially low-lit areas decreases. The former affect can be seen when selecting the 300 lux sDA threshold, the latter when selecting the 100 lux sDA threshold. At this point, it is important to note that the conclusions for  $sDA_{100/50\%}$  are based on a specific design setting (circumstantial, given the surrounding buildings to one side of atrium only) and would not hold for other designs.

Whereas optima for sDA<sub>300/50%</sub> were found in southward orientation from 4<sup>th</sup> to bottom floors, optima were seen around the central orientation (slightly south or northward oriented atria) on the top floor and for more northward orientations on the 5<sup>th</sup> floor. Results largely stem from the room depth (or location of the atrium on the floor plan) and the location of spaces failing the threshold. But also the splay angles of the atrium well walls and the exposure to the skylight influenced the results.

*Optimum orientations across floors.* Whereas optima for sDA<sub>300/50%</sub> were identified in southward orientations from the 4<sup>th</sup> to the bottom floors, optima were seen around the central orientation (slightly south or northward oriented atria) on the top floor and for more northward orientations on the 5<sup>th</sup> floor. The different optimum solutions for the different floors stem from differences in room depth (or location of the atrium on the floor plan) and the location of spaces failing the threshold. Notably, northward orientations on the top floors splayed the south-facing atrium well walls in a more perpendicular positions to the solar altitudes angles, thus increasing daylight in spaces to the north of the atrium, as shown by the %space results (see UDI-e and ASE) in Chapter 8.3.1. and 8.3.2. The reason as to why northward orientations were not the optimum orientation for sDA<sub>300/50%</sub> despite this, is because of the increase in room depth and overshadowing from surrounding buildings. Seeing as this result is circumstantial, one can conclude that southward orientations increase daylight on lower floors, while northward orientations increase daylight on top floors.

*Sunlight exposure.* The impact of splay angles on the ASE metric was particularly noticeable for the top floors. On the 6<sup>th</sup> and 5<sup>th</sup> floors, northmost orientations with 50% and 60% WWR had the highest ASE – a result of the southward-facing atrium well walls being splayed towards the skylight of the atrium. On the 4<sup>th</sup> floor, as a result of an increase of atrium depth and consequent obstruction of the north-facing atrium well

wall, north-ward, rather than northmost orientations showed the highest ASE. On the 3<sup>rd</sup> floor, results shifted again towards more central and finally southward orientations receiving more direct sunlight, supporting the argument of a deeper daylight penetration into the atrium well for southward orientations. It is concluded that northward orientations have a higher risk for the occurrence of glare on the top two to three floors, especially in spaces located to the north of the atrium well.

*Trade-offs.* Overall, design choices require making compromises as optimum solutions vary between floor levels and for different performance criteria. For one, there was a trade-off between upper and lower floors, i.e. southward orientations increased daylight on lower, but not necessarily on upper floors; reducing the WWR on upper floors increased daylight levels on lower floors, but reduced daylight levels on upper floors; reducing the atrium base areas reduced daylight on lower floors, but increase sDA performance on the top floor. Secondly, there is a trade-off in performance between metrics, i.e. design solutions with higher sDA performance have a higher risk for occurrences of glare, orientations that perform better in terms of sDA<sub>300/50%</sub>, fared worse for the sDA<sub>100/50%</sub> metric (as seen for results on the ground to 3<sup>rd</sup> floor, Chapter 7.1).

*Shifts in trends.* While as trends in daylight performance are easily identified, the particular optimum design for performance metrics are hard to predict from the identified trends alone. This is especially true when shifts in a pattern or trend stem from a change in location of spaces passing or failing the absolute thresholds set by the spatial metrics. For example, with smaller atrium areas, spaces to the north of the atrium started failing the sDA<sub>100/50%</sub> metric for northward orientations on the lowest two floors, so that southward orientations showed higher sDA<sub>100/50%</sub> with smaller, but not larger atria. Such shift in pattern are sensitive can further change with the

adjustment of radiance parameter settings. Thus, it is concluded that, a) optimum design results are not necessarily intuitive, b) spatial metric results are susceptible to shifts in pattern (as a result of the absolute pass/fail threshold), and c) underlying reason for changes in daylight performance need to be understood, so as to avoid a misinterpretation of performance metric results.

*Interrelation of design variables.* Overall, daylight performance results are influenced by the combination of design choices. For example, the magnitude of impact, that a design choice has on daylight performance, may vary depending on other design choices made. To illustrate, reducing the atrium base area had a much larger impact in reducing  $sDA_{100/50\%}$  for southward, rather than northward orientations on the ground and second floors. Thus, the 'negative affect' of design choice can vary depending on other design choices made. Hence, the combination of variables needs to be taken into consideration when aiming for a performance-driven design outcome.

### 9.2.2 *Evaluation of metrics as a measure of daylight performance*

*Complementary information.* The  $sDA_{100/50\%}$ ,  $sDA_{300/50\%}$  and ASE1000,250h metrics were used to assess the performance of design variants for a central atrium. The three metrics showed differences in patterns and trends (e.g. in terms of optima), each providing unique additional information. For example,  $sDA_{300/50\%}$  was higher for southward orientations on the lower floors, but at the same time, underlit areas could increase for the same design solutions (lower  $sDA_{100/50\%}$ ). In the current work,  $sDA_{300/50\%}$  showed the influence of splaying the atrium well walls, while  $sDA_{100/50\%}$  showed the impact of the atrium well location, which changed as a result of the parametric operation. Importantly, information drawn from different metrics was often complementary. Thus, for instance, a higher ASE on lower floors was seen for

southward orientations rather than northward orientations on the top floors. This shift was an indicator for deeper daylight penetration for southward orientations and therefore explained the higher  $sDA_{300/50\%}$  performance of said orientation on lower floors.

*Limitations arising from lux thresholds.* Some of the chosen illuminance thresholds used in spatial metrics (i.e. 100, 300, 1000 lux) showed a limited application, i.e., when a certain threshold was met for all design solutions, or not met by any design solutions. For example, performance results did not vary for the  $sDA_{100/50\%}$  metric on upper floors, regardless of the design change implemented, because all spaces passed the 100 lux threshold for 50% of occupied hours. Similarly, ASE results did not vary on lower floors, as no spaces met received direct sunlight exceeding 1000 lux for more than 250 hours in a year. Hence, in this work,  $sDA_{100/50\%}$  could not be used to compare the daylighting performance on the top floors and  $ASE_{1000,250h}$  could not be used to compare the performance of design variants on the bottom floors. In conclusion, depending on the design and floor level, some metrics cannot be used to differentiate between the daylight performance of different design solutions.

*Sensitivity.* All daylight performance metrics had different sensitivity to design changes. For example, the magnitude in change of performance varied between the metrics. This meant that the influence of some design changes was more noticeable for one, and less for another metric. In particular,  $sDA_{100/50\%}$  showed large variations in performance between design variants on lower floors, i.e. when daylight availability was low.  $sDA_{300/50\%}$ , in comparison, showed greater variations on upper floors, i.e. when the conditions for daylighting were good. Where patterns in sDA results for the 300 and 100 lux thresholds aligned (i.e. in reducing daylight when the atrium area decreased, or when increasing daylight for southward orientations) the variation in

performance was much larger for the  $sDA_{100/50\%}$  than the  $sDA_{300/50\%}$  metric. To conclude, changing the thresholds of the metrics can help to better visualise the impact of some design changes on daylight performance. However, optimum solutions can also vary between metrics. This means that one threshold cannot simply be used to replace another, as each threshold can provide unique information.

*sDA target criteria.* The  $sDA_{100/50\%}$  for 95% of space was a more lenient target, more easily achieved than the  $sDA_{300/50\%}$  target for 50% space. However, as this may only hold true for the case study of the present work and not always be transferable, further investigation is recommended.

*Irreconcilability.* Performance targets, as set by the threshold targets (i.e.  $sDA_{100/50\%}$  for at least 95% of space,  $sDA_{300/50\%}$  for at least 50% of space and ASE for not more than 10% of space), may not be reconcilable each other. As demonstrated in this work, the ASE target could not be simultaneously achieved with the  $sDA_{300/50\%}$  and  $sDA_{100/50\%}$  targets. Achieving the sDA targets of 95 and 50% of space therefore meant exceeding the ASE target of 10% space and increasing the risk of glare. To conclude, metrics are likely not reconcilable. Therefore, choosing design objectives using specific target criteria should be carefully considered, keeping in mind the trade-off between daylight availability, occupant well-being, visual comfort.

*Performance optimisation of zones, vs. performance optimisation of an entire building.* The impact of design changes is more visible in spaces that receive more daylight (especially for the  $sDA_{300/50\%}$  metric). For example,  $sDA_{300/50\%}$  results showed a much greater variation on top, than bottom floors. However, daylight trends often vary or contrast each other. E.g., on upper floors, northward orientations, larger WWR and smaller atrium areas showed higher  $sDA_{300/50\%}$  performance. However, all of these design choices resulted in lower  $sDA_{300/50\%}$  performance on the bottom floor.

Consequently, because the variation in performance is much lower on bottom floors, the optimisation of an entire building would result in a design outcome detrimental to daylight performance on lower floors (as shown in Chapter 7.3.4). Ironically, daylight performance improvements are most relevant on lower floors, where daylighting conditions are poorest (as shown by floors failing the  $sDA_{300/50\%}$  threshold in Chapter 7.1). Therefore, as a means of avoiding bias during optimisation, local (i.e. per floor or zone), rather than global (i.e. for the whole building) optimisation is recommended.

### 9.2.3 *Spatial and temporal daylight results*

*Complementary information.* The % time results provided valuable additional information to the % space results. For one, % time results provide explanations for the observed % space results. The percentage of time results visualised on the floor plan provide valuable information additional to the % of space results used to compare the performance of design decisions. For one, performance space results can be explained when looking at the % time results. For example, in the current work, a deeper daylight penetration for southward orientations became comprehensible looking at % time results for ASE and UDI-e mapped onto the floor plan on the ground floor, providing an explanation for southward orientations showing higher  $sDA_{300/50\%}$  results on lower floors. Similarly, on the top floor, where slight northward to slight southward orientations showed the highest  $sDA_{300/50\%}$  performance, the distribution of  $DA_{300}$  results made it possible to understand the trade-off and shifts in trend for the  $sDA_{300/50\%}$  metric by highlighting the spaces that were likely to fail the  $DA_{50}$  threshold.

*Daylight-distribution-informed decisions.* An important finding of the present work is that %time plots can make especially under- or overlit locations visible, thereby highlighting the problematic zones of a design solution. By using the information on

where spaces tend to fail or pass the threshold, this can inform layout design (e.g., placing hallways where there is less light, classrooms where there is more daylight available) or interventions (e.g. where risk of glare is higher). This makes the %time results a valuable design tool for the early design stages.

*Limitations of %space results.* Overall, there is reason to scrutinise design outcomes produced by optimising %space results. This is because the target criteria give an absolute threshold (e.g. a DA50 threshold), whereas in reality daylight is continuous. Judging merely based on threshold criteria may therefore misrepresent design strategies. For example, in the current work, northward orientation showed optimum sDA<sub>300/50%</sub> performance on the 5<sup>th</sup> floor (see Chapter 8.3.2). However, because the majority of areas failing to meet the threshold were in one location, northward orientations overall had the lowest DA<sub>300</sub>. In comparison, southward orientations had a spread of areas failing to meet the DA50 threshold surrounding the atrium well. As a result, daylight did not fall as low as it did for northward orientations. Therefore, in terms of a better daylight distribution, southward orientation, which received daylight for more hours than northward orientations, would appear as a more favourable design solution than the design optimum, which had a northward orientation. In conclusion, design optimisation with %space metrics may not always lead to the best design outcome.

*Limitations of %time results.* The readability of %time results is conditional to actual available daylight in a building and the thresholds used. What this means, is the %time visualisations may require adjustment to the colour scale or require overlays, in order to highlight the differences in daylight, especially when the impact of design changes is subtle. For example, on lower floor, the 2000 lux threshold was rarely exceeded. Hence, in this work, the UDI-e colour scale was adjusted so as to avoid single-

color plots for the metric (e.g. compare DA and UDI-e colour scale in Chapter 8). Similarly, when assessing the impact of design changes on daylight performance, some design could hardly be differentiated visually. For example, the impact of WWR distribution on lower floors was apparent in the %space results (sDA<sub>300/50%</sub> and sDA<sub>100/50%</sub>), but not in the %time results (DA<sub>300</sub> and DA<sub>100</sub>, see Chapter 8.2.2.). Therefore, overlays may be helpful in highlighting the differences between design (as shown in Chapter 8.1 and 8.2). In conclusion, whereas important information may be withheld in %space performance metrics (e.g. on the distribution of daylight), % time explorations may be unable to capture or highlight the difference between designs, as there is no absolute cut-off in performance thresholds. These limitations would need to be addressed in design exploration tools for designers, so as to provide the necessary information required for well-balanced decisions.

#### 9.2.4 *Limitations and future work*

The above-noted interpretations and conclusions on daylight performance analyses are only complete when keeping the limitations in mind. These limitations concern the quality of simulations undertaken, the choice of metrics used to assess performance, and the type of atrium design solutions analysed.

The daylight simulation results were obtained in connection with the 3-phase method, radiance parameter settings, and daylight grid settings specified in this study. Notably, simulation results were not validated against real world readings due to the complexity of replicating annual climate data. Simulation accuracies may also be low for atrium buildings in general, especially so for narrow atria (those with smaller atrium base areas), as the probability of rays tracing back to the sun may decrease (Diéguez *et al.*, 2016). Daylight simulations for atrium design will therefore still need to

validated in future work. Another limitation concerns the use of the ASE metric, which was employed in this work to assess direct sunlight penetration. The ASE metric has been shown to vary greatly between simulation software and settings, thus appearing to be more unreliable than other performance metrics (Brembilla and Mardaljevic, 2019). Taken together, the systematic errors in simulation, may certainly be mirrored in the ANNs. Therefore, this allowed to draw exclusively general conclusions on the impact of design changes on daylight performance. Any specific findings (e.g. regarding design optima and turning points in trends) will need to be validated in future research.

In this work, the main metrics used to assess the performance of design solutions were  $sDA_{300/50\%}$ ,  $sDA_{300/50\%}$ , UDI-e and ASE. The  $sDA_{300/50\%}$  threshold is based on extensive research to ensure better daylight quality and occupant satisfaction (Heschong Mahone Group, 2012), and relies on the 300 lux threshold required for office activities (ISO 8995-1, CIE S 008/E, EN12464-1). The thresholds used for the other metrics is however more difficult to interpret in terms of overall daylight quality. This aspect has been thoroughly discussed in the literature review (Chapter 2). An upper lux threshold and a maximum % of space for it (e.g., >2000/3000 lux or  $ASE_{1000,25h}$  for max 10% of space) may be indicators for a higher risk for glare. Yet, they rarely align with the  $sDA_{300/50\%}$  threshold. Additionally, lux levels exceeding the threshold such as 5000 lux may actually be preferred by occupants and positively affect comfort levels (Heschong Mahone Group, 2012). It may therefore be worth-while to clearly distinguish between direct and indirect lighting in future work. The current work offers but a starting point by using both UDI-e and ASE. Similarly, a 100 lux threshold does account for low available daylight levels, but the daylight quality in such spaces is questionable. It may therefore be less valuable as an optimisation metric, but rather a constraint to ensure that solutions meeting the  $sDA_{300/50\%}$  do not have larger areas falling below the

100 lux threshold. Seeing how the 95% target criteria for  $sDA_{100/50\%}$  was more easily achieved than the 50% criteria for  $sDA_{300/50\%}$ , it may also be worthwhile to increase the 100 lux specification to 150 or 200 lux, in order to ensure a better daylight distribution. This, as well as the differentiation between higher lux levels received from either direct or indirect lighting would need to be implemented in future research, perhaps within the visualisation or interface to improve readability of daylight performance results.

Current work may also be extended by using metrics that assess visual comfort (such as Daylight Glare Probability, Visual Comfort Index, Unified Glare Rating etc.), although they may be less suitable for the early design stages associated with form-finding and changes to the interior layout. Another metrics that would be excellent to extend current work on, is the EML (Equivalent Melanopic Lux), which allows to gain a human-centric perspective on daylight performance. This metric was not used in this work as simulation tools for the EML metric had not been developed at the time of conducting this research.

We have talked about limitations in regard to simulation settings and the metrics applied. There are also limitations in terms of the atrium types analysed. The study investigated square-shaped central atria. Central atria were not shown to be effective design strategies to increase daylight in atrium adjacent spaces. They are better as an architectural design feature, and mainly increase daylight levels because the internal space that needs to be daylit decreases with the placement of an atrium. Research can therefore be extended to include linear and semi-attached atrium types which are joined on one or more sides to the exterior façade and may therefore allow for a deeper daylight penetration into atrium adjacent spaces on lower floors. Future work could additionally compare different shapes, including morphing atria with different forms on top and lower floors, e.g. a square plan on top floors to increase reflected daylight

and rectangular plan on lower floors to increase the light admitting areas. Additionally, a comparison to reflective daylight systems (e.g. see Cunningham, Zaferiou and Lagios, 2014; Indarto *et al.*, 2017), or light tubes and fibre optic dish concentrators (e.g. Oh *et al.*, 2013) could provide a valuable addition to the body of knowledge.

### 9.3 Conclusions on efficacy

ANNs were used to reduce the computational load of performing daylight simulations in a design optimisation process. The efficacy of an ANN-integrated, compared to a purely simulation-based approach was deduced from the number of simulations that could be replaced minus the time required to train and optimise an ANN model:

$$\textit{Time Savings} = \textit{Omitted simulations} - \textit{ANN network optimisation and ANN training}$$

ANNs were adapted for the reason that, once trained, they can provide instantaneous predictions for unseen cases. By using the ANN models, overall simulation time could be reduced, which was extensive for annual daylight simulations. In this work, ANN predictions substituted 66% to 78% of simulations compared to a brute-force approach without affecting predictions accuracies.

ANN network optimisation and training time greatly varied with the size of network architecture (number of hidden layers and number of neurons in the hidden layers), the number of architectures tested and the number of training samples. Optimisation of network architecture can take up several hours to several days. The optimisation only needs to be undertaken once for a given design problem and the identified architecture can then be applied to similar solution spaces. In order to reduce the computational load of optimising the architecture, it is recommended to a.) not iterate through all possible architecture by adding one neuron at a time but increasing the increment, e.g. to 3 or 5 neurons at a time. Heuristic approaches can also be adopted,

in which the increments in architecture size is reduced when ANN training and test performance start to converge. b.) a smaller subset of the data can be used to configure a suitable network architecture. This overall performance would then need to be re-evaluated in one training run for the complete data set and c.) the network ensemble can be reduced, e.g. 4 networks parallelised across 4 cores instead of 10 networks.

ANN training time also greatly varied with the size of network architecture and training data. The cost of a second hidden layer was especially high. To illustrate, on a 2.6 GHz Intel Core i9 virtual machine, iterating an ensemble of 10 networks through all possible architectures, i.e. a 4-layered architecture with 2 hidden layers, tested for 5 to 40 neurons in the first hidden layers and 1 to 20 neurons in the second hidden layer, took approximately 40 hours with 12 out of 64 simulations used as training data. In comparison, iterating through only 38 to 40 neurons in a three-layered architecture only took 30 minutes. Iterating through a second layer with 19 to 20 neurons in said layer, ANN training time was 2.5 hours. When increasing the training data to 45 out of 162 simulations, ANN training of a 4-layered architecture (iterating through 19 to 20 neurons in the second hidden layer), drastically increased to approximately 14 hours. Therefore, the cost of ANN training needs to be weighed against the desired prediction accuracies. In this work, a conservative approach with both a large network architecture and a higher number of training samples was taken to ensure accuracy for the analysis of daylight performance results. Taken together, after deducting ANN training time, overall simulation time compared to the brute-force approach, was reduced by 65% to 71% without much impact on prediction accuracy.

Time savings were measured in comparison to a brute-force approach. Using other optimisation methods such as genetic algorithms (GA), the simulated space would be reduced as not all possible combinations of design variables are simulated. The

efficacy of an ANN integrated approach to genetic optimisation is therefore expected to drop. Previous research (Zhou and Haghghat, 2009) has nonetheless shown that adopting ANNs as part of the fitness function into the GA facilitate optimisation. It is therefore expected that integrating ANNs into GA will also be effective in reducing the computational effort in daylight optimisation problems.

Overall, ANN predictions have been shown capable of replacing simulations and mapping the performance of design solution spaces. The innate potential of the approach lies in that design exploration may become feasible where it was not before. With further research and development of the methodology, it is therefore the vision provide the possibility of finding solutions to design problems that may not have been deliverable before due to computational restraints.

#### 9.4 Potentials of an ANN-integrated approach to design exploration

The study shows how ANNs could be used to more efficiently explore the impact of design changes on the daylight performance in a parametric design environment. In this way, decisions can be made from the solution as a starting point towards the design as an informed outcome of the process. Such a solution to design approach can thereby ensure that design objectives (e.g. in performance) are met early on in the design stage.

The ANN models were integrated into a brute-force approach, as this gave the opportunity to visualise trends in design solutions across the entire solution space and enabled identification of turning points in performance and shifts in pattern. Brute force was deemed essential, firstly because causal relationships can be learned from the trends, and secondly because this provides designers with the freedom of choice to make informed decisions.

As previously mentioned, it is expected that ANNs can also be integrated in other optimisation algorithms such as the GA. This work however emphasises the usefulness of iterating through all possible design solutions.

A few other advantages of brute force over optimisation algorithms shall be named: in comparison to a design proposal that was optimised by selectively choosing design variables based on an objective function (as with a GA), brute-force maintains the flexibility to change design objectives post optimisation (in a GA, the optimisation would require to be rerun as fitness criteria change). This is because all partial results remain available. To illustrate, the designer can search for design variants that achieve increased daylight levels on the lower floors rather than a higher overall building daylight performance (total across all floors). In comparison, an algorithm that selectively evolved the available design solutions towards improving the overall building daylight performance will have omitted the design choices that result in increased daylight levels on the lower floors but therefore lower overall building daylight levels (i.e. the design solutions with lower atrium well glazing area but higher reflected daylight). To conclude, optimisation methods such genetic optimisation pose the risk of producing optimised solutions where the consequences of design choices remain understood. It is also not possible to view results for new the fitness criteria (optimisation towards other metrics, weighted differently) without rerunning the GA. Therefore, even if optimal solutions are rejected, the decision is informed as the consequences are known.

Brute force was overshadowed by optimisation techniques due the computational burden it imposes. ANNs can be trained to emulate simulations in order to reduce this burden. The proposed integration of ANNs therefore provides an opportunity to readapting the brute-force approach into the design process, consequently broadening the universe of choice for designers.

What is missing is the integration of instantaneous ANN predictions into design exploration tools so as to enable interactive exploration of designs (live design exploration). Currently available plug-ins such as Design Explorer<sup>5</sup> and Design Space Exploration<sup>6</sup> provide the possibility to facilitate design exploration and user interaction with the results. To integrate ANNs dynamically with such tools, several processes still need to be automated. These are a) architectural model parametrisation b) automated feature extraction, ANN training, validation and optimisation c) automated transfer of results into the existing interface for visualisation and feedback of performance results to the designer. Lastly, as part of the process, information essential to designers needs to be identified in order to prevent an overload of information and instead identify those criteria essential for a design problem (research into design decision making as well as interface design). This information may vary from designer to designer, and project to project and would need to be researched in future work.

Based on the findings of this work, it is expected that the application of ANNs can be extended to further performance assessment metrics, e.g. EML and solar irradiance. Similarly, it is also expected that ANNs can be implemented to map the performance of more complex design solution spaces. What was found to be important is that the variables between the different generated design solutions (that result in a different performance) need to be captured as input features for training the ANN models. The particular limitations of ANNs in emulating simulations and the complexity of design under which ANNs cannot anymore correctly perform predictions still need to be identified and are a topic for future research. In

---

<sup>5</sup> *Design Explorer v2*. Tomasetti, T., *CORE Studio*. Last updated by Peng, M. (2019). Available at: <https://tt-acm.github.io/DesignExplorer/> (accessed Oktober 21, 2019).

<sup>6</sup> *Design Space Exploration*. *Digital Structures*. Available at: <https://www.food4rhino.com/app/design-space-exploration#lg=1&slide=0> (accessed Oktober 21, 2019).

an ideal future scenario, ANNs would be integrated to perform predictions for a variety of design variables and performance metrics and would be integrated into an interface for live design explorations. The envisioned scenario, towards which future work is intended to lead, would therefore further broaden the horizon of evaluating design strategies and solutions to reach an outcome that best considers daylight (in terms of daylight availability, glare, overheating), energy performance, and human health and well-being.

## References

- Ahn, B. L. *et al.* (2014) 'Effect of LED lighting on the cooling and heating loads in office buildings', *Applied Energy*. Elsevier Ltd, 113(2014), pp. 1484–1489. doi: 10.1016/j.apenergy.2013.08.050.
- Alraddadi, T. A. (2004) 'The effect of the stepped section atrium on daylighting performance', *Architectural Science Review*, 47(3), pp. 303–310. doi: 10.1080/00038628.2000.9697536.
- Aries, M. B. C., Aarts, M. P. J. and Van Hoof, J. (2013) 'Daylight and health: A review of the evidence and consequences for the built environment', *Lighting Research and Technology*, pp. 1–22. doi: 10.1177/1477153513509258.
- Aschehoug, O. (1986) 'Daylight design for glazed spaces', in *Proceedings from the International Daylighting Conference*. CA, USA, pp. 237–243.
- Aschehoug, O. (1992) 'Daylight in glazed spaces', *Building Research & Information*, 20(4), pp. 242–245.
- Attia, S. *et al.* (2013) 'Assessing gaps and needs for integrating building performance optimization tools in net zero energy buildings design', *Energy and Buildings*. Elsevier B.V., 60, pp. 110–124. doi: 10.1016/j.enbuild.2013.01.016.
- Benardos, P. G. and Vosniakos, G.-C. (2007) 'Optimizing feedforward artificial neural network architecture', *Engineering Applications of Artificial Intelligence*, 20, pp. 365–382. doi: 10.1016/j.engappai.2006.06.005.
- Bhooshan, S. (2017) 'Parametric design thinking: A case-study of practice-embedded architectural research', *Design Studies*. Elsevier Ltd, 52, pp. 115–143. doi: 10.1016/j.destud.2017.05.003.
- Boubekri, M. (1995) 'The effect of the cover and reflective properties of a four-sided atrium on the behaviour of light', *Architectural Science Review*, 38(1), pp. 3–8.
- Boubekri, M. and Anninos, W. Y. (1996a) 'Daylight Efficiency of an Atrium: Part II—The Three-Sided Type', *Architectural Science Review*, 39(2), pp. 83–88. doi: 10.1080/00038628.1996.9697362.
- Boubekri, M. and Anninos, W. Y. (1996b) 'Daylight Efficiency of an Atrium: Part III—The Four-Sided Type', *Architectural Science Review*, 39(4), pp. 179–186. doi: 10.1080/00038628.1996.9697362.
- Boubekri, M. and Anninos, W. Y. (1996c) 'Daylighting Efficiency of an Atrium : Part I - The Four-Sided Type', *Architectural Science Review*, 39(2), pp. 75–81. doi: 10.4067/S0718-07642011000200003.
- Brembilla, E. and Mardaljevic, J. (2019) 'Climate-Based Daylight Modelling for compliance verification: Benchmarking multiple state-of-the-art methods', *Building and Environment*. Elsevier, 158(April), pp.

151–164. doi: 10.1016/j.buildenv.2019.04.051.

Calcagni, B. and Paroncini, M. (2004) 'Daylight factor prediction in atria building designs', *Solar Energy*, 76(6), pp. 669–682. doi: 10.1016/j.solener.2004.01.009.

Chow, T. T. *et al.* (2002) 'Global optimization of absorption chiller system by genetic algorithm and neural network', *Energy and Buildings*, 34, pp. 103–109. doi: 10.1016/S0378-7788(01)00085-8.

Cole, R. J. (1990) 'The effect of the surfaces adjoining atria on the daylight in adjacent spaces', *Building and Environment*, 25(1), pp. 37–42.

Conraud-bianchi, J. (2008) *A Methodology for the Optimization of Building Energy, Thermal, and Visual Performance*.

Cook, D. F., Ragsdale, C. T. and Major, R. L. (2000) 'Combining a neural network with a genetic algorithm for process parameter optimization', *Engineering Applications of Artificial Intelligence*, 13(4), pp. 391–396. doi: 10.1016/S0952-1976(00)00021-X.

Cunningham, P., Zaferiou, P. and Lagios, K. (2014) 'A Case Study in Reflective Daylighting', *Perkins+Will Research Journal. Special Issue : Innovation Incubator Research. Design Investigations In Practice*, 6(1).

El Daly, H. M. T. (2014) 'Automated fenestration allocation as complying with LEED rating system', *Alexandria Engineering Journal. Faculty of Engineering, Alexandria University*, 53(4), pp. 883–890. doi: 10.1016/j.aej.2014.09.011.

Deb, K. *et al.* (2002) 'A fast and elitist multiobjective genetic algorithm: NSGA-II', *IEEE Transactions on Evolutionary Computation*, 6(2), pp. 182–197. doi: 10.1109/4235.996017.

Diéguez, A. P. *et al.* (2016) 'Daylight utilization with light pipe in farm animal production: A simulation approach', *Journal of Daylighting*, 3(1), pp. 1–11. doi: 10.15627/jd.2016.1.

Doulos, L., Tsangrassoulis, A. and Topalis, F. (2008) 'Quantifying energy savings in daylight responsive systems: The role of dimming electronic ballasts', *Energy and Buildings*, 40(1), pp. 36–50. doi: 10.1016/j.enbuild.2007.01.019.

Du, J. and Sharples, S. (2009) 'Daylight Prediction in Atrium Buildings: Measurement, Theoretical Analysis and Simulation', in *PLEA 26th Conference on Passive and Low Energy Architecture*. Quebec City, Canada. Available at: <http://plea-arch.org/ARCHIVE/2009/2.STRATEGIES/2.1 Daylighting/POSTER/2-1-19-PLEA2009Quebec.pdf> (Accessed: 10 August 2017).

EEA (2018) *CO2 emission intensity, Monitoring Mechanism provided by European Environment Agency (EEA). Supply, transformation, consumption - all products - annual data provided by Statistical Office of the*

European Union (Eurostat). Available at: [https://www.eea.europa.eu/data-and-maps/daviz/co2-emission-intensity-5#tab-googlechartid\\_chart\\_11\\_filters=%7B%22rowFilters%22%3A%7B%7D%3B%22columnFilters%22%3A%7B%22pre\\_config\\_ugeo%22%3A%5B%22European Union \(current composition\)%22%5D%7D%7D](https://www.eea.europa.eu/data-and-maps/daviz/co2-emission-intensity-5#tab-googlechartid_chart_11_filters=%7B%22rowFilters%22%3A%7B%7D%3B%22columnFilters%22%3A%7B%22pre_config_ugeo%22%3A%5B%22European Union (current composition)%22%5D%7D%7D) (Accessed: 17 June 2020).

EFA (2014) 'EFA Daylight Design Guide Rev02', (January), pp. 1–10.

EIA (2017) *Trends in Lighting in Commercial Buildings*, U.S. Energy Information Administration. Available at: [https://www.eia.gov/consumption/commercial/reports/2012/lighting/?src=Consumption Commercial Buildings Energy Consumption Survey \(CBECS\)-b1](https://www.eia.gov/consumption/commercial/reports/2012/lighting/?src=Consumption Commercial Buildings Energy Consumption Survey (CBECS)-b1) (Accessed: 17 June 2020).

Eltaweel, A. and Su, Y. (2017) 'Parametric design and daylighting: A literature review', *Renewable and Sustainable Energy Reviews*, 73, pp. 1086–1103. doi: 10.1016/j.rser.2017.02.011.

Erlendsson, Ö. (2014) *Daylight Optimization : A Parametric Study of Atrium Design*. Royal Institute of Technology Stockholm, Sweden.

Evins, R. (2013) 'A review of computational optimisation methods applied to sustainable building design', *Renewable and Sustainable Energy Reviews*. Elsevier, 22, pp. 230–245. doi: 10.1016/j.rser.2013.02.004.

Figueiro, M. G. *et al.* (2017) 'The impact of daytime light exposures on sleep and mood in office workers', *Sleep Health*. National Sleep Foundation., 3(3), pp. 204–215. doi: 10.1016/j.sleh.2017.03.005.

Galasiu, A. D. and Reinhart, C. F. (2008) 'Current daylighting design practice: A survey', *Building Research and Information*, 36(2), pp. 159–174. doi: 10.1080/09613210701549748.

Ganatra, A. *et al.* (2011) 'Initial Classification Through Back Propagation In a Neural Network Following Optimization Through GA to Evaluate the Fitness of an Algorithm', *International Journal of Computer Science & Information Technology (IJCSIT)*, 3(1). doi: 10.5121/ijcsit.2011.3108.

Gen, M. and Cheng, R. (2000) *Genetic algorithms and engineering optimization*. Wiley. Available at: [https://books.google.co.uk/books?hl=de&lr=&id=U7MuV1q6P1oC&oi=fnd&pg=PR13&dq=genetic+optimization+architecture&ots=5-DqIqvrnw&sig=Gm-Bs88MFu0L\\_Iy90\\_T3dkBJw9g&redir\\_esc=y#v=onepage&q&f=false](https://books.google.co.uk/books?hl=de&lr=&id=U7MuV1q6P1oC&oi=fnd&pg=PR13&dq=genetic+optimization+architecture&ots=5-DqIqvrnw&sig=Gm-Bs88MFu0L_Iy90_T3dkBJw9g&redir_esc=y#v=onepage&q&f=false) (Accessed: 18 June 2017).

Gerber, D. J. and Lin, S.-H. E. (2013) 'Geometric complexity and energy simulation: Evolving performance driven architectural form', in *CAADRIA: Proceedings of the 18th International Conference on Computer-Aided Architectural Design Research in Asia*. Singapore, pp. 97–96. doi: [http://cumincad.scix.net/cgi-bin/works/Show?\\_id=caadria2013\\_006&sort=DEFAULT&search=gerber&hits=7](http://cumincad.scix.net/cgi-bin/works/Show?_id=caadria2013_006&sort=DEFAULT&search=gerber&hits=7).

- Hafiz, D. (2015) 'Daylighting, Space, and Architecture: A Literature Review', *Enquiry: A Journal for Architectural Research*, 12(1), pp. 1–8. doi: 10.17831/enq:arcc.v12i1.391.
- Hecht-Nielsen, R. (1989) 'Theory of the Backpropagation Neural Network', in *Proceedings of the International Joint IEEE Conference on Neural Networks*. San Diego, CA, USA, pp. 593–605. doi: 10.1109/IJCNN.1989.118638.
- Heschong, L. *et al.* (2012) 'DAYLIGHT METRICS REPORT for the CEC PIER Daylighting Plus Research Program'. doi: 10.13140/RG.2.2.33003.59689.
- Heschong, L., Wright, Roger L and Okura, S. (2002) 'Daylighting Impacts on Human Performance in School', *Journal of the Illuminating Engineering Society*, 31(2), pp. 101–114. doi: 10.1080/00994480.2002.10748396.
- Heschong, L., Wright, Roger L. and Okura, S. (2002) 'Daylighting impacts on retail sales performance', *Journal of the Illuminating Engineering Society*, 31(2), pp. 21–25. doi: 10.1080/00994480.2002.10748389.
- Heschong Mahone Group (2003) *System Design, Modular Skylight Systems for Suspended Ceilings. Project 5.3.5*. doi: 10.1016/B978-0-323-29644-1.00029-3.
- Heschong Mahone Group (2012) *Daylight Metrics - PIER Daylighting Plus Research Program Final Report to the California Energy Commission*. CA, USA.
- Hudson, R. (2010) *Strategies for parametric design in architecture: An application of practice led research*. Universtiy of Bath.
- Iyer-Raniga, U. (1994) 'Daylighting in atrium spaces', *Architectural Science Review*, 37(4), pp. 195–208.
- Jagannath, A. *et al.* (2017) 'The genetics of circadian rhythms, sleep and health', *Human Molecular Genetics*, 26(R2), pp. R128–R138. doi: 10.1093/hmg/ddx240.
- Janjai, S. and Plaon, P. (2011) 'Estimation of sky luminance in the tropics using artificial neural networks: Modeling and performance comparison with the CIE model', *Applied Energy*. Elsevier Ltd, 88(3), pp. 840–847. doi: 10.1016/j.apenergy.2010.09.004.
- Jenkins, D. and Newborough, M. (2007) 'An approach for estimating the carbon emissions associated with office lighting with a daylight contribution', *Applied Energy*, 84(6), pp. 608–622. doi: 10.1016/j.apenergy.2007.02.002.
- Jones, N. L. and Reinhart, C. F. (2019) 'Effects of real-time simulation feedback on design for visual comfort', *Journal of Building Performance Simulation*, 12(3), pp. 343–361. doi:

10.1080/19401493.2018.1449889.

Kayri, M. (2016) 'Predictive Abilities of Bayesian Regularization and Levenberg–Marquardt Algorithms in Artificial Neural Networks: A Comparative Empirical Study on Social Data', *Mathematical and Computational Applications*, 21(2), p. 20. doi: 10.3390/mca2102020.

Kazanasmaz, T., Gunaydin, M. and Binol, S. (2009) 'Artificial neural networks to predict daylight illuminance in office buildings', *Building and Environment*, 44, pp. 1751–1757. doi: 10.1016/j.buildenv.2008.11.012.

Kearney, W. T. (2016) *Using Genetic Algorithms to Evolve Artificial Neural Networks*. Colby College.

Klusmann, D. L. and Murphy, M. S. (2015) 'Intelligent Lighting Control System and Network Comprising Multiple-Channel Photo Sensor'.

Köster, H. (2018) *Daylighting Controls, Performance, and Global Impacts*, *Encyclopedia of Sustainability Science and Technology*. doi: 10.1007/978-1-4939-2493-6\_198-4.

Koza, J. R. and Rice, J. P. (1991) 'Genetic generation of both the weights and architecture for a neural network', in *IJCNN-91-Seattle International Joint Conference on Neural Networks*. Seattle, WA, USA: IEEE, pp. 397–404. doi: 10.1109/IJCNN.1991.155366.

Laouadi, A. (2004) 'Design with SkyVision: a computer tool to predict daylighting performance of skylights', in *CIB 2004 World Building Congress*. Toronto, Canada, pp. 1–11.

Lauridsen, P. K. B. and Petersen, S. (2014) 'Integrating indoor climate, daylight and energy simulations in parametric models and performance-based design', in *Proceedings of the third international workshop on design in civil and environmental engineering*, pp. 111–118.

LeCun, Y. *et al.* (1998) 'Efficient BackProp', in *Neural Networks: Tricks of the trade*. Berlin, Germany: Springer. Available at: <http://yann.lecun.com/exdb/publis/pdf/lecun-98b.pdf> (Accessed: 27 June 2017).

Li, D. H. W. (2010) 'A review of daylight illuminance determinations and energy implications', *Applied Energy*. Elsevier Ltd, 87(7), pp. 2109–2118. doi: 10.1016/j.apenergy.2010.03.004.

Lopez, G. and Gueymard, C. A. (2007) 'Clear-sky solar luminous efficacy determination using artificial neural networks', *Solar Energy*, 81(7), pp. 929–939. doi: 10.1016/j.solener.2006.11.001.

Machairas, V., Tsangrassoulis, A. and Axarli, K. (2014) 'Algorithms for optimization of building design: A review', *Renewable and Sustainable Energy Reviews*, 31(1364), pp. 101–112. doi: 10.1016/j.rser.2013.11.036.

Maesano, C. and Annesi-Maesano, I. (2012) 'Impact of Lighting on School Performance in European

Classrooms', *Clima2016*, doi 10, pp. 1–14.

Magnier, L. and Haghighat, F. (2010) 'Multiobjective optimization of building design using TRNSYS simulations, genetic algorithm, and Artificial Neural Network', *Building and Environment*. Elsevier Ltd, 45(3), pp. 739–746. doi: 10.1016/j.buildenv.2009.08.016.

Mardaljevic, J. (2006) 'Examples of Climate-Based Daylight Modelling', in *CIBSE National Conference: Engineering the future*. London, U.K.

Mardaljevic, J. (2008) 'Climate-Based Daylight Analysis for Residential Buildings Impact of various window configurations, external obstructions, orientations and location on useful daylight illuminance', *IESD Technical report*. De Montfort University. Available at: <http://www.thedaylightsite.com/>.

Mardaljevic, J. et al. (2012) 'Daylighting Metrics: Is There a Relation Between Useful Daylight Illuminance and Daylight Glare Probability?', *Ibpsa-England Bso12*, (September), pp. 189–196.

Mardaljevic, J. (2015) 'Climate-Based Daylight Modelling And Its Discontents', in *CIBSE Technical Symposium*. London, pp. 1–12. Available at: <http://www.cibse.org/knowledge/knowledge-items/detail?id=a0q20000008I76T>.

Mardaljevic, J. and Christoffersen, J. (2016) "'Climate connectivity" in the daylight factor basis of building standards', *Building and Environment*. Elsevier Ltd, pp. 1–10. doi: 10.1016/j.buildenv.2016.08.009.

Mardaljevic, J., Hescong, L. and Lee, E. (2009) 'Daylight metrics and energy savings.', *Lighting Research and Technology*, 41, pp. 261–283. doi: 10.1177/1477153509339703.

Mardaljevic, J. and Nabil, A. (2005) 'Useful daylight illuminance: a new paradigm for assessing daylight in buildings', *Lighting Research and Technology*, 37(1), pp. 41–59. doi: 10.1191/1365782805li128oa.

Mardaljevic, J. and Nabil, A. (2006) 'Useful Daylight Illuminances: A Replacement for Daylight Factors', *Energy and Buildings*, 38, pp. 905–913.

Marill, T. and M. Green, D. (1963) 'On the effectiveness of receptors in recognition systems', *Information Theory, IEEE Transactions on*, 9, pp. 11–17. doi: 10.1109/TIT.1963.1057810.

Marquardt, D. (1963) 'An Algorithm for Least-Squares Estimation of Nonlinear Parameters', *SIAM Journal on Applied Mathematics*, 11(2), pp. 431–441.

McHugh, J. et al. (2004) 'Effectiveness of Photocontrols with Skylighting', in *IESNA Annual Conference*, pp. 1–18.

McNeil, A. and Lee, E. S. (2012) 'A validation of the Radiance three-phase simulation method for modelling annual daylight performance of optically complex fenestration systems', *Journal of Building*

- Performance Simulation*, 6(1), pp. 24–37. doi: 10.1080/19401493.2012.671852.
- Mohsenin, M. and Hu, J. (2015) 'Assessing daylight performance in atrium buildings by using Climate Based Daylight Modeling', *Solar Energy*, 119, pp. 553–560. doi: 10.1016/j.solener.2015.05.011.
- Morimoto, T., Takeuchi, T. and Hashimoto, Y. (1993) 'Growth optimization of plant by means of the hybrid system of genetic algorithm and neural network', *Proceedings of 1993 International Joint Conference on Neural Network*, pp. 2979–2982. doi: 10.1109/IJCNN.1993.714348.
- Neto, A. H. and Fiorelli, F. A. S. (2008) 'Comparison between detailed model simulation and artificial neural network for forecasting building energy consumption', *Energy and Buildings*, 40(12), pp. 2169–2176. doi: 10.1016/j.enbuild.2008.06.013.
- Nguyen, A.-T., Reiter, S. and Rigo, P. (2014) 'A review on simulation-based optimization methods applied to building performance analysis', *Applied Energy*, 113, pp. 1043–1058. doi: 10.1016/j.apenergy.2013.08.061.
- Oh, S. J. *et al.* (2013) 'Computational analysis on the enhancement of daylight penetration into dimly lit spaces: Light tube vs. fiber optic dish concentrator', *Building and Environment*. Elsevier Ltd, 59, pp. 261–274. doi: 10.1016/j.buildenv.2012.08.025.
- Parent, M. D. and Murdock, J. B. (1989) 'Skylight Dome Well System Analysis from Intensity Distribution Data', *Lighting Research & Technology*, 21(3), pp. 111–123.
- Pattanasethanon, S., Lertsatitthanakorn, C. and Atthajariyakul, S. (2008) 'An accuracy assessment of an empirical sine model, a novel sine model and an artificial neural network model for forecasting illuminance / irradiance on horizontal plane of all sky types at Mahasarakham, Thailand', 49, pp. 1999–2005. doi: 10.1016/j.enconman.2008.02.014.
- Pudil, P., Novovi, J. and Kittler, J. (1994) 'Floating search methods in feature selection', *Pattern Recognition Letters*, 15(November), pp. 1119–1125.
- Reinhart, F. C., Mardaljevic, J. and Rogers, Z. (2013) 'Dynamic Daylight Performance Metrics for Sustainable Building Design', *The journal of the illuminating Engineering Society of North America*, 3(1), pp. 7–31. doi: 10.1582/LEUKOS.2006.03.01.001.
- Reinhart, C. F. (2004) 'Lightswitch-2002: A model for manual and automated control of electric lighting and blinds', *Solar Energy*, 77(1), pp. 15–28. doi: 10.1016/j.solener.2004.04.003.
- Reinhart, C. F., Mardaljevic, J. and Rogers, Z. (2013) 'Dynamic Daylight Performance Metrics for Sustainable Building Design', *The journal of the illuminating Engineering Society of North America*, 3(1),

pp. 7–31. doi: 10.1582/LEUKOS.2006.03.01.001.

Reinhart, C. F. and Walkenhorst, O. (2001) 'Validation of dynamic RADIANCE-based daylight simulations for a test office with external blinds', *Energy and Buildings*, 33(7), pp. 683–697. doi: 10.1016/S0378-7788(01)00058-5.

Ritchie, M. D. *et al.* (2003) 'Optimization of neural network architecture using genetic programming improves detection and modeling of gene-gene interactions in studies of human diseases', *BMC Bioinformatics* 2003 4:1. BioMed Central, 105(1), pp. 60–61. doi: 10.1002/1096-8628(20010108)105:1<60::aid-ajmg1062>3.0.co.

Roache, L. (2002) 'Summertime Performance of an Automated Lighting and Blinds Control System', *International Journal of Lighting Research and Technology*, 34(1).

Samant, S. (2017) 'Atrium and its adjoining spaces: a study of the influence of atrium façade design Swinal Samant Atrium and its adjoining spaces: a study of the influence of atrium façade design', *Architectural Science Review*, 54(4). doi: 10.1080/00038628.2011.613640.

Samant, S. and Yang, F. (2007) 'Daylighting in atria: The effect of atrium geometry and reflectance distribution', *Lighting Research and Technology*, 39(2), pp. 147–157. doi: 10.1177/1365782806074482.

Schaffer, J. D., Whitley, D. and Eshelman, L. J. (1992) 'Combinations of genetic algorithms and neural networks: a survey of the state of the art', in *[Proceedings] COGANN-92: International Workshop on Combinations of Genetic Algorithms and Neural Networks*. Baltimore, MD, USA: IEEE Comput. Soc. Press, pp. 1–37. doi: 10.1109/COGANN.1992.273950.

Schon, D. A. (1991) *The Reflective Practitioner: How Professionals Think in Action*. 3rd editio. Farnham, Surrey: Ashgate.

Sharples, S. and Lash, D. (2007) 'Daylight in Atrium Buildings: A Critical Review', *Architectural Science Review*, 50(4), pp. 301–312. doi: 10.3763/asre.2007.5037.

Sharples, S. and Shea, A. D. (1999) 'Roof obstructions and daylight levels in atria: A model study under real skies', *Lighting Research & Technology*, 31(4), pp. 181–185. doi: 10.1177/096032719903100408.

Suyoto, W., Indraprastha, A. and Purbo, H. W. (2015) 'Parametric Approach as a Tool for Decision-making in Planning and Design Process. Case study: Office Tower in Kebayoran Lama', *Procedia - Social and Behavioral Sciences*. Elsevier B.V., 184(August 2014), pp. 328–337. doi: 10.1016/j.sbspro.2015.05.098.

Tian, L. and Noore, A. (2005) 'Evolutionary neural network modeling for software cumulative failure time prediction', *Reliability Engineering & System Safety*, 87(1), pp. 45–51. doi: 10.1016/j.res.2004.03.028.

- Torczon, V. (1995) 'PATTERN SEARCH METHODS FOR NONLINEAR OPTIMIZATION', in. Available at: [https://pdfs.semanticscholar.org/895d/9505bc355499a1a3dc73745a539992689d1e.pdf?\\_ga=2.244359493.1921429837.1497702832-1620719719.1497702832](https://pdfs.semanticscholar.org/895d/9505bc355499a1a3dc73745a539992689d1e.pdf?_ga=2.244359493.1921429837.1497702832-1620719719.1497702832) (Accessed: 17 June 2017).
- Torres, S. and Lo Verso, V. R. M. (2015) 'Comparative analysis of simplified daylight glare methods and proposal of a new method based on the cylindrical illuminance', *Energy Procedia*. Elsevier B.V., 78, pp. 699–704. doi: 10.1016/j.egypro.2015.11.074.
- Tresidder, E. (2014) *Accelerated optimisation methods for low-carbon building design*. De Montfort University, Leicester. Available at: <https://www.dora.dmu.ac.uk/xmlui/handle/2086/10512>.
- Turrin, M. *et al.* (2010) 'Integrated design of a large span roof: A parametric investigation on structural morphology, thermal comfort and daylight', *Proceedings of the ICCCB*.
- Twomey, J. M. and Smith, A. E. (1995) 'Performance measures, consistency, and power for artificial neural network models', *Mathematical Computer Modelling*, 21(1/2), pp. 243–258.
- Whitney, A. W. (1971) 'A Direct Method of Nonparametric Measurement Selection', *Computers, IEEE Transactions on*, 20, pp. 1100–1103. doi: 10.1109/T-C.1971.223410.
- Wilamowski, B. M. (2009) 'Neural network architectures and learning algorithms', *IEEE Industrial Electronics Magazine*, 3(4), pp. 56–63.
- Wong, S. L., Wan, K. K. W. and Lam, T. N. T. (2010) 'Artificial neural networks for energy analysis of office buildings with daylighting', *Applied Energy*. Elsevier Ltd, 87(2), pp. 551–557. doi: 10.1016/j.apenergy.2009.06.028.
- Wronski, L. (2013) *Infinity Tower/SOM*. Available at: <https://www.archdaily.com/331128/in-progress-infinity-tower-som> (Accessed: 12 May 2018).
- Yavuz, C., Yanikoglu, E. and Güler, Ö. (2012) 'Evaluation of daylight responsive lighting control systems according to the results of a long term experiment', *Light and Engineering*, 20(4), pp. 75–83.
- Zhang, S., Zang, H. and Hapeshi, K. (2010) *A Review of Nature-Inspired Algorithms*. Edited by H. Persaei. New York, Chichester, Weinheim, Brisbane, Singapore, Toronto: Wiley-Interscience Publication. doi: 10.1016/S1672-6529(09)60240-7.
- Zhao, H. X. and Magoulès, F. (2012) 'A review on the prediction of building energy consumption', *Renewable and Sustainable Energy Reviews*. Elsevier Ltd, 16(6), pp. 3586–3592. doi: 10.1016/j.rser.2012.02.049.
- Zhou, L. and Haghghat, F. (2009) 'Optimization of ventilation system design and operation in office

environment, Part I: Methodology', *Building and Environment*. Elsevier Ltd, 44(4), pp. 651–656. doi: 10.1016/j.buildenv.2008.05.009.

Zhou, S. and Liu, D. (2015) 'Prediction of Daylighting and Energy Performance Using Artificial Neural Network and Support Vector Machine', *American Journal of Civil Engineering and Architecture*, Vol. 3, 2015, Pages 1-8, 3(3A), pp. 1–8. doi: 10.12691/AJCEA-3-3A-1.

Zongker, D. and Jain, A. (1996) 'Algorithms for Feature Selection: An Evaluation', in *Proceedings of 13th International Conference on Pattern Recognition*. Vienna, Austria, pp. 18–22.

## Publications

Lorenz, C. L. *et al.* (2020) 'Artificial Neural Networks for parametric daylight design', *Architectural Science Review*. Taylor & Francis, 63(2), pp. 210–221. doi: 10.1080/00038628.2019.1700901.

Lorenz, C.L. *et al.* (2019) 'Input Feature Selection and Optimization for ANNs Predicting Daylight in Buildings', in *EG-ICE 26th Workshop on Intelligent Computing in Engineering*.

Lorenz, C.L. *et al.* (2019) 'Machine Learning in Design Exploration: An Investigation of the Sensitivities of ANN-Based Daylight Predictions.', in *CAAD Futures Conference Proceedings*. Deajeon, South Korea, pp. 153–165.

Lorenz, C.L. *et al.* (2018) 'Artificial Neural Network-Based Modelling for Daylight Evaluations', in *Symposium on Simulation for Architecture + Urban Design*. Delft, The Netherlands.

Lorenz, C.L. and Jabi, W. (2017) 'Predicting Daylight Autonomy Metrics Using Machine Learning', in *International Conference for Sustainable Design of the Built Environment*. London, U.K.

## Appendix A

### Daylight Analysis: Percentage-of-Space Results

This appendix chapter presents the analysis of %-space results for all assessed design solutions, with key findings presented in the chapter 7 of the thesis. Focus is laid on the influence of atrium well geometry, atrium well orientation, and WWR distribution on daylight levels (as measured by %-space performance), with results presented in the following order:

- Impact of atrium well geometry on  $sDA_{300/50\%}$ , with magnitudes assessed based on minimum and maximum  $sDA_{300/50\%}$  values for each given floor area
- Impact of WWR distribution on  $sDA_{300/50\%}$ , with magnitude assessed based on minimum and maximum  $sDA_{300/50\%}$  ranges across the different WWR in each given floor area
- Impact of atrium orientation on  $sDA_{300/50\%}$ , with magnitude assessed based on minimum and maximum  $sDA_{300/50\%}$  ranges across the different orientations for each WWR option in each given floor area
- Combined impact of all design changes on  $sDA_{300/50\%}$  across all floors
- Impact of atrium well geometry on  $sDA_{100/50\%}$ , with magnitudes assessed based minimum and maximum  $sDA_{100/50\%}$  values for each given floor area, taking into account the previous  $sDA_{300/50\%}$  results
- Impact of WWR distribution on  $sDA_{100/50\%}$ , with magnitude assessed based on minimum and maximum  $sDA_{100/50\%}$  ranges across the different WWR in each given floor area, taking into account the previous  $sDA_{300/50\%}$  results

- Impact of atrium orientation on  $sDA_{100/50\%}$ , with magnitude assessed based on minimum and maximum  $sDA_{100/50\%}$  ranges across the different orientations for each WWR option in each given floor area, taking into account the previous  $sDA_{300/50\%}$  results
- ◆ Impact of atrium well geometry on ASE, with magnitudes assessed based on minimum and maximum ASE values for each given floor area, taking into account the previous  $sDA_{300/50\%}$  and  $sDA_{100/50\%}$  results
- ◆ Impact of WWR distribution on ASE, with magnitude assessed based on minimum and maximum ASE ranges across the different WWR in each given floor area, taking into account the previous  $sDA_{300/50\%}$  and  $sDA_{100/50\%}$  results
- ◆ Impact of atrium orientation on ASE, with magnitude assessed based on minimum and maximum ASE ranges across the different orientations for each WWR option in each given floor area, taking into account the previous  $sDA_{300/50\%}$  and  $sDA_{100/50\%}$  results

## A.1 Analysis of $sD_{300/50\%}$ results

$sDA_{300/50\%}$  results for the ground, third and top floor are shown in Figure 1. In atrium adjacent spaces, overall  $sDA_{300/50\%}$  ranged between 21 and 29 % on the ground floor, 37 and 46 % and on the third floor and between 75 - 95% on the top floor (Figure 1). When the atrium well area is included to the results of ground floor,  $sDA_{300/50\%}$  range increased overall to 24 to 41%. The magnitude of variation in  $sDA_{300/50\%}$  results on the top floor is therefore quite high (up to 20 percentage points) and lower on the ground floor (7 percentage points).

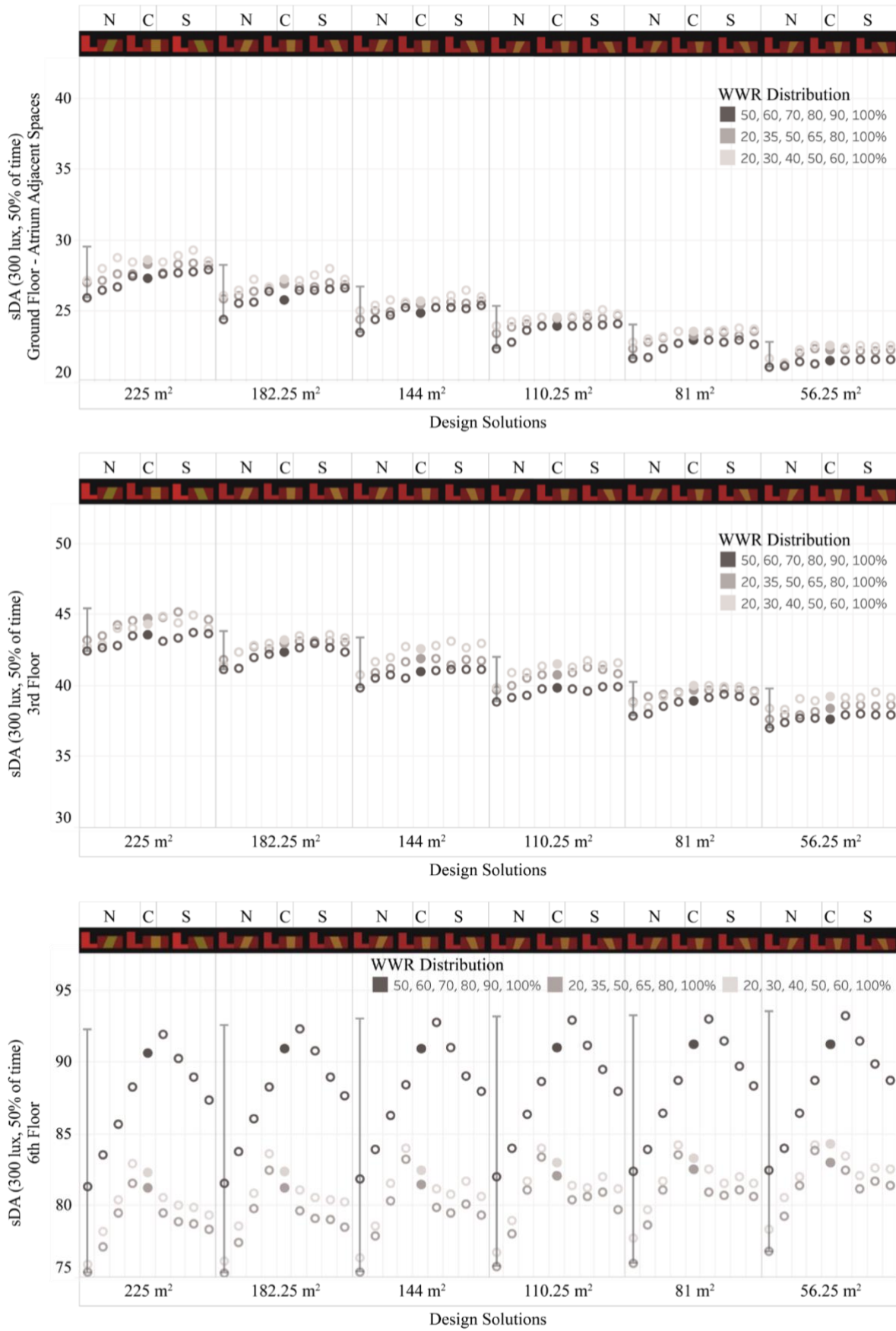


Figure 1 sDA<sub>300/50%</sub> performance in atrium adjacent spaces: ground, 3<sup>rd</sup>, and 6<sup>th</sup> floor

### A.1.1 *Impact of Atrium Well Geometry on $sDA_{300/50\%}$*

For the ground floor, the smaller the atrium base area, the lower the  $sDA_{300/50\%}$  levels in atrium adjacent spaces. The same is true for the third, but not the top floor.

On the ground floor,  $sDA_{300/50\%}$  for a given atrium base area varied between 26 and 29% for the largest atrium base area and between 21 and 23% for smallest atrium base area (as indicated in Figure 1). On the third floor,  $sDA_{300/50\%}$  ranged between 42 and 45% for the largest atrium base area and between 37 and 40 % for the smallest atrium base areas. From the ground to the 5<sup>th</sup> floor,  $sDA_{300/50\%}$  was lower for smaller atrium base areas. From the 5<sup>th</sup> floor onwards, this pattern starts changing. On the 6<sup>th</sup> floor,  $sDA_{300/50\%}$  ranged between 75 and 92 % for the largest atrium base area and increased to 77 and 93% for the smallest atrium base area. The magnitudes illustrate that a change in the atrium base floor area has a larger impact on ground and 3<sup>rd</sup> floor, with the smallest impact and a reverse effect apparent on the top floor.

The identified trend in which reducing the atrium base area reduces  $sDA_{300/50\%}$  can largely be explained by the increase in the floor area of atrium adjacent space and the associated increase in overall room depth. This increases the percentage of space in which daylight sparsely reaches. The reverse effect that is noticeable from the 5<sup>th</sup> floor onwards can be explained by the splay angles of the atrium well walls that result in an increase of visible sky area (top light rather than side light). This increases  $sDA_{300/50\%}$  despite the slight increase in room depth. This shows that splay angles can only improve daylight performance if additional gains from top light are not negated by a scarce daylight penetration into the depth of the atrium well and a substantial increase in room depth.

### A.1.2 Impact of WWR distribution on $sDA_{300/50\%}$

Figure 2 shows the maximum and minimum ranges in  $sDA_{300/50\%}$  for the different WWR options on the top floor. The WWR distribution series starting with 50% showed significantly higher  $sDA_{300/50\%}$  compared to both WWR distribution series starting with 20%, which showed very similar results to each other. Changing the WWR distribution showed a greater impact on  $sDA_{300/50\%}$  when the atrium well was oriented towards south. The variation in  $sDA_{300/50\%}$  results between the different WWR distribution options was the lowest for northward-oriented atria (as indicated in Figure 2).

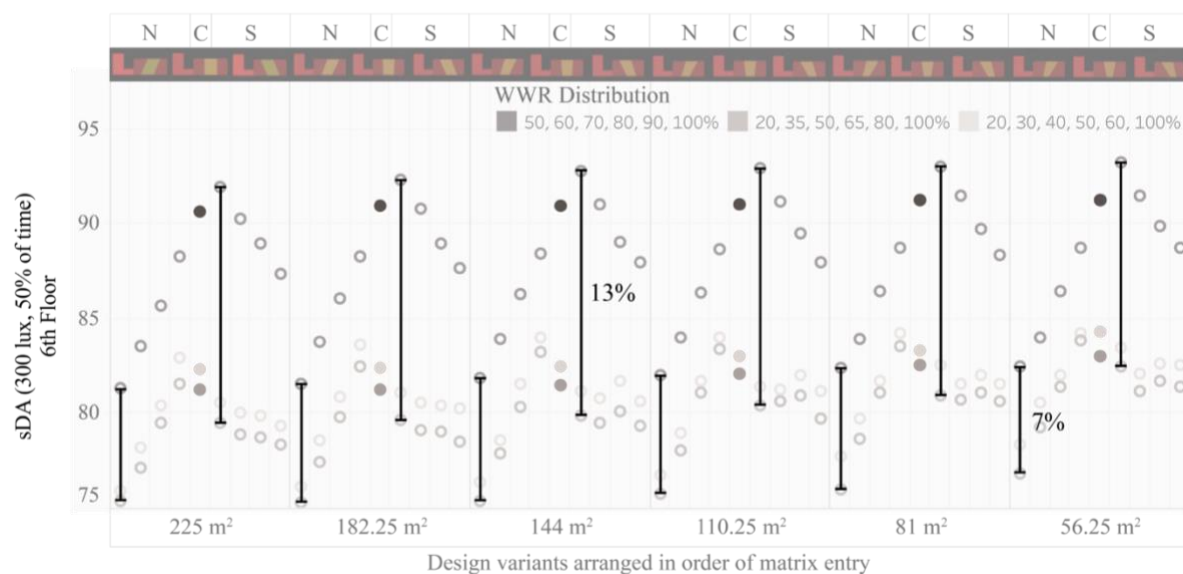


Figure 2 Maximum and minimum  $sDA_{300/50\%}$  ranges for WWR options on the 6<sup>th</sup> floor

On the top floor, the maximum range of variation in  $sDA_{300/50\%}$  was 13%, whereas the minimum range was 7%. Maximum ranges occurred for solutions with a slight southern orientation and minimum ranges occurred for atria with the northernmost orientation. On the top and fifth floor, the 50% WWR distribution series consistently performed better. This pattern started to change for the fourth and lower floors. On the third and ground floors, the WWR distribution series of 20, 30, 40, 50, 60, 100% tended to perform better than the others. The magnitude of variation in  $sDA_{300/50\%}$  based on WWR is much lower on the third and ground floors (as shown in Figure 2), with a

difference lower than 2.3%  $sDA_{300/50\%}$ . Although this may appear to be a small improvement, it matters for two reasons. First, the improvement occurs on lower floors where daylight levels fall below the target and space are considered poorly lit. Second, the difference accounts for around 28m<sup>2</sup> (i.e. on the ground floor), which means that additional daylight is provided to the otherwise under lit areas in the proximity of the atrium well. This area could thus potentially accommodate more suitable work environments.

A reduction in window area significantly diminished  $sDA_{300/50\%}$  results on the top floor improve  $sDA_{300/50\%}$  in the lower floors. This is a result of larger opaque surfaces on the upper floors that increase the inter-reflected light within the atrium well. This effect is especially noticeable on the third floor, where the majority of design solutions with 65% WWR underperformed design solutions with 50% WWR. The turning point and exception to this can be found in design solutions with an atrium base area of 225m<sup>2</sup>. For design solutions with this atrium base area, the increase in daylight resulting from the increased inter-reflected daylight could not anymore offset the additional daylight received through larger windows.

It is important to notice that these effects can further be exacerbated, and by the number of simulation ambient bounces. To an extent, the higher the number of bounces, the deeper and further daylight will travel into atrium adjacent spaces. In addition, an higher daylight levels on lower floors may also be achieved by increasing the reflectance of materials in the atrium well. Since both affect  $sDA_{300/50\%}$  results, further studies are needed to validate realistic settings for climate-based daylight simulations in atrium buildings.

### A.1.3 *Impact of Atrium Orientation on $sDA_{300/50\%}$*

The northmost orientation showed the weakest  $sDA_{300/50\%}$  performance on all floors except the 5<sup>th</sup> floor. The optimum performing orientations varied, although they were similar across all design solutions from ground to 4<sup>th</sup> floor.

On the top floor, the WWR distribution series starting with 50% showed a different optimum orientation than both WWR distribution series starting with 20%, which showed similar results to each other. The optimum for the 50% WWR distribution series was found in slightly southward-oriented atria whereas the optima for the other two WWR series were found in slightly northward-oriented atria. This pattern remained consistent across all atrium base areas. On both the third and ground floor, the optimum orientation was southward for all WWR distribution series. A difference between the optimum orientations on these two floors was that the optima on the ground floor were more steeply oriented towards south than on the third floor. The turning point for optimum orientations from south to north occurs on the fifth floor. On this floor, a steeper northward orientation consistently provided the highest  $sDA_{300/50\%}$  for all WWR distribution series.

Figure 3 shows the  $sDA_{300/50\%}$  ranges for the different orientations on the top floor, per WWR distribution series for each given atrium base area. The maximum range of variation, 11%  $sDA_{300/50\%}$ , was found in the 50% WWR distribution series and the minimum range, 6%  $sDA_{300/50\%}$ , in the 20, 30, 40, 50, 60, 100% WWR distribution series. The range of variation in  $sDA_{300/50\%}$  based on orientation is much lower on the third and ground floors (as shown in Figure 1), with a difference lower than 2.5%  $sDA_{300/50\%}$ .

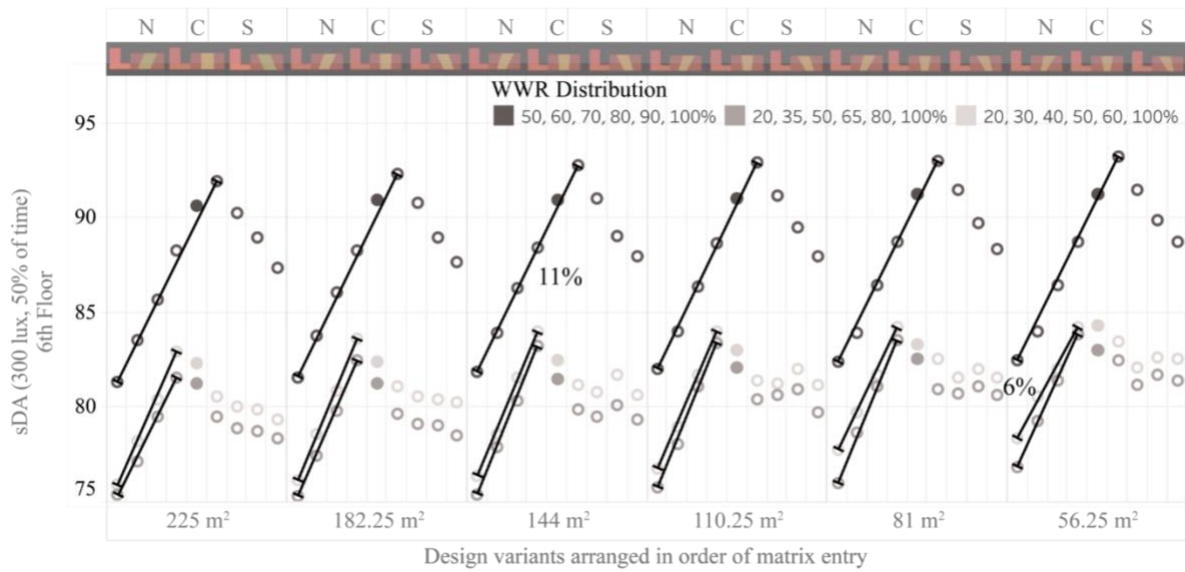


Figure 3 Maximum and minimum  $sDA_{300/50\%}$  ranges for Orientation on the 6<sup>th</sup> floor

Both orientation and atrium base area alter the splay angles of the atrium well walls. To aid in understanding the association between splay angles, orientation, and daylight performance, the splay angles are given in ranges for each of the nine orientations (Figure 4). The range encompasses the minimum and maximum splay angles resulting from the smallest and largest atrium base area. Figure 4 also shows the points at which the splay angles were measured.

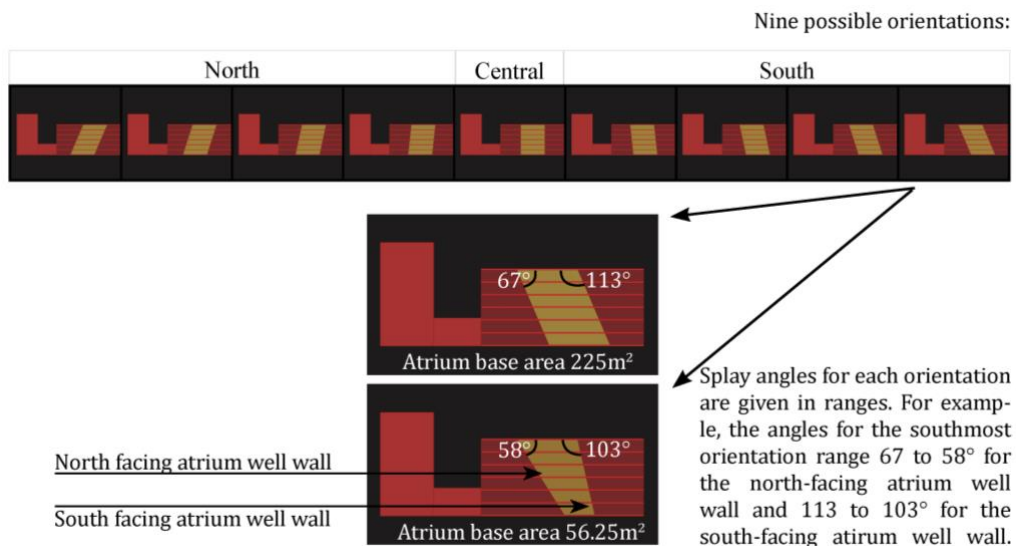


Figure 4 Graphic format explaining the atrium well splay angle ranges

Table 1 shows the splay angles of the orientations that most commonly resulted in the highest sDA<sub>300/50%</sub> on the ground, third and top floor. The optimum splay angles for the fifth floor are also displayed as the turning point in performance pattern occurred on this floor. The northward orientations, for the most part, have obtuse splay angles on the north-facing atrium well wall and acute splay angle of the south-facing atrium well wall. This is vice versa the case for southward orientations. The exception in which both north and south-facing atrium well walls have acute splay angles occurs for slightly north and northward orientations as well as the central orientation (Table 1, underlined and bolded values). Specifically, atrium design solutions with a slight north and southward orientation and an atrium base area of 110.25m<sup>2</sup> and lower have acute splay angles on both atrium well walls. In the same way, atrium design solutions with a central orientation and an atrium base area smaller than 225 m<sup>2</sup> have acute splay angles on both atrium well walls. These design solutions therefore slightly differ from the remaining solutions in that both atrium well walls expose surface area to the atrium skylight, whereas other solutions have at least on atrium well wall withdrawing surface area from the atrium skylight.

Orientation	North-most	North	North	North	Central	South	South	South	South-most
Splay angle of north-facing wall	113.2 to 102.6°	107.8 to 96.7°	102.1 to 90.8°	96.1 to <b><u>84.8</u></b> °	90 to 78.9°	83.9 to 73.2°	77.9 to 67.9°	72.2 to 62.9°	66.8 to 58.4°
Splay angle of south-facing wall	66.8 to 58.4°	72.2 to 62.9°	77.9 to 67.9°	83.9 to 73.2°	90 to 78.9°	96.1 to <b><u>84.8</u></b> °	102.1 to 90.8°	107.8 to 96.7°	113.2 to 102.6°
Atrium base area: 225 m <sup>2</sup>	113° 67°				90° 90°				67° 113°
Atrium base area: 56.25 m <sup>2</sup>	103° 58°				79° 79°				58° 103°
	5 <sup>th</sup> Floor	6 <sup>th</sup> Floor	6 <sup>th</sup> Floor (20%WWR)	6 <sup>th</sup> Floor (50%WWR)	3 <sup>rd</sup> Floor	Ground Floor			

Table 1 Splay angles of design solutions grouped according to orientation; results of best performing orientations are encircled

The smaller the window area and the lower the floor level, the lower the impact of orientation on  $sDA_{300/50\%}$ . This is noticeable when comparing design solutions with 50 and 20% WWR on the top floor and results on top floor to those on the lower floors (Figure 1). Thus, those spaces that had a greater availability of daylight were more affected by the choice of orientation.

Southward oriented atria typically showed higher  $sDA_{300/50\%}$  levels on the fourth and lower floors. The optimum orientation changed to steeply southward oriented atria, the lower the floor. This is because the lower floor levels require a deeper penetration of daylight into the atrium well. This is achieved by aligning the splay angles with the solar altitude. As a consequence, daylight reaches deeper into the building and lower floors therefore perform better with increasingly southward orientations. As for the upper floors, northward orientations perform better as this means that the glazing area is more perpendicular to the solar altitude and spaces therefore receive more direct daylight.

Less intuitive results were found on the top two floors where optimal orientations vary. Especially on the top floor where north/ south orientations perform better for different WWR options, the relationship between orientation and splay angles becomes difficult to entangle. The derivation of conclusions would therefore need a more detailed analysis of the spatial distribution of daylight and of the climate data itself as well as further validation of the results. Nonetheless, the following lines of argument provide possible explanations for the presented results:

On the fifth floor, there was a shift in pattern as north oriented atria displayed higher  $sDA_{300/50\%}$  levels regardless of the WWR. This situation also holds true for 20% WWRs on the top floor level. The higher  $sDA_{300/50\%}$  values for north oriented atria can be

explained by several aspects: Northward orientations allow more direct sunlight and acute splay angles of the south-facing atrium well walls expose more floor area in the south of the atrium towards the sky (top light rather than side light). At the same time, the south facing atrium well walls provide an orthogonal surface to prevailing solar angle thus enabling deeper daylight penetration into atrium adjacent spaces in the south. Additionally, more daylight is reflected from the south facing atrium well walls as the percentage of opaque surfaces is particularly high with the low WWR.

A few arguments also explain the higher  $sDA_{300/50\%}$  levels for the southward orientation on the top floor for 50% WWR: Southward orientation and acute splay angles of the north-facing atrium well wall expose more floor area in the north of the atrium towards the sky (top light rather than side light). For design solutions with an atrium base area of  $110.25\text{m}^2$  and smaller, the atrium well walls have acute splay angles on both the north and south facing walls, meaning additional exposure to skylight and direct light on floor areas to both sides of the atrium well. For solutions with a larger atrium base area, obtuse splay angles of the south-facing atrium well wall have the potential to improve the distribution of daylight (more diffuse light) and daylight levels in spaces to the south of the atrium well. This argument is based on studies by Parent and Murdock (1989) and Laouadi (2004) , who showed that skylights with obtuse splay angles would improve daylight in spaces below the skylight. All in all, the results suggest that, if the window area is large enough (50% WWR on the top floor), improvements in daylight that result from obtuse or mildly acute angles of the north-facing atrium well wall are greater than the improvements in daylight resulting from an increase in direct penetration via perpendicular orientation towards south. It is noted that the current study used a simplified model with zero wall-thickness. Consequently, results may change, and optimum orientations may shift when including wall-thickness in the simulation models.

#### A.1.4 Combined impact of all design changes across all floors on $sDA_{300/50\%}$

Figure 5 shows the total  $sDA_{300/50\%}$  performance across all floor levels (average weighted according to floor area).  $sDA_{300/50\%}$  within the design solution space ranged between 45 and 55% and therefore contained design variants that both meet and fail the  $sDA_{300/50\%}$  threshold. The smaller the atrium base area, the lower the  $sDA_{300/50\%}$ . The WWR distribution series starting with 50% consistently outperformed the other two, which showed overlapping results. The optimum orientation across all floor levels was the same as the one shown previously for the top floor, i.e. with a slightly south and slightly north orientation showed the highest  $sDA_{300/50\%}$  for WWR distribution series starting with 50% and 20% respectively.

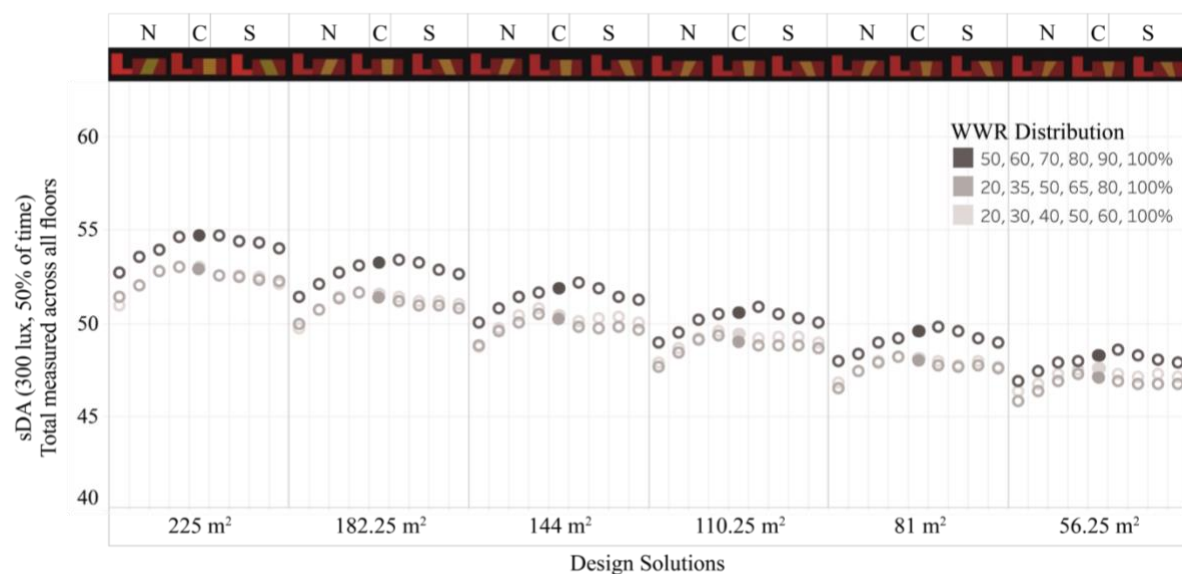


Figure 5  $sDA_{300/50\%}$  performance across all floor levels

The  $sDA_{300/50\%}$  results ranged between 51 and 55%, and 46 and 49%  $sDA_{300/50\%}$  for the largest and smallest atrium base area respectively. The variation between WWR distribution options as well as orientations was below 3%  $sDA_{300/50\%}$ . Changing the atrium base area therefore had the biggest influence on the overall  $sDA_{300/50\%}$  of the building.

The highest  $sDA_{300/50\%}$  relating to WWR distribution was seen for the WWR distribution series starting with 50%, a result which is only representative of the optimum design solutions on top two floors. The highest  $sDA_{300/50\%}$  relating to orientation was seen on slight north/south orientations, again a result seen true only for the top floor. This means the top floor is skewing the results, making the overall weighted  $sDA_{300/50\%}$  performance across the building unsuitable to base design decisions on.

This also becomes clear when considering that, on the top floor, even the weakest design variants achieved  $sDA_{300/50\%}$  higher than 75%, a threshold indicating 'preferred daylight sufficiency' (Heschong Mahone Group, 2003; IESNA, 2012). The 'worst case' design choices, as suggested by the combined  $sDA_{300/50\%}$  performance, therefore do not lower daylight levels on the top floor below recommended 75% or 50%  $sDA_{300/50\%}$  targets. In comparison however, these design choices do negatively affect daylight on the lower floors, where the availability of daylight is especially critical, and the recommended targets cannot be met. To conclude, it is important to consider the impact of design choices locally (i.e. per floor or even per room) rather than simply globally (i.e. for the whole building).

## A.2 Analysis of $sD_{100/50\%}$ results

$sDA_{100/50\%}$  results for the ground and third floor are shown in Figure 6. Results for the top floor are not shown, as they were consistently at 100% for all design solutions. In atrium adjacent spaces, overall  $sDA_{100/50\%}$  ranged between 46 and 78% on the ground floor and between 86 and 100% on the third floor. When the atrium well area was included in the calculation of results on the ground floor, the range increased to 48 and 82%  $sDA_{100/50\%}$ . The magnitude of variation in results on the ground floor is therefore quite high (up to 32 percentage points) and lower on the third floor (14 percentage

points). The variation in results for the 100 lux  $sDA_{100/50\%}$  threshold is therefore much higher than those seen for the 300 lux  $sDA_{300/50\%}$  threshold, which were at 7 and 9 percentage points for ground and third floor respectively.

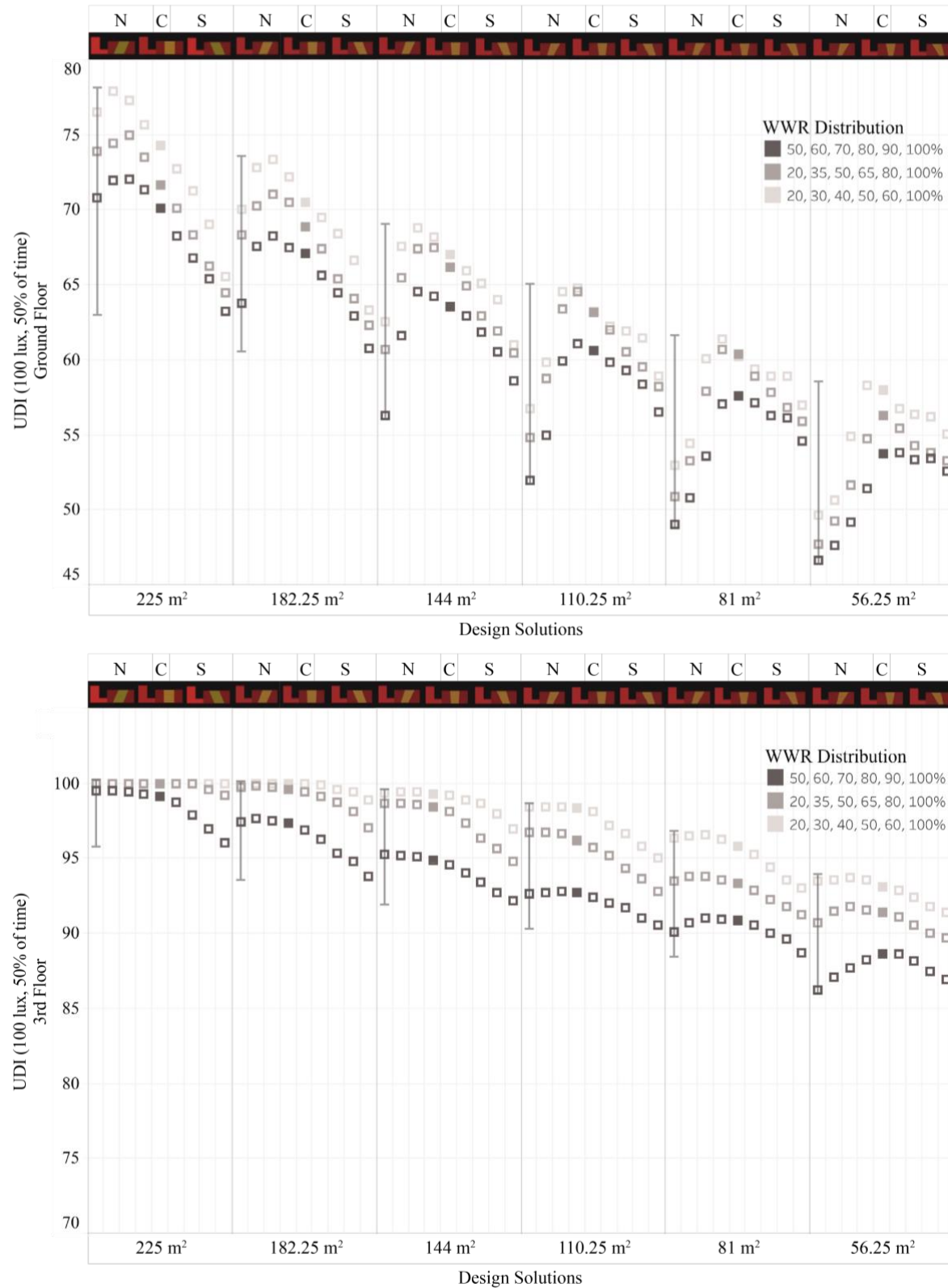


Figure 6  $sDA_{100/50\%}$  performance in atrium adjacent spaces: ground and 3rd floor

### *A.2.1 Impact of atrium well geometry on $sD_{100/50\%}$*

For the ground floor, the smaller the atrium base area, the lower the  $sDA_{100/50\%}$  in atrium adjacent spaces. The same is true for the third floor. On the third floor, the influence of atrium base area on daylight performance could not further investigated with the  $sDA_{100/50\%}$  criteria, as performance was at its maximum.

On the ground floor,  $sDA_{100/50\%}$  for a given atrium base area varied between 63 and 78% for the largest atrium base area and between 46 and 58% for smallest atrium base area (Figure 6). On the third floor,  $sDA_{100/50\%}$  ranged between 96 and 100% for the largest atrium base area and between 86 and 94% for the smallest atrium base areas. From the 4<sup>th</sup> floor onwards, daylight performance using the  $sDA_{100/50\%}$  criteria could not further investigated, as performance was at its maximum. The magnitudes illustrate that a change in the atrium base floor area has a larger impact on ground than on the 3<sup>rd</sup> floor, with performance dropping more heavily. Seen in combination with orientation, which is discussed further down, reducing atrium base area had a much larger impact in reducing daylight for southward than northward orientations. Compared to previous results, reducing the atrium base area has a much larger influence on  $sDA_{100/50\%}$  than  $sDA_{300/50\%}$  results. The  $sDA_{100/50\%}$  metric therefore showed a greater sensitivity to design changes on lower floors.

### *A.2.2 Impact of WWR distribution on $sD_{100/50\%}$*

Figure 7 shows the maximum and minimum ranges in  $sDA_{300/50\%}$  for the different WWR options on the ground and third floor. The WWR distribution series with the lowest overall glazing area (20, 30, 40, 50, 60, 100% WWR) showed significantly higher  $sDA_{100/50\%}$  in comparison to the other both WWR distribution series.

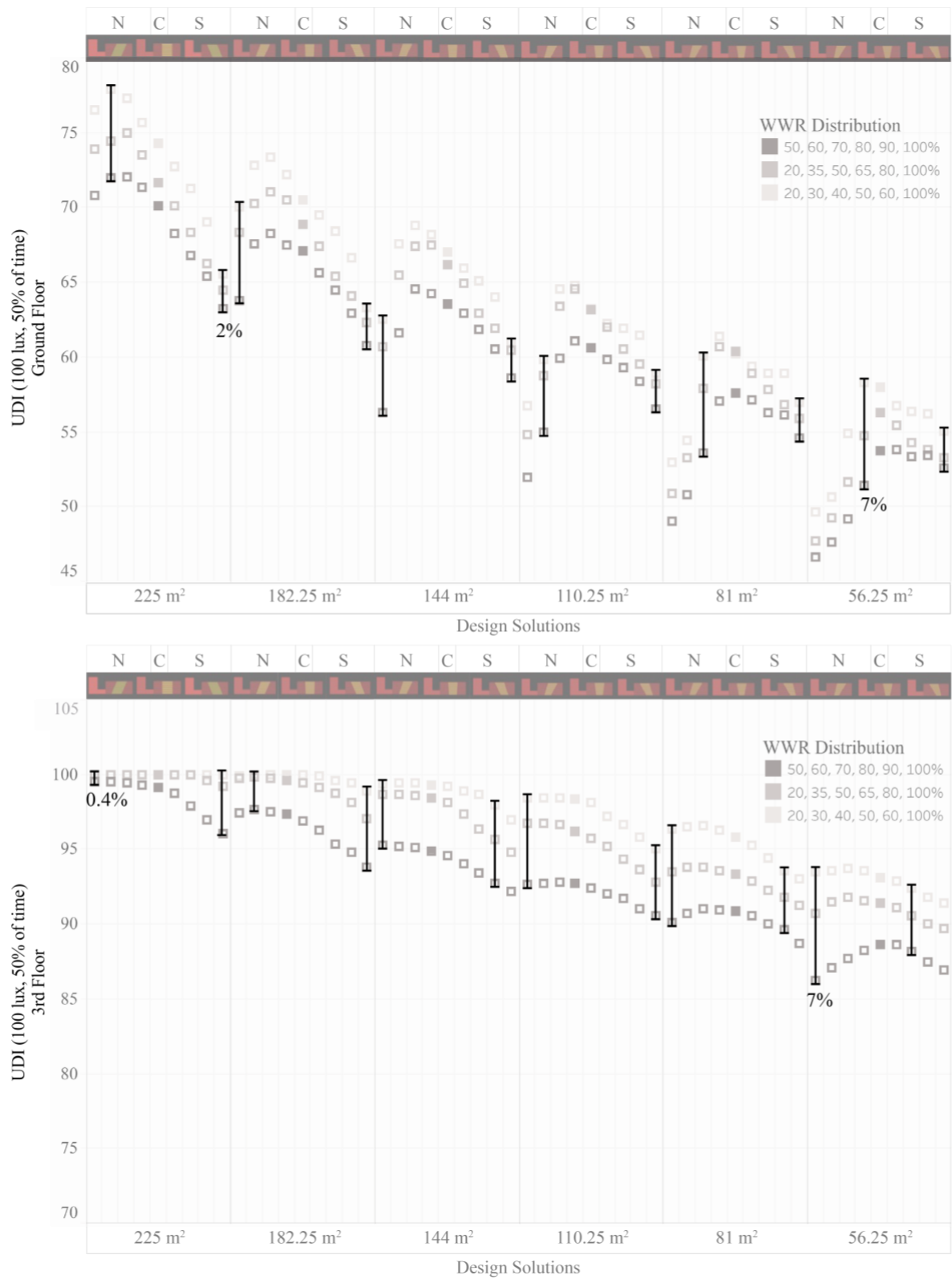


Figure 7 Maximum and minimum  $sDA_{100/50\%}$  ranges for WWR options on the ground and 3<sup>rd</sup> floor

On the ground floor, the maximum range of variation in  $sDA_{100/50\%}$  was 7%, whereas the minimum range was 2%. Minimum ranges occurred for design solutions

with the southernmost orientation and maximum ranges occurred for atria with a southern orientation. On the third floor, the maximum range of variation in  $sDA_{100/50\%}$  was also 7%, and the minimum range less than 1% due to design solutions reaching maximum performance (100%). The maximum and minimum ranges did not occur at a specific orientation, but varied depending on the atrium base area. Thus, the sensitivity of  $sDA_{100/50\%}$  daylight performance to changes in WWR distribution could not be pinpointed to specific orientations.

The WWR distribution series of 20, 30, 40, 50, 60, 100% consistently performed better than the WWR distribution series of 20, 35, 50, 65, 80, 100%, which consistently performed better than the WWR distribution series starting with 50%. This is true for all floors and reflects the results seen for the  $sDA_{300/50\%}$  metric on lower floors. The reason is the same explained for the  $sDA_{300/50\%}$  results: The larger opaque surfaces increase inter-reflected light and therefore daylight levels in atrium adjacent spaces on lower floors. That is why the 20, 30, 40, 50, 60, 100% shows a better performance, even though the window area of the other two distribution series is larger. Compared with the  $sDA_{300/50\%}$  metric, the variation in results for  $sDA_{100/50\%}$  is higher for the lower floors (up to 7 compared to 2.3 percentage points) and therefore more clearly shows an increase in daylight based on an increase in reflected light.

### *A.2.3 Impact of orientation on $sD_{100/50\%}$*

The optimal orientations varied depending on atrium base area, WWR distribution and floor level. On the ground floor, more steeply northward orientations showed higher results for design solutions with larger atrium base areas. For smaller atrium base areas, optima shifted towards shallow northward, central and shallow southward orientations. On the third floor, more northward orientations showed higher  $sDA_{100/50\%}$  for the most

part, a central and shallow southward orientation only performed better for the smallest atrium base area in combination with the WWR distribution series starting with 50%.

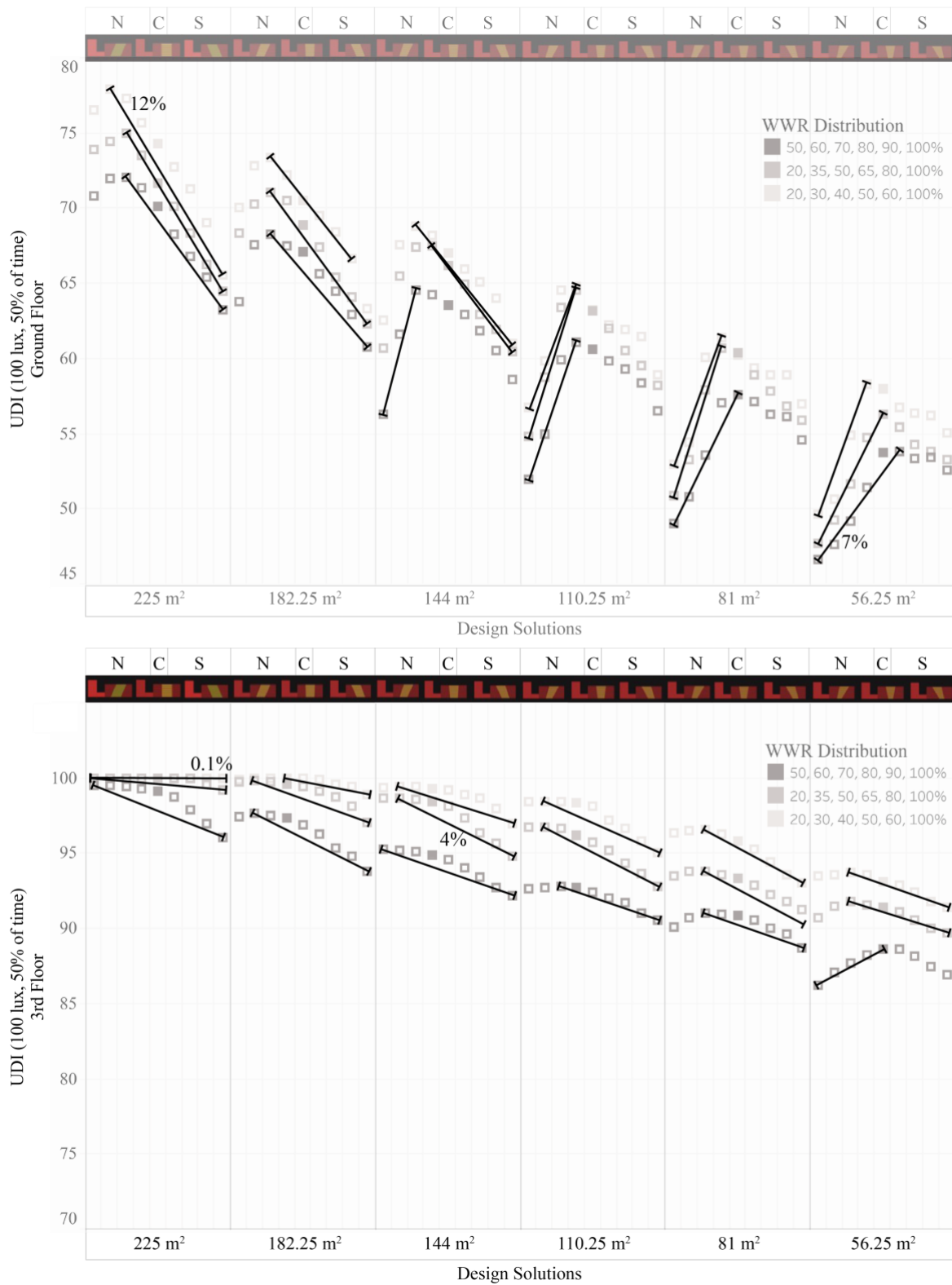


Figure 8 Maximum and minimum  $sDA_{100/50\%}$  ranges for orientation on the ground and 3rd floor

Figure 8 shows the  $sDA_{100/50\%}$  ranges for the different orientations on the ground and third floor, per WWR distribution series for each given atrium base area. On the ground floor, the maximum range of variation of 12%  $sDA_{100/50\%}$  was found in the 50% WWR distribution series and the minimum range of 7% in the 20, 30, 40, 50, 60, 100% WWR distribution series. The magnitudes in variation were much lower on the third floor. There, the maximum range of variation of 4% was found in the 20, 35, 50, 65, 80, 100% WWR distribution series. The minimum ranges found neared 0%. This sensitivity of  $sDA_{100/50\%}$  to orientation stands in contrast to  $sDA_{300/50\%}$  results, where variation was highest on the top floor (11 percentage points), and much lower for ground and third floors (less than 2.5 percentage points).

On the ground floor, the optimum orientations for all WWR distribution series were similar to each other. This is true for the second floor as well, with a change in pattern visible on the third floor. There, the WWR distribution series starting with 20% showed similar results to each other, with northward orientations showing higher results regardless of the atrium base area. Only for the smallest atrium base area of the 50% WWR distribution series, an exception is visible. Here, the pattern follows what was seen on ground and second floors, and the central to slightly southern orientation showed a higher  $sDA_{100/50\%}$  performance.

The  $sDA_{300/50\%}$  results in comparison showed that optimum orientations remained unaffected by the atrium base area. Thus, southward orientations consistently showed better performance on the lowest four floors. On the top two floors again, optimum orientations (whether northward or southward) remained consistent, regardless of the atrium base area.

Table 2 shows the splay angles of the orientations that resulted in the highest  $sDA_{100/50\%}$  on the ground floor. Table 3 shows the splay angles of the orientations that

resulted in the highest  $sDA_{100/50\%}$  on the third floor, with results omitted for  $sDA_{100/50\%}$  100%. Where optimum orientations differ between the three WWR distribution series, this is highlighted by coloured markers. On the ground floor, optimum orientation gradually shifted from northward to southward orientations with every smaller atrium base area. Obtuse splay angles on the north-facing atrium well wall and acute splay angle of the south-facing atrium well wall showed higher results for larger atria. Once the atrium area was  $110.25\text{m}^2$  and lower however, acute splay angles on all atrium well walls resulting in 'v' shaped atria showed higher  $sDA_{100/50\%}$ . On the third floor, more northward orientations showed higher results for the most part. Only for design solutions of the WWR distribution series starting with 50% WWR, 'v' shaped atria with acute splay angles on all atrium well walls started to show higher  $sDA_{100/50\%}$  when the atrium base area was  $81\text{m}^2$  and smaller.

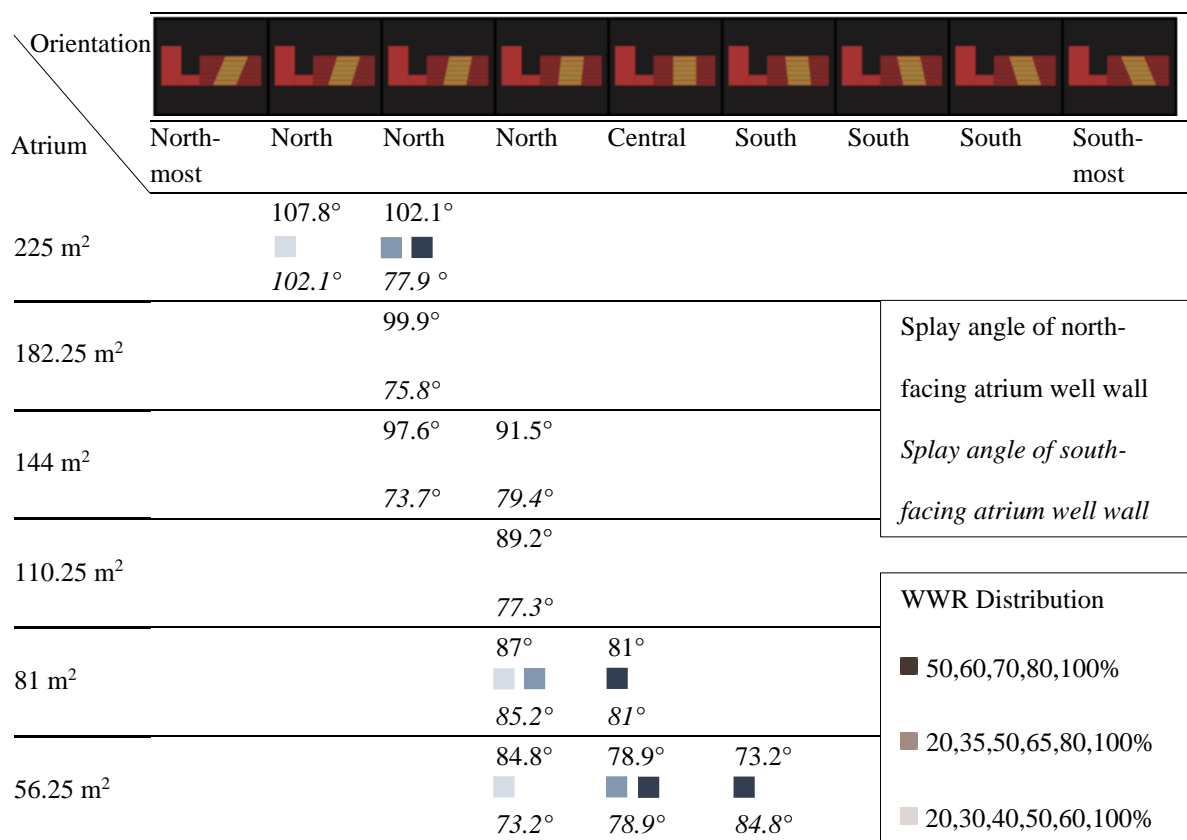


Table 2 Splay angles of design solutions with the highest  $sDA_{100/50\%}$  performance on the ground floor. The splay angles of the north and south-facing atrium well walls are written at the top and bottom of each row respectively.

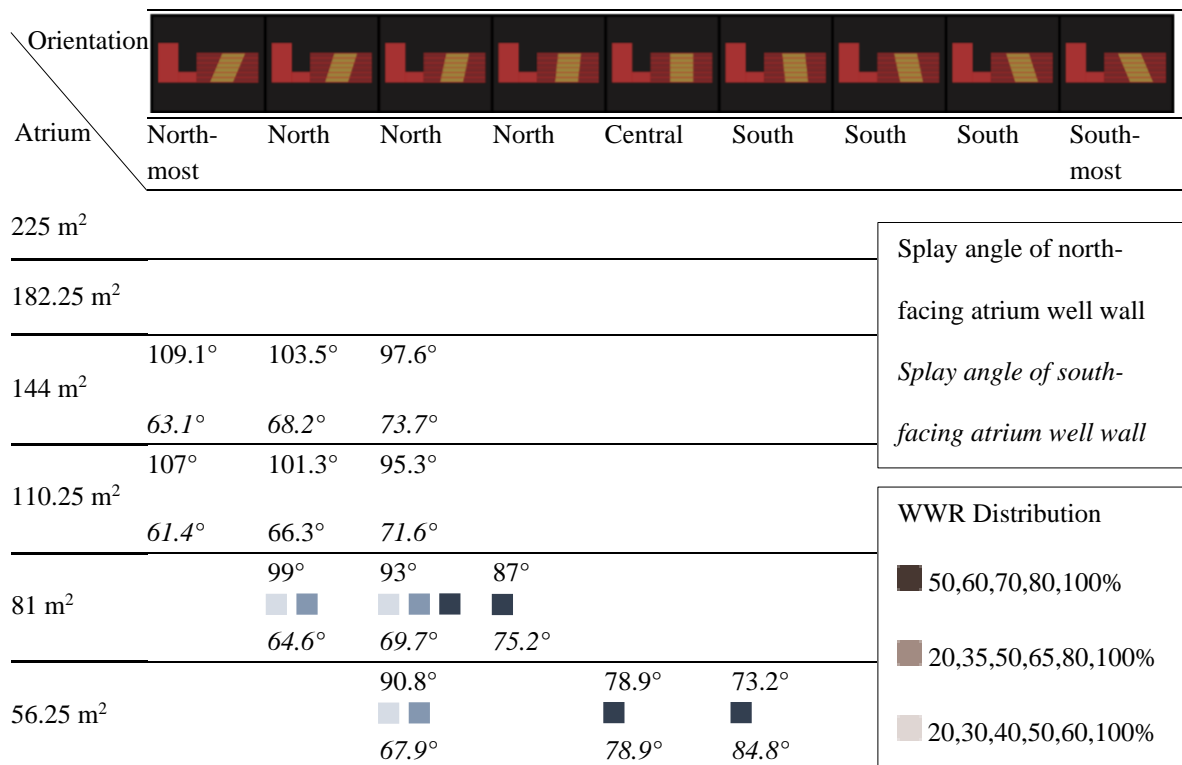


Table 3 Splay angles of design solutions with the highest  $sDA_{100/50\%}$  performance on the third floor. The splay angles of the north and south-facing atrium well walls are written at the top and bottom of each row respectively.

It stands out that the optimum orientations for  $sDA_{100/50\%}$  on lower floors stand in contrast to those seen for the  $sDA_{300/50\%}$  metric on lower floors, yet echo the results seen on the fifth and sixth floors. On the fifth floor, more steeply northward oriented atria had shown a higher  $sDA_{300/50\%}$  performance, a result seen for  $sDA_{100/50\%}$  on the third floor and partially on the second and ground floors. On the sixth floor, optimum orientations had shifted towards the centre (shallow north and southward orientations), a result seen for  $sDA_{100/50\%}$  on the second and ground floor for smaller atrium base areas and on the third floor for only the distributions series starting with 50% WWR. Optimum orientations diverge especially for this WWR distribution series using both metrics. On the sixth floor for example, a shallow south orientation had higher  $sDA_{300/50\%}$  results than north orientations only for this series. In the same way,  $sDA_{100/50\%}$  results favoured central or southward orientations on ground to third floor first for this WWR distribution series, followed by the WWR distributions series of 20, 35, 50, 65, 80, 100% and lastly

the distribution series of 20, 30, 40, 50, 60, 100%. This shows that optimum orientations depend on the specific window area on the simulated floor level (as seen for  $sDA_{300/50\%}$  on the sixth floor) as well as the overall areas of opaque and glazed surfaces on atrium well walls (as seen for  $sDA_{100/50\%}$  ground to third floor): central to shallow southward orientations outperform northward orientations for smaller atria with less overall surface area, once the glazing area is large enough. The threshold at which this occurs may however change with the specific applied radiance simulation settings and further details of the architectural model (such as wall-thickness and window depth). Hence, further validation would need to be undertaken before developing a general rule.

Overall, the lower threshold of 100 lux showed a more distinct sensitivity to the applied design variables compared to the 300 lux threshold. It therefore allowed for a more in-depth investigation and understanding of the influence of atrium well area, glazing area, splay angles and so forth on daylight. At the same time however, some results of the  $sDA_{300/50\%}$  metric could not be drawn from  $sDA_{100/50\%}$ . For example,  $sDA_{300/50\%}$  results showed that more steeply southward orientations enabled deeper daylight penetration into the atrium well, which resulted in higher daylight levels on the ground to fourth floor. Southward orientations were therefore identified a key strategy to improving daylight levels on lower floors. This could not be seen when using  $sDA_{100/50\%}$ . Therefore, using only the lower 100 lux threshold may have biased results and design decisions. In the next section, yet another perspective is taken on the results. ASE results are discussed alongside  $sDA_{300/50\%}$  and  $sDA_{100/50\%}$  results, highlighting differences and new findings that can be won from the metric.

### A.3 Analysis of ASE results

ASE results for the third and top floor are shown in Figure 9. Results for the ground floor are not shown, as they were consistently at 0% for all design solutions. In atrium adjacent spaces, overall ASE was around 1% on the third floor and ranged between 11 to 16% on the top floor. The magnitude of variation in ASE results was less than 0.5 percentage points on the third floor and around 5 percentage points on the top floor.

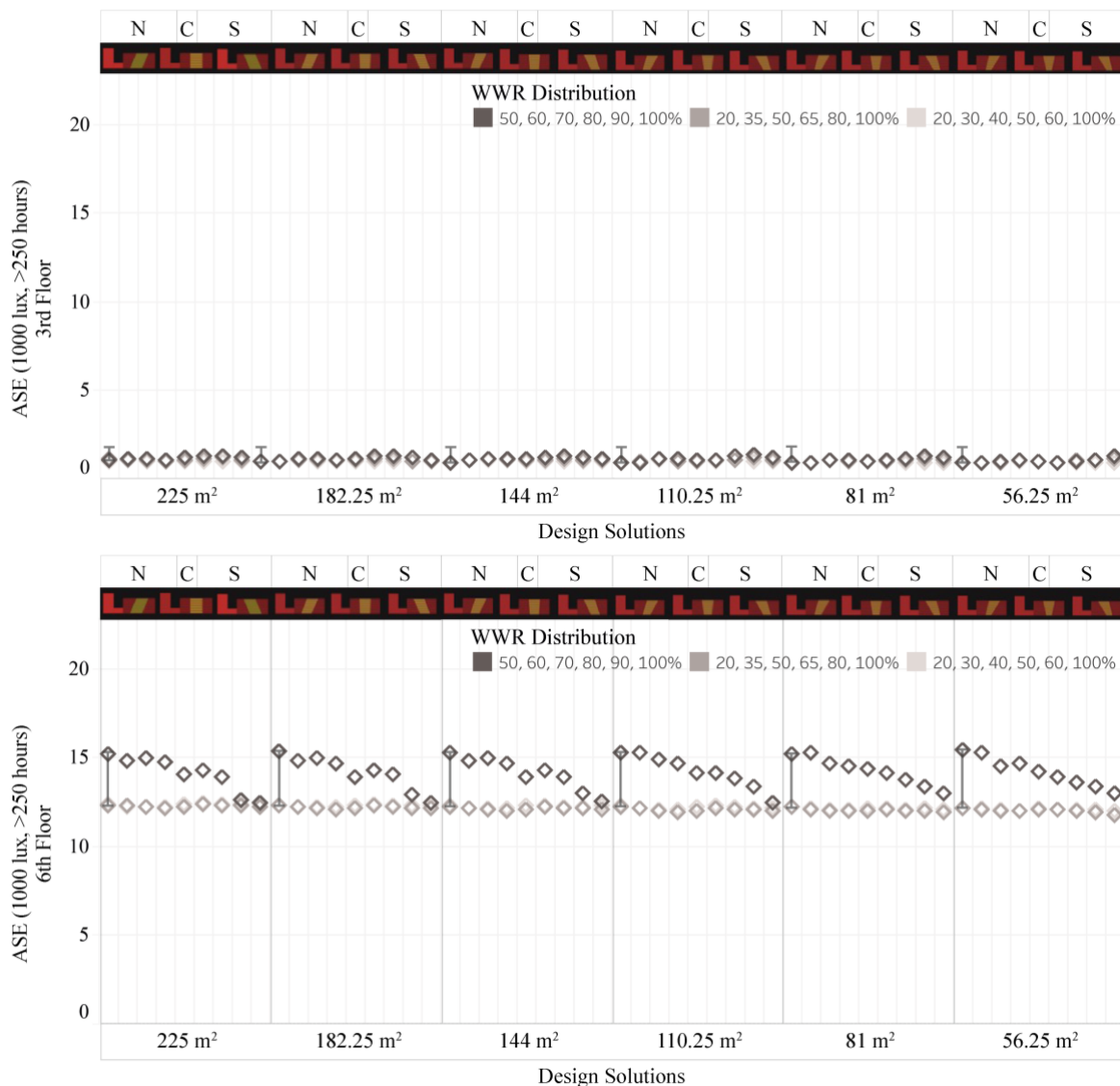


Figure 9 ASE performance in atrium adjacent space: 3rd and 6th floor

### *A.3.1 Impact of atrium well geometry on ASE*

Reducing the atrium base area only showed minimal impact in ASE results. Even as the atrium base area was reduced for each design solution, ASE remained similar. Nonetheless, a marginally lower ASE was noticed for smaller atrium base areas on the fourth to fifth floor. This trend was not evident in result on the third floor. In contrast to these results, a marginally higher ASE was noticed on the sixth floor when reducing the atrium base area. The increase in ASE from the largest to the smaller atrium base area on the top floor reached up to 0.5 percentage points. A distinct difference between this metric,  $sDA_{300/50\%}$  and  $sDA_{100/50\%}$  is that the latter two showed a much greater impact on daylight levels following the scaling down of atrium base area. A similarity between ASE and sDA exists in that both show a reduction of daylight levels for smaller atrium areas on some lower floors, but a minor increase on the top floor.

The identified trend, in which reducing the atrium base area increased ASE on the top floors, correlates with  $sDA_{300/50\%}$  results and can be explained in the same way. Reducing the atrium base area resulted in a splayed of atrium well wall toward the atrium well skylight. Thus, visible sky area and direct sunlight exposure increased. The decrease in sunlight exposure on lower floors resulting from scaling down the atrium area can be explained as a consequence of the overall smaller surface areas of the atrium well façade, and therefore smaller light admitting areas. ASE on bottom floors could not anymore be differentiated, as less than 0.1% of space exceeded the 250h threshold of direct sunlight exposure. Although the %space could not capture the impact of design changes on direct sunlight exposure for these floors, %time results analysed in the next chapter will provide further information on this matter.

### A.3.2 Impact of WWR distribution on ASE

From the fourth to the top floor, the WWR distribution series starting with 50% showed higher ASE results than the WWR distribution series starting with 20%. On the third floor, there was no apparent variation in results based on changes to WWR distribution. Similarly, on the second and ground floors, ASE was 0%, or close to, 0% and the impact of WWR distributions could not be assessed.

Figure 10 shows the maximum and minimum ranges in ASE for the different WWR options on the top floor. The WWR distribution series starting with 50% showed significantly higher ASE compared to both WWR distribution series starting with 20%. Changing the WWR distribution showed a greater impact for northward orientations and declined, the more southward the orientation. The variation in ASE between the WWR distributions series was highest for an atrium base area of 56.25m<sup>2</sup>. Here, the maximum difference in ASE was 3.3% for the northmost orientation and 1.2% for the southmost orientation. By comparison, the largest atrium base area showed a difference in ASE of 2.9% for the northmost orientation and 0.2% for the southmost orientation (as indicated in Figure 10).

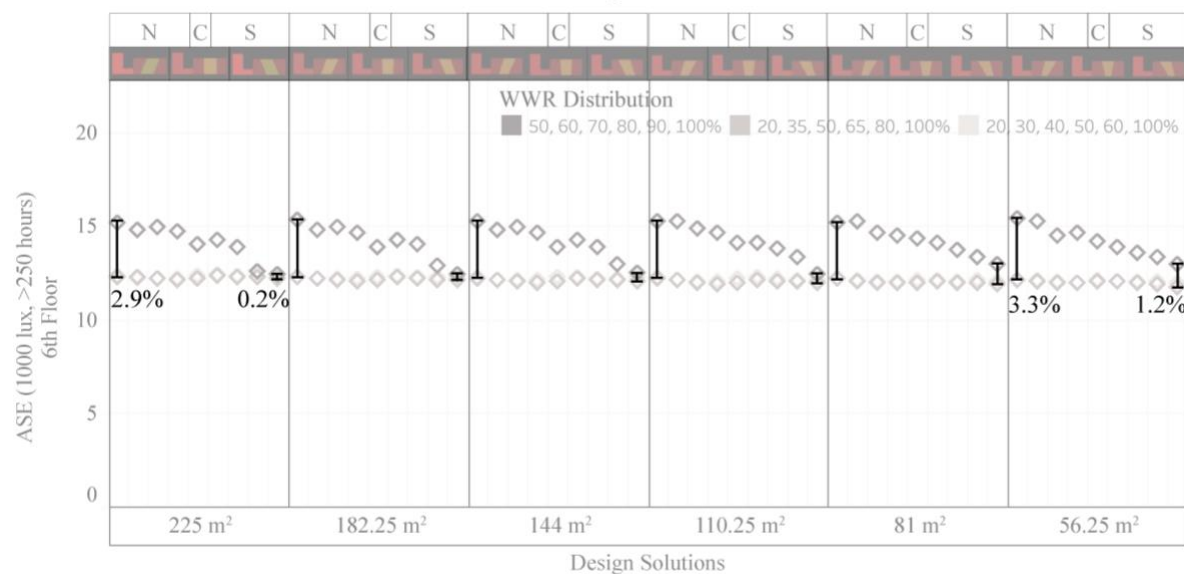


Figure 10 Maximum and minimum ASE ranges for WWR options on the 6th floor

On top floor, larger windows were expected to result in higher ASE as a consequence of a larger light admitting area for direct sunlight penetration. Although this was indeed the case, the difference in ASE for southward orientations between the different WWR options was small (increase to 0.2% to 1.2% of space). This result can be easily explained as a consequence of the atrium well splay angles. For northward orientations, the south-facing atrium well was splayed towards the skylight, thus increasing the visible sky area (Figure 11 b, d). Vice versa, for southward orientations, the south-facing atrium well walls were withdrawn, thus reducing visible sky (Figure 11 a, c). This also explains why the difference in ASE for different WWR options was higher, the smaller the atrium. This is because smaller atrium areas reduced the atrium well splay angles (Figure 11 c, d). Hence, the observed results showed the combined influence of atrium base area and orientation on varying ASE performance for different WWR options.

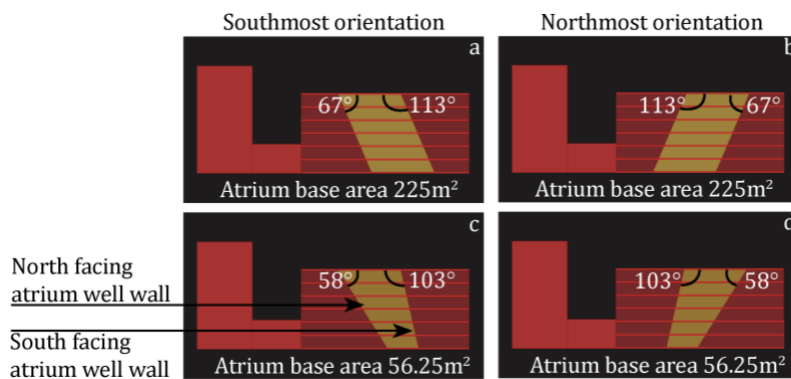


Figure 11 Illustration of atrium well splay angles and orientation towards the skylight

### A.3.3 Impact of orientation on ASE

The northmost orientation showed the highest, and the southmost orientation the lowest ASE results on the top and 5<sup>th</sup> floors. The orientations with highest ASE result on the fourth floor varied, from northmost to shallow northward orientations. On the third floor,

central to southward orientations showed marginally higher ASE. ASE on the second and ground floors remained at 0.1% to 0%.

Figure 12 shows the maximum range in ASE for the different orientations of the WWR distribution series starting with 50%. The range of variation in ASE was highest on the top floor. Here, northmost orientations had the highest ASE results, and showed that 2.5% to 2.9% more space was affected from direct sunlight exposure compared to southmost orientations. In comparison, the range of variation in ASE was less than 0.4 on the third floor. Here, a trend was visible in which central to southward orientations showed higher ASE than northmost and northward orientations.

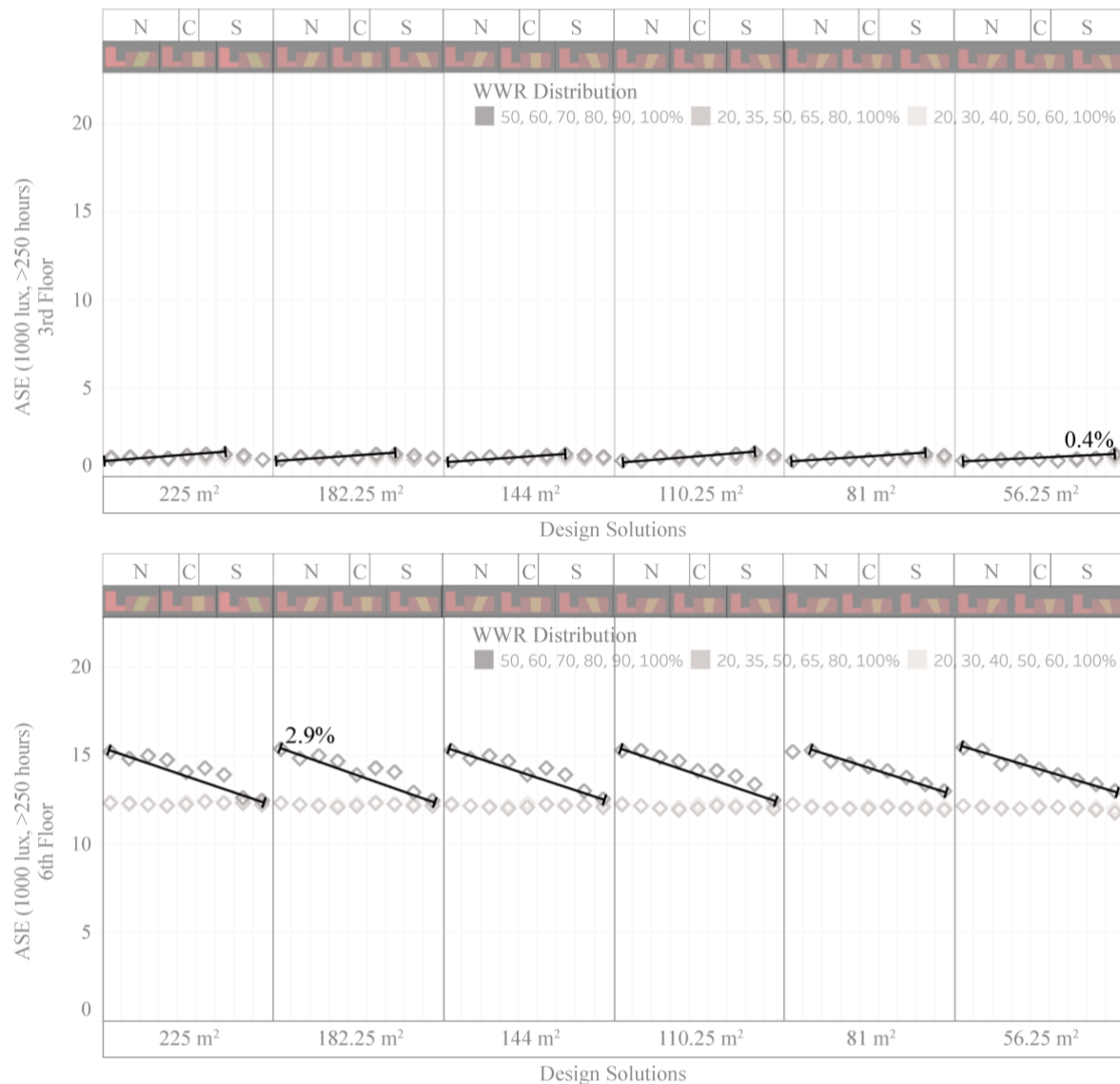


Figure 12 Maximum ASE range for orientation on the 3<sup>rd</sup> and 6<sup>th</sup> floor

Explanations for the observed results have already been provided in previous sections. On the top floors, the splay angles of the atrium well either tilted the south-facing atrium wall towards the skylight in northward orientations, or away from the skylight in southward orientations (as shown in Figure 11), thus resulting in higher ASE for northward orientations and a lower ASE for southward orientations. This began to change from the fourth floor downwards. On lower floors, the atrium well depth (e.g. height from third to the top floor) increased, and the north-facing atrium well walls began to obstruct direct sunlight penetration. This effect was reduced for central to southward orientations, as this aligned the atrium well with solar altitude angles and therefore allowed for a deeper daylight penetration into the atrium well. Due to the susceptibility of ASE to radiance parameter settings and the specific daylight simulation method (Brembilla and Mardaljevic, 2019), trends in ASE could not be distinguished when the window areas were too small (as seen for 20% WWR on the top floor).

Taken together, ASE allowed to trace direct sunlight exposure, while the sDA and UDI metrics represented results including reflected daylight. Nonetheless, ASE showed little variation in results and suggested that only little direct sunlight penetrated deep into the atrium well and reached atrium adjacent spaces. All metrics are limited by an absolute threshold (e.g. 250 h for ASE, 50% DA for sDA<sub>300/50%</sub>) and thus do not provide information on the distribution of daylight within the atrium and atrium adjacent spaces. In order to verify the explanations provided in the discussion of this chapter, as well as supplement the findings with additional information on the distributions of %time results, the next chapter analyses the daylight simulation plots for the various design solutions.

## Appendix B

### Daylight Analysis: Percentage-of-Time Results

This appendix chapter presents the analysis of the %time results, or more accurately, the distribution of %time results for DA<sub>300</sub>, DA<sub>100</sub>, DA<sub>2000</sub> and ASE<sub>1000</sub> that led to the previously detailed results for sDA<sub>300/50%</sub>, sDA<sub>100/50%</sub>, and ASE<sub>1000,250h</sub>. With this, some of the previous results can be explained. Interestingly, different conclusions can be drawn from the %time and %space results. By comparing these conclusions, the set target thresholds of the %space results (i.e. 50% time for 50% of space for sDA<sub>300/50%</sub>; 50% time for 95% of space for sDA<sub>100/50%</sub> and 10% for ASE<sub>1000,250h</sub>) are scrutinized. Thus, the limitations of setting such thresholds as target criteria, and the severe implications this can have for optimisation processes are illustrated in this chapter.

DA<sub>300</sub>, DA<sub>100</sub>, DA<sub>2000</sub> and ASE<sub>1000</sub> results for all six floors of the 162 design solutions were obtained from the ANN models and were visualised in Grasshopper, resulting in a total of  $4 \times 6 \times 162 = 3888$  visualisations for the daylight distribution. From these 3888 visualisations, select examples were used to analyse the influence of atrium well geometry, WWR distribution and orientation on daylight distribution. These examples also help explain previous findings for sDA<sub>300/50%</sub>, sDA<sub>100/50%</sub>, UDI-e and ASE<sub>1000,250h</sub>.

The analysis is structured in accordance with the main findings from the previous chapter on the impact of atrium well geometry, atrium well orientation and WWR distribution on daylight performance in Sections 8.1, 8.2 and 8.3, respectively. The sections are sub-structured to present the key results for each floor, going from the 6<sup>th</sup> to the ground floor. Thus, current %time results are always compared with the findings from the previous chapter, highlighting how %time and %space results can explain each

other or provide additional information crucial to understanding the impact of design changes.

## B.1 Impact of atrium geometry on daylight performance

The main findings from the previous chapter on the impact of atrium geometry on daylight performance can be summarised as follows:

1. 6<sup>th</sup> floor:  $sDA_{300/50\%}$  showed marginally higher results for smaller atrium base areas.  $sDA_{100/50\%}$  was achieved by 100% of the floor area by all design solutions.  $ASE_{1000, 250h}$  results remained similar regardless of changes to atrium base areas.
2. 5<sup>th</sup> to ground floor: Starting from the 5<sup>th</sup> floor, reducing the atrium base areas also reduced  $sDA_{300/50\%}$  results. This decrease was more pronounced on the 3<sup>rd</sup> to ground floors.  $sDA_{100/50\%}$  results remained at 100% of the floor area for all design solutions from the 6<sup>th</sup> to 4<sup>th</sup> floor. On the 3<sup>rd</sup> and lower floors, reducing the atrium base area reduced daylight performance of the  $sDA_{100/50\%}$  metric. The decrease was more pronounced on the second and ground floor. For the ASE metric, only southward oriented atria of the 50% WWR distribution series on the 5<sup>th</sup> floor showed results similar to the 6<sup>th</sup> floor, and ASE slightly increased from the largest to smallest atrium base area. For all other design solutions, results showed a tendency of marginal reduction in ASE on the 5<sup>th</sup> to 3<sup>rd</sup> floors, which was more noticeable for northward and central oriented than southward oriented atria.

### *B.1.1 Impact of atrium geometry on daylight performance on the 6<sup>th</sup> floor*

“ $sDA_{300/50\%}$  showed marginally higher results for smaller atrium base areas.  $sDA_{100/50\%}$  was achieved by 100% of the floor area by all design solutions.  $ASE_{1000,250h}$  results remained similar regardless of changes to atrium base areas.”

To aid in further understanding the findings described, %time results are shown for three selected design solutions on the 6<sup>th</sup> floor. The selected design solutions are highlighted in Figure 1. The three design variants have a central orientation and a WWR of 50% on the 6<sup>th</sup> floor.

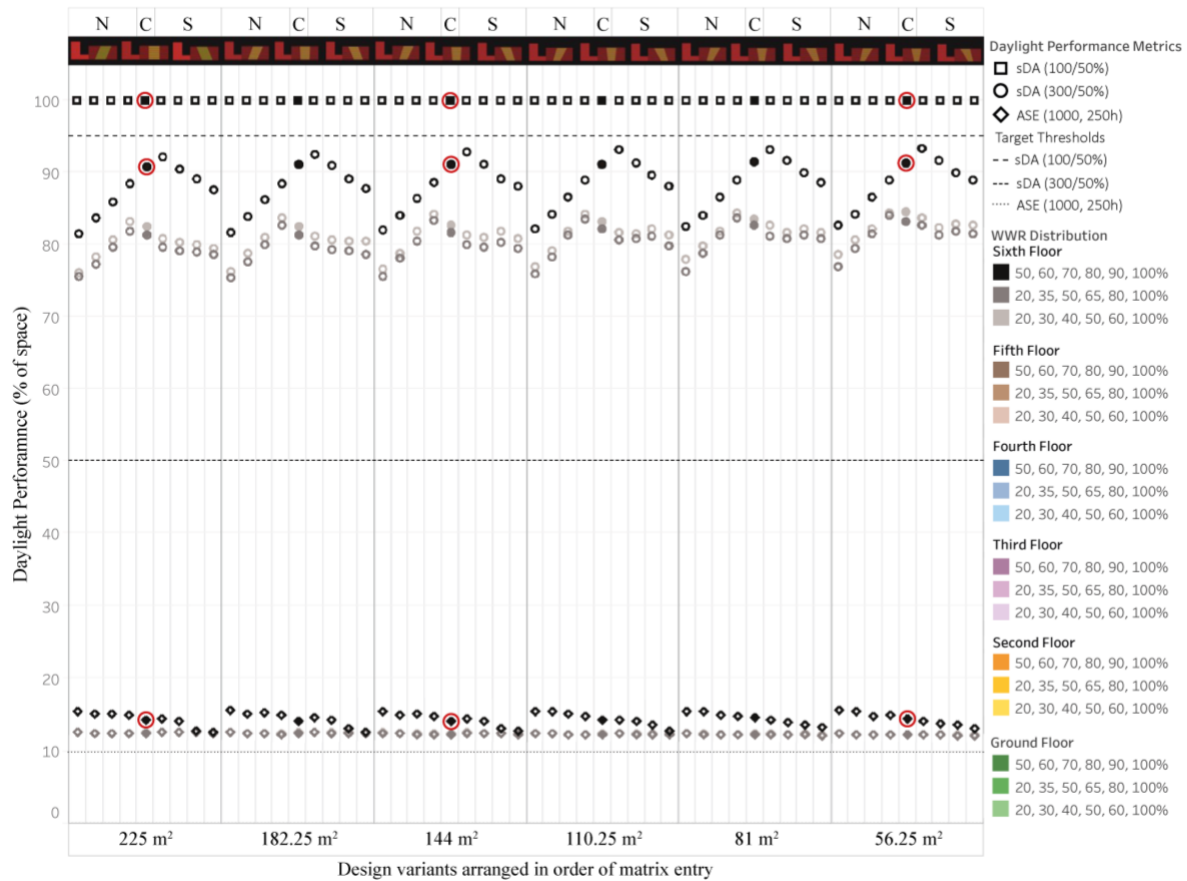


Figure 1 sDA<sub>300/50%</sub>, sDA<sub>100/50%</sub> and ASE results on the 6<sup>th</sup> floor. Metric results for the marked design solutions are plotted in Figure 2 and Figure 3.

DA<sub>300</sub> and sDA<sub>300/50%</sub> plots for the specified design solutions on the 6<sup>th</sup> floor are shown in Figure 2. Decreasing the atrium base area only slightly impacted daylight levels on the 6<sup>th</sup> floor, which remained similar to each other. Nonetheless, there was a marginal increase in sDA<sub>300/50%</sub> with every smaller atrium base area. As this barely stands out visually, an overlay of the plot from the largest and smallest atrium base areas is illustrated below (Figure 2, G). The areas highlighted in blue show additional spaces that passed the sDA<sub>300/50%</sub> threshold. For central oriented design solutions, these spaces were

mostly in areas directly surrounding the atrium well, as slanting the atrium well facades exposed more floor area towards the skylight. Therefore, an increase could be seen in  $sDA_{300/50\%}$  results despite the increase in room depth, which would usually reduce daylight levels. This increase in room depth was 2,59m on each side of the atrium well, or 26,82 m<sup>2</sup> when comparing the largest to the smallest atrium base area (Figure 2, G).

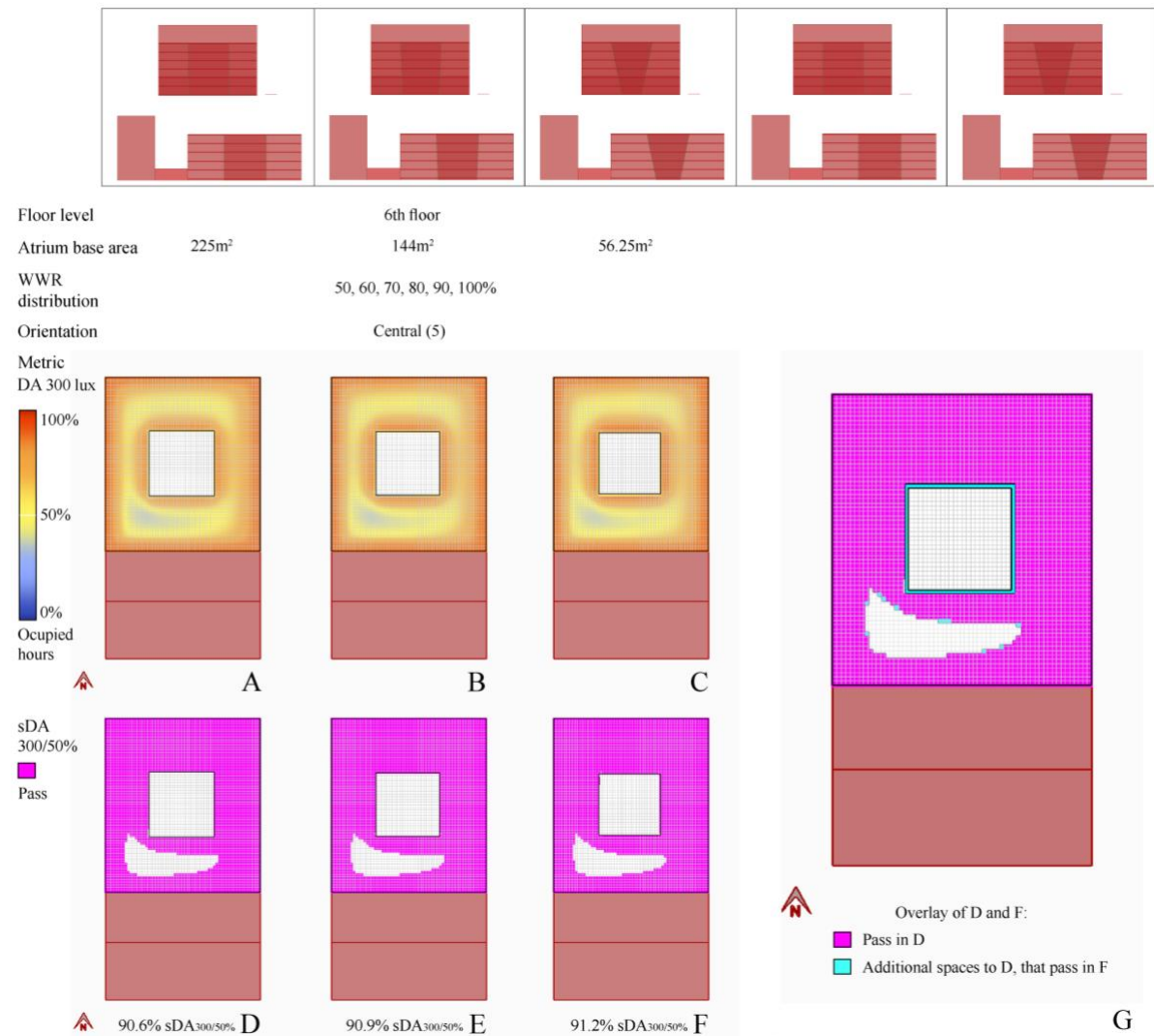


Figure 2  $DA_{300}$  and  $sDA_{300/50\%}$  results plots for the specified design solutions, highlighting the impact of atrium geometry on daylight results on the 6<sup>th</sup> floor

UDI-e and ASE results are shown in Figure 3. Both show a marginal increase in daylight levels exceeding 1000 lux, the smaller the atrium base areas. An overlay highlights this difference between UDI-e for the largest and smallest atrium base areas by subtraction of the results (Figure 3, N). Especially areas to the north of the atrium

receive more daylight when reducing the atrium base area, a consequence of splaying the atrium well walls to be more perpendicular to solar altitude angles.

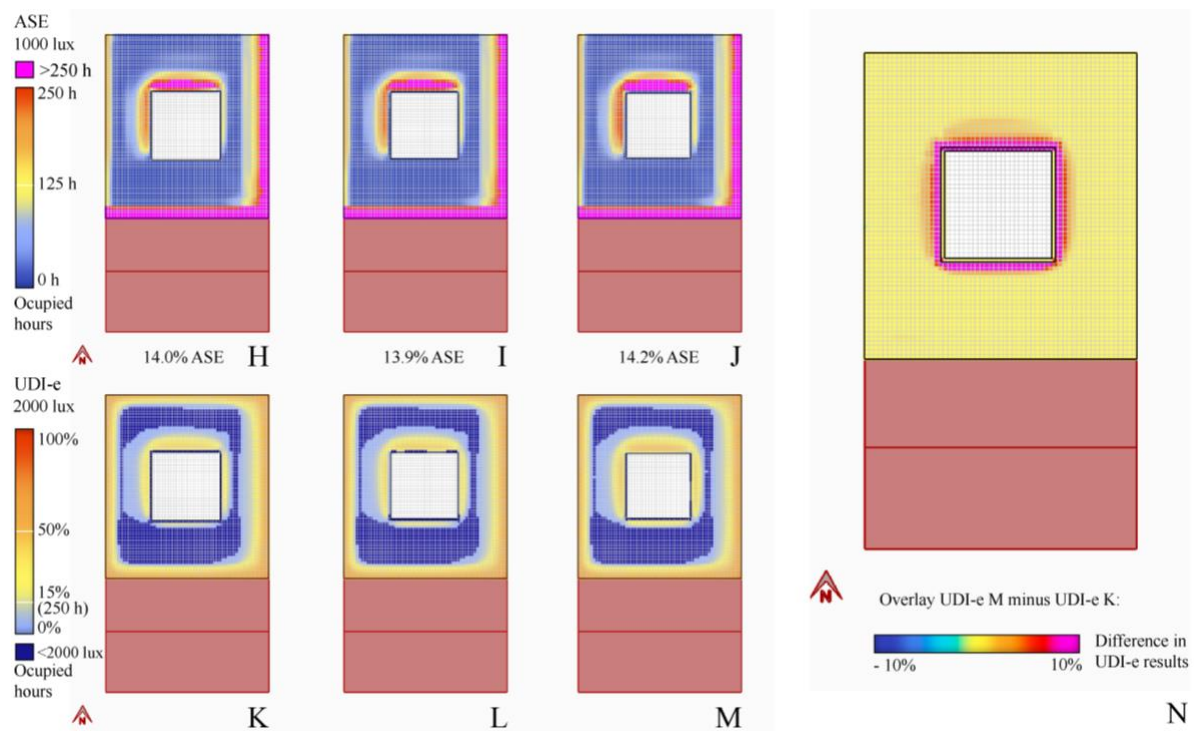


Figure 3 ASE and UDI-e results plots for the specified design solutions, highlighting the impact of atrium geometry on daylight results on the 6th floor

### B.1.2 Impact of atrium geometry on daylight performance on the 5<sup>th</sup> to ground floor

“Starting from the 5<sup>th</sup> floor, reducing the atrium base areas also reduces  $sDA_{300/50\%}$  results. This decrease was more pronounced on the 3<sup>rd</sup> to ground floors.  $sDA_{100/50\%}$  results remained at 100% of the floor area for all design solutions from the 6<sup>th</sup> to 4<sup>th</sup> floor. On the 3<sup>rd</sup> and lower floors, reducing the atrium base area reduced daylight performance for the  $sDA_{100/50\%}$  metric. The decrease was more pronounced on the second and ground floor. For the ASE metric, only southward oriented atria of the 50% WWR distribution series on the 5<sup>th</sup> floor showed results similar to the 6<sup>th</sup> floor, and ASE slightly increased from the largest to smallest atrium base area. For all other design solutions, results showed a tendency of

marginal reduction in ASE on the 5<sup>th</sup> to 3<sup>rd</sup> floor, which was more noticeable for northward and central oriented than southward oriented atria.”

The impact of altering the atrium base area on daylight performance on lower floors significantly differed from what was seen on the 6<sup>th</sup> floor. To aid in further understanding the findings described, %time results are shown for three selected design solutions on the 3<sup>rd</sup> floor. The selected design solutions are highlighted in Figure 4. The three design variants have a central orientation and a WWR of 50% on the 3<sup>rd</sup> floor.

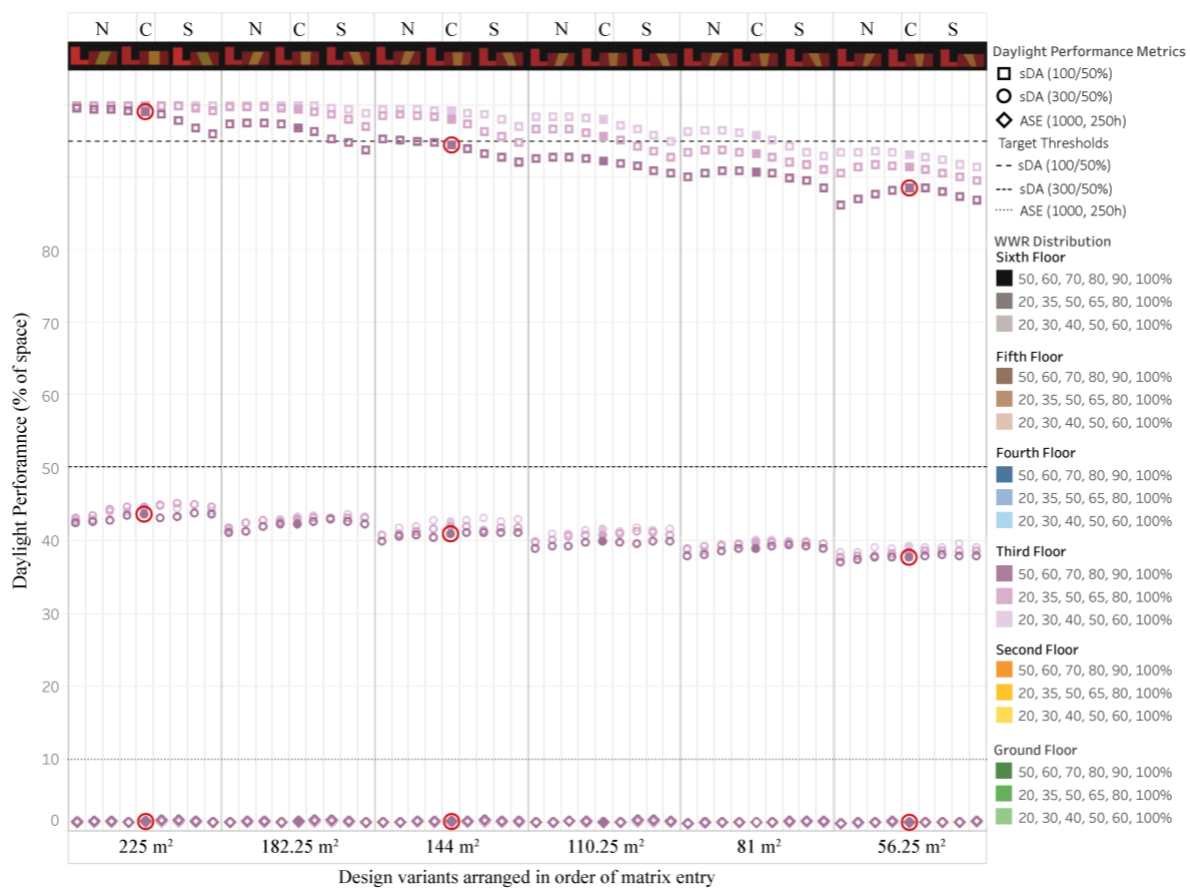


Figure 4 sDA<sub>300/50%</sub>, sDA<sub>100/50%</sub> and ASE results on the 3<sup>rd</sup> floor. Metric results for the marked design solutions are plotted in the following sections.

DA and sDA plots for the specified design solutions on the 3<sup>rd</sup> floor are shown in Figure 5. Decreasing the atrium base area reduced daylight performance. The overlay of sDA results (Figure 5 G) showed that this decrease in sDA<sub>300/50%</sub> results could largely be attributed to the increase in room depth. The DA<sub>300</sub> results (Figure 5 A to C) revealed that

this increase in room depth was also responsible for the occurrence of especially low illuminances (as shown by an increase of dark blue spaces). This can be seconded looking at  $sDA_{100/50\%}$  and  $DA_{100}$  results (Figure 6). Reducing the atrium area and increasing the room depth resulted in an increase in areas to the south of the atrium well failing to meet the threshold (Figure 6 K to M). The overlay of  $sDA_{100/50\%}$  results for the largest and smallest atrium areas accentuated the difference in  $DA_{100}$  (Figure 6 N). This difference was shown for the atrium with a central orientation. The magnitude of impact however that decreasing the atrium base area had on  $sDA_{100/50\%}$  results varied between orientations, such that the decrease in  $sDA_{100/50\%}$  was much higher for southward than northward oriented atria. The pattern could be seen starting from the 3<sup>rd</sup> floor and was more apparent on the 2<sup>nd</sup> and ground floor. As this result is concerned with atrium well orientation, it is discussed in more detail in another section of this chapter.

UDI-e and ASE results for the specified design solutions on the 3<sup>rd</sup> floor are shown in Figure 7. The plots show that it was mainly the area surrounding the atrium well that was affected by illuminances exceeding the ASE and UDI-e thresholds. Notably, for smaller atria, the depth of affected area increased toward the south of the atrium well (Figure 7 R to U). This was again a consequence of splaying the atrium well walls to be more perpendicular to solar altitude angles.

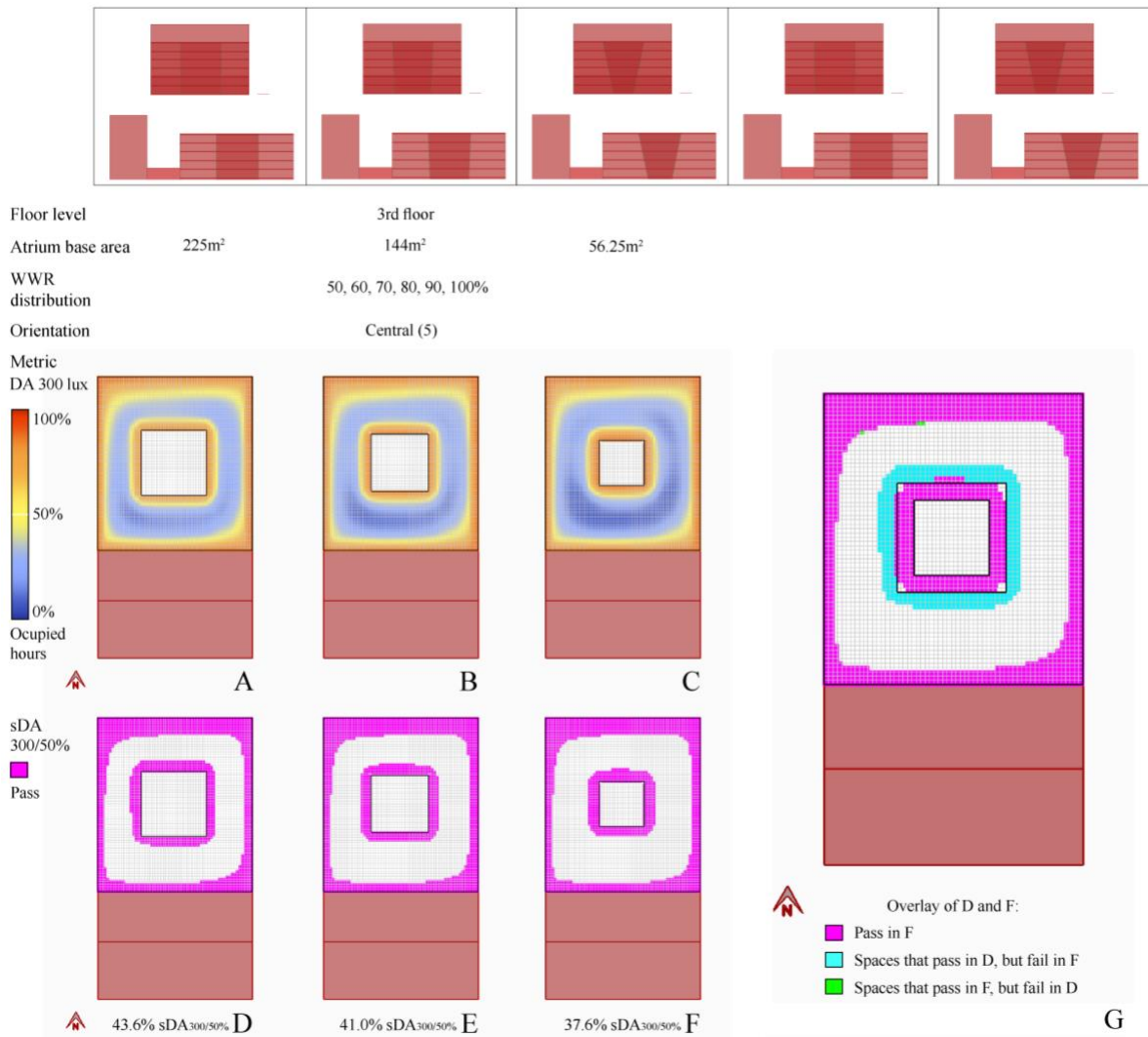


Figure 5 DA<sub>300</sub> and sDA<sub>300/50%</sub> results plots for the specified design solutions, highlighting the impact of atrium geometry on daylight results on the 3rd floor

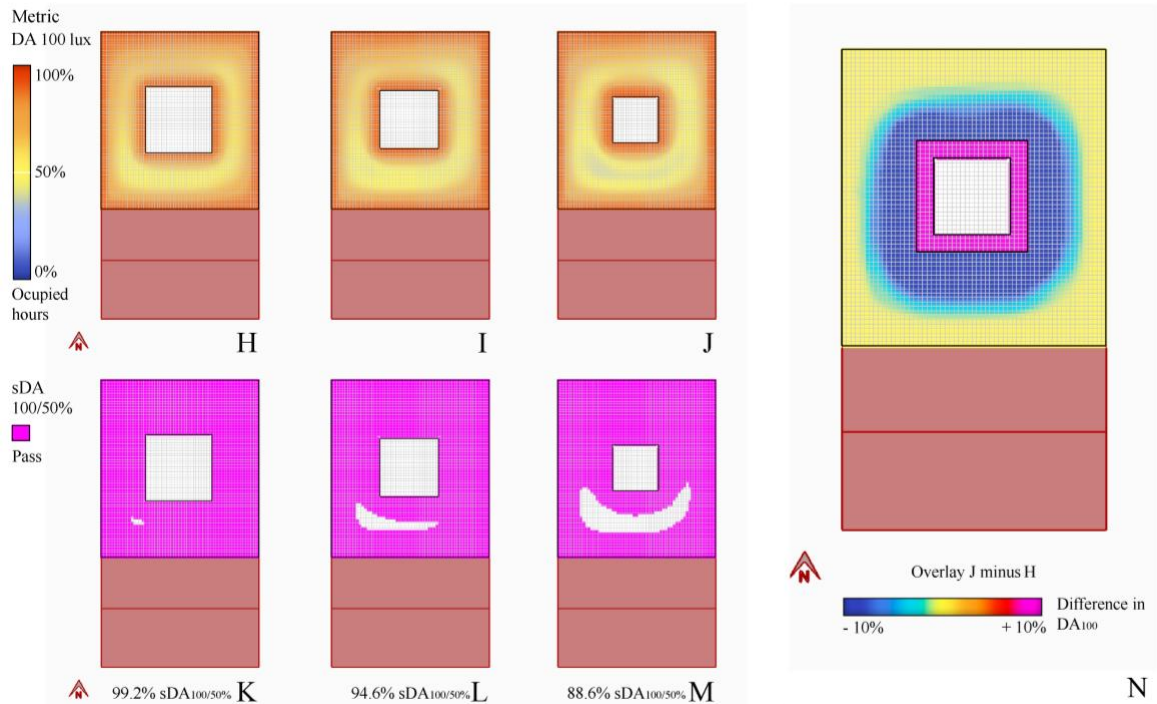


Figure 6 DA<sub>100</sub> and sDA<sub>100/50%</sub> results plots for the specified design solutions, highlighting the impact of atrium geometry on daylight results on the 3rd floor

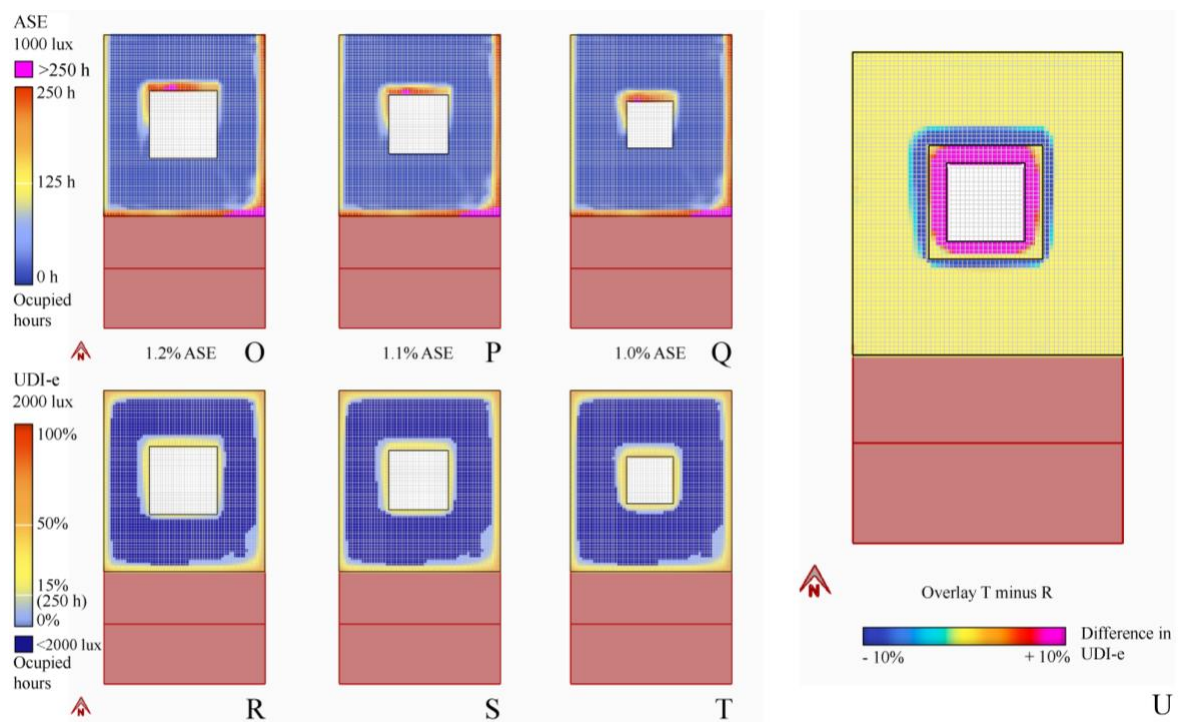


Figure 7 UDI-e and ASE results plots for the specified design solutions, highlighting the impact of atrium geometry on daylight results on the 3rd floor

## B.2 Impact of atrium WWR distribution on daylight performance

The main findings from the previous chapter on the impact of atrium geometry on daylight performance can be summarised as follows:

1. 6<sup>th</sup> to 4<sup>th</sup> floor: A smaller WWR resulted in lower  $sDA_{300/50\%}$  performance on the 6<sup>th</sup> and 5<sup>th</sup> floors.  $sDA_{100/50\%}$  was achieved by 100% of the floor area by all design solutions.  $ASE_{1000,250h}$  results differed between the WWR distribution series, such that the WWR distribution series starting with 50% WWR showed a higher ASE than the WWR distribution series starting with 20% WWR for northward orientations. For southward to southmost orientations however,  $ASE_{1000,250h}$  results became more similar between WWR distribution series. On the 4<sup>th</sup> floor,  $sDA_{300/50\%}$  performance results were similar for any given WWR distribution series, showing that there was hardly any impact of WWR distribution on  $sDA_{300/50\%}$  for this floor. In terms of ASE, the WWR distribution starting with 50% WWR showed higher results than the WWR distribution series starting with 20% WWR.
2. 3<sup>rd</sup> to ground floor: On these floors, the WWR distribution series starting with 20% WWR on the top floor showed the highest  $sDA_{300/50\%}$  and  $sDA_{100/50\%}$  performance. ASE results overlapped and showed no difference in sunlight exposure regardless of the WWR distribution series. On the 2<sup>nd</sup> and ground floors, ASE results are at 0%.

### *B.2.1 Impact of WWR distribution on daylight performance on the 6<sup>th</sup> to 4<sup>th</sup> floors*

“A smaller WWR resulted in lower  $sDA_{300/50\%}$  performance on the 6<sup>th</sup> and 5<sup>th</sup> floors.  $sDA_{100/50\%}$  was achieved by 100% of the floor area by all design solutions.  $ASE_{1000,250h}$  results differed between the WWR distribution series, such that the WWR distribution series starting with 50% WWR showed a higher ASE than the

WWR distribution series starting with 20% WWR for northward orientations. For southward to southmost orientations however, ASE<sub>1000,250h</sub> results became more similar between WWR distribution series. On the 4<sup>th</sup> floor, sDA<sub>300/50%</sub> performance results were similar for any given WWR distribution series, showing that there was hardly any impact of WWR distribution on sDA<sub>300/50%</sub> for this floor. In terms of ASE, the WWR distribution starting with 50% WWR showed higher results than the WWR distribution series starting with 20% WWR.”

To aid in further understanding the findings described, %time results are shown for four selected design solutions on the 5<sup>h</sup> floor. The selected design solutions are highlighted in Figure 8. The four design variants have northmost and southmost orientations and a WWR of 60% and 30% on the 5<sup>th</sup> floor.

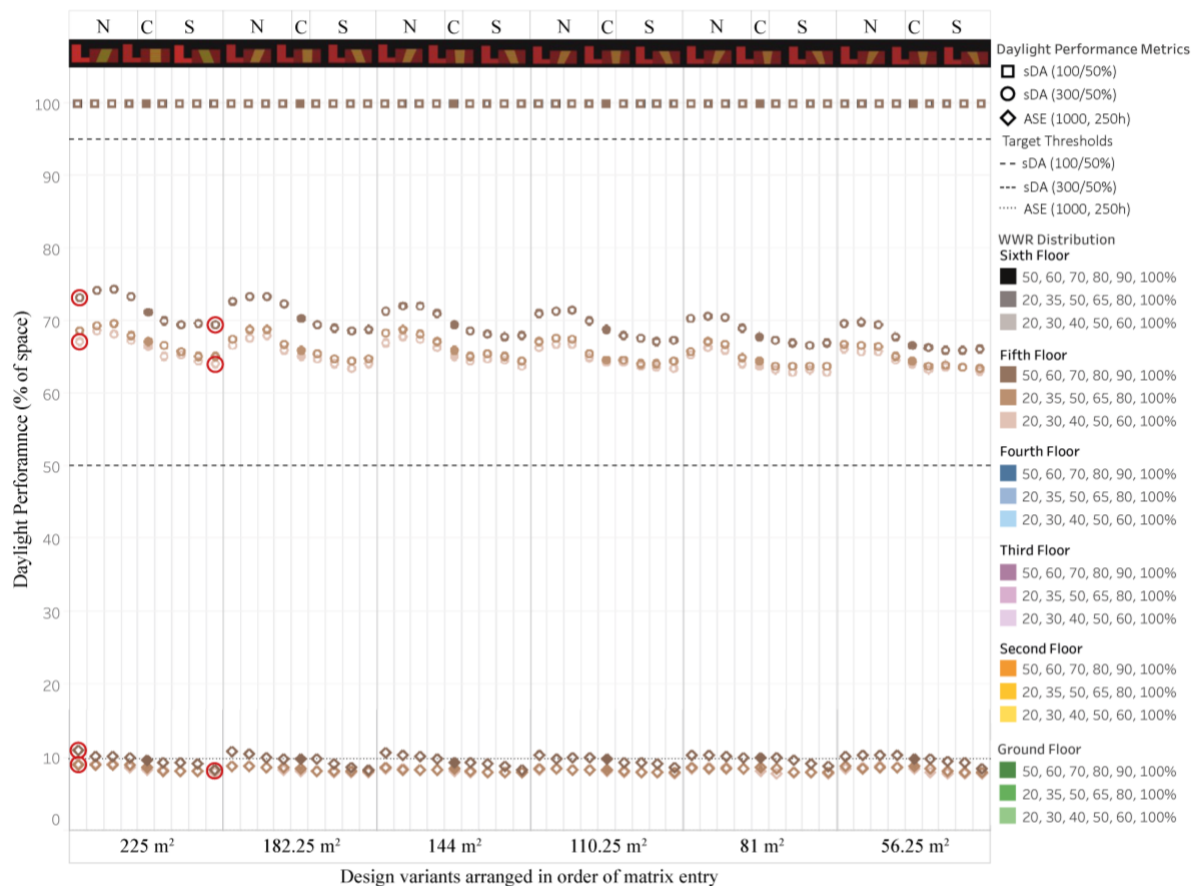


Figure 8 sDA<sub>300/50%</sub>, sDA<sub>100/50%</sub> and ASE results on the 5<sup>th</sup> floor. Metric results for the marked design solutions are plotted in the following sections.

DA<sub>300</sub> and sDA<sub>300/50%</sub> plots for the specified design solutions on the 5<sup>th</sup> floor are shown in Figure 9. The WWR distribution series starting with 50% (with a WWR of 60% on the 5<sup>th</sup> floor) showed a higher sDA<sub>300/50%</sub> performance than the WWR distribution series starting with 20% (with a WWR of 30% on the 5<sup>th</sup> floor). This result is self-explanatory considering the difference in light admitting window area. The DA<sub>300</sub> plots additionally revealed that larger window areas improved daylight in areas to the south of the atrium when the atrium had a northward orientation, and vice versa improved daylight in areas to the north of the atrium when the atrium had southward orientations (see difference of daylight levels into the depth of atrium adjacent spaces, as shown by the blue hue in Figure 9 E and E2). The difference in daylight as a result of smaller windows was most pronounced in spaces to the south of the atrium as a consequence of overshadowing from the surround buildings (see dark blue hue in in Figure 9 E). Thus, although norward orientations showed higher sDA<sub>300/50%</sub>, the decrease in DA<sub>300</sub> resulting from smaller windows was more noticeable for this orientation.

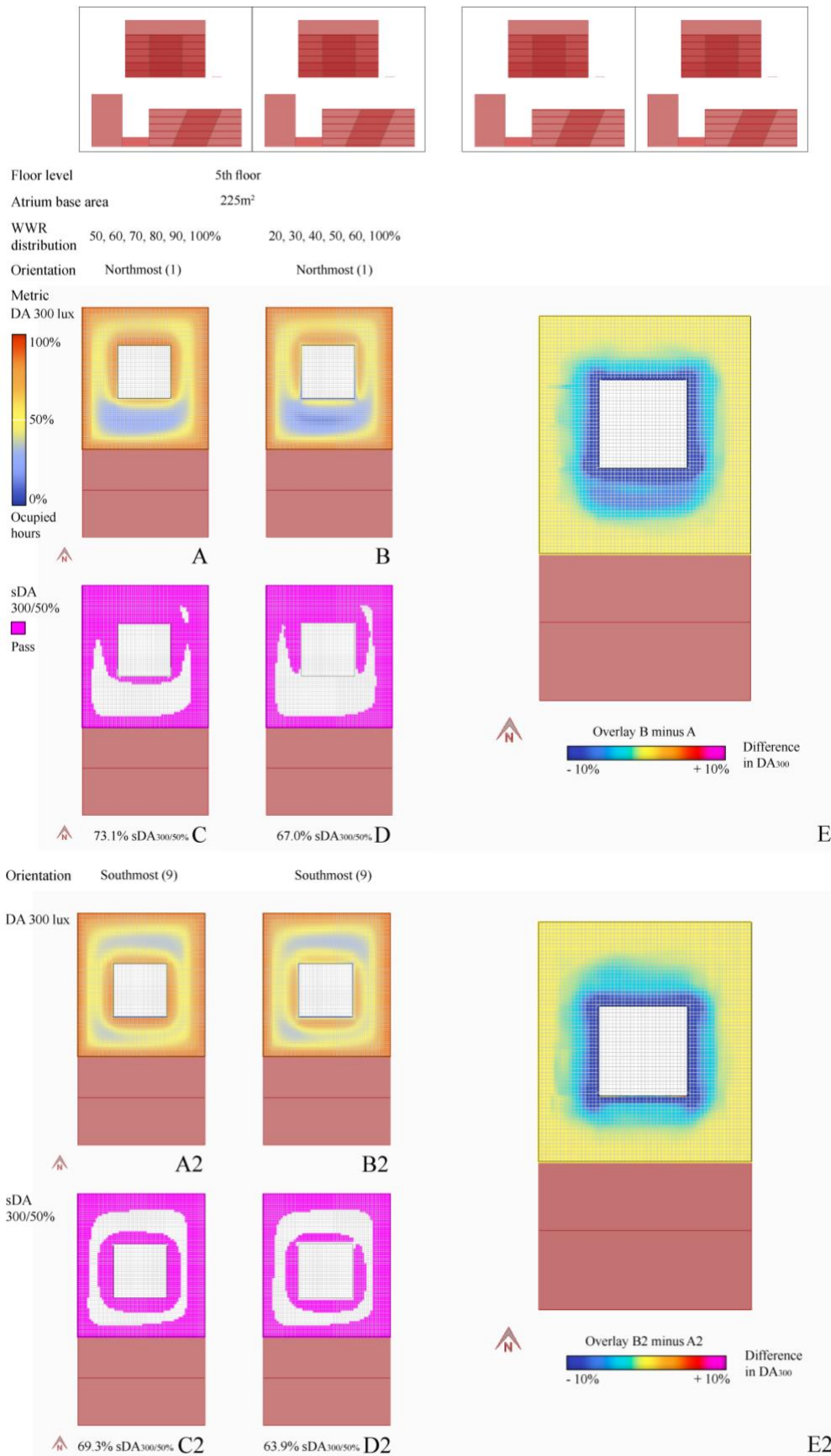


Figure 9 DA<sub>300</sub> and sDA<sub>300/50%</sub> result plots for the specified design solutions, highlighting the impact of WWR distribution on daylight results on the 5<sup>th</sup> floor

UDI-e and ASE results are shown in Figure 10. These plots provide information additional information to the DA plots. Lux levels exceeding 1000/2000 occurred mostly in spaces north of the atrium well attributing to the south-facing atrium well façade (pink hue around atrium in Figure 10 F, G, F2, G2; orange and yellow hue in Figure 10 H, I, H2, I2). Reducing the window area therefore reduced both ASE and DA<sub>2000</sub> in those spaces (e.g. see Figure 10 G and I compared to F and H). Although the %space result for the ASE metric showed a bigger difference in ASE only for northward orientations, the %time plots indicate that this difference in ASE is also true for southward orientations (Figure 10 F2 and G2). However, as the direct sunlight exposure did not exceed the 250h threshold for southward orientations, the difference was not captured by the %space results. To conclude, reducing window area reduces risk of glare for northward as well as southward orientations. Reducing window area also reduced DA<sub>300</sub> and sDA<sub>300/50%</sub>. However, the decrease in DA<sub>300</sub> resulting from a smaller WWR was higher for northward orientations. This trend was seen only for the 6<sup>th</sup> and 5<sup>th</sup> floors. On the 4<sup>th</sup> floor, a smaller WWR did not anymore significantly reduce sDA<sub>300</sub> or DA<sub>300</sub>. Instead, the 4<sup>th</sup> floor was the turning point for an opposite trend, whereby lowering the WWR increased daylight levels on lower floors. This is investigated in more detail in the next section.

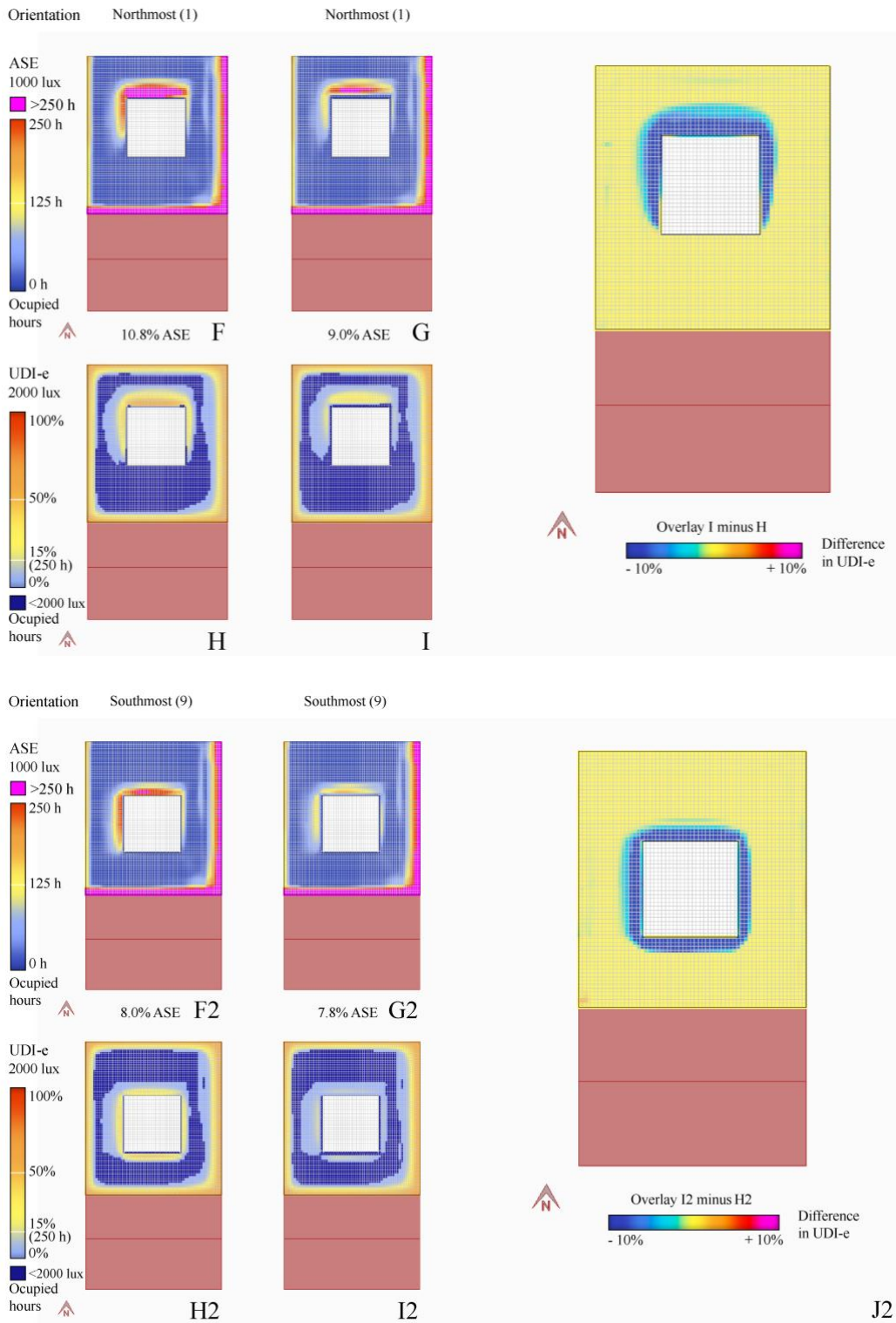


Figure 10 ASE and UDI-e result plots for the specified design solutions on the 5<sup>th</sup> floor

## B.2.2 Impact of WWR distribution on on daylight performance on the 3<sup>rd</sup> to ground floors

“On these floors, the WWR distribution series starting with 20% WWR on the top floor showed the highest  $sDA_{300/50\%}$  and  $sDA_{100/50\%}$  performance. ASE results overlapped and showed no difference in sunlight exposure regardless of the WWR distribution series. On the 2<sup>nd</sup> and ground floors, ASE results are at 0%.”

To aid in further understanding the findings described, %time results are shown for four selected design solutions on the ground floor. The selected design solutions are highlighted in Figure 11. The four design variants have northmost and southmost orientations and a WWR distribution of 50, 60, 70, 80, 90, 100% and 20, 30, 40, 50, 60, 100%.

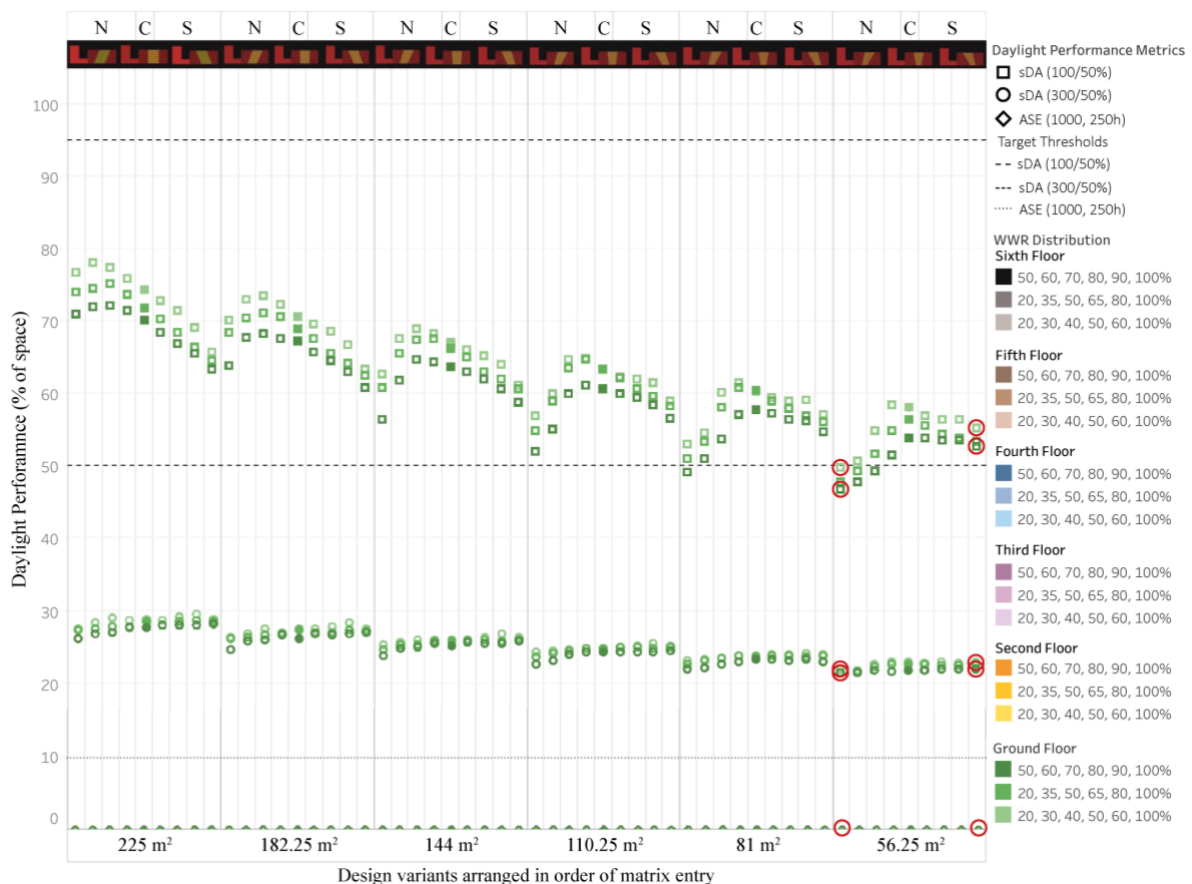


Figure 11  $sDA_{300/50\%}$ ,  $sDA_{100/50\%}$  and ASE results on the ground floor. Metric results for the marked design solutions are plotted in the following sections

DA<sub>300</sub> and sDA<sub>300/50%</sub> plots for the specified design solutions on the ground floor are shown in Figure 12. DA<sub>100</sub> and sDA<sub>100/50%</sub> plots are shown in Figure 13. In contrast to the 6<sup>th</sup> and 5<sup>th</sup> floors, the WWR distribution series starting with 50% and a higher overall light admitting area showed lower sDA<sub>300/50%</sub> performance than the WWR distribution series starting with 20% and smaller overall light admitting area improved sDA<sub>300/50%</sub>. As previously explained, this a result stems from the increase in reflected daylight. The increase in daylight resulting from lower WWR across the atrium façade is displayed by means of an overlay of DA plots in Figure 12 and Figure 13 E, E2. As shown in the figures, the WWR distributions series with 20, 30, 40, 50, 60, 100% showed a deeper daylight penetration into atrium adjacent spaces. Areas surrounding the atrium were able to achieve DA for at least 10% more occupied hours in a year (see pink hue Figure 12 , Figure 13 E, E2).

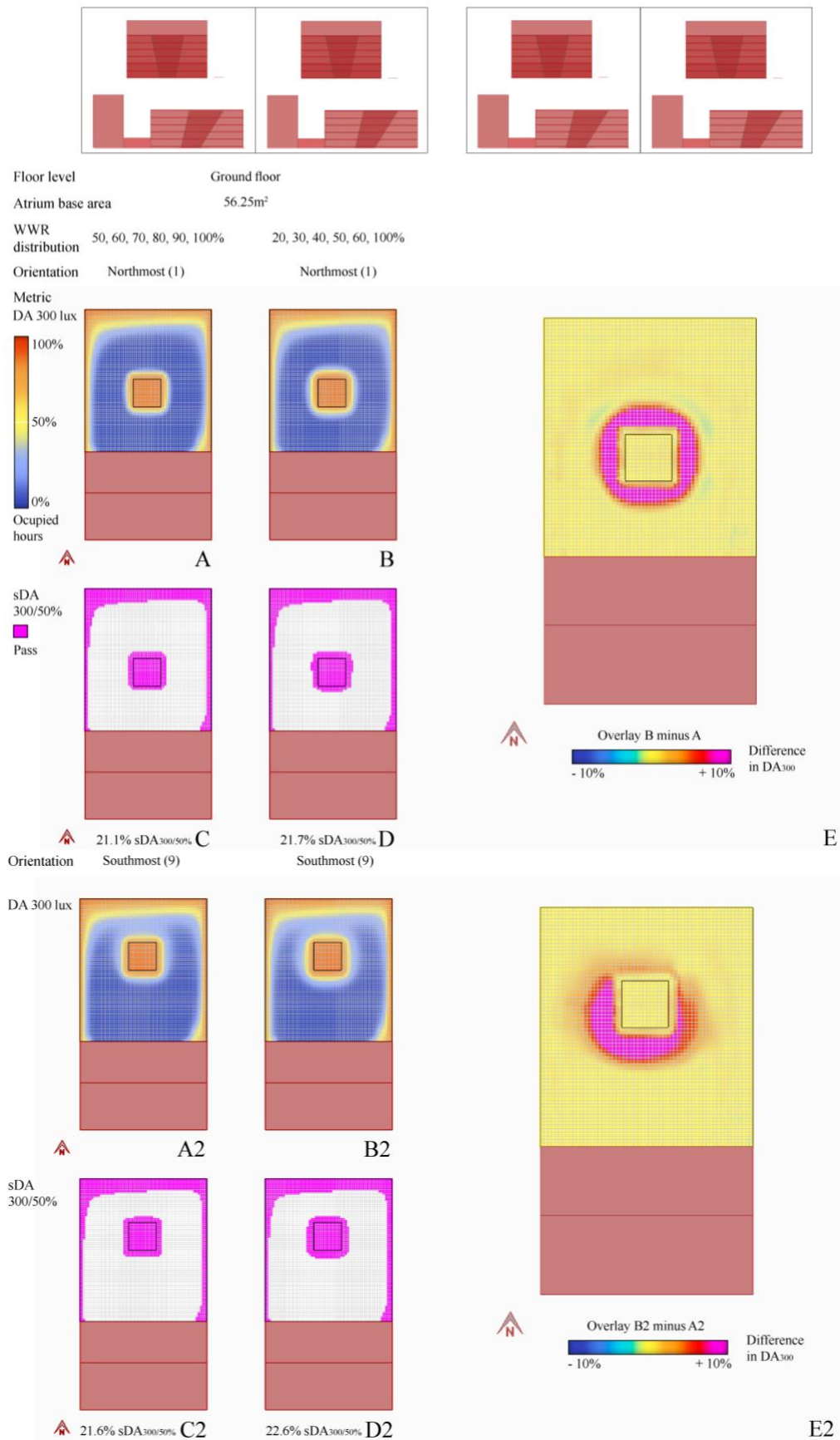


Figure 12 DA<sub>300</sub> and sDA<sub>300/50%</sub> result plots for the specified design solutions, highlighting the impact of WWR distribution on daylight results on the ground floor. The %space sDA results provided below the plots refer to atrium adjacent spaces only

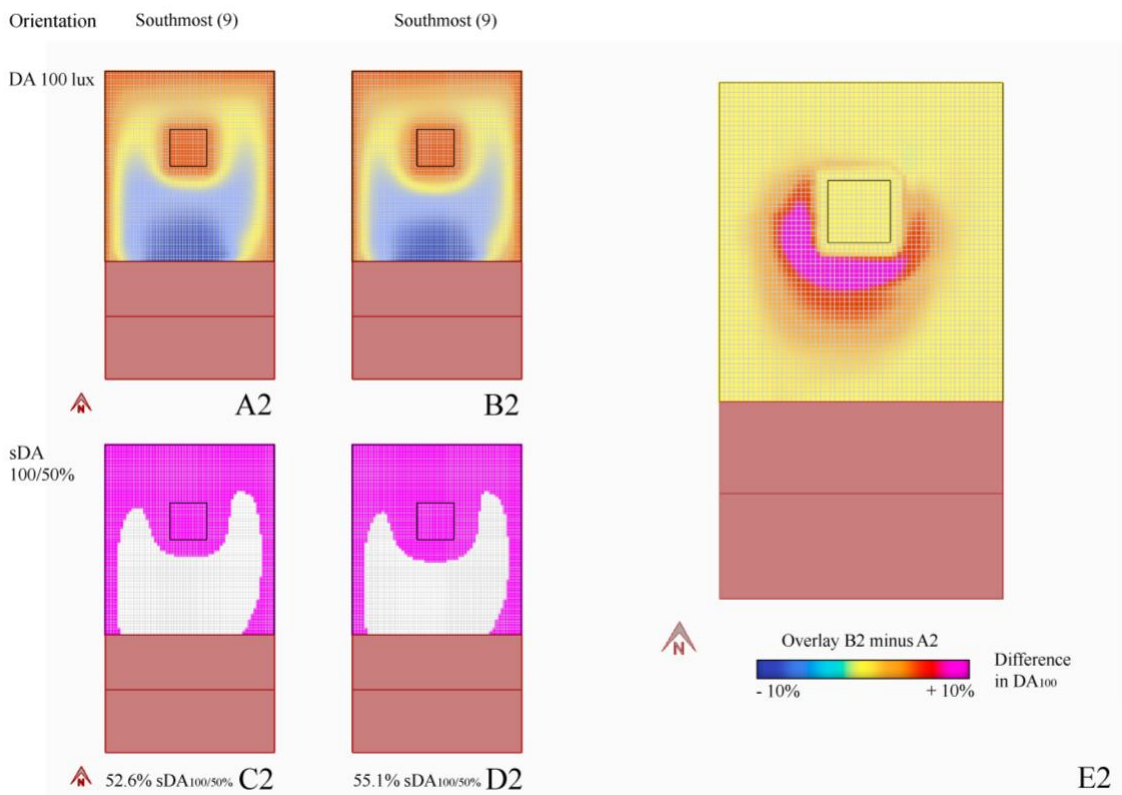
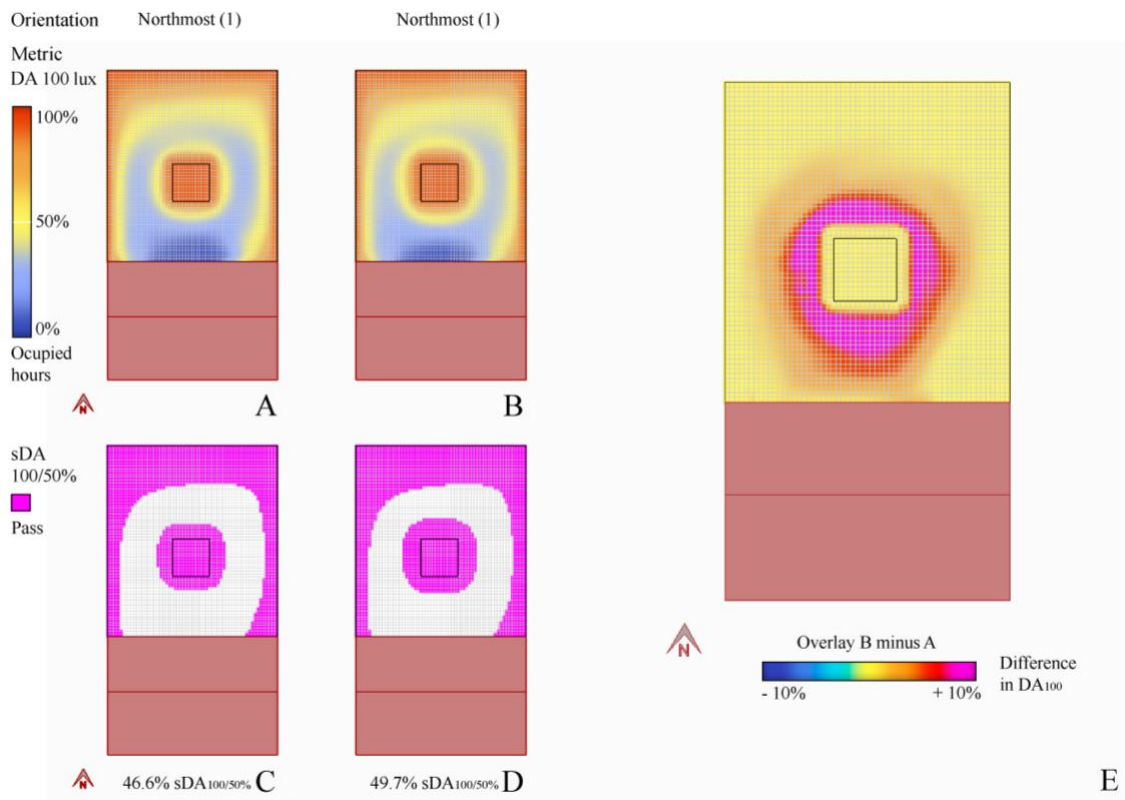


Figure 13 DA<sub>100</sub> and sDA<sub>100/50%</sub> result plots for the specified design solutions on the ground floor. The %space sDA results provided below the plots refer to atrium adjacent spaces only

Figure 14 shows the ASE and UDI-e result plots. Whereas ASE results did not show any difference in direct sunlight penetration between the two WWR distribution series, UDI-e showed that reflected daylight increased DA exceeding 2000 lux in atrium adjacent spaces (yellow hue in Figure 14 H compared to I, H2 compare to I2). For northmost orientations,  $DA_{2000}$  increased mostly in spaces to the north of the atrium well. For southmost orientations, the increase in  $DA_{2000}$  in atrium adjacent spaces was more noticeable (thicker pink hue surrounding the atrium in Figure 14 J2 compared to J). Here,  $DA_{2000}$  increase in all directions surrounding the atrium, but most notably in spaces to the south, east and west. To conclude, reducing WWR across the atrium well façade improved daylight penetration into atrium adjacent spaces on lower floors. The impact of WWR on daylight performance varied between orientations, such that daylight reached deeper into spaces either north or south of the atrium well. For northward orientations, reducing the WWR improved  $DA_{100}$  especially in spaces to the south of the atrium well, where overall DA fell short. In contrast,  $DA_{300}$  and UDI-e showed that southward, rather than northward orientations increased daylight in spaces to the south of the atrium. Lastly, the impact of WWR distribution on the ground floor, as described in this and previous sections, was mostly visualised by means of an overlay of results. The differences were not evident from the DA and sDA plots alone, indicating a limitation of such visualisations.

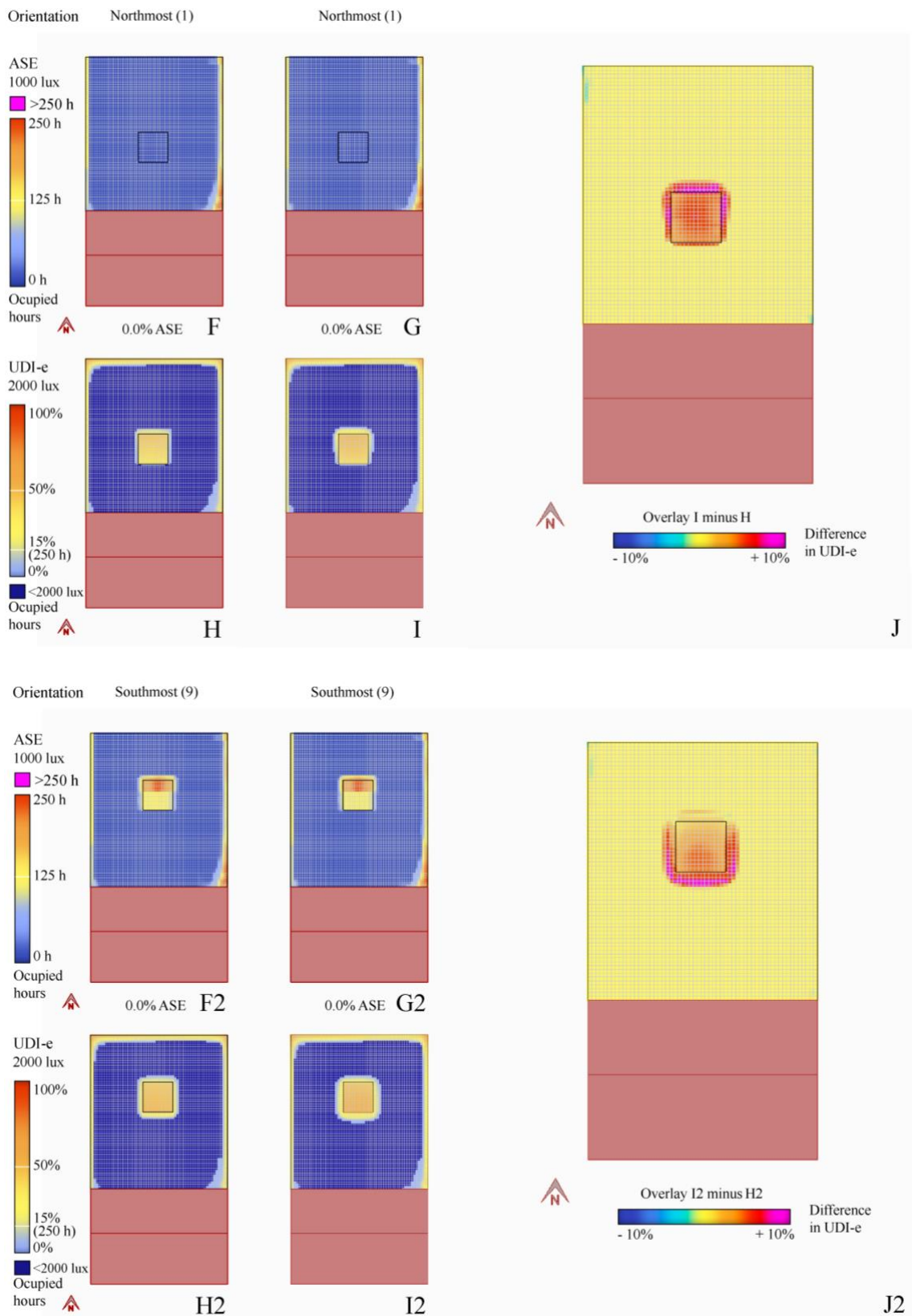


Figure 14 ASE and UDI-e result plots for the specified design solutions on the ground floor

### B.3 Impact of atrium orientation on daylight performance

The main findings from the previous chapter on the impact of atrium geometry on daylight performance can be summarised as follows:

3. 6<sup>th</sup> floor: Shallow north- and southward orientations displayed the highest  $sDA_{300/50\%}$  performance and the north-most orientation the lowest.  $sDA_{100/50\%}$  was achieved by 100% of the floor area by all design solutions.  $ASE_{1000,250h}$  results showed that, with a WWR of 50%, northward oriented atria received more direct sunlight than southward oriented atria. As for a WWR of 20%, ASE results remained similar regardless of changes to atrium well orientation.
4. 5<sup>th</sup> floor: Northward orientations displayed the highest  $sDA_{300/50\%}$  performance and southward orientations the lowest. This pattern was consistent for all three WWR distribution series.  $sDA_{100/50\%}$  was achieved by 100% of the floor area by all design solutions.  $ASE_{1000,250h}$  displayed progressively lower direct sunlight penetration from north to southward orientations in a linear fashion, with northmost orientations consistently displaying the highest ASE and southmost orientations the lowest. The gradient was steepest (difference in ASE between northmost and southmost orientations was greatest) for the WWR distribution series starting with 50% WWR (with a WWR of 60% on the fifth floor). I.e., the difference in ASE between northmost and southmost orientations was greatest for this WWR distribution series. The difference in ASE between northmost and southmost orientations for the two WWR distribution series starting with 20% WWR (with a WWR of 30% and 35% on the fifth floor) was minimal.
5. 4<sup>th</sup> floor:  $sDA_{300/50\%}$  performance hardly differed between the different orientations on this floor. Nonetheless, a tendency for southward orientation to show higher

sDA<sub>300/50%</sub> results, and northward orientations to show lower sDA<sub>300/50%</sub> results became apparent, more so for smaller atrium base areas. sDA<sub>100/50%</sub> was achieved by 100% of the floor area by all design solutions. ASE displayed a higher value for north than south orientations. For design solutions with the largest atrium base area, the northmost orientations displayed the highest ASE result. For all other atrium base areas, the smaller the atrium base area became, the shallower the orientation with the highest ASE, and the lower the ASE of northmost orientations. This pattern was consistent across all WWR distribution series.

6. 3<sup>rd</sup> floor: Southward orientations displayed the highest sDA<sub>300/50%</sub> performance. In contrast, northward orientations displayed the highest sDA<sub>100/50%</sub> performance and southmost orientations the lowest. Only design solutions with the smallest atrium base area of 56.25m<sup>2</sup> and a WWR distribution series starting with 50% WWR showed a shift in pattern, whereby central and slight southward orientations gave higher sDA<sub>100/50%</sub> results than northward orientations. ASE results hardly varied between the different orientations, with differences less than 0.5% ASE. Nonetheless, northmost orientations, with the exception of design solutions with the largest atrium base area of 225m<sup>2</sup>, now started to show the lowest ASE.
7. 2<sup>nd</sup> floor: Southward orientations displayed the highest sDA<sub>300/50%</sub> performance and northmost the lowest. This trend was true for all atrium base areas. In contrast, sDA<sub>100/50%</sub> results changed with a decrease in atrium base area, from more northward to central orientations achieving a higher sDA<sub>100/50%</sub> result. For larger atrium base areas, southmost orientations showed the lowest sDA<sub>100/50%</sub>. For smaller atrium base areas, northmost orientations showed the lowest sDA<sub>100/50%</sub> result. ASE results were at 0% for all design solutions on this floor.

8. Ground floor: Southward orientations displayed the highest  $sDA_{300/50\%}$  performance and northmost the lowest. This trend was true for all atrium base areas. In contrast,  $sDA_{100/50\%}$  results changed with a decrease in atrium base area, from more northward to central and slight southward orientations achieving a higher  $sDA_{100/50\%}$  result. For larger atrium base areas, southmost orientations showed the lowest  $sDA_{100/50\%}$ . For smaller atrium base areas, northmost orientations showed the lowest  $sDA_{100/50\%}$  result. ASE results were at 0% for this floor.

### *B.3.1 Impact of atrium orientation on daylight performance on the 6<sup>th</sup> floor*

“Shallow north- and southward orientation displayed the highest  $sDA_{300/50\%}$  performance and the north-most orientation the lowest.  $sDA_{100/50\%}$  was achieved by 100% of the floor area by all design solutions.  $ASE_{1000,250h}$  results showed that, with a WWR of 50%, northward oriented atria received more direct sunlight than southward oriented atria. As for a WWR of 20%,  $ASE_{1000,250h}$  results remained similar regardless of changes to atrium well orientation.”

To aid in further understanding the findings described, %time results are shown for five selected design solutions on the 6<sup>th</sup> floor. The selected design solutions are highlighted in Figure 15. Among the selected design variants are those with a northmost, northward and southward orientation for the 50% WWR distribution series and a northward and southward orientation for the 20% WWR distribution series. Thus, both the optimum southward orientation (in terms of  $sDA_{300/50\%}$  performance) for the 50% WW distribution series and the optimum northward orientation for the 20% WWR distribution series are displayed for further analysis.

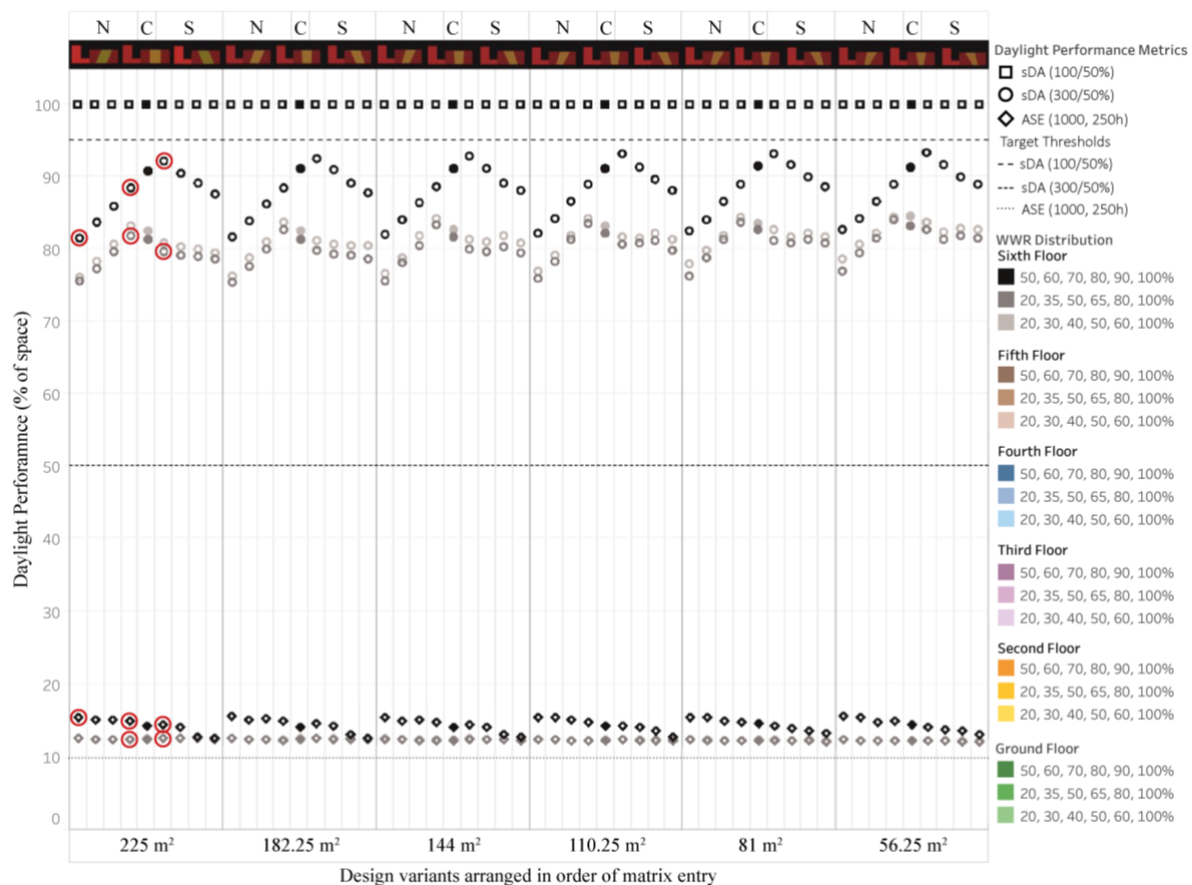


Figure 15 sDA<sub>300/50%</sub>, sDA<sub>100/50%</sub> and ASE results on the 6<sup>th</sup> floor. Metric results for the marked design solutions are plotted in the following sections.

Figure 16 shows DA<sub>300</sub> and sDA<sub>300/50%</sub> results of the selected design solutions on the 6<sup>th</sup> floor. The steeper the orientation towards north or south, the lower the sDA<sub>300/50%</sub> performance. As evident from the figure, this was because changing the orientation increased the room depth on either side of the atrium well, resulting in particularly low DA<sub>300</sub> for those spaces (blue patches in Figure 16 A, B, C, D, E). Due to overshadowing from adjoining and surrounding buildings, the spaces prone to receiving less daylight were concentrated in the south of the atrium well. As a result, northward orientations generally showed lower performance than southward orientations on this floor.

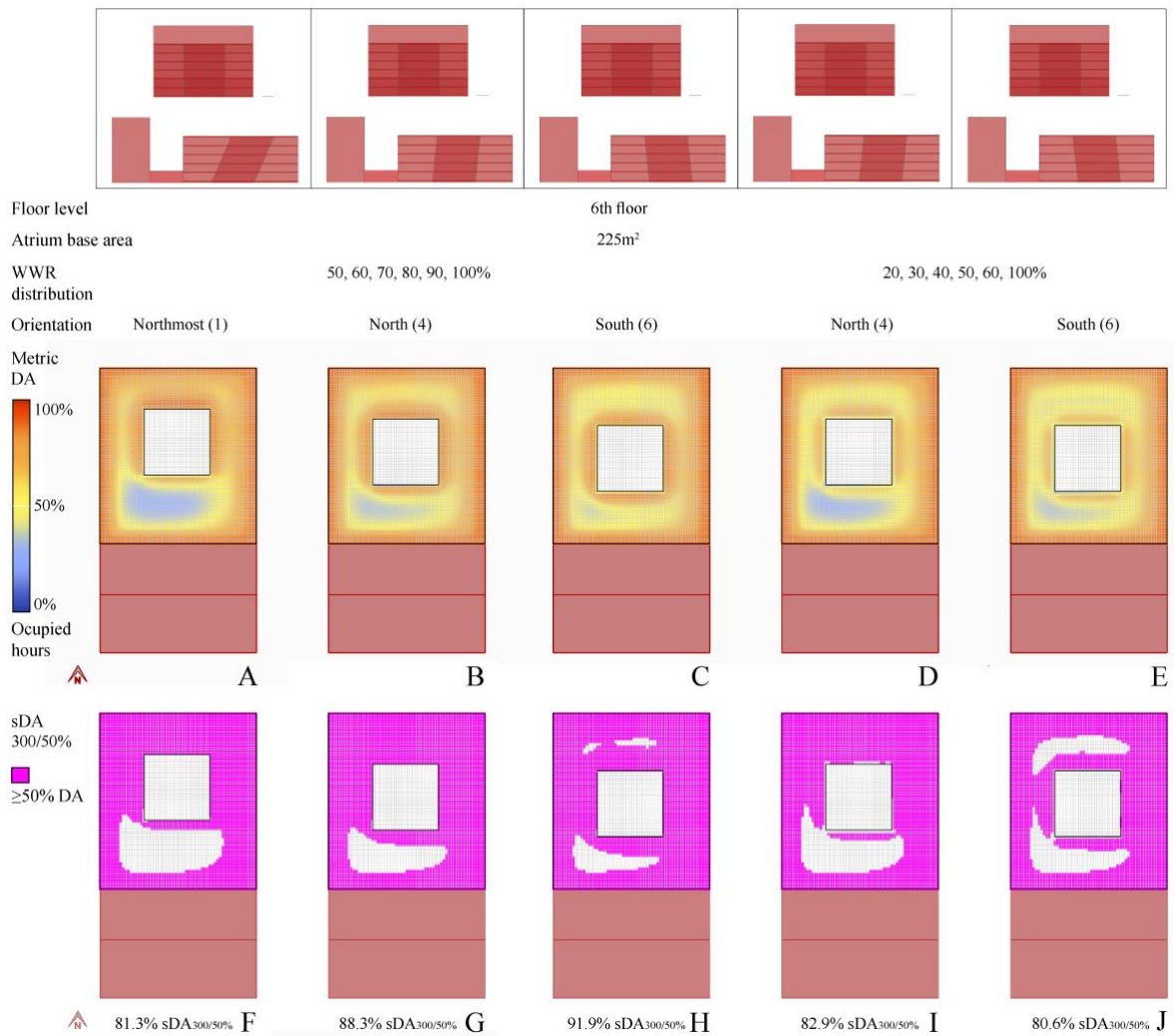


Figure 16 DA<sub>300</sub> and sDA<sub>300/50%</sub> result plots for the specified design solutions, highlighting the impact of atrium orientation on daylight performance on the 6<sup>th</sup> floor

Despite receiving the lowest DA<sub>300</sub> in spaces to the south of the atrium well, northward orientations also received the highest DA<sub>300</sub> in spaces to the north of the atrium. While the low DA was a result of the increase in room depth and effect of surrounding buildings, the high DA values stem from a more perpendicular positioning of the south-facing atrium well wall to the sun (as shown by a thicker and darker orange hue around the atrium in Figure 16 A, B, D compared to C, E). This becomes evident when looking at the ASE and UDI-e results (Figure 17). Both confirmed that northward orientations received more daylight in spaces to the north and also west of the atrium (Figure 17, P, Q compared to R, S compared to T). Northward orientations therefore

resulted in a higher occurrence of lux levels above 1000/ 2000 and overall greater daylight availability for some areas while other areas received less daylight as a result of the room depth and surrounding buildings. A trade-off therefore existed between the orientations. In terms of  $sDA_{300/50\%}$  performance, with a WWR of 50%, the northward orientation received sufficient daylight in spaces to the north of the atrium to exceed the 50%  $DA_{300}$  threshold for the most part (Figure 16 H). Where the WWR was 20% however, daylight levels could no longer achieve the 50% threshold in space to the north of the atrium and the floor area failing the threshold increased (Figure 16 J). This explains the mixed results seen for optimum orientations on the 6<sup>th</sup> floor. Nonetheless, optimum orientations remained close to the central orientation, where the room depth was minimal on either side of the atrium well.

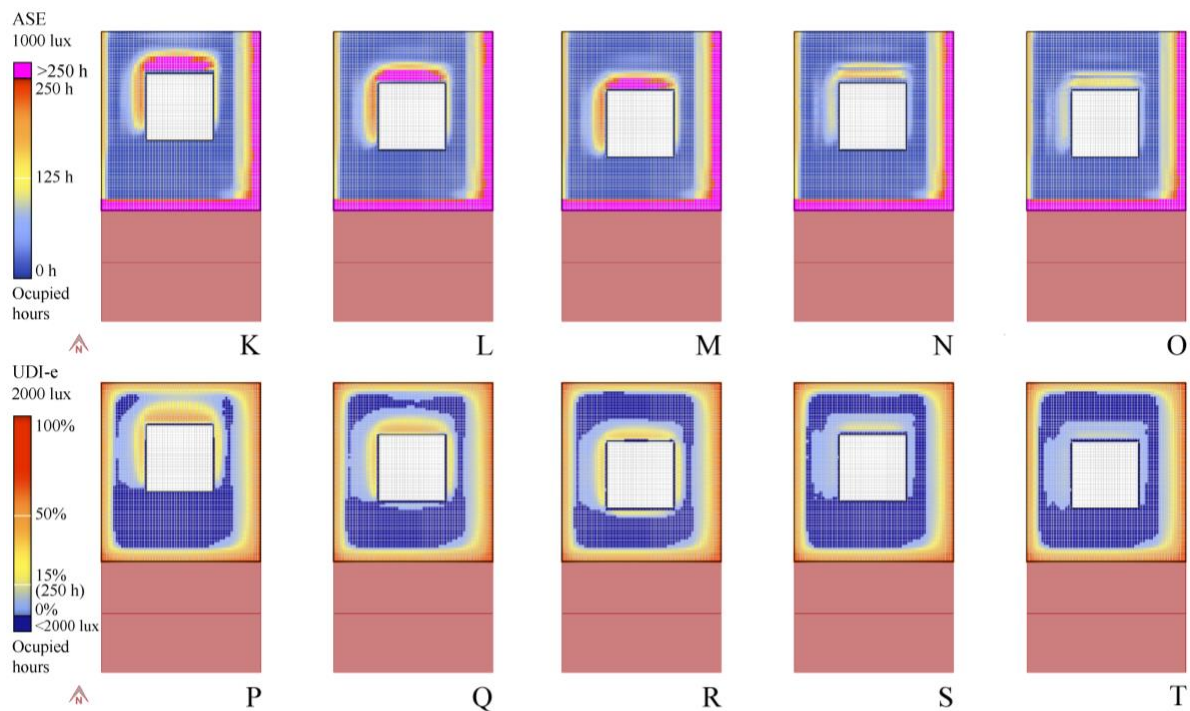


Figure 17 ASE and UDI-e result plots for the specified design solutions on the 6<sup>th</sup> floor

### B.3.2 Impact of atrium orientation on daylight performance on the 5<sup>th</sup> floor

“Northward orientations displayed the highest  $sDA_{300/50\%}$  performance, and southward orientations the lowest. This pattern was consistent for all three WWR

distribution series.  $sDA_{100/50\%}$  was achieved by 100% of the floor area by all design solutions.  $ASE_{1000,250h}$  displayed progressively lower direct sunlight penetration from north to southward orientations in a linear fashion, with northmost orientations consistently displaying the highest ASE and southmost orientations the lowest. The gradient was steepest (difference in ASE between northmost and southmost orientations was greatest) for the WWR distribution series starting with 50% WWR (with a WWR of 60% on the fifth floor). I.e., the difference in ASE between northmost and southmost orientations was greatest for this WWR distribution series. The difference in ASE between northmost and southmost orientations for the two WWR distribution series starting with 20% WWR (with a WWR of 30% and 35% on the fifth floor) was minimal.”

To aid in further understanding the findings described, %time results are shown for five selected design solutions on the 5<sup>th</sup> floor. The selected design solutions are highlighted in Figure 18. The selected design variants are those with a northmost, northward, central, southward and southmost orientation. As patterns were consistent for all three WWR distribution series, design variants are selected from the 50% WWR distribution series.

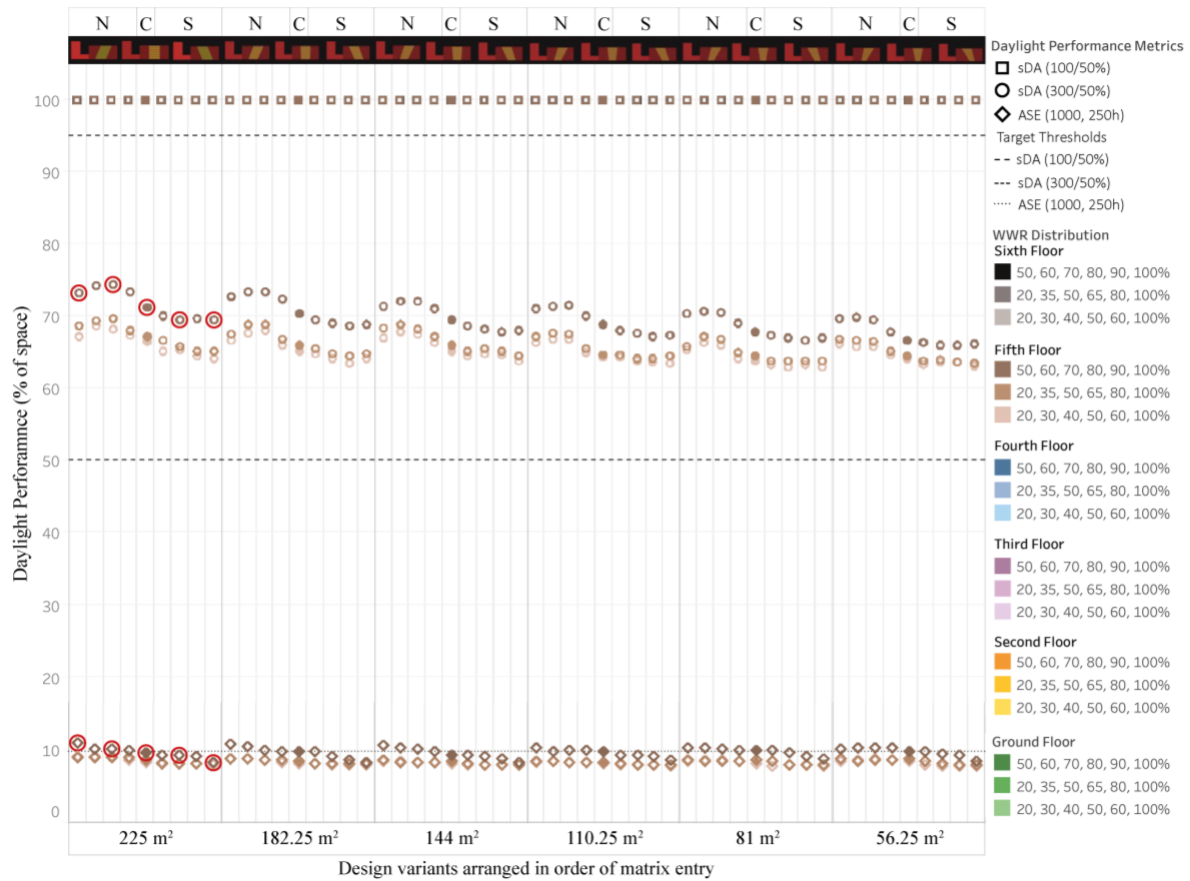


Figure 18 sDA<sub>300/50%</sub>, sDA<sub>100/50%</sub> and ASE results on the 5<sup>th</sup> floor. Metric results for the marked design solutions are plotted in the following sections

Figure 19 shows DA<sub>300</sub> and sDA<sub>300/50%</sub> results for the selected design solutions on the 5<sup>th</sup> floor. Many of the observations made for the top floor held true on this floor as well: spaces to the south of the atrium well received less daylight as a result of overshadowing from adjoining and surrounding buildings (see blue patches in Figure 19 A to E). Also, spaces to the north and north-west received more daylight as a result of the southward facing atrium well walls (see Figure 20 M and R). Northward orientations further increased DA in spaces to the north of the atrium well, as this splayed the south-facing atrium well wall into a more perpendicular positions to solar altitude angles (see increasing depth of orange hue Figure 20 T to P). The one difference to the top floor was the increase of depth into the atrium well (from 6<sup>th</sup> to 5<sup>th</sup> floor), which resulted in overall lower DA in areas surrounding the atrium. As a consequence, design solutions with a

central atrium and equal room depth on either side of the atrium well, had areas both to the north and south of the atrium well failing the  $sDA_{300/50\%}$  threshold (Figure 19 C). Northward orientations, which increased DA in spaces to the north of the atrium, resulted in DA passing the 50% threshold, thus increasing  $sDA_{300/50\%}$  for northward orientations (Figure 19 F, G). Consequently, optima were seen for more steeply northward oriented atria on the 5<sup>th</sup> floor, rather than central, shallow northward or southward orientations, which showed the highest  $sDA_{300/50\%}$  on the 6<sup>th</sup> floor.

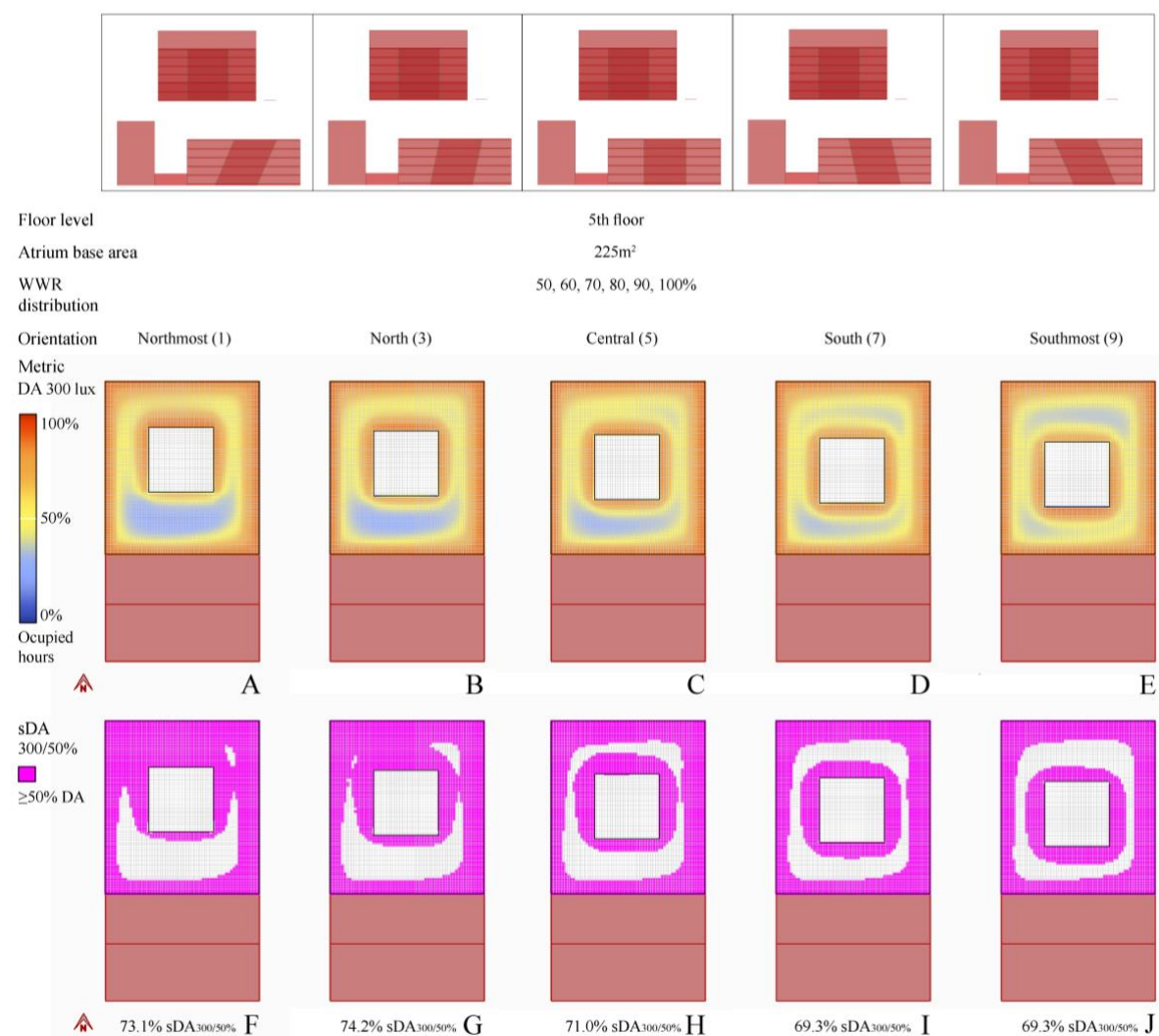


Figure 19  $DA_{300}$  and  $sDA_{300/50\%}$  result plots for the specified design solutions, highlighting the impact of atrium orientation on daylight performance on the 5<sup>th</sup> floor

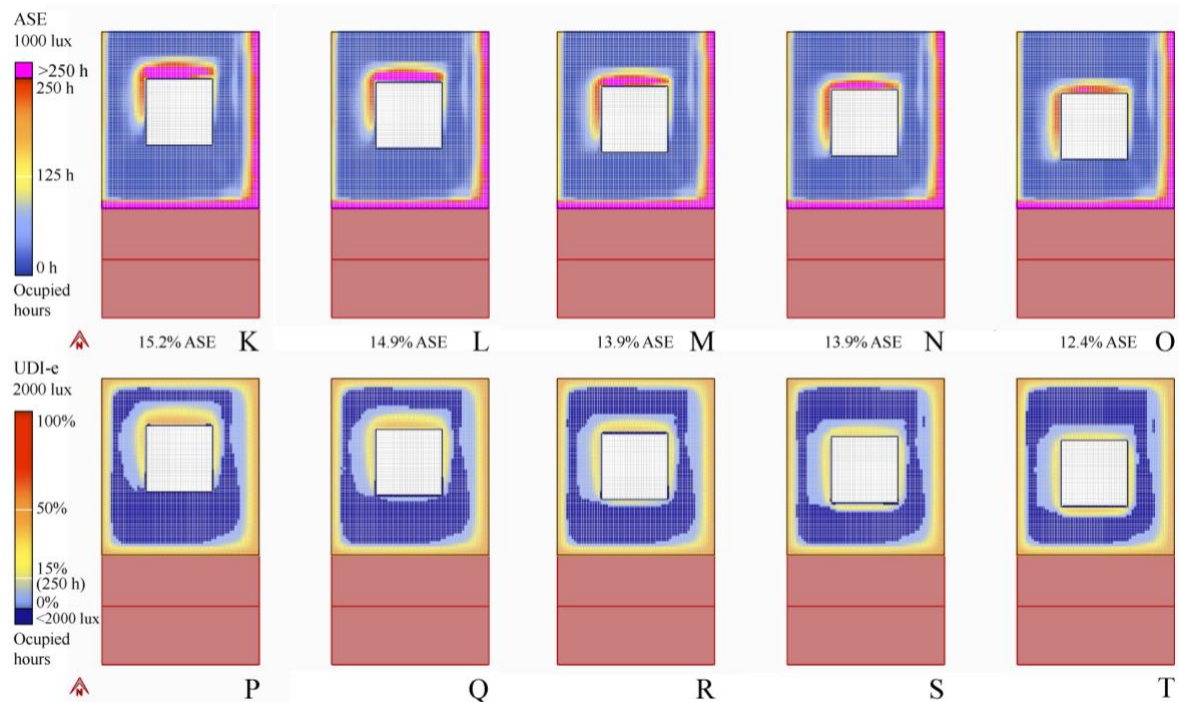


Figure 20 ASE and UDI-e result plots for the specified design solutions on the 5<sup>th</sup> floor

In terms of spatial daylight quality, an important observation could be made by further analysing the northward orientation with optimum  $sDA_{300/50\%}$  performance (Figure 19 B). As already mentioned, spaces to the south of the atrium well received less daylight as a consequence of overshadowing from surrounding buildings. Northward orientations, which resulted in an increase in room depth to the north of the atrium, emphasised this detriment and resulted in particularly low  $DA_{300}$  in those spaces. The optimum design variant thus showed lower  $DA_{300}$  in larger areas than what could be seen for southward orientations (compare blue patches Figure 19 B to D, E). Thus, even though more spaces passed the 50%  $sDA$  threshold in northward orientations (Figure 19 A, B, F, G), the overall distribution of daylight was better in southward orientations, as  $DA_{300}$  did not fall as low (Figure 19 D, E). This was observed for the top floor as well. Importantly, a better daylight distribution can be considered a more desirable design outcome than meeting the  $sDA$  threshold. However,  $sDA_{300/50\%}$  did not lead to this design outcome, and  $sDA_{100/50\%}$  was still too low of an indicator to show this result. For designers, this means

that optimisation towards objectives with absolute pass/fail thresholds such as the sDA need to be carefully considered, firstly because important factors can be overlooked, and secondly because turning points in trends (e.g. from 6<sup>th</sup> to 5<sup>th</sup> floor) can easily change. Understanding the underlying patterns behind the obtained performance results (e.g. by including the %time results in the design considerations) therefore appears imperative to making well informed decisions.

### *B.3.3 Impact of atrium orientation on daylight performance on the 4<sup>th</sup> floor*

“sDA<sub>300/50%</sub> performance hardly differed between the different orientations on this floor. Nonetheless, a tendency for southward orientation to show higher sDA<sub>300/50%</sub> results, and northward orientations to show lower sDA<sub>300/50%</sub> results became apparent, more so for smaller atrium base areas. sDA<sub>100/50%</sub> was achieved by 100% of the floor area by all design solutions. ASE displayed a higher value for north than south orientations. For design solutions with the largest atrium base area, the northmost orientations displayed the highest ASE result. For all other atrium base areas, the smaller the atrium base area became, the shallower the orientation with the highest ASE, and the lower the ASE of northmost orientations. This pattern was consistent across all WWR distribution series.”

To aid in further understanding the findings described, %time results are shown for five selected design solutions on the 4<sup>th</sup> floor. These are highlighted in Figure 21. The selected design variants have a northmost, northward, central, southward and southmost orientation. Results are shown for design solutions with largest, as well as the smallest atrium base areas. As patterns were consistent for all three WWR distribution series, design variants are selected from the 50% WWR distribution series.

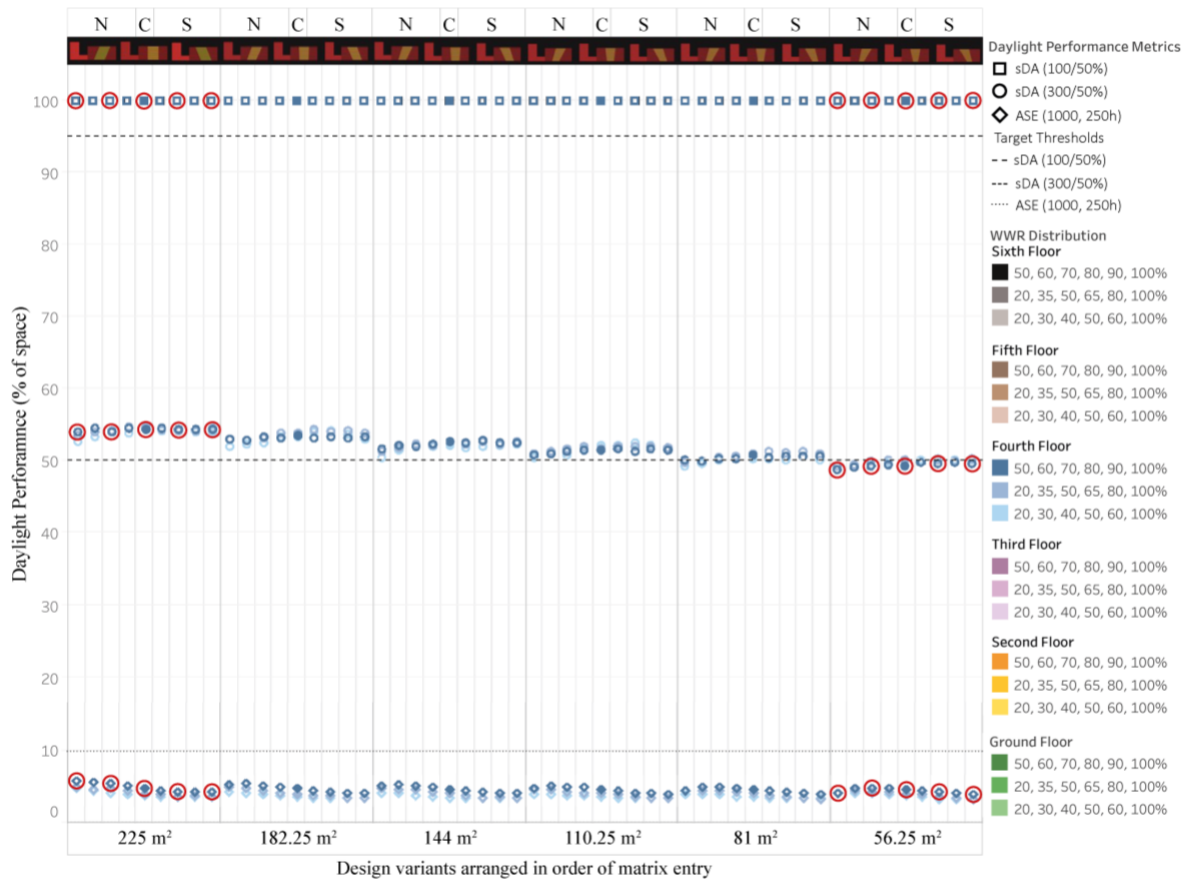


Figure 21 sDA<sub>300/50%</sub>, sDA<sub>100/50%</sub> and ASE results on the 4<sup>th</sup> floor. Metric results for the marked design solutions are plotted in the following sections.

Figure 22 shows the DA<sub>300</sub> and sDA<sub>300/50%</sub> results for the largest and smallest atrium base areas on the 4<sup>th</sup> floor. The following findings seen on the 5<sup>th</sup> and 6<sup>th</sup> floors are true for the 4<sup>th</sup> floor as well: northward orientations allowed more area on the north of the atrium to have higher DA<sub>300</sub>, but also showed lowest DA<sub>300</sub> in spaces to the south of the atrium. Nonetheless, the difference between spaces that met and failed the sDA<sub>300/50%</sub> target on the 4<sup>th</sup> floor was minimal.



Figure 22 DA<sub>300</sub> and sDA<sub>300/50%</sub> result plots for the specified design solutions, highlighting the impact of atrium orientation on daylight performance on the 4<sup>th</sup> floor

ASE and UDI-e results for the 4<sup>th</sup> floor are shown in Figure 23. ASE results mirrored those seen on the 5<sup>th</sup> floor, such that design solutions with southward oriented atria received more direct sunlight in spaces to the south, west and east of the atrium, but therefore also less direct sunlight in spaces to the north of the atrium (e.g. compare Figure 23 K to O and K2 to O2). The UDI-e results too mirrored those seen on the 5<sup>th</sup> floor. Thus, in addition to spaces to the west and east of the atrium, spaces to the south of the atrium received more indirect sunlight when the atrium had a southward orientation (e.g. compare Figure 23 P to T and P2 to T2). The ASE results however differed from those seen on the 5<sup>th</sup> and 6<sup>th</sup> floor, in that the northmost orientation no longer had the highest ASE for all atrium base areas (Figure 23 K2). Instead, less steep northward orientated atria showed higher ASE (Figure 23 L2, M2, N2). This indicated a shift in pattern and suggested that, due to the depth of the atrium well (from the 4<sup>th</sup> floor to the skylight of the atrium well), the north facing atrium well walls obstructed direct sunlight penetration. A southward orientation and consequent alignment of the atrium well with solar altitude angles therefore enabled a deeper daylight penetration. This is confirmed in later sections, when looking at the %time results for the 3<sup>rd</sup> to ground floors.

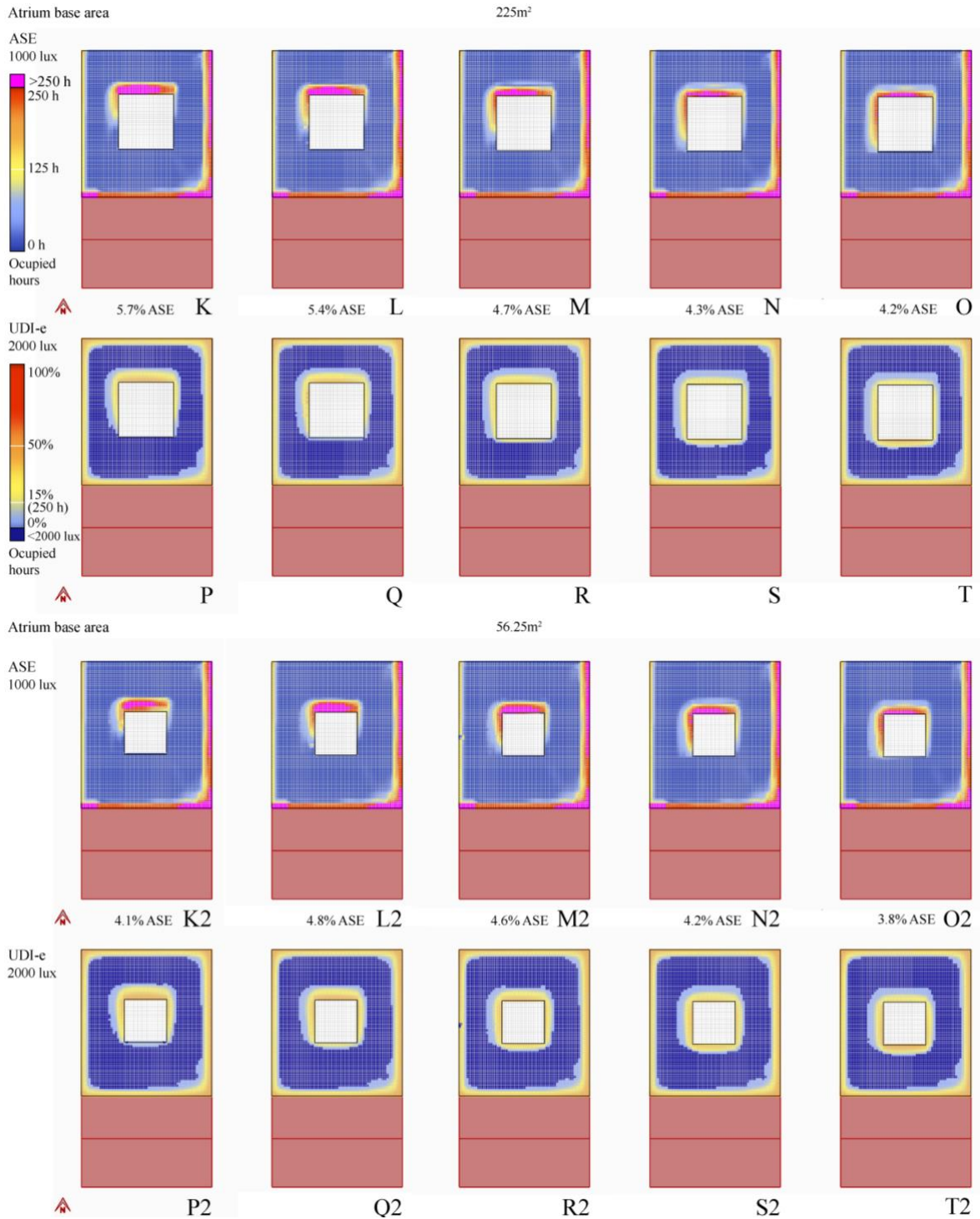


Figure 23 ASE and UDI-e result plots for the specified design solutions on the 4<sup>th</sup> floor

Lastly, DA<sub>100</sub> results for the 4<sup>th</sup> floor are shown in Figure 24. Although all design solutions passed the sDA<sub>100/50%</sub> target criteria, it stands out that, southward, more than northward orientations, had a higher percentage of space exceeding a DA<sub>100</sub> of 50 (indicated by fewer areas in yellow hue). With this metric, southmost orientations

therefore appear to be favourable design solutions as, overall, a minimum of  $DA_{100}$  was achieved for more occupied hours in a year. This is again a result that only becomes visible when looking at the spatial distribution of the %time results, as  $sDA_{100/50\%}$  gives 100% for all orientations.

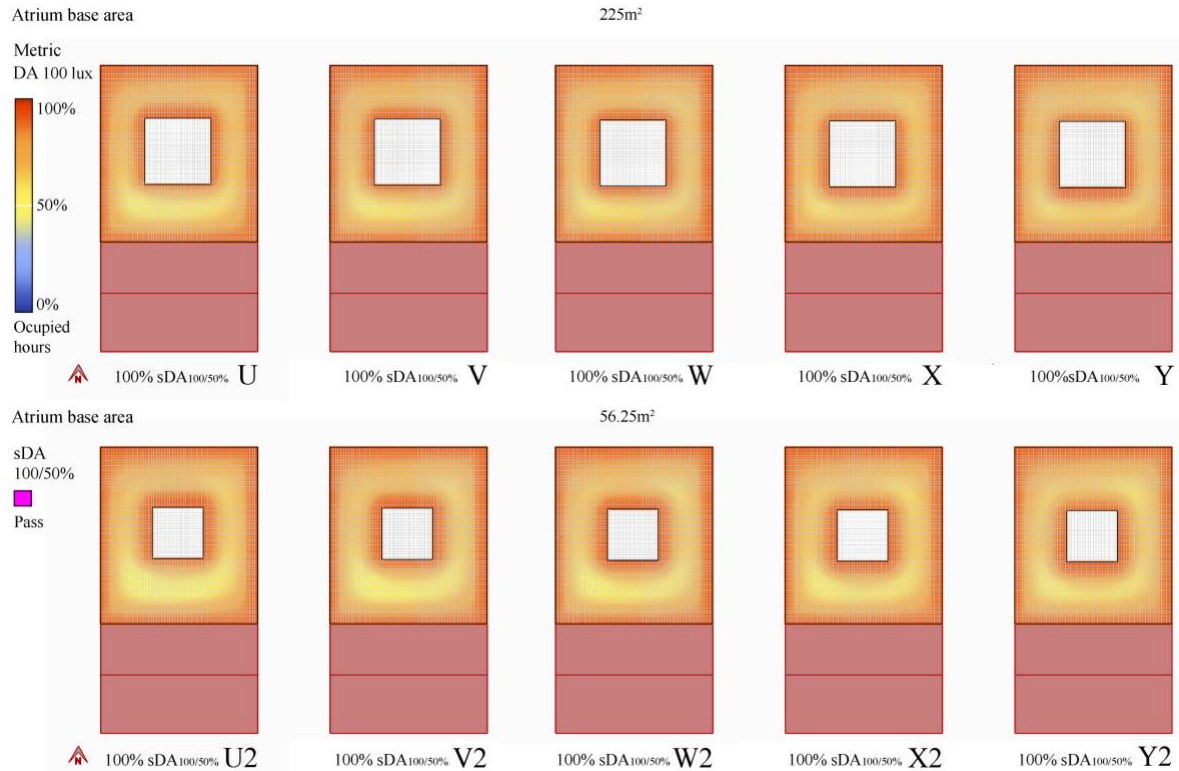


Figure 24  $DA_{100}$  results plots for the specified design solutions on the 4<sup>th</sup> floor

### B.3.4 Impact of atrium orientation on daylight performance on the 3<sup>rd</sup> floor

“Southward orientations displayed the highest  $sDA_{300/50\%}$  performance. In contrast, northward orientations displayed the highest  $sDA_{100/50\%}$  performance and southmost orientations the lowest. Only design solutions with the smallest atrium base area of  $56.25m^2$  and a WWR distribution series starting with 50% WWR showed a shift in pattern, whereby central and slight southward orientations gave higher  $sDA_{100/50\%}$  results than northward orientations. ASE results hardly varied between the different orientations, with differences less than 0.5% ASE. Nonetheless, northmost

orientations, with the exception of design solutions with the largest atrium base area of 225m<sup>2</sup>, now started to show the lowest ASE.”

To aid in further understanding the findings described, %time results are shown for five selected design solutions on the 3<sup>rd</sup> floor. These are highlighted in Figure 25. The selected design variants have a northmost, central, and southmost orientation with an atrium base area of 182.25m<sup>2</sup> and northmost and central orientation with an atrium base area of 56.25m<sup>2</sup>. Results are shown for design solutions from the 50% WWR distribution series.

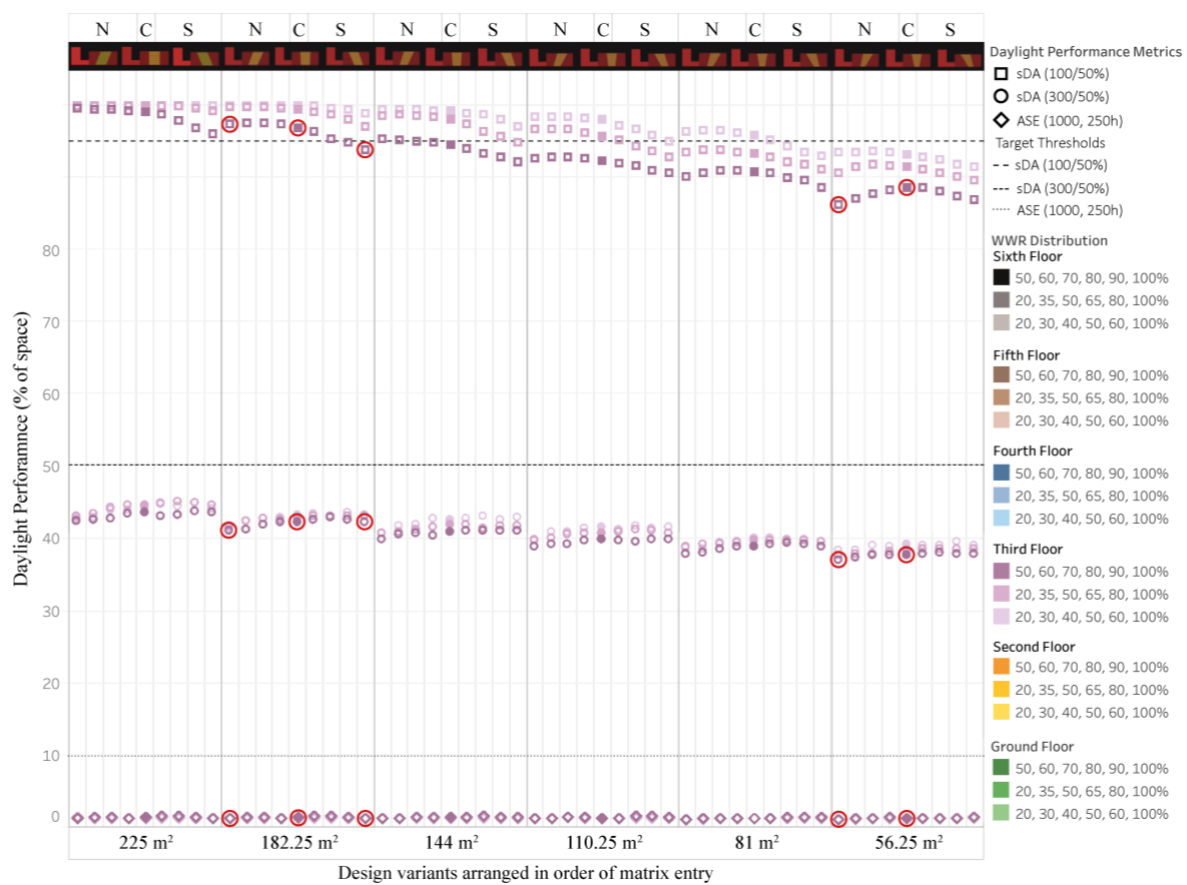


Figure 25 sDA<sub>300/50%</sub>, sDA<sub>100/50%</sub> and ASE results on the 3<sup>rd</sup> floor.

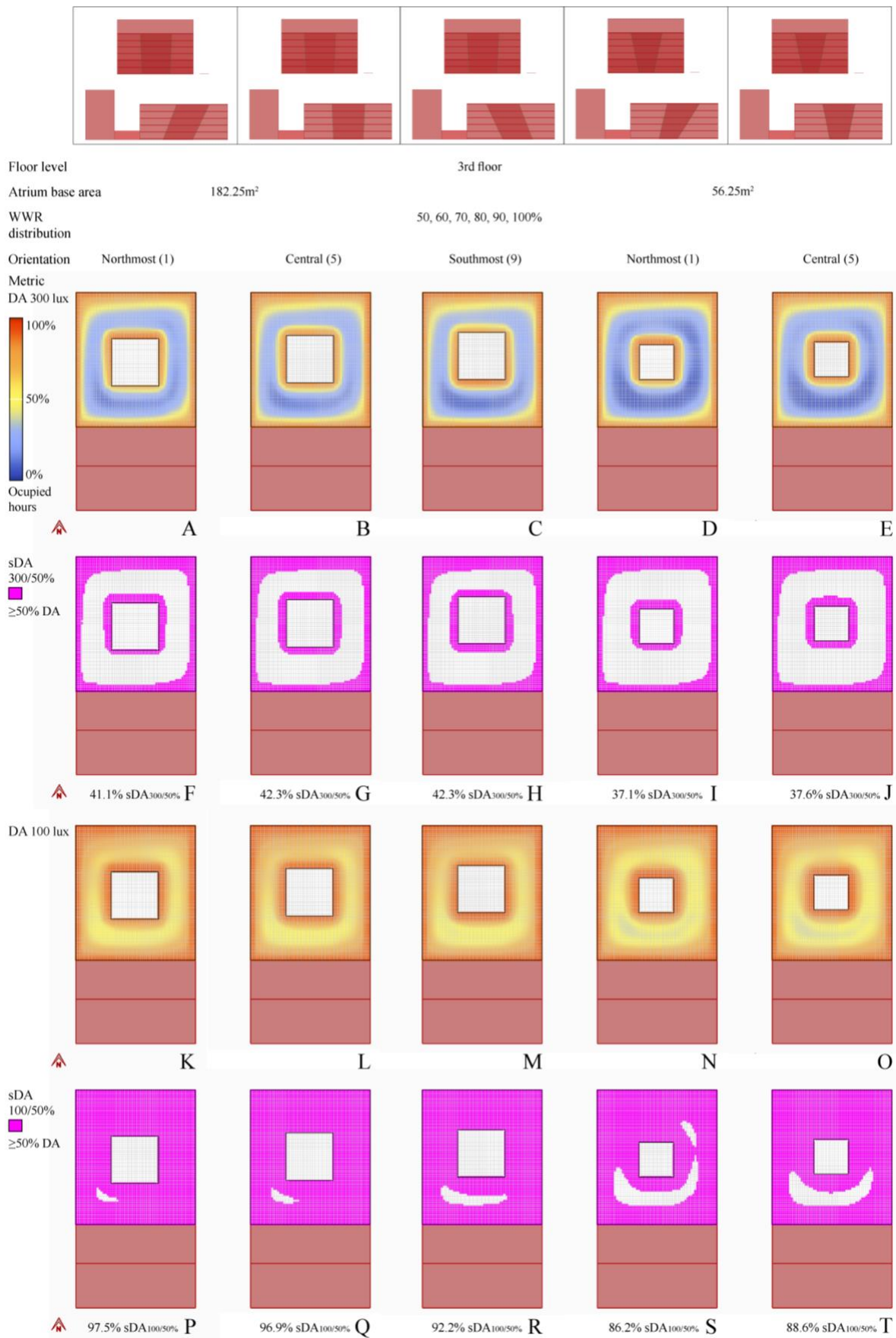


Figure 26 DA<sub>300</sub>, sDA<sub>300/50%</sub>, DA<sub>100</sub> and sDA<sub>100/50%</sub> result plots for the specified design solutions, highlighting the impact of atrium orientation on daylight performance on the 3rd floor

DA and sDA plots for the specified design solutions on the 3<sup>rd</sup> floor are shown in Figure 26. sDA<sub>100/50%</sub> fell below 100% starting from this floor downwards. While central to southward orientations showed higher sDA<sub>300/50%</sub> performance, northward orientations showed higher sDA<sub>100/50%</sub> performance for the most part. Both metrics therefore appear to contrast one another.

From the spatial distribution of DA results, it is apparent that some of the previously explained conditions held true on this floor as well: spaces to the south of the atrium were more prone to being underlit (as seen for all floors), and central to southward orientations allowed daylight to reach more deeply into spaces to the south, east and west of the atrium, as seen on the 4<sup>th</sup> floor (Figure 27 L, M, O and Q, R, T compared against K, N and P, S). A major difference to the above floors arose from the location of the pivot point for tilting the atrium, which was located in the vertical centre of the building (between the 3<sup>rd</sup> and 4<sup>th</sup> floor). As a result, the centre point of the atrium well on each floor changed and so did the room depth in atrium adjacent spaces. Specifically, from the 4<sup>th</sup> to 6<sup>th</sup> floors, northward orientations increased the room depth in spaces to the south of the atrium. Southward orientations on the other hand increased the room depth in spaces to the north of the atrium. This was vice versa for the ground to third floors: northward orientations increased the room depth in spaces to the north of the atrium, and southward orientations increased the room depth in spaces to the south of the atrium. Another difference to the above floors was that, with increasing depth of the atrium well, less daylight reached atrium adjacent spaces. Thus, atrium adjacent spaces benefited from aligning the atrium well orientation with solar altitude angles and splaying the north-facing atrium well walls (as opposed to the south-facing atrium well walls, as seen on the top floors) towards the skylight.

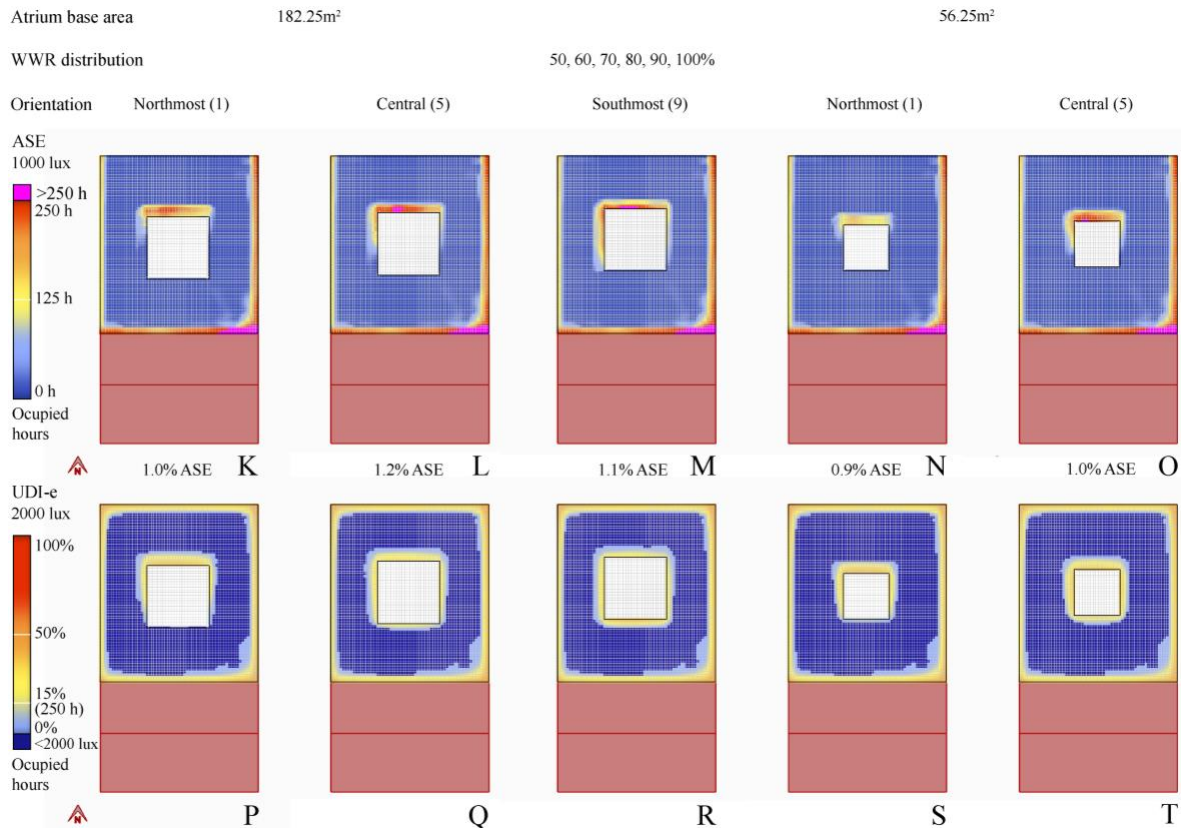


Figure 27 ASE and UDI-e result plots for the specified design solutions on the 3<sup>rd</sup> floor

The advantage of aligning the atrium well orientation with solar altitude angles can be seen by looking at the  $sDA_{300/50\%}$  results. As only a sparse amount of daylight travelled into atrium adjacent spaces, only those spaces directly surrounding the atrium well meet the  $DA_{300} 50$  threshold. Therefore, central to southward orientations, which receive more daylight in spaces directly surrounding the atrium well (e.g. see Figure 27 L, M, O and compared to K, N; or depth of dark orange hue in Figure 27 E compared to D, or depth of pink hue to the north of the atrium in **Error! Reference source not found.** H compared to the depth of the pink hue to the south of the atrium in F), outperformed northward orientations for the  $sDA_{300/50\%}$  metric.

Looking at  $sDA_{100/50\%}$ , patterns resembled those identified on the 5<sup>th</sup> floor for the  $sDA_{300/50\%}$  results. Southward orientations increased the room depth in spaces south of the atrium and therefore for areas failing the threshold in those spaces (Figure 27 P to T). Hence, southward orientations, for the most part, showed the lowest  $sDA_{100/50\%}$  on

the 3<sup>rd</sup> floor. This was already visible in the DA<sub>300</sub> results (Figure 27 A to E), which showed that lowest DA<sub>300</sub> results fell in those spaces to the south of the atrium (visible from a dark blue hue). In the sDA<sub>300/50%</sub> metric however, this information disappeared (Figure 27 F to J). Instead, the low DA<sub>300</sub> was only reflected in the sDA<sub>100/50%</sub> results (Figure 27 P to R). Therefore, the sDA<sub>100/50%</sub> optima for northward orientations could be explained by the %time results of the DA<sub>300</sub> metric. A shift in trend for sDA<sub>100/50%</sub> was only seen on for the smallest atrium base area and is further explored within the results of the 2<sup>nd</sup> and ground floor.

### *B.3.5 Impact of atrium orientation on daylight performance on the 2<sup>nd</sup> floor*

“Southward orientations displayed the highest sDA<sub>300/50%</sub> performance and northmost the lowest. This trend was true for all atrium base areas. In contrast, sDA<sub>100/50%</sub> results changed with a decrease in atrium base area, from more northward to central orientations achieving a higher sDA<sub>100/50%</sub> result. For larger atrium base areas, southmost orientations showed the lowest sDA<sub>100/50%</sub>. For smaller atrium base areas, northmost orientations showed the lowest sDA<sub>100/50%</sub> result. ASE results were at 0% for all design solutions on this floor.”

To aid in further understanding the findings described, %time results are shown for five selected design solutions on the 2<sup>nd</sup> floor. These are highlighted in Figure 28. The selected design variants have a northmost, northward, central, southward and southmost orientation with an atrium base area of 182.25m<sup>2</sup> and 56.25m<sup>2</sup>. Results are shown for design solutions from the 50% WWR distribution series.

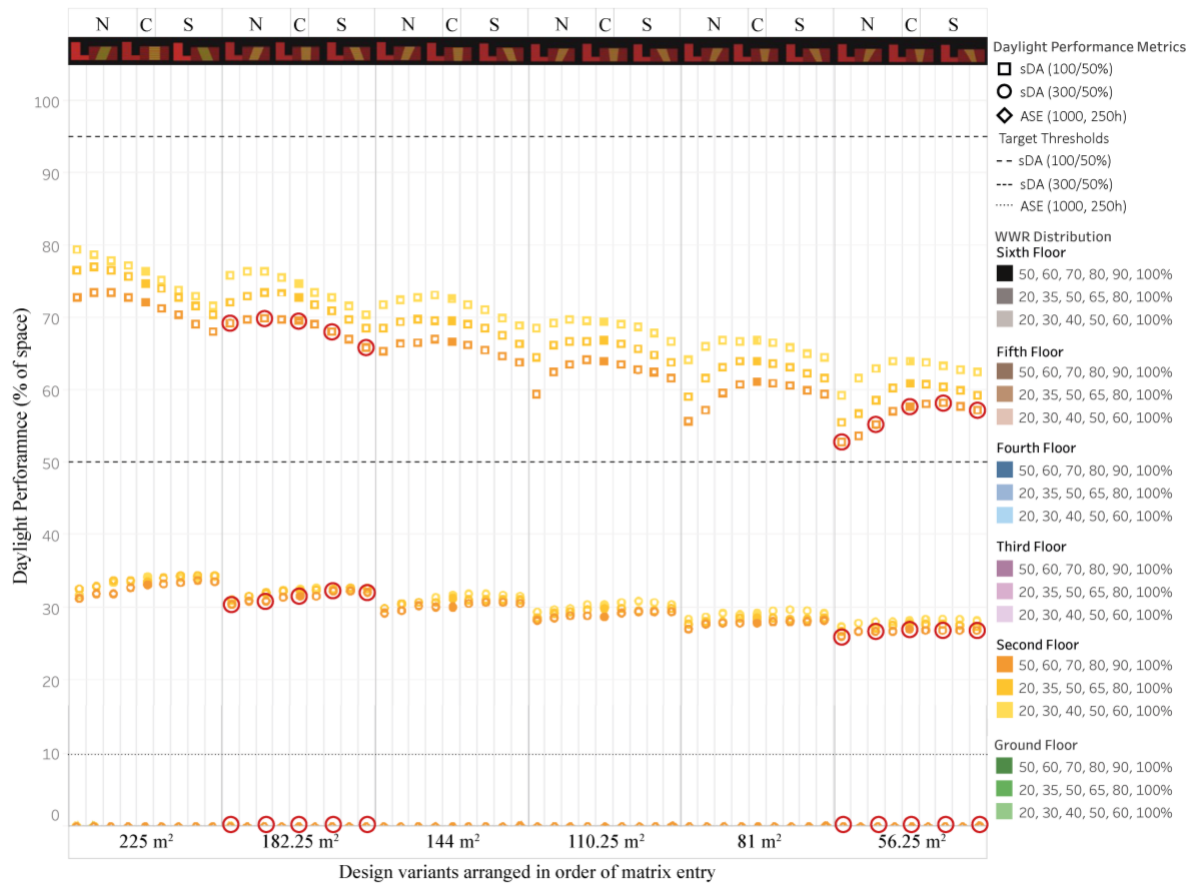


Figure 28 sDA<sub>300/50%</sub>, sDA<sub>100/50%</sub> and ASE results on the 2<sup>nd</sup> floor.

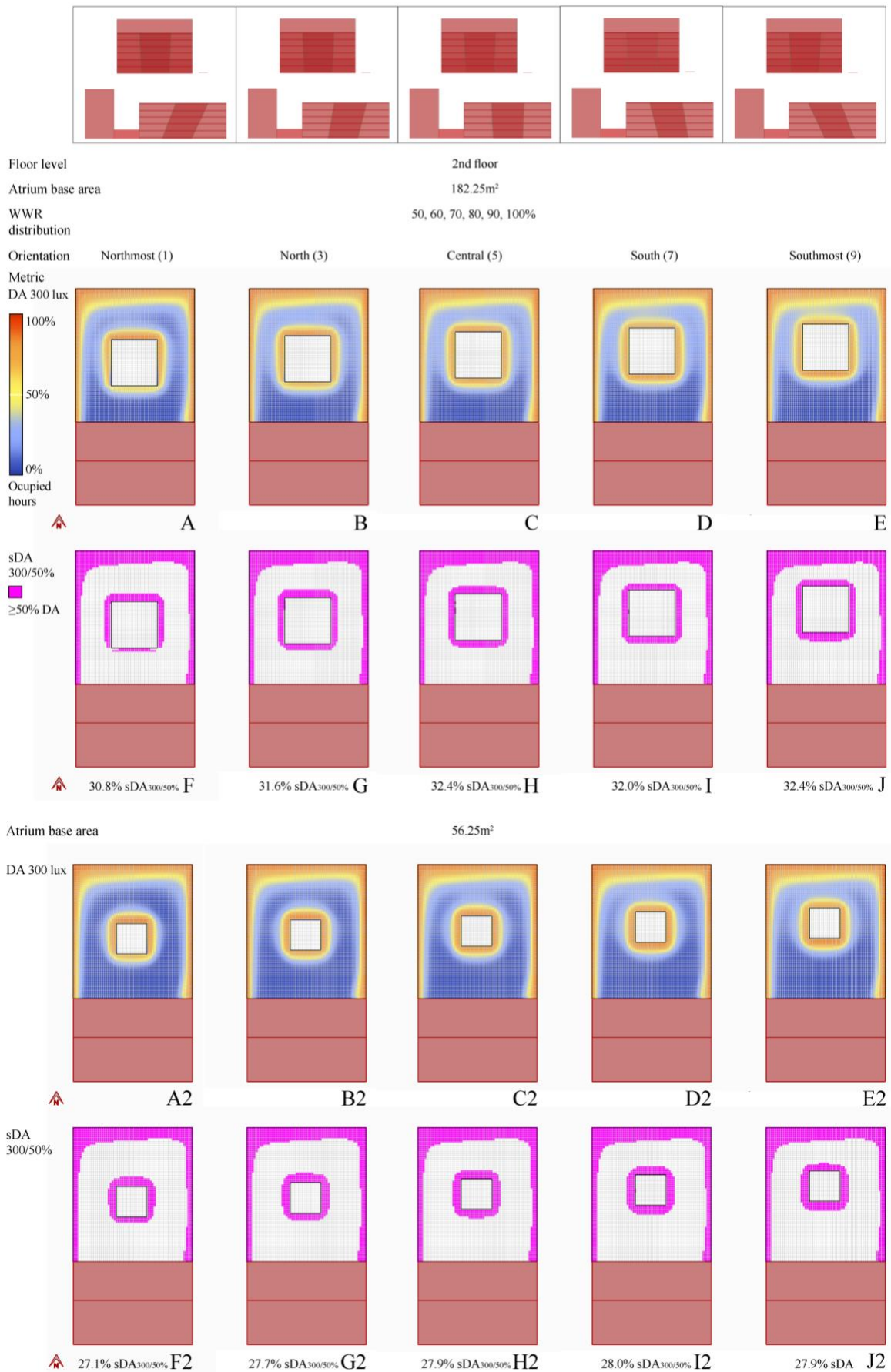


Figure 29 DA<sub>300</sub> and sDA<sub>300/50%</sub> result plots for the specified design solutions, highlighting the impact of atrium orientation on daylight performance on the 2<sup>nd</sup> floor

DA<sub>300</sub> and sDA<sub>300/50%</sub> plots for the specified design solutions on the 2<sup>nd</sup> floor are shown in Figure 29. The patterns for DA<sub>300</sub> were quite straight forward. The lowest DA<sub>300</sub> were in spaces to the south of the atrium well (dark blue patches, Figure 29 A to E and A2 to E2). For southward oriented atria, these underlit areas increase in size due to the increased room depth (dark blue patch Figure 29 E). For northward oriented atria, these areas also extended to spaces in the north of the atrium (dark blue patches Figure 29 A). For design solutions with smaller atrium base areas, spaces to the north of the atrium were more affected by low daylight levels and hence more affected by northward orientations (dark blue patches Figure 29 A2 to D2). These observations explain the varying results for sDA<sub>100/50%</sub> for different atrium base areas. In the sDA<sub>300/50%</sub> metric however, these trends did not show, as only those spaces in direct proximity of the facades were able to meet the 50% DA threshold. As the distribution of daylight around the atrium well was better for southward orientations (as explained previously for the results on the 3<sup>rd</sup> floor), these achieved slightly higher sDA<sub>300/50%</sub>.

Figure 30 shows the DA<sub>100</sub> and sDA<sub>100/50%</sub> results for the specified design solutions on the 2<sup>nd</sup> floor. For an atrium base area of 182.25m<sup>2</sup>, the atrium well was large enough for spaces to the north of the atrium to receive daylight exceeding DA 50 for 100 lux (Figure 30 A to E). As northward orientations minimised the room depth of spaces to south of the atrium, the underlit areas in those spaces were reduced. Thus, northward orientations showed higher sDA<sub>100/50%</sub> performance for design solutions with larger atrium base areas. For smaller atrium base areas however, spaces to the north and south of the atrium were underlit (Figure 30 F2, G2). Central to southward orientations, which had a smaller room depth in spaces to the north of the atrium and a better daylight distribution, reduced the areas failing to meet the threshold in those spaces (Figure 30

H2, J2). Thus, central to southward orientations showed higher  $sDA_{100/50\%}$  performance for design solutions with smaller atrium base areas.

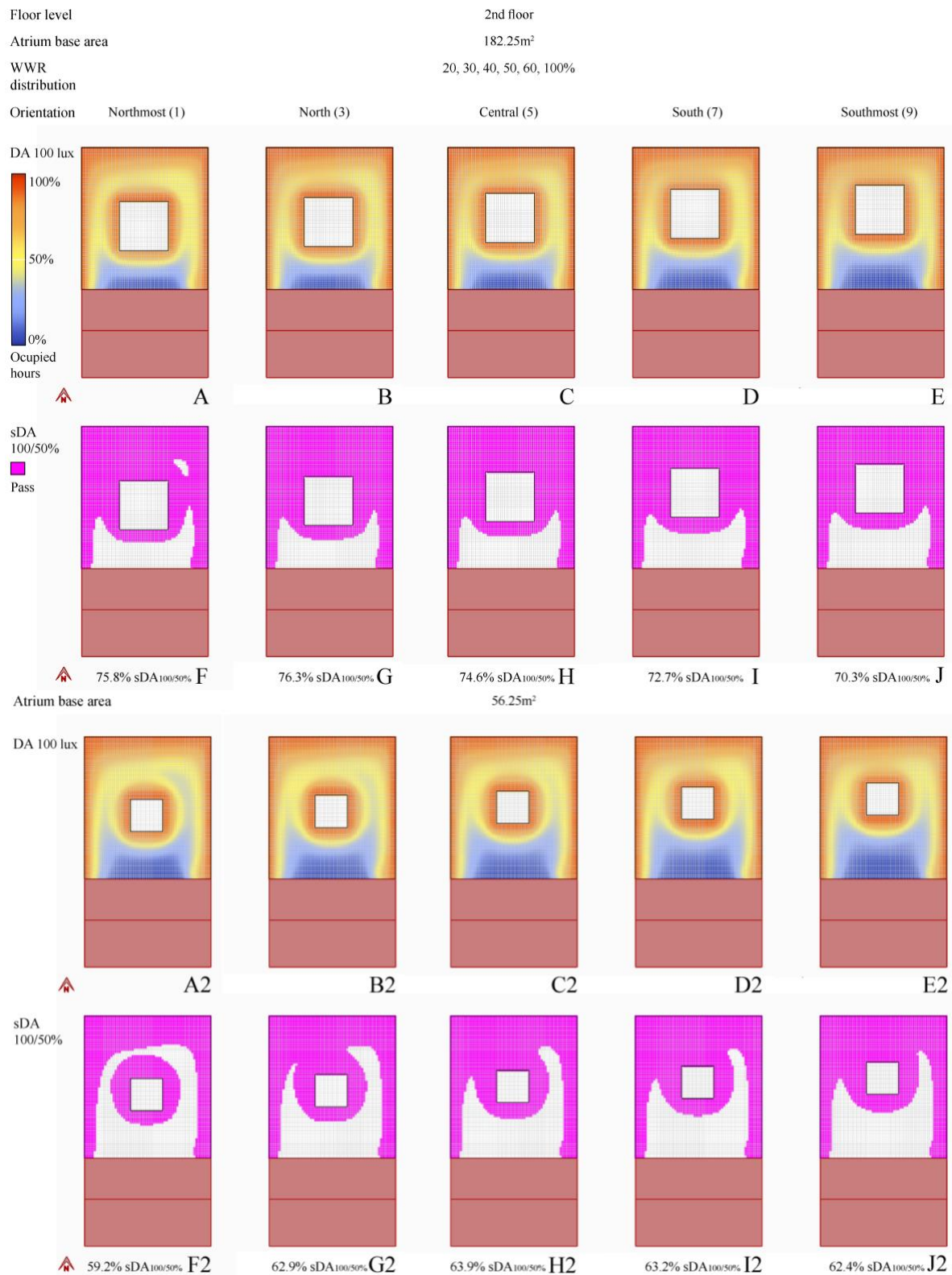
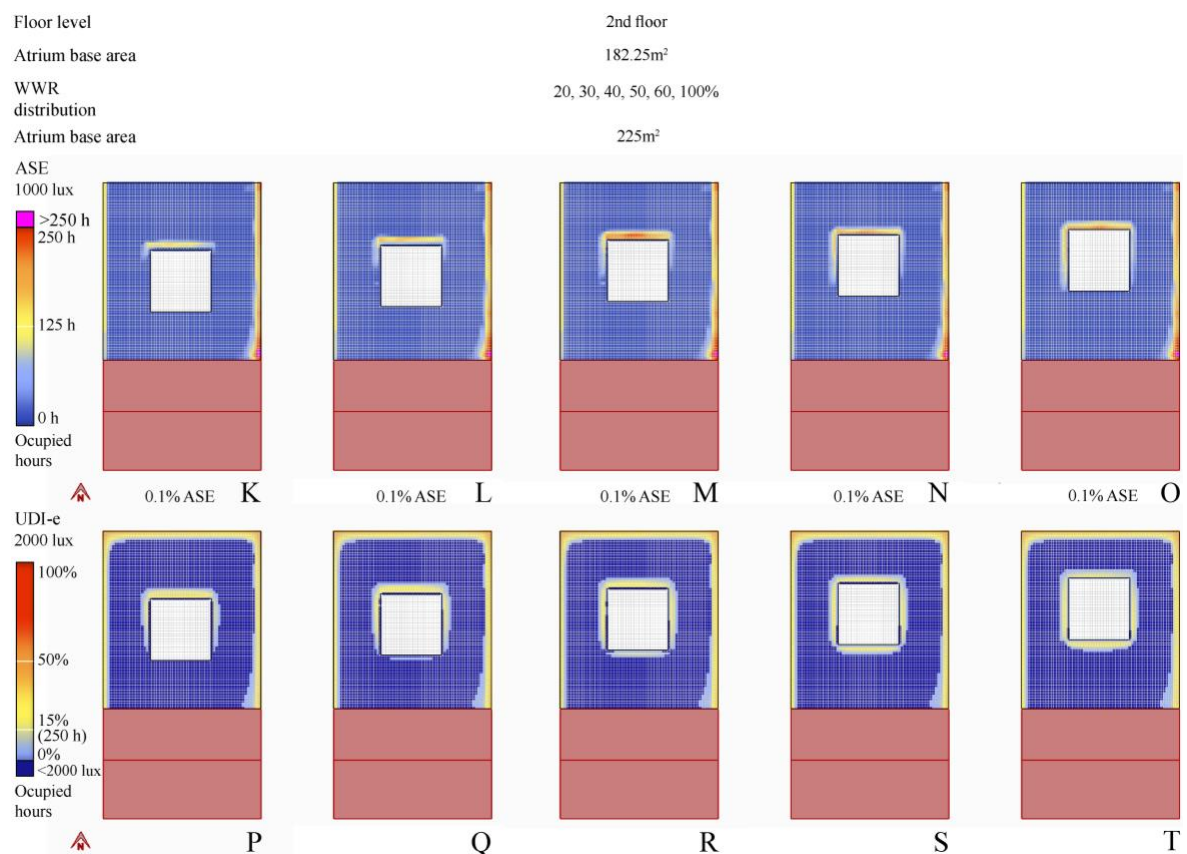


Figure 30  $DA_{100}$  and  $sDA_{100/50\%}$  results plots for the specified design solutions on the second floor

Figure 31 shows the ASE and UDI-e results for the specified design solutions on the 2<sup>nd</sup> floor. The highest ASE was found in central or southward orientations, depending on the atrium base area and atrium well splay angles (red patches Figure 31 M and N2). The areas receiving some form of direct sunlight were larger for southward orientations. Here, direct sunlight reached spaces not only to the north, but also east and west of the atrium (light blue to light yellow patches to the east and west of the atrium Figure 31 N and O, N2 and O2). UDI-e results, by comparison, showed that daylight additionally reached deeper into spaces to the south of the atrium for southward orientations (Figure 31 S, T, and R2, S2, T2 compared with P and P2). Consequently, UDI-e results suggest that southward orientations resulted in an overall better penetration of daylight into atrium adjacent spaces.



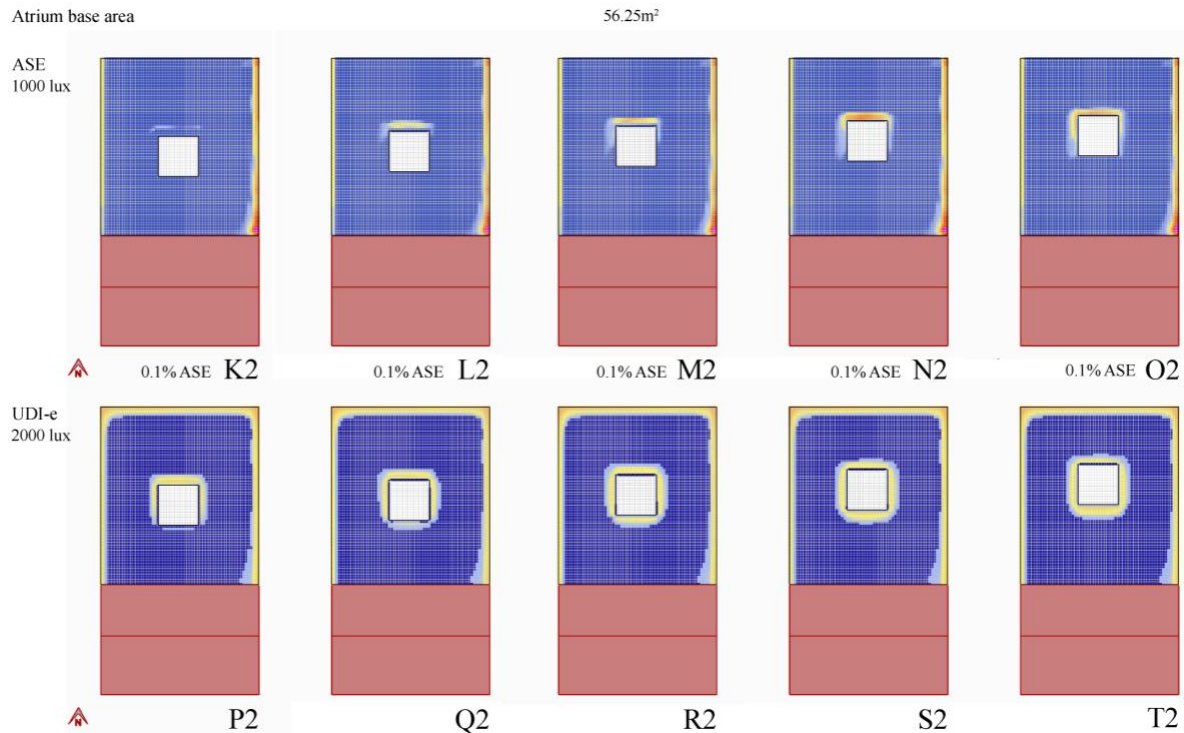


Figure 31 ASE and UDI-e result plots for the specified design solutions on the ground floor

### B.3.6 Impact of atrium orientation on daylight performance on the ground floor

“Ground floor: Southward orientations displayed the highest  $sDA_{300/50\%}$  performance and northmost the lowest. This trend was true for all atrium base areas. In contrast,  $sDA_{100/50\%}$  results changed with a decrease in atrium base area, from more northward to central and slight southward orientations achieving a higher  $sDA_{100/50\%}$  result. For larger atrium base areas, southmost orientations showed the lowest  $sDA_{100/50\%}$ . For smaller atrium base areas, northmost orientations showed the lowest  $sDA_{100/50\%}$  result. ASE results were at 0% for this floor.”

To aid in further understanding the findings described, %time results are shown for five selected design solutions on the ground floor. These are highlighted in Figure 32. The selected design variants have a northmost, northward, central, southward and southmost

orientation with an atrium base area of 182.25m<sup>2</sup> and 56.25m<sup>2</sup>. Results are shown for design solutions from the 50% WWR distribution series.

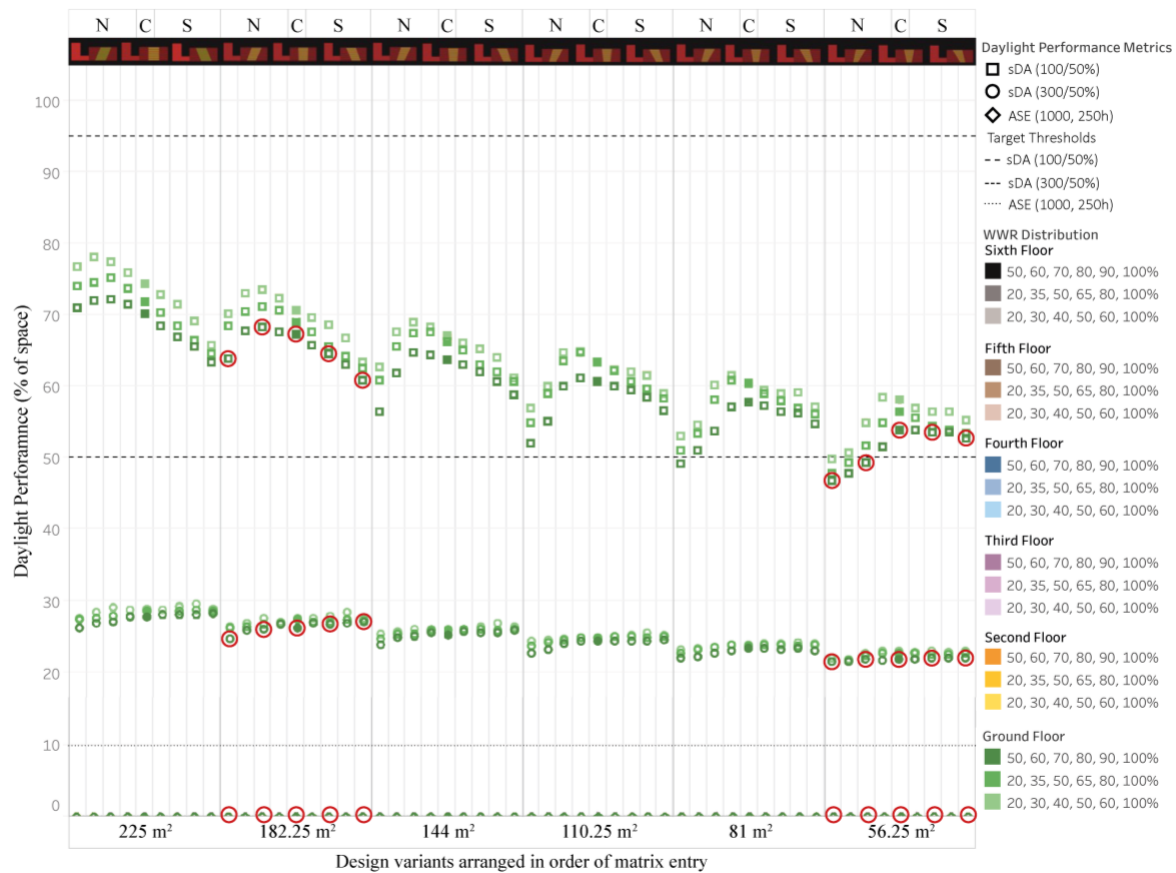
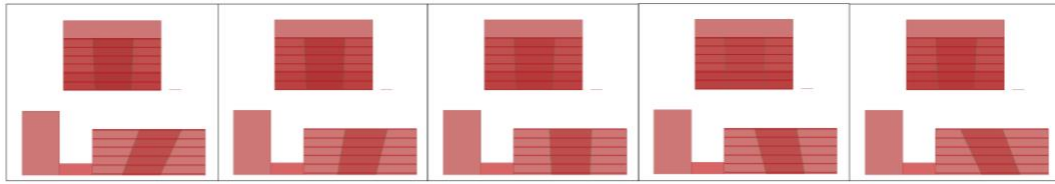


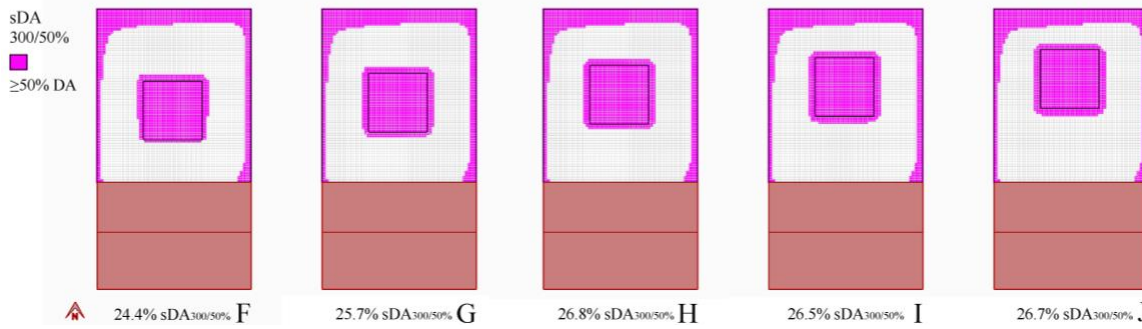
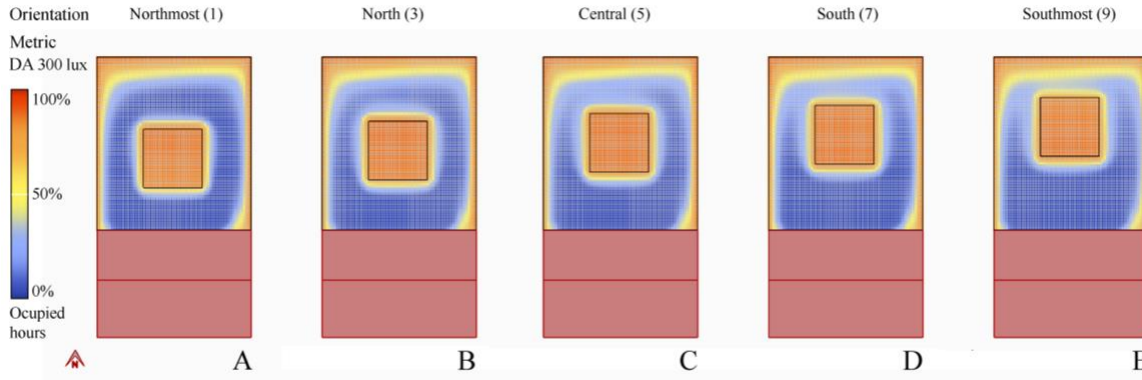
Figure 32 sDA<sub>300/50%</sub>, sDA<sub>100/50%</sub> and ASE results on the ground floor. Metric results for the marked design solutions are plotted in the following sections.

Figure 33 shows the DA<sub>300</sub> and sDA<sub>100/50%</sub> for the specified design solutions on the ground floor. The patterns and trends were similar to those described for the 2<sup>nd</sup> floor, with the main difference being that less daylight reached the ground floor. As noted previously, central to southmost orientations showed overall higher DA<sub>300</sub> (more light blue patches in central to southmost orientations in Figure 33 C to E and D2 to E2). This difference was however only apparent from the %time plots for DA. Nonetheless, sDA<sub>100/50%</sub> performance results also favoured southward orientations, albeit with marginal differences between results (Figure 33 A to E and A2 to E2). The results also showed that, as would be expected, sDA<sub>100/50%</sub> performance was 100% within the atrium well.



Floor level  
 Atrium base area  
 WWR distribution

Ground floor  
 182.25m<sup>2</sup>  
 50, 60, 70, 80, 90, 100%



Atrium base area  
 56.25m<sup>2</sup>

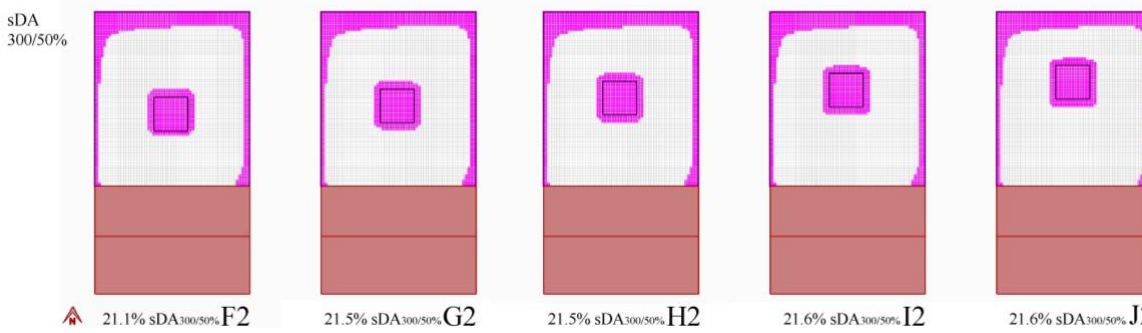
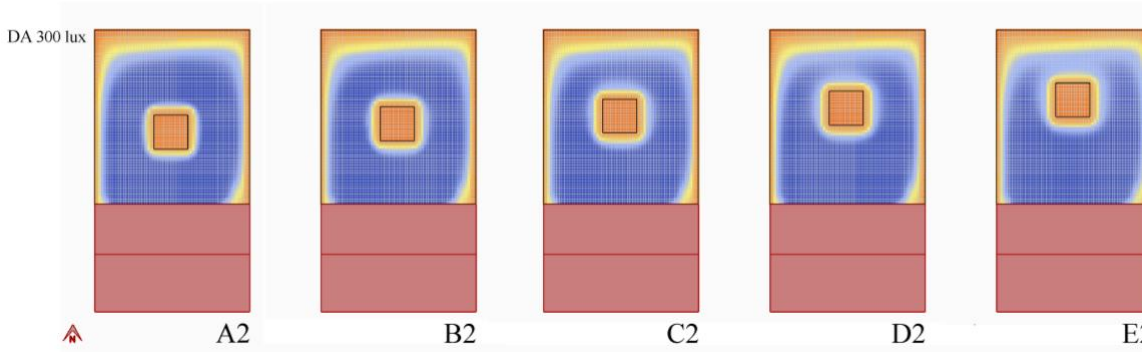


Figure 33 DA<sub>300</sub> and sDA<sub>300/50%</sub> result plots for the specified design solutions, highlighting the impact of atrium orientation on daylight performance on the ground floor. The %space sDA results provided below the plots refer to atrium adjacent spaces only.

Findings on DA<sub>100</sub> and sDA<sub>100/50%</sub> remained the same as those previously described for the 2<sup>nd</sup> floor (Figure 34.). However, the change from north to southward oriented atria showing a higher DA<sub>100</sub> and sDA<sub>100/50%</sub> performance occurred more abruptly than on the previous floor. Overall, sDA<sub>100/50%</sub> performance was similarly high on the 2<sup>nd</sup> and ground floor despite the additional depth. This was because the atrium well façade on the ground floor was fully glazed (as opposed to a WWR of 60%, 80%, 90% on the second floor).

The %time plots for DA<sub>100</sub> results show that southward orientations increased areas with especially low daylight (dark blue patches Figure 33 C to E and C2 to E2). Rather than due to orientation itself, this result was a product of the increase in room depth and overshadowing from surrounding buildings. Southward orientations however also improved daylight in spaces directly surrounding the atrium well, as shown with the sDA<sub>300/50%</sub> results. An increase of daylight in those spaces could be confirmed by looking at the UDI-e and ASE plots in Figure 35. ASE result showed that southmost orientations received the most direct sunlight, a result of alignment of the atrium well with solar altitude angles (Figure 35 N, O and N2, O2). UDI-e results also confirmed a better daylight distribution around the atrium well for southward than northward orientations (light blue hue all around the atrium well instead of only to the north of the atrium, Figure 35 S, T and S2, T2).

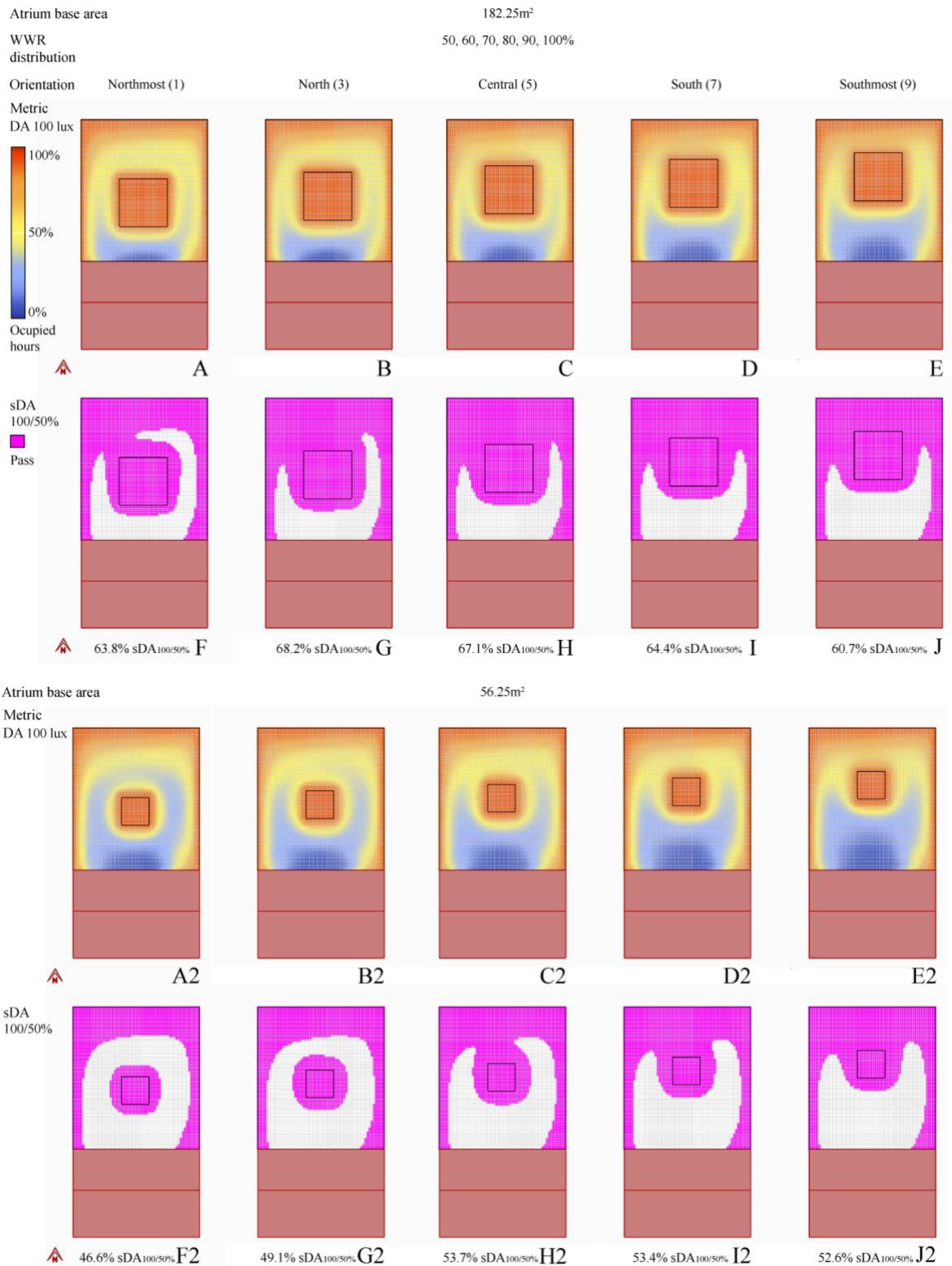


Figure 34 DA<sub>100</sub> and sDA<sub>100/50%</sub> results plots for the specified design solutions on the ground floor. The %space sDA results provided below the plots refer to atrium adjacent spaces only

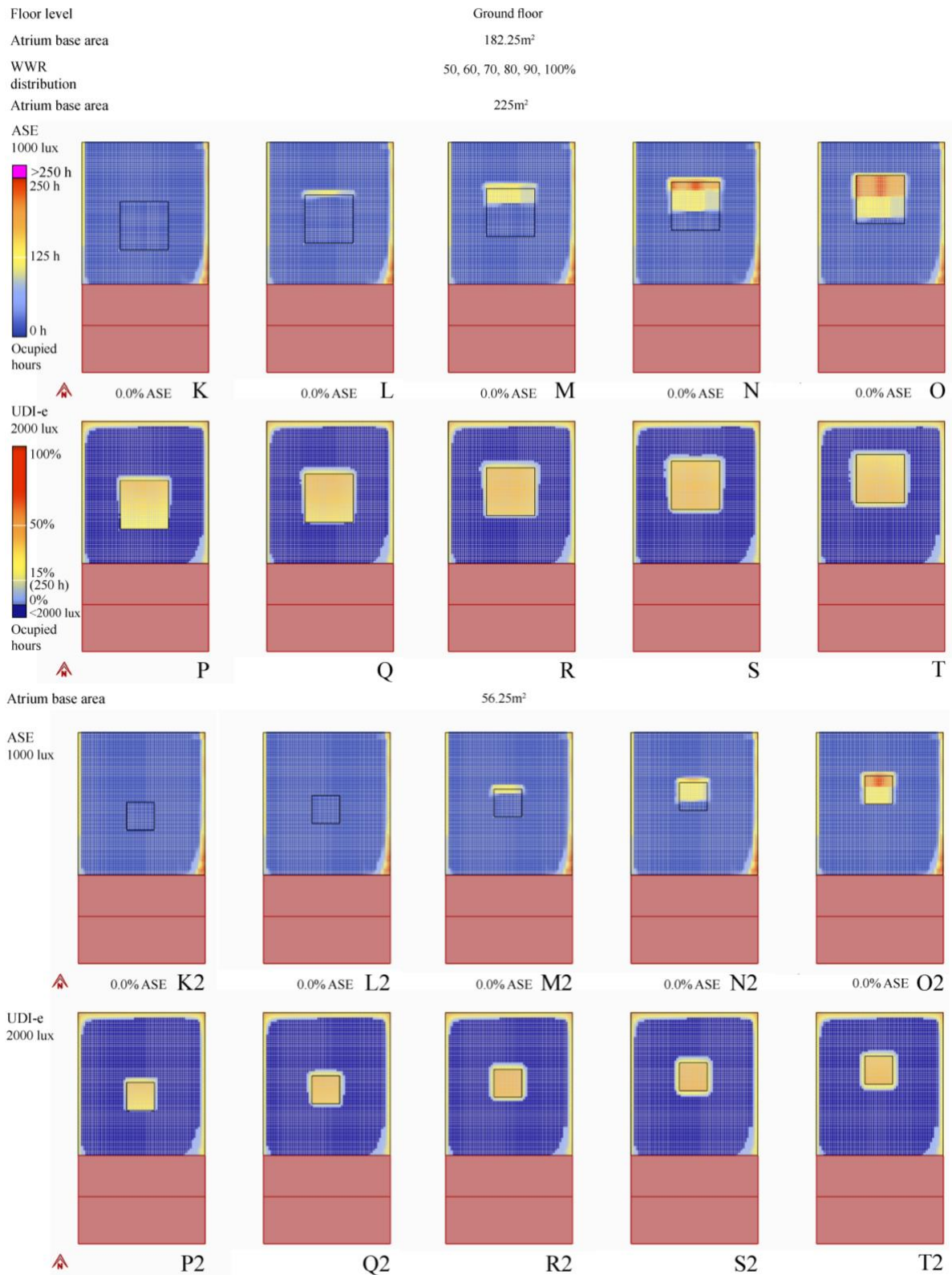


Figure 35 ASE and UDI-e result plots for the specified design solutions on the ground floor

In conclusion, southward orientations appear to perform better in that they allow for a deeper daylight penetration into the building and improve daylight distribution in

areas surrounding the atrium well, whereas northward orientations appear to perform better in that the amount of especially low DA decreases. The latter however is largely a result of the location of the atrium well on the floor plan. When this is understood, designers can make informed design changes: e.g., a southward orientation can be selected to improve daylight distribution in spaces surrounding the atrium well, and the atrium well location can be moved towards the south of the building floor plan in order to reduce underlit areas in these spaces.

The %time results helped more accurately understand the impact of design changes on daylight performance. The results provided explanations for the observed patterns and trends in daylight performance analysed in the previous chapter, and also uncovered additional information and differences between design solutions that were not evident from the %space results. For example, ASE performance of all design solutions on the 3<sup>rd</sup> floor was similar to each other. Differences could only be identified from the %time plots, which showed that southward orientation increased direct sunlight penetration in spaces to the east and west of the atrium well. Also, some of the design solutions that showed the highest sDA, revealed particularly low DA in the %time plots and an overall worse daylight distribution (as seen on the 5<sup>th</sup> and 4<sup>th</sup> floors). The analysis further highlighted, that turning points in trends may easily change. For example, by increasing the radiance parameter setting (e.g. to 7 ab), the optimum orientations identified on the 6<sup>th</sup> and 5<sup>th</sup> floors may shift. Taken together, daylight performance metrics with absolute cut-off thresholds (such as the sDA) may obscure design strategies that could lead to better qualitative daylighting of a space. The %time visualisations provided a quick aid to understanding the underlying patterns and trade-offs for the desired performance targets and assisted in identifying bias introduced by the thresholds. Alternatively, using multiple thresholds (e.g. DA<sub>100</sub>, DA<sub>200</sub> and DA<sub>300</sub>) or

multiple metrics (e.g. uniformity as additional metric) may also provide additional control.